STAT

Next 1 Page(s) In Document Denied

STAT

TECHNICAL INTELLIGENCE TRANSLATION

(Title Unclassified)
FUNDAMENTALS OF INFRARED TECHNOLOGY
(Osnovy Infrakrasnoy Tekhniki)

by

I. A. Margolin and
N. P. Sumyantsev

Source: Military Publishing House,
Ministry of Defense USSR

Moscow

1955

263 Pages

DEPARTMENT OF THE AIR FORCE
UNITED STATES OF AMERICA

AIR TECHNICAL INTELLIGENCE CENTER
WRIGHT-PATTERSON AIR FORCE BASE
OHIO

I.A.Margolin and N.P.Sumyantsev (deceased)

FUNDAMENTALS OF INFRARED TECHNOLOGY

Military Publishing House
Ministry of Defense USSR
Moscow, 1955

STAT

STAT

AUTHORS' PREFACE

Infrared rays are being increasingly used in various fields of science and technology. The rising interest in this field of the spectrum of electromagnetic oscillations is therefore understandable.

During recent years many works on the principles of physics and technology of the radiation and registration of infrared rays have appeared. The authors of the book have set themselves the task of systematizing and summarizing these scattered data.

In this book, presented for the attention of the reader, are the principles of the physics and technology of radiation, propagation, and reception of infrared rays including a number of data of handbook character.

This review makes no claim to exhaustive coverage of the questions discussed, since it is one of the first attempts to systematize the materials in this field. It may be used as a handbook and a textbook.

The introduction, Chapters I-VII, and Section 75-76 of Chapter VIII, Sections 82-84 of Chapter IX, and Chapter XIII have been written by I.A.Kargolin; Section 77 of Chapter VIII, Sections 78-81 and 85 of Chapter IX, and Chapters X to XII by the late N.P.Rumyantsev.

INTRODUCTION

The historic directives of the Nineteenth Congress of the Communist Party USSR on the Fifth Five-Year Plan of development of the USSR for 1951-1955 point out the necessity of widespread automation of the production process, and of increasing, within the Five-Year Plan, the production of instruments for control, automation, and telemechanics by about 2.7 times.

A number of such instruments use elements of infrared technology. Infrared technology is a new branch of modern technical physics, covering a wide range of problems connected with the physics of radiation, propagation, and recording of infrared rays, with the technology of development and manufacture of infrared radiators, with the technology of the development of indicators (radiation receivers), special optical systems and optical filters, and with the application of these elements to various scientific research fields, as well as to industrial and military purposes.

The development of infrared technology is inseparably linked with the names of our greatest Russian scientists.

In 1878, the outstanding Russian electrode technologist P.N.Yablochkov invented a radiator with an incandescent body in the form of a rod made of a mixture of kaolin and magnesia. This radiator is a very good source of infrared rays and is therefore widely used in various scientific studies.

In 1888, the outstanding Russian physicist A.G.Stoletov was the first to give a scientific explanation of the phenomenon of the external photoelectric effect, establish its basic laws, and construct the first prototype of the photoelectric

cell.

In 1895, the great Russian physicist P.N.Lebedev designed the first prototype of the vacuum thermoelectric cell, one of the basic forms of indicators of infrared rays.

In the postwar years, Soviet industry achieved great success in the introduction and mass production of various forms of modern infrared instruments to meet the requirements of the national economy. These instruments, designed under the guidance and participation of great Soviet scientists and specialists such as A.A.Levedev, G.S.Landsberg, G.G.Slyusarev, A.I.Tudorovskiy, I.A.Shoshin, and others, are superior in a number of basic parameters to analogous foreign prototypes, which is evidence of the high scientific and technical level of the mechanical optics industry.

The design of the individual elements of infrared technology and the solution of the complex theoretical questions were propagated by the Soviet scientists S.I.Vavilov, A.A.Glagoleva, Arkad'yeva, M.L.Veyngerov, B.P.Kozyrev, M.A.Levitskya, N.C.Smirnov, N.N.Terenin, P.V.Timofeyev, M.S.Khlebnikov, V.V.Shuleykin, and many others.

There is no doubt that in future years, infrared technology will make new and great advances in its development.

CHAPTER I

BASIC CONCEPTS AND DEFINITIONS RELATING TO RADIANT ENERGY

Section 1. Radiant Energy

The energy of visible and invisible rays is known as radiant energy. Radiation in the visible region of the spectrum (visible rays) is called light.

In modern physics, light is considered a flux of material particles possessing wave and quantum properties. Certain optical phenomena are well explained by the wave mechanics of light, others by the quantum theory. The wave properties are due to the fact that light consists of electromagnetic waves. The quantum properties are characterized by variations in the energy of light in definite portions known as light quants.

Table 1

Relation between Units of Measurement of Energy

Unit	erg	joule	kilojoule	cal	kcal
1 erg	1	10^{-7}	10^{-10}	2.39×10^{-8}	2.39×10^{-11}
1 joule	10^{7}	1	10^{-3}	0.239	2.39×10^{-4}
1 kilojoule	10^{10}	10^{3}	1	239	0.239
1 cal	4.18×10^{7}	4.18	4.18×10^{-3}	1	10^{-3}
1 kcal	4.18×10^{10}	4.18×10^{3}	4.18	10^{3}	1

This is also true of the radiant energy of the invisible part of the spectrum.

If radiant energy is absorbed by bodies on the path of its propagation, it is transformed into other forms of energy, thermal, electric, or chemical, with the law

of conservation of energy being obeyed.

Radiant energy is measured in ergs (erg); joules (j) and calories (cal). Table 1 gives the relations between these units.

Section 2. Quantities Characterizing the Oscillatory Process

Electromagnetic oscillations are characterized by the same fundamental quantity as mechanical harmonic oscillations.

If a point executes harmonic oscillatory motions about a point of equilibrium, the deviation y from this position for any instant of time t is found from the formula

$$y = A \cos\left(2\pi \frac{t}{T} + \varphi\right) \qquad (1)$$

where A = amplitude of oscillations (maximum deviation from the position of equilibrium);

T = period of oscillation (time of one full oscillation);

φ = initial phase (quantity defining the deviation from the point of equilibrium at the initial instant t = 0).

By laying off the time on the abscissa and the value of the deviation y on the ordinate, we obtain a graph of the harmonic oscillatory motion (Fig.1).

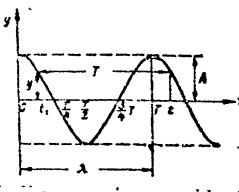

Fig.1 - Graph of Harmonic Oscillatory Motion

The quantity $2\pi \frac{t}{T} + \varphi$ is called the phase of the oscillations at the instant of time t. After every period, i.e., at t equal to T, 2T, 3T, etc, the deviations y are the same in magnitude and sign, for example at the instants of time t_1 and t_2. This corresponds to the same phase of oscillation.

The number of full cycles of oscillations in unit time is called the frequency of oscillations ν. This quantity is reciprocal to the oscillation period. The cycle (c) has been adopted as the unit of oscillation frequency. This is the frequency at which one full oscillation takes place in one second.

The propagation of oscillatory (wave) motion in any medium is characterized by: the wavelength λ, equal to the distance between the two nearest points corresponding to the same amplitudes and differing in phase by the period T; the velocity of propagation of the wave motion v, equal to the distance at which the wave is propagated in unit time:

$$v = \frac{\lambda}{T} \qquad (2)$$

In a medium with a refractive index of n, the velocity of propagation of the wave motion will be

$$v = \frac{c}{n} \qquad (3)$$

where c is the velocity of propagation of light in a medium with the refractive index of n = 1, equal to 299775 ± 11 km/sec.

Table 2

Relations between Units of Wavelength

Unit	m	cm	mm	μ	mμ	Å	X
1 m	1	10^2	10^3	10^6	10^9	10^{10}	10^{13}
1 cm	10^{-2}	1	10	10^4	10^7	10^8	10^{11}
1 mm	10^{-3}	10^{-1}	1	10^3	10^6	10^7	10^{10}
1 μ	10^{-6}	10^{-4}	10^{-3}	1	10^3	10^4	10^7
1 mμ	10^{-9}	10^{-7}	10^{-6}	10^{-3}	1	10	10^4
1 Å	10^{-10}	10^{-8}	10^{-7}	10^{-4}	10^{-1}	1	10^3
1 X	10^{-13}	10^{-11}	10^{-10}	10^{-7}	10^{-4}	10^{-3}	1

The wavelength λ, the velocity of light c, the period T and the frequency ν are correlated by the radiation

$$\lambda = cT = \frac{c}{\nu} \qquad (4)$$

Electromagnetic waves have a very wide range of wavelengths; therefore, to-

STAT

gether with the units of length used for measuring radio waves (m, cm, mm), units like the micron (μ), millimicron (mμ), Angstrom (Å), and roentgen (X) are also used in the short-wave region of the spectrum. Table 2 gives the relations between these units.

Section 3. The Spectrum of Electromagnetic Waves

The totality of all electromagnetic waves forms a spectrum of electromagnetic waves with wavelengths from 1×10^{-11} to 3×10^{10} cm. This spectrum can arbitrarily

Table 3

Scale of Spectrum of Electromagnetic Waves

Spectrum region		Wavelength	
		In conventional units	in cm
Low-frequency oscillations		Longer than 20,000 m	Longer than 2×10^6
Radio waves	Long	20,000-2000 m	$2 \times 10^6 - 2 \times 10^5$
	Medium	2000-200 m	$2 \times 10^5 - 2 \times 10^4$
	Short	200-10 m	$2 \times 10^4 - 1 \times 10^3$
	Ultrashort	10-0.5 m	$1 \times 10^3 - 0.5 \times 10^2$
	Microwaves	shorter than 0.5 m	shorter than 0.5×10^2
Infrared rays	Long-wave	420-100 μ	4.2×10^{-2} to 1×10^{-2}
	Medium-wave	100-15 μ	1×10^{-2} to 1.5×10^{-3}
	Short-wave	15-0.76 μ	1.5×10^{-3} to 0.76×10^{-4}
Visible rays	Red	7600-6200 Å	0.76×10^{-4} to 0.62×10^{-4}
	Orange	6200-5900 Å	0.62×10^{-4} to 0.59×10^{-4}
	Yellow	5900-5600 Å	0.59×10^{-4} to 0.56×10^{-4}
	Green	5600-5000 Å	0.56×10^{-4} to 0.5×10^{-4}
	Blue	5000-4800 Å	0.5×10^{-4} to 0.48×10^{-4}
	Deep blue	4800-4500 Å	0.48×10^{-4} to 0.45×10^{-4}
	Violet	4500-4000 Å	0.45×10^{-4} to 0.4×10^{-4}
Ultraviolet rays		4000-50 Å	0.4×10^{-4} to 5×10^{-7}
X-rays		50-0.04 Å	5×10^{-7} to 4×10^{-10}
Gamma rays		40 X and shorter	4×10^{-10} and shorter

be divided into separate regions which, in part, overlap.

Figure 2 gives the range of the spectrum of electromagnetic waves on a logarithmic scale. Table 3 also gives the division of the spectrum into separate regions.

The gamma rays are the extreme, shortest rays of the spectrum and are radiated by radioactive elements.

X-rays are very short electromagnetic waves emitted by solid bodies struck by high-speed electrons. X-rays have high penetrating power and act strongly on the human organism.

The region of ultraviolet rays is bounded by the regions of X-rays and visible rays. The electric arc, as well as quartz and mercury lamps, are good technical sources of ultraviolet rays.

Ultraviolet rays can be detected by photographic methods, by the fluorescence and phosphorescence caused by these rays, and by means of photocells and thermoelectric cells.

The visible rays occupy the narrowest segment in the electromagnetic spectrum: 0.4-0.76 μ. It has been demonstrated by Soviet scientists, particularly by N.I.Pinegin, that the boundary of the visible region of the spectrum is determined by the power of the radiation source and the degree of adaptation of the eye. Thus, in the infrared region of the spectrum, the threshold of sensitivity of the eye goes as far as 0.85-0.90 μ when the power of the radiation source is increased by hundreds of thousands of times. The properties and regions of application of the visible rays are known from courses in physics.

Infrared rays, invisible to the eye, occupy the region of the spectrum from about 0.76 to 400-420 μ, lying between the red rays of the visible part of the spectrum and the ultrashort radio waves. They possess the same properties as the visible and ultraviolet rays, i.e., their propagation is rectilinear, and they are refracted and polarized. Infrared rays are radiated by the outer electrons of atoms and molecules as a result of rotary and oscillatory motions of the molecules.

These rays are sometimes called thermal rays since their radiation is determined by the temperature of the radiating body.

The methods of excitation and detection of infrared rays vary according to the spectral areas.

The region of infrared rays may be arbitrarily divided into three regions of

STAT

the spectrum: short-wave (0.76-15μ), medium-wave (15-100μ) and long-wave (110-420μ). The short infrared rays (0.76-15μ) are the most fully investigated and utilized in technology. They may be divided into separate zones according to the type of receivers used.

Infrared rays of a wavelength from 0.76 to 9.3-1.5μ are detected by photocells with external photoeffect, by specially treated (infrared-sensitized) photographic plates, and by the methods of extinction of phosphorescent screens. For the recording of infrared radiation in this zone, all forms of thermoelectric receivers and photocells with internal photoeffect and with photoeffect in the blocking layer are also used.

Sources of infrared rays in this portion of the spectrum are electric incandescent lamps, various gas-discharge lamps, and all heated bodies with temperature above 280°K.

To detect waves of wavelength from 1.3 to 7μ, photocells with internal photoeffect are used, as well as all thermoelectric indicators. Sources for such waves are electric incandescent lamps, high-pressure and extreme-pressure mercury lamps, special rod and cup radiators, and

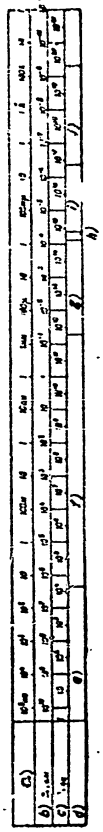

Fig.2 - Scale of Spectrum of Electromagnetic Waves
a) λ (Logarithmic scale); b) f, cps; c) Name of spectral region; d) Low-frequency oscillations; e) Radio waves; f) Infrared rays; g) Visible rays; h) Ultraviolet rays; i) X-rays; j) Gamma rays

all heated bodies with temperatures above 70°K.

The boundary wavelength of 15μ for the 7 to 15μ portion of the spectrum is determined by the absorption of infrared rays in the atmosphere; water vapor, always present in the atmosphere, almost completely absorbs infrared rays of wavelengths longer than 14-15μ.

Sources of infrared rays of this part of the spectrum are all heated bodies of temperatures above 45°K as well as rod and cup radiators.

Infrared rays of the long-wave portion of the spectrum have not yet been studied much. Their sources are all bodies at temperatures above absolute zero; but the energy radiated by them is so small that it can hardly be detected by sensitive thermoelectric receivers. Works by the noted Soviet physicist A.A.Glagoleva-Arkad'yeva are devoted to this region of the infrared spectrum. He has built a special radiator (mass "radiator" emitting infrared rays of wavelengths up to about 0.1 mm).

Radio waves are waves which have wavelengths from millimeters to a few kilometers, and are widely used for radio communication, radio broadcasting, radio location, television, etc.

Low-frequency oscillations have the longest wavelength. Their sources are industrial alternating-current generators.

STAT

CHAPTER II

ENERGETIC AND LIGHT-TECHNOLOGICAL QUANTITIES

Section 4. Energetic Quantities

Radiant energy and all quantities related to it are measured in energetic or light-technical units according to the spectral composition of the radiant energy and to the features of the receiver used for the measurement. Energetic quantities are used when the receiver reacts in the same way to radiant energy over a wide range of the spectrum of infrared rays. Receivers of this type are called nonselective. Such receivers are, for example, thermoelectric cells which transform radiant energy into thermal energy.

If selective receivers whose reaction depends on the spectral composition of the radiant energy are used for the measurement (such as photocell or photographic plates), then the selection of the unit of measurement depends on the band of the spectrum in which the receiver operates. In the infrared region of the spectrum energetic quantities are usually employed. For measuring radiant energy in the visible region of the spectrum, optical-engineering units are used permitting an evaluation of the perception of light by the eye which reacts to a radiant flux only in the visible region of the spectrum.

Radiant Flux

The quantity of energy radiated (absorbed or transferred) in unit time is called the radiant flux Φ.

If, during the time interval t, the radiant energy Q is radiated, then the radiant flux

$$\Phi = \frac{Q}{t} \qquad (5)$$

Radiant flux is measured in units of power. The relations between these units are given in Table 4.

Table 4

Relations between Certain Units of Power

Unit	erg/sec	cal/sec	watt	kw
1 erg/sec	1	2.39×10^{-8}	10^{-7}	10^{-10}
1 cal/sec	4.18×10^{7}	1	4.18	4.18×10^{-3}
1 watt	10^{7}	0.239	1	10^{-3}
kw	10^{10}	239	10^{3}	1

Energetic Power of Light

The energetic power of light I_{en} represents the radiant flux per unit solid angle ω, through which it is propagated:

$$I_{en} = \frac{d\Phi}{d\omega} \qquad (6)$$

If the radiant flux is uniformly distributed within the limits of the solid angle ω, then

$$I_{en} = \frac{\Phi}{\omega} \qquad (7)$$

The energetic power of light is measured in w/ster, erg/sec-ster and cal/sec-ster.

Note. If the area S, equal to the square of the radius of the sphere r is cut out of a sphere and the boundaries of this area are connected with the center of the sphere, then the solid angle will be equal to unity, since at $S = r^2$

$$\omega = \frac{S}{r^2} = 1 \qquad (8)$$

Therefore the solid angle, cutting out on the surface of a sphere an area equal to the square of the radius of this sphere, is taken as the unit of solid angle and is called a steradian (ster).

The solid angle ω is related to the plane angle α by the relation

$$\omega = 2\pi(1 - \cos\alpha) \qquad (9)$$

The quantity ω is dimensionless.

Energetic Illumination

The radiant flux incident on unit irradiated surface is called the energetic illumination, or surface density of incident flux, and is expressed by the formula

$$E_{en} = \frac{d\Phi}{dS} \qquad (10)$$

where dS = element of illuminated surface;

$d\Phi$ = flux incident on this element of surface.

If the surface is illuminated by a point source over the definite solid angle $d\omega$, eq.(10) takes the form

$$E_{en} = I_{en}\frac{d\omega}{dS} \qquad (11)$$

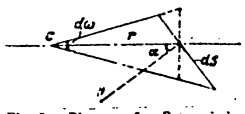

Fig.3 - Diagram for Determining Energetic Illumination

Let us imagine that the point source of light C (Fig.3) with the energetic light intensity I_{en} illuminates the surface element dS in the solid angle $d\omega$. Then the solid angle in which the element of surface is illuminated is equal to

$$d\omega = \frac{dS}{r^2}\cos\alpha \qquad (12)$$

where α = angle formed by ray incident on the surface and the normal N to it;

r = distance from the source to the center of the area dS.

Substituting the value of $d\omega$ from eq.(12) in eq.(11), we get

$$E_{en} = \frac{d\Phi}{dS} = \frac{I_{en}}{r^2}\cos\alpha \qquad (13)$$

Equation (13) expresses the law of inverse squares, according to which the illumination of a surface is directly proportional to the light intensity and inversely proportional to the square of the distance between the radiator and the irradiated surface.

Energetic illumination is measured in watt/cm^2, erg/sec-cm^2 and cal/sec-cm^2.

Energetic Luminosity (Illumination)

The radiant flux emitted by unit of radiating surface is called the energetic luminosity, or the surface density of the radiant flux emitted. The energetic luminosity is defined by the formula

$$B_{en} = \frac{d\Phi}{dS} \qquad (14)$$

where $d\Phi$ is the radiant flux radiated by unit surface dS.

Brightness and illumination are measured in the same units and differ only in that the brightness characterizes the radiation from this surface, while the illumination characterizes the incidence of the light flux on a surface.

Energetic Brightness

The radiant energy emitted by unit surface in a specified direction is called energetic brightness. The energetic brightness B_{en} is equal to the quotient of energetic luminous intensity of a surface measured in a given direction by the area of the emitting surface projected onto a plane perpendicular to the direction considered:

$$B_{en} = \frac{dI_\alpha}{dS\cos\alpha} \qquad (15)$$

where dI_α = energetic luminous intensity in the given direction;

STAT

α = angle between normal to the surface and the given direction.

When a luminous flux is emitted uniformly in all directions, the energetic brightness is defined by the formula

$$B_{en} = \frac{dI_{en}}{dS} \qquad (16)$$

Energetic brightness is measured in watt/steradian-cm^2.

The Cosine Law. Relations between Energetic Quantities

The variation in the energetic luminous intensity of light, depending on the direction, obeys the cosine law in most cases: the luminous intensity of a radiating surface of uniform brightness is proportional to the cosine of the angle of radiation. In its mathematical form, this law may be obtained from eq.(15)

$$B_{en} = \frac{I_\alpha}{S \cos \alpha}$$

whence the luminous intensity of the radiating surface is

$$I_\alpha = B_{en} S \cos \alpha \qquad (17)$$

The cosine law gives simple relations between certain quantities.

From eq.(17), if the energetic brightness is known, we can determine the energetic luminous intensity of the surface and, consequently, also the total radiant flux emitted by it:

$$\Phi = \pi B_{en} S \qquad (18)$$

Substituting the value of Φ in eq.(14), we obtain the expression for the luminosity

$$R_{en} = \pi B_{en} \qquad (19)$$

Thus, the luminosity of a surface obeying the cosine law of radiation equals its energetic brightness multiplied by π.

Let us find the relation between the illumination and the brightness of an ideally scattering surface. An ideally scattering surface is a surface reflecting all the incident light flux regardless of the direction of its incidence and distributing the reflected flux by the cosine law of radiation. A white matte surface is an almost ideal scattering surface.

A light flux incident on a surface is characterized by the illumination produced by it on that surface.

An ideally scattering surface completely reflects the incident flux without absorbing any of it; it may therefore be considered that it emits the same radiant flux. Consequently, the energetic luminosity of this surface

$$R_{en} = E_{en} \qquad (20)$$

i.e., the energetic luminosity of an ideally scattering surface is equal to its energetic illumination.

Since the radiant flux is distributed by the cosine law, the energetic brightness is a constant quantity and, according to eq.(19), is equal to (considering that, for an ideally scattering surface, $R_{en} = E_{en}$)

$$B_{en} = \frac{E_{en}}{\pi} \qquad (21)$$

i.e., the energetic brightness of an ideally scattering surface is equal to its energetic illumination divided by π.

Section 5. Certain Properties of the Human Eye

The properties of the eye play a substantial role in visual measurements of radiant energy. When a radiant flux strikes the retina of the eye, a photochemical process takes place. It consists of the stimulation under the action of light of certain photosensitive terminal nerve cells, the so-called rods and cones. This stimulation is then transmitted to the brain.

The cones constitute the apparatus for daytime vision, functioning at high illuminations, and the rods, the apparatus for nocturnal and twilight vision, functioning at low illuminations. The cones enable us to discriminate color, since

STAT

they perceive the frequencies of the light spectrum differently.

The curves for the cones (C) and the rods (R) give the spectral sensitivity of the eye, constructed according to the data of Professor N.F.Fedorov (Fig.4), show that the maximum of rod sensitivity is shifted toward shorter wavelength (λ = 0.507μ) with respect to the maximum of cone sensitivity (λ = 0.555μ).

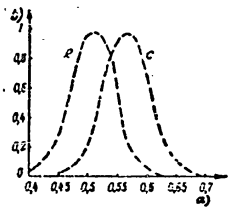

Fig.4 - Spectral Sensitivity of the Eye
R - Rods; C - Cones
a) Wavelength, μ; b) Spectral sensitivity in arbitrary units

The time required for the sensation of light to be produced is from 0.1 to 0.25 sec, according to the intensity of illumination (brightness) and the wavelength of the light.

The minimum radiant flux Φ_e, capable of producing a sensation of light in the eye is called the light threshold of the eye. The light threshold of the eye is about 1×10^{-10} - 5^{-12} erg/sec.

The resolving power of the eye is characterized by the minimum angle of resolution at which the eye is able to distinguish two points or lines of an observed object. The magnitude of the resolving power is inversely proportional to the angle of resolution. Under the conditions of normal illumination and good contrast, this angle is equal to one minute. As the illumination decreases, the resolving power decreases since the angle of resolution increases, reaching 10-17' for observation in twilight or dusk.

The eye is able to distinguish objects because of the contrast between the brightness (or color) of an object and the background against which the object is observed.

The contrast between the brightness of an object and that of the background is defined by the formula

$$K = \frac{B_o - B_b}{B_b} \qquad (22)$$

where B_o = brightness of the object;

B_b = brightness of the background.

Visual (Subjective) Method of Measuring Radiant Energy

The visual (subjective) evaluation of the quantity of radiant energy is based on visual perception so that visual measurements are possible only in the visible portion of the spectrum (0.4-0.76μ). Subjective photometers of various types are used as auxiliary instruments for measurements in this region.

The visual method of measurement, based on a discrimination of different illumination by the eye, has major drawbacks. The human eye is a selective receiver. Even within the visible part of the spectrum, the sensitivity of the eye varies over a wide range, which has a strong effect on the accuracy of light measurements. Moreover, the eye can only approximately estimate the equality or inequality of light fluxes, and this estimate is different with different people.

Section 6. Optical Engineering Quantities

Luminous Flux

The radiant flux of the visible part of the spectrum produces a different visual stimulation of the eye, depending on the spectral composition. The power of the radiant energy estimated from the light sensation of the eye, is called the light flux F.

The human eye does not perceive the light flux uniformly throughout the entire visible part of the spectrum. Its maximum sensitivity is to a monochromatic light flux of wavelength λ = 0.555μ. With increasing or decreasing wavelength of monochromatic radiation, the sensitivity of the eye decreases.

For monochromatic radiation of a wavelength of λ, there exists a definite relation between the radiant flux Φ_λ and the light flux F_λ:

$$F_\lambda = V_\lambda \Phi_\lambda \qquad (23)$$

where V_λ is the monochromatic visibility characterizing the sensitivity of the eye to a monochromatic light flux of a wavelength of λ by comparison with the sensitivity of the eye to a the radiant flux of the same wavelength λ.

In the general form, for the entire visible portion of the spectrum, the light flux

$$F = \int_{\lambda=0.4}^{\lambda=0.76} \Phi V_\lambda d\lambda \qquad (24)$$

The unit adopted for the light flux is the lumen (lm), which is the light flux radiated by an uncovered radiator (an absolute black body) at the solidification temperature of platinum (2046°K) from an area of 5.305×10^{-3} cm^2.

Luminous Intensity

The luminous intensity I is the light flux per unit solid angle ω within which it is radiated:

$$I = \frac{F}{\omega} = \frac{Fr^2}{S} \qquad (25)$$

On radiation within the total solid angle ω = 4π, the luminous intensity will be

$$I = \frac{F_o}{4\pi} \qquad (26)$$

where F_o = total light flux.

The candle (cd), has been adopted as the unit of luminous intensity. An international candle is the luminous intensity that a point source radiates in the directions in which it emits a light flux of one lumen distributed within a solid angle of 1 ster.

Knowing the luminous intensity I of a source under the conditions of uniform distribution over the solid angle ω, the light flux can be calculated by the relation

$$F = I\omega \qquad (27)$$

However, since $\omega = \frac{S}{r^2}$

$$F = \frac{IS}{r^2} \qquad (28)$$

In the total solid angle ω = 4π, the light flux is

$$F = 4\pi I \qquad (29)$$

If the luminous intensity of a source is equal to unity (1 cd), then the light flux emitted by it will be 12.56 lumens.

If a point source of light radiates a light flux within a solid angle of 1 steradian and the luminous intensity is 1 candle, then the light flux is 1 lumen.

Brightness

The brightness B of a radiating (or reflecting) surface S in a given direction is the quotient of the luminous intensity I in this direction to the projection of the surface S on a plane perpendicular to the same direction:

$$B = \frac{I}{S \cdot \cos\alpha} \qquad (30)$$

where α = angle between the given direction and the normal to the luminous surface.

The relation between the brightness of an ideally scattering surface, to which the cosine law of radiation is applicable, and the light flux is expressed by the formula

$$B = \frac{F}{\pi} \qquad (31)$$

The following units are used for measuring brightness:

Stilb (sb), which is the brightness of an extremely small plane surface equally luminous at all points, for which the ratio of luminous intensity in candles to its area in square centimeters is equal to unity, the brightness and the luminous intensity being determined in a direction perpendicular to this surface:

$$1\ sb = \frac{1\ cd}{1\ cm^2}$$

Millistilb (msb), one thousandth of a stilb:

$$1 \text{ msb} = 10^{-3} \text{ sb}$$

decimillistilb (dmsb), one ten-thousandth of a stilb:

$$1 \text{ dmsb} = 1^{-4} \text{ sb}$$

Table 5 gives the brightness characteristics of certain light sources

Table 5

Brightness Characteristics of Certain Light Sources

Light Source	Brightness sb	Light Source	Brightness sb
Extreme-preasure arc	280,000	Filament of incandescent tungsten lamp (1 watt/cd)	150-200
		Neon point lamp	20
Surface of sun visible from earth	165,000	Acetylene flame	8
		Cap burner	4
		White paper, illuminated by sun	3.2
High-intensity arc (200 amp)	82,000	Kerosene flame	1.5-1.2
High-intensity arc (150 amp)	60,000	Sky covered by haze	0.8
Extreme-preasure mercury lamp	60,000	Stearine candle flame	1.0
Ordinary arc lamp (20 amp)	3,000	Surface of moon	0.25
		Sky in overcast weather	0.1
Special incandescent lamp	2,900	Neon bulb with flat electrodes	0.05
Motion picture projection lamp	1,600		
Point lamp (230 watts)	1,500	Screen of motion-picture theater	0.1-0.0005
Gas-filled tungsten lamp (0.5 watt/cd)	600	Moonless night sky	10^{-8}

According to eq.(30), the luminous intensity radiated by a surface of brightness B, in the direction of the normal N to the surface is equal to

$$I = BS \qquad (32)$$

If the light is radiated at a certain angle to the normal N, then eq.(32) takes the form

$$I_\alpha = BS \cos \alpha \qquad (33)$$

Consequently, the intensity of light radiated from a surface of the same brightness is proportional to the cosine of the angle α.

The light threshold of the eye with respect to brightness is equal to 6.4×10^{-11} sb.

At a brightness of more than 16 sb, the eye is blinded.

The region of greatest sensitivity of the eye to white light corresponds to a brightness of 0.0064-0.064 sb.

Illumination

The illumination (or specific illumination) E represents the surface light density of an incident light flux, i.e., the light flux F incident on unit surface S:

$$E = \frac{F}{S} \qquad (34)$$

The specific illumination is connected with the brightness by the relation

$$E = \pi B \qquad (35)$$

Thus to pass from illumination to brightness or vice versa, the corresponding quantity (E or B) must be multiplied or divided by π.

The illumination of a surface of brightness B, when a light flux is incident on it at an angle α, is expressed by the formula

$$E = B\omega \cos \alpha \qquad (36)$$

where ω = solid angle within which the light flux is incident.

The units lux and phot are used to measure illumination.

The lux (lx) is the direct illumination on a surface on each square meter of which light flux of 1 lumen is uniformly distributed:

$$1 \text{ lux} = \frac{1 \text{ lumen}}{1 \text{ m}^2}$$

A phot (f) is the illumination of a surface of one square centimeter on which is uniformly distributed light flux of 1 lumen is incident:

$$1 \text{ phot} = \frac{1 \text{ lumen}}{1 \text{ cm}^2} = 10{,}000 \text{ lux}$$

A milliphot (mf) is equal to one thousandth of a phot:

$$1 \text{ milliphot} = 10^{-3} \text{ phot}$$

Table 6 gives examples of various illuminations.

Table 6

Illuminations Produced by Certain Sources (in Lux)

Illumination produced by sun beyond the limits of the earth's atmosphere	150,000
Illumination produced by sun on the earth's surface at noon:	
in summer	50,000
in autumn and spring	22,000
in winter	7,000
Illumination on open place in cloudy weather	1,000
Illumination necessary for exact work	200
Illumination necessary for writing	30
Illumination produced by street lighting	10
Illumination necessary for orientation	1
Illumination produced on earth's surface by the moon	0.2

In accordance with eq.(36) we may write

$$B = \frac{F}{\omega \cos \alpha} \qquad (37)$$

Luminosity

The luminosity R or the surface light density of the radiated (or reflected) light flux F, is the ratio of the light flux to the area of the radiating (or reflecting) surface:

$$R = \frac{F}{S} \qquad (38)$$

If the cosine law of radiation is applicable to the surface, then the following relation exists between luminosity R and brightness B:

$$R = \pi B \qquad (39)$$

If the surface S is illuminated and completely reflects all the light flux (a perfectly diffusing surface), then its luminosity will be

$$R = E \qquad (40)$$

where E is the specific illumination of the surface.

In this case the illuminated surface acts as though it were a source of light.

The difference between the illumination and luminosity of a self-luminous surface is that the illumination on the surface is defined by the light flux $F_{inc.}$ falling on it, while the luminosity is determined by the reflected light flux $F_{refl.}$.

The reflection of the light flux by the surface is defined by the coefficient of reflection ρ:

$$\rho = \frac{F_{refl.}}{F_{inc.}} \qquad (41)$$

Hence the luminosity of a surface that does not completely reflect the luminous flux is defined by the formula

$$R = \frac{F_{refl.}}{S} = \frac{\rho F_{refl.}}{S} = \rho E \qquad (42)$$

The radphot and radlux are used for measuring the luminosity.

The radphot (rf) is the luminosity of a uniformly radiating plane surface that emits into a hemisphere a light flux of 1 lumen from an area of 1 cm^2:

$$1 \text{ rf} = 1 \text{ lm}/1 \text{ cm}^2$$

A radlux (rlx) is equal to one ten-thousandth of a radphot:

1 rlx = 10^{-4} rf

Section 7. Conversion of Energetic Quantities to Optical Quantities

In measurements, we usually have to do with radiation of complex composition. The invisible portion of the spectrum is characterized by energetic quantities and the visible by optical quantities.

For measuring radiant energy, an objective method is used, based on the transformation of radiant energy into other forms of energy, and a visual method based on the perception of light by the human eye. It is therefore important to establish the relation between the measured energetic and optical units of light flux, allowing transition from energetic to optical quantities.

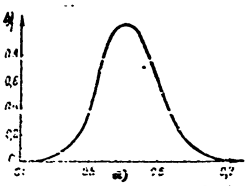

Fig.5 - Curve of Relative Visibility
a) Wavelength, μ; b) Relative visibility factor K_λ

Assume that some part of a complex spectrum of radiation of a source is bounded by the wavelength λ and λ + dλ. If we measure the flux of this part of the spectrum by both methods, then the ratio of the light flux, measured in lumens, to the radiant flux, measured in watts, is called the visibility factor (V_λ) or the light yield of the radiation for a wavelength of λ, defined by the formula

$$V_\lambda = \frac{F}{\Phi} \qquad (45)$$

The value of this factor depends on the wavelength, since the eye does not react uniformly to different wavelengths. The value of V_λ asymptotically tends toward zero at the boundary of the visible portion of the spectrum, and has its maximum (V_{max}) at a wavelength of about 0.555.

The ratio of the visibility factor for a wavelength of λ to the maximum value of this factor (V_{max}) is called the relative visibility factor K_λ for a wavelength of λ:

$$K_\lambda = \frac{V_\lambda}{V_{max}} \qquad (44)$$

The variation in the relative visibility factor K_λ according to wavelength λ may be represented in the form of the relative visibility curve shown in Fig.5. The values of K_λ are plotted on the ordinate and those of the wavelength on the abscissa. At λ = 0.555μ, the curve has its maximum which is arbitrarily taken as unity. To determine the absolute values of the visibility factor V_λ, the ordinates of the curve must be multiplied by the value of V_{max}.

The quantity reciprocal to the visibility factor (the luminous efficiency of radiation) is called the specific radiation consumption. At λ = 0.555μ, i.e., at maximum luminous efficiency, the specific radiation consumption has its minimum value.

The minimum specific consumption is also called the mechanical equivalent of light.

$$M = \frac{1}{V_{max}} = 0.0015 \text{ w/lm} \qquad (45)$$

The mechanical equivalent of light represents the minimum power in watts necessary to produce a light flux of 1 lumen at λ = 0.555μ. The mechanical equivalent of light permits establishing the relation between energetic and optical units.

On the basis of eq.(45), the maximum visibility factor is:

$$V_{max} = \frac{1}{M} = 670 \text{ lm/w} \qquad (46)$$

The ratio between the quantities K_λ, V_λ and M is defined by the expressions

$$V_\lambda = \frac{K_\lambda}{M} \qquad (47)$$

and

$$K_\lambda = V_\lambda M \qquad (48)$$

If the distribution of the radiant flux along the spectrum is expressed by a certain function f(λ), the radiant flux will be

$$\Phi = \int f(\lambda)d\lambda \qquad (49)$$

To determine the luminous flux as that part of the radiant flux perceived by the eye, it is necessary according to eq.(49) to multiply the value of the radiant flux for each wavelength λ by the corresponding visibility factor V_λ.

Integrating the resultant product, we obtain the value of the luminous flux:

$$F = \int_{\lambda=0.4}^{\lambda=0.76} f(\lambda)V_\lambda d\lambda = V_{max} \int_{\lambda=0.4}^{\lambda=0.76} f(\lambda)K_\lambda d\lambda \qquad (50)$$

For an approximate calculation of the luminous flux as a part of the radiant flux we can use the equation

$$F = \sum_{i=1}^{i=n} \Phi_i V_\lambda = V_{max} \sum_{i=1}^{i=n} \Phi_i K_\lambda \qquad (51)$$

where Φ_i = radiant flux in the wavelength range from $\lambda = i$ to $\lambda = i + 1$;

n = number of intervals into which the visible region of the spectrum is arbitrarily divided, for convenience of calculation.

Table 7

Principal Energetic and Optical Values

Energetic quantity	Formula	Units	Optical quantity	Formula	Units
Radiant energy	$W = \int \Phi dt$	erg, j, cal	Luminous energy	$W = Ft$	lm-sec
Radiant flux	$\Phi = \frac{dW}{dt}$	watt, erg/sec	Luminous flux	$F = I\omega = 4\pi I$	lumen
Energetic luminous intensity	$I_{en} = \frac{d\Phi}{d\omega}$	watt/ster	Luminous intensity	$I = \frac{F}{\omega} = BS$	candle
Energetic illumination	$E_{en} = \frac{d\Phi}{dS}$	watt/cm^2	Illumination	$E = \frac{F}{S} = \pi B$	lux, phot
Energetic luminosity	$R_{en} = \frac{d\Phi}{dS}$	watt/cm^2	Luminosity	$R = \frac{F}{S} = \rho E$	radphot
Energetic brightness	$B_{en} = \frac{dI_{en}}{dS}$	watt/ster/cm^2	Brightness	$B = \frac{I}{S} = \frac{\rho E}{\pi 10^4}$	stilb

A summary table of the principal energetic and optical quantities is given above (Table 7).

Section 8. Reflection, Absorption, and Transmission of Radiant Energy

If the radiant flux Φ is incident on the surface of a body S, then a portion of the flux Φ_ρ is reflected (mirror or diffuse reflection), another part Φ_τ passes through the body, and, depending on its refractive index, changes its direction, while a third part Φ_α is absorbed by the body.

The total flux Φ equals the sum of these fluxes:

$$\Phi = \Phi_\rho + \Phi_\tau + \Phi_\alpha \qquad (52)$$

On dividing both sides of eq.(52) by Φ, we obtain

$$1 = \frac{\Phi_\rho}{\Phi} + \frac{\Phi_\tau}{\Phi} + \frac{\Phi_\alpha}{\Phi} \qquad (53)$$

Let us denote the ratios:

$$\frac{\Phi_\rho}{\Phi} = \rho; \quad \frac{\Phi_\tau}{\Phi} = \tau; \quad \frac{\Phi_\alpha}{\Phi} = \alpha \qquad (54)$$

The ratio of the reflected flux to the incident flux is called the coefficient of reflection ρ.

The ratio of the flux passing through the body to the incident flux is called the coefficient of transmission τ.

The ratio of the absorbed flux to the incident flux is called the coefficient of absorption α.

It follows from eq.(53) that the following relation exists between ρ, τ, and α:

$$\rho + \tau + \alpha = 1 \qquad (55)$$

According to the state of the surface, the reflection of the incident flux may be of the mirror type (angle of incidence equal to angle of reflection) or of the diffuse type (scattered).

Mirror reflection is given by polished surfaces, and the value of the coef-

ficient of reflection ρ depends on the degree of polish of the surface.

Table 8

Values of ρ, τ, and α for Certain Materials (Bibl.1)

Type of Material	Coefficients, %			Thickness of material, mm
	ρ	τ	α	
Transparent colorless glass	About 8	89-91	1-3	1-3
Matte glass (sand-blasted inside)	12-15	72-85	3-16	1.8-4.4
Thick opal glass	30-76	10-65	4-28	1.3-6.2
Opal glass of good light transmittance	40-50	45-55	4-6	1.5-2
Polished marble	50-61	3-6	27-47	8.1-9.3
Alabaster (gypsum)	43-53	33-47	11-16	-
Thin white parchment	40-50	35-55	10-15	-
Light paper	33-40	42-50	13-20	-
Dark paper	43-50	30-45	17-23	-
White silk	35	60	5	-
White paint	67-80	-	33-20	-
Black velvet	0.4	-	99.6	-
Black cloth	1.2	-	98.8	-

The coefficients of transmission and absorption depend in a complex manner on the chemical composition and structure of the substance. For liquid and gaseous bodies, the value of these factors also depends on the size and number of the individual particles, for example the molecules, mist or dust particles in the volume which is penetrated by the radiant flux. This question will be considered in more detail below with respect to the passage of infrared rays through the atmosphere.

Table 8 gives the values of ρ, τ, and α for a few materials.

CHAPTER III

THERMAL RADIATION AND ITS BASIC LAWS

Section 9. Thermal Radiation

The process of conversion of the thermal energy of a body into radiant energy is termed thermal radiation.

The thermal state of a body is characterized by its temperature, and therefore thermal radiation is sometimes called temperature radiation.

Two bodies of different temperatures transmitting heat to each other will, after a certain length of time, assume the same temperature, i.e., enter into thermal equilibrium.

If a heated body is placed within an envelope impervious to radiation, the walls of the envelope, absorbing the energy radiated by the body, will be heated, and will in turn commence to radiate energy which will be absorbed by the body. As a result of this heat exchange, the heated body and the surrounding envelope will be thermal equilibrium after a certain interval of time.

Section 10. The Absolute Black Body

A body that completely absorbs the incident radiant flux and possesses maximum power of radiation is called an ideal black body, and its radiation is termed black-body radiation.

In nature there are no bodies having total absorptive power. The most absorptive materials, lampblack, platinum black and bismuth black, absorb about 96-98% of the indicent radiant energy falling.

An ideal-black-body may, however, be artificially produced. An artificial body most closely approaching an ideal black body was first proposed in 1893 by the

famous Russian physicist V.A.Mikhel'son.

This body, whose diagram is shown in Fig.6, consists of a hollow sphere with narrow openings and a blackened inside surface, whose absorptive power is 90%. If a flux of radiant energy is directed through the opening of the sphere, 90% of the energy is absorbed when the ray strikes the inside wall, while the radiant flux reflected by it (10%) then strikes the wall; on a second reflection, the energy of this flux is reduced to 1%, and on the next reflection to 0.1%.

Fig.6 - Diagram of Absolute Black Body

If the radiant flux emerges from the aperture after a triple reflection, then the total absorptive power of such a body will be equal to 0.999, i.e., very close to unity.

The inside surface of such a body not only absorbs but, on heating to a certain temperature, also radiates like an ideal black body.

At present, a number of designs of radiators of the ideal black-body type have been developed, but all of them are based on the principle of the Mikhel'son hollow radiator.

Section 11. Radiating and Absorbing Powers of a Body

The radiating power of a body $e_{\lambda T}$ is the term given to the radiant energy of a definite wavelength λ radiated from 1 cm^2 of surface in 1 sec at a temperature T. Usually, $e_{\lambda T}$ is measured in kcal/m^2 hour, or in w/cm^2 (1 kcal/m^2 hr = 1.163 × × 10^{-4} w/cm^2).

The absorptive power of a body $a_{\lambda T}$ is a quantity indicating what part of the radiant energy incident on its surface, having the definite wavelength λ, is absorbed by it at a temperature T.

The absorptive power of an ideal black body is unity for any wavelength, since it completely absorbs all the flux incident on it. For all other bodies, the absorptive power is less than unity.

The ratio between the emissive power of a body $e_{\lambda T}$ and its absorptive power $a_{\lambda T}$ at a given temperature and wavelength is constant for all bodies; this constant is equal to the emissive power $E_{\lambda T}$ of an ideal black body:

$$\frac{e_{\lambda T}}{a_{\lambda T}} = \text{const} = E_{\lambda T} \qquad (56)$$

It follows from this equation that the emissive power $E_{\lambda T}$ of an ideal black body is greater than the emissive power $e_{\lambda T}$ of any other thermal radiator.

In practice, the values of the emissive power are often replaced by the values of the spectral energetic brightness

$$b_{\lambda T} = \frac{dB_\lambda}{d\lambda} \qquad (57)$$

and of the spectral energetic luminosity

$$r_{\lambda T} = \frac{dR_\lambda}{d\lambda} \qquad (58)$$

where dB_λ and dR_λ = the values of the energetic brightness and luminosity, respectively;

$d\lambda$ = wavelength of the monochromatic radiation.

The total radiation of unit surface of an ideal black body in unit solid angle is defined by the expression

$$R = \int_{\lambda=0}^{\lambda=\infty} E_{\lambda T}\, d\lambda \qquad (59)$$

To determine the emissive power of bodies, the physicist Stefan proposed the expression

$$E_{\lambda T} = \sigma T^4 \qquad (60)$$

where σ = radiation constant;

T = absolute temperature.

The radiation constant σ, determined experimentally, is equal to 5.71 × × 10^{-12} w/cm^2 deg^4, or 4.96 × 10^{-8} kcal/m^2 hr deg^4.

Stefan proposed that the formula found by him should be used for all bodies.

The Russian scientist, Academician B.B.Golitsyn (1893), however, proved theoretically that this was true only for an ideal black body.

In technical calculations, eq.(60) is usually represented in the form

$$E_{\lambda T} = C\left(\frac{T}{100}\right)^4 \qquad (61)$$

where C is the coefficient of radiation of an ideal black body.

The value of C is 4.96 kcal/m^2 hr deg^4, or 5.71×10^{-4} w/cm^2 deg^4.

When the ambient temperature T_o is taken into account, eq.(61) assumes the form

$$E_{\lambda T} = C\left[\left(\frac{T}{100}\right)^4 - \left(\frac{T_o}{100}\right)^4\right] \qquad (62)$$

The energetic brightness B_T of the flux radiated in a given direction, at a black-body temperature equal to T, can be determined by the formula

$$B_T = \frac{\sigma}{\pi} T^4 \text{ w/ster cm}^2 \qquad (63)$$

The total power emitted by an area S of the surface of an ideal black body in all directions is proportional to the fourth power of its absolute temperature:

$$W = S\sigma T^4 \text{ w/cm}^2 \qquad (64)$$

The emissive power within the solid angle ω, whose axis makes the angle α with the normal to the radiating surface, is determined by the formula

$$W = S\frac{\sigma}{\pi} T^4 \cos\alpha\, d\omega \qquad (65)$$

Section 12. Relation between Radiation Energy, Wavelength, and Temperature

The noted Russian physicist V.A.Mikhel'son was the first to study the dependence of the emissivity on the wavelength and temperature. He also made the first attempt to determine the form of this function theoretically.

In the general form, the law of energy distribution in the spectrum of an ideal black body is determined by the function

$$E_{\lambda T} = f(\lambda, T)$$

The equation proposed by Mikhel'son had the form

$$E_{\lambda T} = CT^{\frac{3}{2}}\lambda^{-6} e^{-\frac{c}{\lambda^2 T}} \qquad (66)$$

From this equation, more particularly, it followed that

$$\lambda_{max}^2 T = \text{const} \qquad (67)$$

and

$$E_{max} T^{-4.5} = \text{const} \qquad (68)$$

Later studies made by Wien on the basis of the Second Law of Thermodynamics and the law of light pressure, discovered by the outstanding Russian physicist P.N.Lebedev, allowed a more exact determination of the dependence of radiation energy on λ and T:

$$E_{\lambda T} = \frac{c^2}{\lambda^5} f\left(\frac{\lambda T}{c}\right) \qquad (69)$$

(where c = velocity of light), and yielded the equation of spectral energy distribution as a function of the wavelength λ:

$$E_{\lambda T} = C_1 \lambda^{-5} e^{-\frac{C_2}{\lambda T}} \qquad (70)$$

where $C_1 = 3.7 \times 10^{-12}$ w cm^2,

$C_2 = 1.432$ cm deg.

The same equation as a function of the radiation frequency ν has the form:

$$E_{\nu T} = C_1 \nu^3 e^{-\frac{C_2 \nu}{T}} \qquad (71)$$

It follows from eq.(70) that, at a given temperature T, the radiation reaches its maximum E_{max} at a definite wavelength λ_{max}. The relation between the temperature of the radiating body T and the wavelength λ_{max} has the form

$$\lambda_{max} T = \text{const} \tag{72}$$

The numerical value of the constant in eq.(72) is 2892 μ deg, whence

$$\lambda_{max} = \frac{2892}{T} \tag{73}$$

where λ_{max} is expressed in microns.

It follows from eq.(73) that, at increasing temperature of an ideal black body, the maximum of its radiation curve is shifted toward the shorter waves.

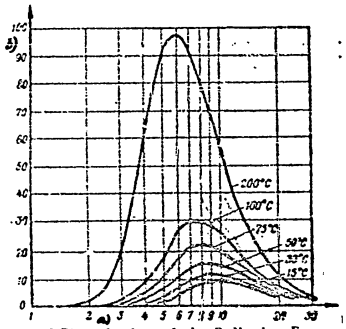

Fig.7 - Curves of Distribution of the Radiation Energy of an Ideal Black Body at Various Temperatures
a) Wavelength, μ; b) Emissivity $E_{\lambda T}$, w/cm³

Using eq.(73), it is possible to determine the wavelength corresponding to maximum radiation of energy in the spectrum for a given black-body temperature, or the black-body temperature itself, if the wavelength corresponding to maximum radiation is known.

Figure 7 gives distribution curves for the radiation energy of an ideal black body at various temperatures. The values of the emissivity in w/cm³ are plotted along the ordinate, and the wavelengths in microns along the abscissa.

The curves indicate that, for an ideal black body at 15°C, the maximum radiation corresponds approximately to λ = 10 μ. At a wavelength of 4μ the emissivity drops to 0.5 w/cm³, i.e., to about 5% of its maximum value. With increasing temperature, the maximum shifts toward shorter wavelengths, and its absolute value rapidly increases.

On the basis of the regularities derived earlier, showing that the emissive power of an ideal black body is proportional to the fourth power of its absolute temperature, and that the radiation maximum shifts toward shorter wavelengths with increasing temperature, Wien proposed the following equation for determining the value of the maximum radiation energy:

$$E_{max} = \beta T^5 \tag{74}$$

where β = constant equal to 4.16×10^{-12} w/cm³ deg⁵. Consequently,

$$E_{max} = 4.16 \times 10^{-12} T^5 \text{ w/cm}^3 \text{ deg}^5 \tag{75}$$

It will be clear from eq.(74) that the value of the radiation maximum in the black-body spectrum increases proportionally to the fifth power of the temperature.

The following formula is convenient for determining the emissivity in the long-wave region of the spectrum

$$E_{\lambda T} = CKT\lambda^{-5} \tag{76}$$

where $CK = 0.412 \times 10^{12}$ w cm/deg.

Section 13. The Quantum Law of Radiation

The equations of energy distribution in the black-body spectrum [eqs.(70) and (76)] were derived on the basis of classical dynamics under the assumption that any radiation of the wavelength λ depends only on the velocity of motion of the molecules, and that these velocities are distributed according to Maxwell's law. As

shown by later investigations, these equations are a limiting expression for some unknown general law, and are true only for certain regions of wavelengths (for which the Maxwell equations were calculated) for certain temperatures.

To find the general energy distribution equation, entirely different conditions must be taken as basis.

These conditions were formulated by Planck, who started from the premise that radiation is a consequence of the oscillations of linear atomic vibrators, which excite electromagnetic waves, where such a vibrator does not emit energy continuously but in discrete portions, or "quanta", and where the energy of a quantum absorbed or emitted by a vibrator depending on the wavelength (or frequency) of the radiation.

The energy of a quantum is determined by the formula

$$\epsilon = h\nu \tag{77}$$

where $h = 6.62 \times 10^{-27}$ erg sec, the calculated universal constant.

On the basis of these quantum conditions, Planck deduced a new energy - distribution equation for the radiation of an ideal black body:

$$E_{\lambda T} = \frac{2\pi c^2 h}{\lambda^5} \cdot \frac{1}{e^{\frac{ch}{\lambda KT}}} \tag{78}$$

where c = velocity of light;

K = the Boltzmann constant, equal to 1.38×10^{-16} erg/deg.

On introducing the notation

$$C_1 = 2\pi hc^2 \text{ and } C_2 = \frac{hc}{K}$$

in eq.(78), the equation may be obtained in a simpler form:

$$E_{\lambda T} = C_1 \lambda^{-5} (e^{\frac{C_2}{\lambda T}} - 1)^{-1} \tag{79}$$

The numerical values of the constants are: $C_1 = 3.74 \times 10^{-12}$ w cm^2, and $C_2 = 1.4384$ cm deg.

Equation (79) expresses the quantum law of radiation.

To pass from wavelength to frequency, or vice versa, the following formula is used:

$$E_{\nu T} = \frac{c}{\nu^2} E_{\lambda T} \tag{80}$$

where c = velocity of light.

Hence eq.(79) takes the following form, as a function of radiation wavelength:

$$E_{\nu T} = C_3 \nu^3 \frac{1}{e^{\frac{C_4 \nu}{T}} - 1} \tag{81}$$

where

$$C_3 = \frac{2h}{c^2} \text{ while } C_4 = \frac{h}{K}$$

Equation (79) not only characterizes the energy distribution over the spectrum, but also permits a determination of the total quantity of energy (the radiant flux Φ) radiated at a given temperature:

$$\Phi = \int_{\lambda=0}^{\lambda=\infty} E_{\lambda T} d\lambda = C_1 \int_{\lambda=0}^{\lambda=\infty} \lambda^{-5} (e^{\frac{C_2}{\lambda T}} - 1)^{-1} d\lambda \tag{82}$$

Experimental verification of eqs.(79) and (82) confirmed their validity for all wavelengths and temperatures. Consequently, they express the general law of energy distribution in the spectrum of an ideal black body.

Section 14. Coefficient of Radiation Efficiency of an Ideal Black Body

The radiation energy of an ideal black body, like that of any other radiator, is received or registered by various receptors, such as the human eye, a thermocouple, etc. To determine the efficiency of the action of energy radiated in a certain part of the spectrum on one receptor or another, the coefficient of efficiency (k.p.d.) of the radiator is used.

Figure 8 gives the spectral distribution curve of the radiation energy of an

ideal black body.

The emissivity of an ideal black body, in relative units, is plotted on the ordinate and the wavelength in microns on the abcissa. By using this curve, the radiation efficiency can be determined.

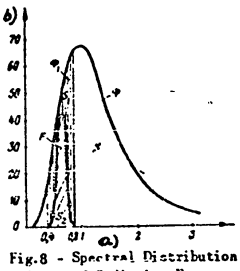

Fig.8 - Spectral Distribution Curve of Radiation Energy of an Ideal Black Body
a) Wavelength, μ; b) Emissivity E_T in relative units

The area S, bounded by the upper curve, represents the total radiated power, i.e., the total radiant flux Φ; the area S_1 (vertically hatched), the power radiated in the visible part of the spectrum Φ_1, the area S_2 (obliquely hatched), the power perceptible to the eye.

The ratio between the power radiated in the visible part of the spectrum (or flux Φ_1) to the total power radiated (or total radiant flux Φ) is called the energetic coefficient of radiation efficiency:

$$\eta_e = \frac{\Phi_1}{\Phi} = \frac{S_1}{S} \qquad (83)$$

To determine the power perceptible to the eye, or the luminous flux F, the total radiant flux Φ must be multiplied by the integral value of the relative visibility factor K_λ for the entire visible region of the spectrum:

$$F = \Phi \int_{\lambda=0.4}^{\lambda=0.8} K_\lambda \, d\lambda \qquad (84)$$

The ratio of the power perceptible to the eye, or the luminous flux F, to the total radiant flux Φ, is called the coefficient of efficiency:

$$\eta_c = \frac{F}{\Phi} = \frac{S_2}{S} \qquad (85)$$

The ratio of the power perceptible to the eye, or the luminous flux F, to the power radiated in the visible part of the spectrum, or the flux Φ_1, is the efficiency of visible radiation:

$$\eta_B = \frac{F}{\Phi_1} = \frac{S_2}{S_1} \qquad (86)$$

These efficiencies are connected by the relation:

$$\eta_c = \eta_e \eta_B \qquad (87)$$

Table 9 gives the values of η_e and η_c for an ideal black body at temperatures from 3000 to 8000° absolute.

Table 9

Values of Efficiencies η_e and η_c for an Ideal Black Body at Various Temperatures

T °K	η_e %	η_c %
3000	8	3
4000	22	8.5
5000	32	12.6
6000	38	14.4
6500	39	14.5
7000	40	14.4
8000	38	13.5

It will be clear from the Table that an ideal black body has its maximum luminous efficiency at T = 6500°K, where it reaches 14.5%. This is the maximum luminous efficiency of temperature radiators. For ordinary incandescent lamps, the luminous efficiency is only about 3%.

Section 15. Radiation of Non-Black Bodies

All the above laws are valid for an ideal radiator, the black body.

Since an ideal black body does not exist in nature, all real bodies capable of radiating energy may be grouped under the common designation of non-black bodies, whose radiation depends on their physical properties and, primarily, on their absorptive power.

Non-black bodies are divided into two groups, bodies with so-called gray radiation, and bodies with selective radiation.

Gray radiation is the term applied to temperature radiation with a spectral energy distribution curve of the same form as that of a black body at the same temperature, but with an intensity of radiation, for any wavelength and for any temperature, which is lower than in a black body; this is determined by the absorptive power of the real body. All laws of black radiation apply to gray radiation, provided these radiations differ only by a constant factor, the absorption coefficient, which is independent of the wavelength.

By analogy to the black-body equations, we may write, for gray bodies:

$$E = C_0 \left(\frac{T}{100} \right)^4$$

where C_0 = emissivity factor of the gray body. C_0 is always less than C, and depends on the temperature.

Comparing the radiation energy of a gray body with that of a black body at the same temperature, we find a new quantity, termed the relative emissivity, or degree of blackness of a body:

$$\varepsilon = \frac{C_0}{C}$$

Table 10 gives the values of ε for various materials.

Knowing ε, the radiation energy of a gray body may be calculated by the equation:

$$E = \varepsilon C \left(\frac{T}{100} \right)^4 \qquad (88)$$

Table 10

Relative Emissivity, or Degree of Blackness ε, of Total Normal Radiation for Various Materials (Bibl.2)

Type of Material	t °C	ε
Polished aluminum	225-575	0.039-0.057
Unpolished aluminum	26	0.055
Polished iron	425-1020	0.144-0.377
Iron, freshly abraded with emery	20	0.242
Oxidized iron	100	0.736
Oxidized iron, smooth	125-525	0.78-0.82
Cast iron, unmachined	925-1115	0.87-0.95
Polished steel casting	770-1040	0.52-0.56
Sheet steel, ground surface	940-1100	0.55-0.61
Iron, machined	830-990	0.60-0.70
Iron oxide	500-1200	0.85-0.95
Gold, carefully polished	225-635	0.018-0.035
Rolled brass plate, with natural surface	22	0.06
Rolled brass plate, abraded with coarse emery	22	0.20
Brass plate, dull	50-350	0.22
Copper, carefully polished, electrolytic	80-115	0.018-0.023
Copper, commercial, polished to brightness; but not mirror-finished	22	0.072
Copper oxide	500-1100	0.66-0.54
Molten copper	1075-1275	0.16-0.13
Molybdenum filament	725-2600	0.096-0.292
Nickel, technical, clean and polished	225-375	0.07-0.087
Nickel-plated pickled iron, unpolished	20	0.11
Nickel wire	185-1000	0.096-0.186
Nickel oxide	650-1255	0.59-0.86
Nichrome	125-1034	0.64-0.76
Tin, bright tinned sheet iron	25	0.043-0.064
Platinum, pure, polished sheet	225-625	0.054-0.104
Platinum strip	925-1115	0.12-0.17
Platinum filament	25-1230	0.036-0.192
Platinum wire	225-1375	0.073-0.182
Mercury, very pure	0-100	0.09-0.12
Lead, gray, oxidized	25	0.281
Silver, polished, pure	225-625	0.0198-0.0324
Chromium	100-1000	0.08-0.26
Zinc, commercial (99.1%), polished	225-325	0.045-0.053
Galvanized sheet iron, bright	28	0.228
Galvanized sheet iron, gray, oxidized	24	0.276
Asbestos cardboard	24	0.96
Asbestos paper	40-370	0.93-0.945
Thin paper bonded to metal plate	19	0.924
Water	0-100	0.95-0.963
Gypsum	20	0.903
Oak, planed	20	0.895
Fused quartz, rough	20	0.932

STAT

Type of Material	t °C	ε
Red brick, rough	20	0.93
Grog brick, glazed	1100	0.75
Refractory brick		0.8-0.9
White enamel varnish on rough iron plate	23	0.906
Black glossy varnish sprayed on iron plate	25	0.875
Black varnish, dull	40-95	0.96-0.98
Black glossy shellac on tinned iron	21	0.821
Black shellac, dull	75-145	0.91
Oil paints of various colors	100	0.92-0.96
Aluminum paint, after heating to 325°C	150-315	0.35
Grayish marble, polished	22	0.931
Smooth glass	22	0.937
Soot, from candle	95-270	0.952
Soot, with waterglass	100-125	0.959-0.947
Lampblack, 0.075 mm and larger	40-370	0.945
Tar paper	21	0.910
Washed coal (0.9% ash)	125-625	0.81-0.79
Carbon filament	1040-1405	0.526
Glazed porcelain	22	0.924
Rough lime stucco	10-80	0.91

Radiation in which energy is emitted within definite narrow portions or bands of the spectrum is called selective radiation.

The radiation of selective bodies, which include almost all metals, differs from black-body radiation in the character of the energy distribution over the spectrum. The radiation energy of selective bodies may be approximately determined by eq.(56), but it must be borne in mind that the absorption factor of a selective body $a_{\lambda T}$ is not the same for the various portions of the spectrum, but depends on the wavelength λ and the temperature T.

Figure 9 shows the characteristic form of the curves of spectral distribution of the energy of black-body, gray-body, and selective radiation. It will be seen from the diagram that the curve of gray-body radiation lies below the curve of radiation of a black body, and that their slopes are similar. The curve of selective radiation has a number of maxima and minima.

The ratio of the energy radiated by a surface element of a given body (spectral energetic brightness $b_{\lambda T}$) to the energy radiated by an equal surface element of a black body (spectral energetic brightness $B_{\lambda T}$) at the same temperature, wavelength,

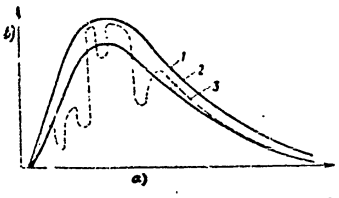

Fig.9 - Curves of Spectral Distribution of Energy of Black-Body (1), Gray-Body (2), and Selective (3) Radiation
a) Wavelength; b) Intensity of radiation

time interval, is called the monochromatic emissivity of the body and is denoted by the symbol $\varepsilon_{\lambda T}$:

$$\varepsilon_{\lambda T} = \frac{b_{\lambda T}}{B_{\lambda T}}$$

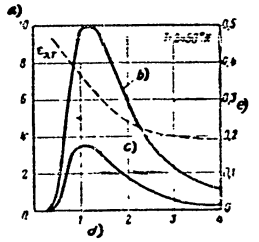

Fig.10 - Spectral Energetic Brightness of Tungsten and of a Black Body
a) Energetic spectral brightness in relative units; b) Black body; c) Tungsten; d) Wavelength, μ; e) Monochromatic emissivity of tungsten

In Fig.10, the broken line shows the curve $\varepsilon_{\lambda T}$ for tungsten at T = 2450°K. The values of $\varepsilon_{\lambda T}$ are calculated by dividing the ordinate of the curve of spectral energetic brightness of tungsten by the corresponding ordinates of the curve of brightness of a black body (solid lines). The gradual decrease in the value of $\varepsilon_{\lambda T}$ with increasing wavelength, which is characteristic for all metals, indicates that the maximum of radiation of metals is shifted toward shorter wavelengths by comparison with the maxima of black-body radiation at the same temperature.

We may also determine the total emissivity ε_T, which represents the ratio of

the energetic brightness of the body b_T at a given temperature T to the energetic brightness B_T of a black body:

$$\varepsilon_T = \frac{b_T}{B_T} \qquad (89)$$

Graphically, this will be represented by the ratio of the area bounded by the emissivity curve of tungsten to the area bounded by the emissivity curve of a black body.

The monochromatic emissivity curves of tungsten in the infrared region of the spectrum, constructed from measurement data (solid lines), are given in Fig. 11.

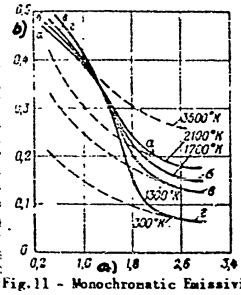

Fig. 11 - Monochromatic Emissivity of Tungsten in the Infrared Region of the Spectrum
a) Wavelength, μ; b) Monochromatic emissivity of tungsten

As indicated in the diagram, within the limits of the visible region of the spectrum and for the short infrared rays, the values of $\varepsilon_{\lambda T}$ decrease with increasing temperature, while in the region of the longer infrared rays, they increase. The overwhelming majority of metals possess this peculiarity.

To determine the basic computational energetic values for non-black bodies, various formulas obtained on the basis of experimental data are used.

To determine the monochromatic emissivity of metals in the infrared part of the spectrum, the following formula has been proposed:

$$\varepsilon_{\lambda T} = 0.365\sqrt{\frac{\rho_e}{\lambda}} \qquad (90)$$

where ρ_e = resistivity of metal in ohm-cm at a temperature T;

λ = wavelength in cm.

Figure 11 gives the curves constructed for tungsten from the values of $\varepsilon_{\lambda T}$ calculated by eq. (90) (dashed lines).

Equation (90) gives results in agreement with the measurements at certain wavelengths, for example, at $\lambda > 2\mu$ for tungsten, at $\lambda > 14\mu$ for silver, etc. With sufficient accuracy, this can be used for determining $\varepsilon_{\lambda T}$ at wavelengths longer than 1μ. For wavelengths in the ultraviolet and visible regions of the spectrum, this formula is unsuitable, since the results of calculation differ from the measured values. This can apparently be explained by phenomena of resonance (absorption bands) in the ultraviolet and visible regions of the spectrum.

To determine the energetic luminosity of radiation of non-black bodies, the following empirical formula has been proposed:

$$R_T = \sigma' T^{\alpha} \qquad (91)$$

where σ' = a certain constant;

α = a quantity depending on the kind of metal used and on its temperature.

The values of σ' for some metals have been experimentally determined. Thus, for example, for platinum, $\sigma' = 3.56 \times 10^{-15}$, for tungsten, 1.51×10^{-15}, for nickel, 1.04×10^{-14}.

For tungsten, eq. (91) has the form

$$R_T = 1.51 \times 10^{-15} T^{4.9} \qquad (92)$$

Equation (92) gives correct results in the temperature range of 2000-3000°K, i.e., precisely at the temperatures corresponding to the working conditions of the filaments of incandescent lamps. To determine temperature at which the intensity of radiation of platinum and that of a black body are comparable, the approximate formula

$$T_{plat} = aT_{bb} \qquad (93)$$

may be used, where

$$a = \frac{2892}{2630} = 1.1$$

The total radiation of metals may be determined by the formula

$$E_{\lambda T} = \frac{\sigma}{\pi} T^4 (1 - e^{\alpha T}) \qquad (94)$$

where σ = a constant taken from eq.(60);

α = a constant depending on the kind of metal.

The values of the constant α for a few metals are given in Table 11.

Table 11

Value of α for Several Metals

Metal	$\alpha \cdot 10^4$
Cesium	1.08
Molybdenum	1.118
Gold	1.20
Platinum	1.25
Tantalum	1.31
Tungsten	1.47
Nickel	1.65

The absorption factor of pure metals in the region of short and medium infrared rays may be determined by the simplified formula

$$a_{\lambda T} = \frac{0.365}{j\lambda} \qquad (95)$$

where j = electric conductivity of the metal in $\frac{1}{\text{ohm-cm}}$.

To determine the maximum radiation of metals, the following formula is recommended:

$$E_{max} = \frac{0.365\sqrt{\rho C_1}}{(\lambda_{max} T)^{5.5}\left(e^{\frac{C_2}{\lambda T}} - 1\right)} T^{5.5} \qquad (96)$$

To determine the total radiation

$$\int_0^\infty E_{\lambda T} d\lambda = C_1 \cdot 8.156 \times 10^{-19} \sqrt{\rho\, T^{4.5}} \qquad (97)$$

Putting $\rho = \rho_o \frac{T}{273}$, which holds for most metals, we obtain:

for selective radiation in the region from λ to $\lambda + d\lambda$

$$E_\lambda = C_1 \cdot 0.0221 \sqrt{\rho_o T} \lambda^{-5.5} \left(e^{\frac{C_2}{\lambda T}}\right)^{-1} \qquad (98)$$

for maximum radiation

$$E_{max} = C_1 \cdot 1.334 \times 10^{-23} \sqrt{\rho_o T^6} \qquad (99)$$

For total radiation

$$\int_0^\infty E_\lambda d\lambda = C_1 \cdot 4.936 \times 10^{-20} \sqrt{\rho_o T^5} \qquad (100)$$

Equations (96)-(100) are true for wavelengths over 4 μ. Table 12, below, gives the emissivity factors of certain bodies.

Table 12

Values of the Emissivity Factors of Certain Bodies (Bibl.3)

Bodies	Kind of Surface	Temperature, °C	Radiation Factor	
			kcal/m² hr deg⁴	watt/cm² deg⁴
Lamphlack	Smooth	0-50	4.3	5.0×10^{-4}
Iron	Carefully polished	40-250	1.31	1.53×10^{-4}
Iron	Bright	30-100	1.60	1.85×10^{-4}
Iron	Dull, oxidized	20-360	4.32	5.02×10^{-4}
Cast iron	Rough, strongly oxidized	40-250	4.39	5.1×10^{-4}
Brass	Dull	50-350	1.05	1.22×10^{-4}
Ice	-	0	3.06	3.56×10^{-4}
Water	-	60	3.20	3.72×10^{-4}
Brick (red)	Rough	22	4.6	5.35×10^{-4}
Silicate brick	Rough	10000	4.0	4.65×10^{-4}
Same	Rough	1100	4.2	4.88×10^{-4}
Refractory brick	Rough	1000	3.5-3.7	$4.07\text{-}4.3 \times 10^{-4}$
Copper	Polished	50	0.53	0.62×10^{-4}
Copper	Dull rolled	50	3.10	3.60×10^{-4}
Copper	Rough	50	3.68	4.28×10^{-4}

We conclude this Chapter by stating the concepts of color temperature and

STAT

brightness temperature, which we will often meet in the sequel.

The color temperature T_c is the temperature of a black body with the same ratio of brightness between two given spectral regions as the given body at the temperature T. For all metals the color temperature T_c is higher than the true temperature of the body T.

The brightness temperature T_B is the temperature of a black body of the same visual monochromatic brightness for a given wavelength as the given radiator at temperature T.

The brightness temperature is always less than the true temperature of the body.

CHAPTER IV

SOURCES OF INFRARED RAYS

Section 16. Classification of Sources of Infrared Rays

The sources of radiation used today in various fields of infrared technology may be divided into three groups, according to the physical nature of the radiation.

The first group comprises sources of incandescent radiation in which the infrared radiation takes place as a result of the combustion of a fuel or the heating of a body to a definite temperature.

The second group consists of electroluminescent sources of radiation operating on the principle of electroluminescence, or luminescence due to the passage of an electric current through rarefied gas.

The third group comprises sources of radiation of combined type, making simultaneous use of incandescent radiation and luminescence.

The "mass radiator" of A.A.Glagoleva-Arkad'yeva occupies a special position. In its physical nature this radiator is a source of electromagnetic radiation in the transitional region between radio waves and infrared rays and cannot be classified in any of the three above groups.

Table 13 enumerates a few sources of infrared rays which are used in technology and scientific research, and are considered in the present Chapter.

Section 17. Requirements for a Source of Infrared Rays

The basic requirement for a source of infrared rays is high efficiency in the infrared region of the spectrum. An effective source of infrared rays is chosen on

STAT

the basis of the general laws of thermal radiation (cf. Chapter III), taking into account the spectral characteristics of the receptor to be used for the infrared rays.

Table 13

A Few Sources of Infrared Rays

Type of Source	Nature of Radiation	Radiator
Group I Sources of Temperature Radiation		
Electric incandescent lamps with pure-metal filaments	Thermal radiation	Filament of tungsten or other refractory metal, heated to incandescence by an electric current
Electric incandescent lamps with filaments of metal compounds	Same	Filament of carbide or other compound, heated to incandescence by an electric current
Lamps with special incandescent body	Thermal selective radiation	Plate of kaolin in plug form, heated to incandescence by an electric current
Incandescent-mantle lamp	Same	Silk mantle impregnated with thorium oxide, heated to incandescence by the flame of a gas or a liquid fuel
Group II Electroluminescence Sources of Radiation		
Helium lamps	Luminescence	Positive column glowing under silent discharge in an inert gas
Cesium lamps	Same	Positive column glowing under arc discharge in cesium vapor
Mercury-arc lamps	Same	Positive column glowing under arc discharge in mercury vapor
Group III Combined Sources of Radiation		
Simple electric arc	Thermal radiation and luminescence	Electrodes heated to incandescence by electric current, incandescent gases, and luminescent positive column of an arc discharge
High-intensity electric arc	Same	Same
Arc lamp with tungsten electrodes (point lamp)	Same	Same
Extreme-pressure mercury-tungsten lamp	Same	Tungsten spiral heated to incandescence by electric current and luminescent positive column of arc discharge in mercury vapor

In addition to high efficiency, sources of infrared rays must also satisfy a number of other requirements, namely:

- they must be suitable for use with optical systems;
- they must not require special handling or observation;
- they must have a sufficiently long life and stability in operation;
- they must have minimum possible weight and over-all size;
- they must allow DC and AC power supply under emergency operation and must permit convenient adjustment of that operation.

Table 14 gives the energetic characteristics of a few sources of infrared radiation, for illustrative purposes.

Of the artificial sources of radiation in the Table, only the incandescent lamp, electric arc, mercury and helium lamps are used in technology. The incandescent mantle and the plug lamp, although they are sources of infrared rays, produce it in such an insignificant amount that they are used primarily only in the laboratory.

Section 18. Incandescent Lamps

The first incandescent electric lamp used for practical purposes was developed in 1873 by the prominent Russian electrical engineer A.N.Lodygin. This lamp was the prototype of all the succeeding designs of electric lamps. Incandescent

STAT

electric lamps are successfully used as sources of infrared radiation.

The source of radiant energy in the incandescent electric lamp is a filament of

Table 14

Characteristics of a Few Sources of Infrared Radiation (Bibl.4)

Source of Radiation	Total Radiation Energy, watt/cm²	Energy of Infrared Rays in Region 0.8-12 μ, watt/cm²	Energy in Different Parts of Region 0.8-12 μ, in %		
			0.8-1.4 μ	1.4-2.4 μ	2.4-12 μ
Mercury lamp	0.026	0.010	39	21	-
Tungsten filament incandescent lamp (gas-filled)	0.0125	0.007	3.2	20.5	51.o
Electric arc	0.034	0.024	12.8	54	26
Incandescent mantle	0.001	0.00077	5	63	20
Plug lamp	0.0007	0.0005	50	20	-
Helium lamp	0.021	-	≈ 100	-	-

a pure refractory metal or of refractory metal compound, a class including the carbides, borides, and nitrides. Table 15 gives data on the melting points of these materials. As indicated in this Table, the number of refractory pure metals and refractory compounds used for making incandescence filaments is relatively small.

The main characteristics for which a material for the incandescent filaments of a lamp is selected are:

high melting point;

minimum rate of vaporization of the material, which determines the life of the filament;

ease of machining and strength;

spectral characteristic of radiation, as required for the lamp.

Of the pure metals, tungsten best satisfies these requirements and therefore is the principal material used for incandescent filaments of electric bulbs. Other refractory metals, such as tantalum, osmium, iridium, platinum, and zirocaium, have not found widespread use.

Of the refractory compounds, tantalum carbide is most suitable for incandescent filaments and has a number of advantages over tungsten. Its working temperature is

Table 15

Melting Points of Refractory Metals and Compounds

Metals		Carbides and Mixtures		Nitrides		Borides	
Material	T °K	Material	T °K	Material	T °K	Material	T °K
Carbon	3773	4TaC + HfC	4215	TaC + TaN	3645	HfB	3335
Tungsten	3663	4TaC + ZrC	4205	HfN	3580	ZrB	3065
Rhenium	3440	HfC	4160	TiC + TiN	3505	[illegible]	3195
Tantalum	3303	TaC	4150	TaN	3360		
Molybdenum	2893	ZrC	3805	ZrN	3255		
Osmium	2773	NbC	3770	TiN	3220		
Iridium	2622	TiC	3410	BN	3000		
Zirconium	2300	WC	3140				
Platinum	2044	W_2C	3130				
Nichrome	1823	MoC	2965				
Iron	1783	Mo_2C	2960				
Nickel	1723	VaC	2830				
		ScC	2650				
		SiC	2540				

400-500°K higher than that of tungsten, which improves all the illumination parameters of the lamp. The rate of vaporization of tantalum carbide is about 30% lower than that of tungsten, and the total radiation is about 30% higher, which corresponds to an increase in brightness of about 33% as compared with tungsten.

An obstacle to the wide use of tantalum carbide filaments is their low mechanical strength.

Incandescent-lamp filaments are usually made in the form of a cylindrical coil bent into circular shape and placed in a plane perpendicular to the axis of the lamp (for a short filament), or in zigzag form (for longer filaments).

Gas tubes have relatively high thermal losses. One of the methods of reducing these losses is shortening the coil and increasing its diameter, but this is possible only to a certain degree, since the strength of a filament decreases with in-

STAT

creasing diameter. A solution of the problem has been to design filaments in the form of a double spiral, or "bispiral" (Fig.12).

Lamps with a bispiral filament have a higher luminous efficiency than lamps with only a single spiral filament. The increase in luminous efficiency, amounting to 8-20%, depending on the type of lamp, is explained by the reduction in the heat losses due to the modified form of the filament. The greatest advantage in using a bispiral filament is obtained for low-power bulbs at 220 volts, which have the highest heat losses.

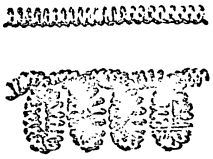

Fig.12 - Double Spiral Filament ("Bispiral")

In motion-picture projection, searchlight, and other special bulbs and lamps, incandescent bodies of maximum brightness and minimum size of luminous surface are used. A filament stretched spirally on a spherical or ellipsoidal surface, or a sphere or ellipsoid of compressed powder material, constitute typical examples of such incandescent bodies.

Vacuum or gas-filled incandescent lamps with tungsten filaments radiate most of their radiant energy in the region of short-wave infrared rays (cf.Table 14).

For example, a vacuum incandescent lamp, at a tungsten filament temperature of T = 2500°K, has its maximum radiation in the region λ = 1.15 μ, and a gas-filled lamp, at a filament temperature of T = 3000°K, in the region λ = 0.96 μ.

If the total energy radiated by a vacuum lamp is taken as 100%, then only 7-12% of the radiant energy is contributed by the energetic radiation in the visible portion of the spectrum, and the energy perceptible by the eye amounts to only about 3%. The remainder of the energy, except for small losses in the holders, is radiated into space, mainly in the form of infrared rays.

The properties of tungsten incandescent lamps and the simplicity of their manufacture, permit their use as sources of infrared rays.

Table 16 gives an idea of the energetic balance of a vacuum incandescent lamp and of lamps filled with various gases.

One of the main drawbacks of incandescent lamps, as in other temperature radiators, is the very low selectivity of their radiation, requiring the use of special

Table 16

Distribution of Radiation Energy (in percent) in Various Incandescent Lamps (Bibl.5)

Type of Radiation	Vacuum Lamp	Argon-Filled Lamp	Argon-Filled "Bispiral" Lamp	Krypton-Xenon Filled Lamp
Visible radiation	7	10	12	13
Invisible radiation	86	68	74	76
Loss in holders	7	3	2	2
Losses through gas	0	19	12	9

filters to cut out the required portion of the infrared spectrum.

Section 19. Basic Parameters of Incandescent Electric Bulb

The incandescent electric bulb is characterized by the following illumination and energetic parameters: filament temperature, brightness, luminous flux, luminous efficiency, power consumed, and working voltage. The filament temperature is the main characteristic determining all the illumination-engineering and energetic parameters of the lamp.

The brightness of radiation is determined by the working filament temperature: the higher the temperature, the greater the brightness.

Table 17 gives data showing the relation of brightness and temperature. The brightness increases sharply at a relatively small increase in temperature in the working region of 2500-3000°K.

One of the main parameters characterizing the operation of a bulb is the luminous efficiency, defined as the ratio of the luminous flux to the total power radiated, and measured in lumens per watt (lm/w).

The luminous efficiency characterizes the economy of the lamp or bulb: the greater the light flux radiated by a lamp per watt of power input, the more economical the bulb will be.

STAT

creasing diameter. A solution of the problem has been to design filaments in the form of a double spiral, or "bispiral" (Fig.12).

Lamps with a bispiral filament have a higher luminous efficiency than lamps with only a single spiral filament. The increase in luminous efficiency, amounting to 8-20%, depending on the type of lamp, is explained by the reduction in the heat losses due to the modified form of the filament. The greatest advantage in using a bispiral filament is obtained for low-power bulbs at 220 volts, which have the highest heat losses.

Fig.12 - Double Spiral Filament ("Bispiral")

In motion-picture projection, searchlight, and other special bulbs and lamps, incandescent bodies of maximum brightness and minimum size of luminous surface are used. A filament stretched spirally on a spherical or ellipsoidal surface, or a sphere or ellipsoid of compressed powder material, constitute typical examples of such incandescent bodies.

Vacuum or gas-filled incandescent lamps with tungsten filaments radiate most of their radiant energy in the region of short-wave infrared rays (cf.Table 14).

For example, a vacuum incandescent lamp, at a tungsten filament temperature of T = 2500°K, has its maximum radiation in the region λ = 1.15 μ, and a gas-filled lamp, at a filament temperature of T = 3000°K, in the region λ = 0.96 μ.

If the total energy radiated by a vacuum lamp is taken as 100%, then only 7-12% of the radiant energy is contributed by the energetic radiation in the visible portion of the spectrum, and the energy perceptible to the eye amounts to only about 3%. The remainder of the energy, except for small losses in the holders, is radiated into space, mainly in the form of infrared rays.

The properties of tungsten incandescent lamps and the simplicity of their manufacture, permit their use as sources of infrared rays.

Table 16 gives an idea of the energetic balance of a vacuum incandescent lamp and of lamps filled with various gases.

One of the main drawbacks of incandescent lamps, as in other temperature radiators, is the very low selectivity of their radiation, requiring the use of special

Table 16

Distribution of Radiation Energy (in percent) in Various Incandescent Lamps (Bibl.5)

Type of Radiation	Vacuum Lamp	Argon-Filled Lamp	Argon-Filled "Bispiral" Lamp	Krypton-Xenon Filled Lamp
Visible radiation	7	10	12	13
Invisible radiation	86	68	74	76
Loss in holders	7	3	2	2
Losses through gas	0	19	12	9

filters to cut out the required portion of the infrared spectrum.

Section 19. Basic Parameters of Incandescent Electric Bulb

The incandescent electric bulb is characterized by the following illumination and energetic parameters: filament temperature, brightness, luminous flux, luminous efficiency, power consumed, and working voltage. The filament temperature is the main characteristic determining all the illumination-engineering and energetic parameters of the lamp.

The brightness of radiation is determined by the working filament temperature: the higher the temperature, the greater the brightness.

Table 17 gives data showing the relation of brightness and temperature. The brightness increases sharply at a relatively small increase in temperature in the working region of 2500-3000°K.

One of the main parameters characterizing the operation of a bulb is the luminous efficiency, defined as the ratio of the luminous flux to the total power radiated, and measured in lumens per watt (lm/w).

The luminous efficiency characterizes the economy of the lamp or bulb: the greater the light flux radiated by a lamp per watt of power input, the more economical the bulb will be.

STAT

The values of the luminous efficiency of vacuum and gas-filled lamps can be determined from the curves in Fig. 13.

When a lamp burns, the tungsten filament is gradually vaporized, and the walls of the bulb are covered with a dark film, which attenuates the luminous flux radiated by the incandescent body. To reduce this harmful phenomenon, all modern incandescent electric bulbs (from 60 watts up) are filled with an inert gas (usually a mixture of argon and nitrogen) which helps to reduce filament vaporization.

Table 17

Relation between Temperature and Brightness of Filament

Temperature of Filament °K	Brightness, Stilb
1000	0.000126
2000	20.7
2500	246
3000	1326
3500	4540
3655	6131

As stated above, an increase in temperature leads to an increase in the energetic efficiency of a radiation source. Since, in gas-filled lamps the working temperature of the filament can be increased without shortening its life, the advantage of charging a bulb with gas becomes evident.

However, this is true only for bulbs of medium and high amperage, which, as a rule, have a relatively heavy incandescent filament. In low-amperage bulbs, with a fine incandescent filament, the temperature cannot be significantly increased, since this would accelerate the vaporization of the filament. The greater the diameter of the filament, the higher the temperature it can withstand.

Consequently, for lamps at the same feed voltage, the luminous efficiency and filament temperature are higher in the higher-amperage lamps. The variation of the parameters of incandescent lamps with applied voltage is shown by the curves in Fig. 14.

Section 20. Features of the Design of Incandescent Lamps for Searchlights

The principal differences between searchlight lamps and ordinary illuminating lamps lie in the form of the incandescent body and the form and dimensions of the bulb.

The selection of the type of lamp is determined by the dimensions of the lens system of the searchlight and by its purpose.

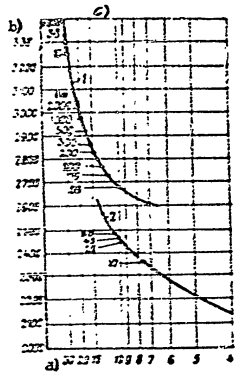

Fig. 13 - Relation of Luminous Efficiency and Temperature:
1- For gas-filled lamps with tungsten filament; 2- For vacuum lamps with tungsten filament
a) Luminous efficiency, lm/w;
b) Temperature, °K

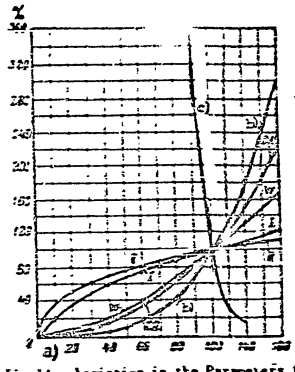

Fig. 14 - Variation in the Parameters (in %) of Incandescent Lamps as a Function of Voltage Input
F- Luminous flux; C.O.- Luminous efficiency; W- Power; I- Current; R- Resistance
a) Applied voltage, volts; b) F;
c) Duration of burning

Figure 15 shows characteristics modern searchlight lamps. By filament form and bulb shape, such lamps may be roughly classified into four groups.

The lamps of the first group (fig. 15,a) have a cylindrical spiral filament of small diameter but relatively great length. The axis of the spiral is perpendicular to the axis of the lamp, and the shape of the bulb is usually spherical. This posi-

tion of the filament allows a small angle of diffusion in the vertical plane and a large angle in the horizontal plane to be obtained from such lamp in a searchlight.

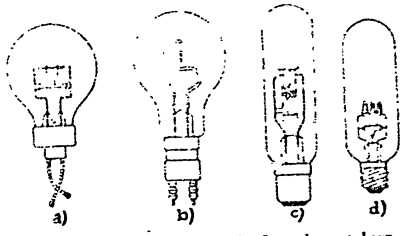

Fig.15 - Types of Searchlight Incandescent Lamp.

In lamps of the second group (Fig.15,b) the incandescent filament is the same as in the lamps in the first group but is installed along the axis of the lamp; the shape of the bulb is spherical. In using lamps with such a filament, the utilization factor of the lens system of the searchlight is increased.

To increase the efficiency of certain projector lamps, the front surface of the spherical bulb, is coated with a mirror layer serving to direct the luminous flux from the filament into the lens system of the projector.

In lamps of the third types (Fig.15,c), the spiral filament is arranged in zigzag in a single plane (which gives the incandescent body a rectangular form) and is placed in a bulb of cylindrical shape. Such a filament form allows the necessary angles of radiation in the vertical and horizontal plane to be selected by varying the ratio between the sides of the rectangles.

In lamps of the fourth group (Fig.15,d), the incandescent filament is drawn out in the form of a spiral. The bulb is cylindrical or has a spherical bulge at the center.

Table 18 gives the main design, electrical and illumination-engineering data of a few types of searchlight and motion-picture projection incandescent lamps. The range of voltages is from 11-220 volts, and the range of power from 250 to 3000 watts.

Table 18

Principal Characteristics of Certain Types of Searchlight and Motion-Picture Projection Incandescent Lamps (Bibl.7)

Purpose of Lamp	Voltage, v	Power, Watts	Dimensions, mm: Diameter of Bulb	Total Length	Height of Light Center	Form of Incandescent Body	Overall Dimensions of Incandescent body, mm: Width or Length	Height or Diameter	Socket	Form of Bulb	Illumination Engineering Data: Luminous Flux Lumen	Luminous Efficiency lm/w	Overall Luminous Intensity, Stilb	Life Hours
Lighthouse	11	250	65	115	77	Filament along axis	6.5	3	Light signal	Spherical	6,750	26.5	2,930	30
Lighthouse	23	250	65	115	77	Double filament	8	4	Same	Same	6,125	24.5	1,150	30
Motion-picture projection lamps	110	300	35	141	70	Rectangular	9	9	Plug	Cylindrical	6,450	21.5	751	50
"	110	500	35	151	81.5	Same	9.5	8.5	Special focusing, with flange	Same	11,000	22	1,565	30
Searchlight	110	750	35	151	81.5	"	10.4	10	Same	"	17,250	23	1,795	30
"	110	500	65	135	75	"	13	14.5	"	"	10,500	21	540	100
"	110	1,000	70	240	135	"	15	12.5	Screw	"	22,200	22.2	840	100
"	110	1,500	75	305	135	"	21.5	15.5	Goliath	"	34,500	23.0	940	100
"	110	2,000	80/115	360	180	"	32.5	18.5	"	Cylindrical with pinched bulge	47,400	23.7	970	100
"	110	3,000	95/120	378	180	"	39	16	"	Same	72,300	24.1	1,000	300
"	220	500	65	135	75	"	16	14	Form of bulb	Cylindrical	9,800	19.6	455	100
"	220	1,000	70	240	135	"	19.5	16	Same	Same	21,000	21	675	100
"	220	1,500	75	305	135	"	26.5	16	Goliath	"	32,550	21.7	675	100

STAT

The over-all brightness ranges from 455 to 3000 stilbs. The forms and types of the sockets vary (according to the function of the lamp).

The life of the lamps shown in Table 18 corresponds to normal voltage conditions. By shortening the life of the lamp under forced conditions, the lamps will yield a higher luminous efficiency and brightness, which sometimes exceeds 3000-4000 stilbs.

Section 21. Special Infrared Radiators

The Rod Lamp

The idea of designing a lamp with a luminous body made of a kaolin plate, heated to incandescence by a current, was conceived by the famous Russian scientist inventor, P.N.Yablochkov.

Figure 16 schematically shows the construction of the rod lamp in which the

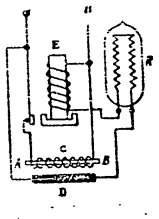

Fig. 16 - The Rod Lamp

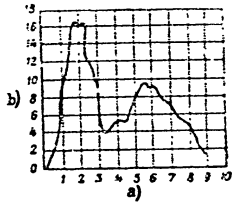

Fig. 17 - Radiation Spectrum of the Rod Lamp
a) Wavelength, μ; b) Intensity of radiation in relative units

incandescent body is a compressed cylinder, the rod R, made of a mixture of zirconium dioxide and yttrium oxide.

The diameter of the rod is 0.4-0.6 mm, its length 12-20 mm, its supply voltage 100-250 v, its current 0.25-1 amp. In view of the fact that such a rod, in the cold state, has a very high resistance and therefore conducts almost no current, the cylinder is preheated by the incandescent platinum wire c, wound on the porcelain pin AE.

After preheating for 30-45 sec, the resistance of the rod is considerably reduced. In order to limit the increasing current, the resistor P is connected in the circuit of the rod.

The electromagnet E serves for automatic switching of the rod from the preheating circuit to the working circuit with the resistor P.

The radiation spectrum of the rod lamp (Fig.17) has two principal maxima, one in the region 1.6-2.4 μ and the other in the region 5.5-6 μ. The rod lamp is a good

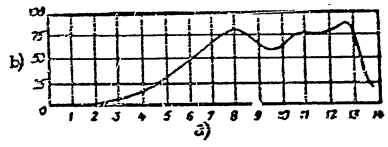

Fig. 18 - Spectrum of Radiation of Incandescent Mantle
a) Wavelength, μ; b) Intensity of radiation, %

selective source of infrared rays, but at the same time has the following main disadvantages:

Sensitivity to fluctuations in voltage, requiring stabilization by means of a barretter;

Low radiation power, allowing the rod lamp to be used primarily only under laboratory conditions;

Rapid disintegration of the rod with increasing temperature.

The Incandescent Mantle

In its design, this mantle consists of a cap heated to incandescence by the flame of a liquid fuel or gas.

The body of the mantle is made of silk impregnated with thorium oxide, with a few percent cerium oxide added.

STAT

A feature of the incandescent burner is its radiation over a very wide range of the infrared region of the spectrum, beginning from 1 μ (Fig.18) up to 100-150 μ. Because of the low intensity of its radiation, however, the incandescent mantle is used only for laboratory studies.

Section 22. Electroluminescent Radiators

While temperature radiators yield a continuous spectrum, electroluminescent sources of radiation have a discontinuous line or band spectrum. Electroluminescent

Table 19

Atomic and Electrical Data of a Few Gases and Vapors

Gas	Atomic Number	Atomic Weight	First Resonance Potential, v	Ionization Potential, v
Hydrogen	1	1.018	-	13.53
Helium	2	4.002	19.77	24.48
Nitrogen	7	14.008	-	14.48
Oxygen	8	16.0	-	13.55
Neon	10	20.18	16.77	21.47
Sodium vapor	11	23.0	2.1	5.12
Argon	18	39.94	11.57	15.69
Mercury vapor	80	200.16	4.86	10.38

radiators make it possible to build high-intensity selective radiators with a maximum of radiation in a very narrow region of the spectrum, depending on the gas used for filling.

Electroluminescent radiators have a number of disadvantages: the relative complexity of their circuits, which requires the use of chokes and transformers; the considerable time required for establishing a steady state, etc. These disadvantages limit, to a certain extent, the use of electroluminescent radiators as technical sources of infrared rays.

Electroluminescent radiators of the type of gas-discharge tubes and gas-discharge lamps are being used widely in infrared technology. In their design, radiators of this type consist of a glass or quartz bulb filled with gas or with a vapor of certain metals. Metal electrodes are fused into the bulb, and the voltage necessary to produce a discharge inside the bulb is applied to them. The construction and design features of various gas-discharge lamps used in infrared technology will be considered below.

Section 23. Gases and Metal Vapors Used for Filling Gas-Discharge Lamps

The following gases are used for filling gas-discharge lamps: neon, helium, argon (as an additive), and the vapor of mercury and sodium. Sodium vapor is chemically active and reacts with the glass of the lamp bulbs. Since the vapor pressure of sodium in the pure state is very low (0.0002 mm Hg), a certain amount of neon, argon, or other inert gas which is chemically inactive and does not combine with the electrodes and the glass, must be added to obtain the discharge.

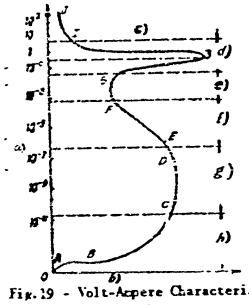

Fig.19 - Volt-Ampere Characteristic of Gas Discharge
a) Current, amp; b) Voltage, v; c) Arc discharge; d) Anomalous glow discharge; e) Normal glow discharge; f) Transitional regions; g) Silent independent discharge; h) Silent non-independent discharge

Table 19 gives the atomic and electrical data of a few gases and vapors used to fill gas-discharge lamps.

Section 24. Forms of Discharge in Gas

The most convenient way of studying the various forms of electric discharge in a gas is by plotting the volt-ampere characteristic of the gas discharge, as shown in Fig.19. This diagram shows that, for the initial section OA, direct proportionality between current and voltage exists. The subsequent voltage rise does not lead to an increase in current, and over the segment AE the curve runs almost parallel to the abscissa. A further rise in voltage leads to an increase in current along the segment BC. Taken as a whole, the region OC is called the region of silent non-independent discharge.

The segment CG is characterized by constant voltage with rise of current. Along

STAT

the segment DE, a voltage drop occurs, while the region CE is the zone of silent independent discharge.

Along the segment EF (in the transitional region) the voltage drops rapidly, the current increases, the gas in the lamp begins to glow, and a normal glow discharge forms in the region FG (where the current does not depend on the voltage). A further increase in current leads first to a sharp voltage rise (up to point H), and then to a sharp voltage drop (up to point I), and in the region GI an anomalous glow discharge takes place.

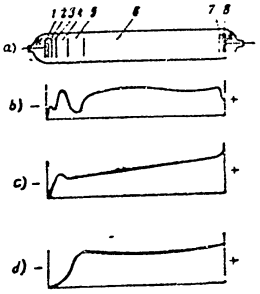

Fig. 20 - Electrical and Luminous Characteristics of a Glow Discharge in a Gas-Discharge Tube
1- Cathode dark space; 2- Region of cathode glow; 3- Nonluminous negative dark space; 4- Region of negative glow discharge; 5- Faraday dark space; 6- Positive column; 7- Region of anode glow; 8- Anode dark space; a- Gas-discharge tube; b- Intensity of luminescence; c- Distribution of potential; d- Density of electron flux

The last region, IJ, in which an arc discharge occurs, is characterized by high current and low voltage.

The gas-discharge lamps used as sources of infrared rays usually operate under glow or arc discharge.

Section 25. The Glow Discharge

The gas contained in a gas-discharge lamp is always in a state of partial ionization due to the action of external ionizing forces: ultraviolet, radioactive, and cosmic radiations. Under the action of voltage applied between the anode and cathode, the electrons begin to be displaced. In addition to this electron current there also appears a current due to the positive ions moving in the direction of the cathode. As a result, the total current increases. For a glow discharge, low current density and great voltage drop are characteristic. Such a discharge is characterized by a bright glow, whose color is determined by the kind of gas in the lamp.

Figure 20 shows the electrical and luminous characteristics of a glow discharge in a gas-discharge tube.

Figure 20,a shows that directly at the cathode (k) there is a narrow region (1) called the cathode dark space. This is adjoined by the region of cathode glow (2), followed by the region of nonluminous negative dark space (3). The negative dark space is in turn adjoined by the region of negative glow discharge (4), passing over into the Faraday dark space (5), which in turn changes over into the brightly glowing positive column (6), terminating in the region of anode glow (7), separated from the anode A by the narrow anode dark space (8).

It will be clear from Fig.20,b that the intensity of luminescence is distributed nonuniformly along the lamp. In the region of the cathode dark space there is no luminescence. In the region of the cathode glow there is a small maximum of intensity, diminishing on transition to the region of the negative dark space and again sharply rising in the region of negative glow discharge. In the region of the Faraday dark space, the intensity of luminescence drops sharply and then rises gradually, assuming a constant value in the region of the positive column. The anode glow has a small maximum of intensity and then falls in the anode dark space.

The potential is also distributed irregularly between the electrodes (Fig.20,c). In the region of the dark cathode space there is a cathode potential drop. In the region of the negative glow discharge there is a maximum of potential, which declines first in the region of the Faraday dark space and then smoothly rises almost to the anode, where a small upward jump of potential is noted.

The density of the electron flux (Fig.20,d), beginning from the cathode, rises gradually to the region of the Faraday dark space where a small maximum occurs, and then remains unchanged almost to the anode, where it increases slightly.

Section 26. Helium Lamps

The helium gas-discharge spectral lamp, which is a resonant source of infrared rays, is schematically shown in Fig.21. This lamp differs in design from ordinary gas-discharge tubes in that its bulb contains a special capillary tube in which a

current density of 500 amp/cm^2 is reached.

The brightness of radiation of the helium lamp is up to 600 sb, and the maximum radiation is in the region 0.8-1 μ, i.e., is a source of near infrared rays.

Fig.21 - Diagram of Helium Lamp

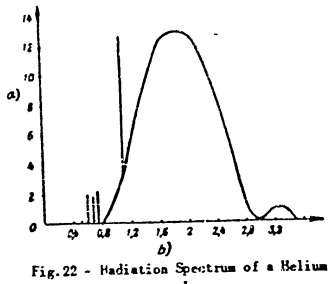

Fig.22 - Radiation Spectrum of a Helium Lamp

a) Intensity of radiation in relative units; b) Wavelength μ

In 1934, Ye.Devyatkova and N.Devyatkov developed an original type of helium gas discharge lamp (Bibl.6). The tube is made of molybdenum glass. The anode and cathode are located at the ends of the tube. The cathode is made of oxide-coated tantalum, and has the form of a cylinder, within which a tungsten spiral for heating the oxide layer of the cathode is placed. The helium charge of the tube is under a pressure of 4.5-12 mm Hg. The voltage required for a discharge to occur is 40-90 volts at a current of 2-12 amp.

The radiation spectrum of this lamp (Fig.22) is mixed. Together with a strong resonance line of helium at the wavelength 1.08 μ, the spectrum has a continuous region of radiation of the incandescent cathode in the range 0.8-2.95 μ, with the maximum of radiation at 1.8 μ. Both types of helium lamps may be used as radiators of short infrared rays.

Section 27. The Cesium Resonance Lamp

The cesium resonance lamp consists of a bulb filled with cesium vapor. Inside the bulb is attached a tube with electrodes. The lamp is a selective source of near infrared rays of great radiation intensity in this region. To prevent the destruction of the glass due to absorption of cesium vapor, the inner surface of the bulb is coated with a thin layer of a special composition. The lamp is produced in 50-100 and 500 watt sizes.

The 100-watt lamp (Fig.23) consists of the tube A, 125 mm long and 35 mm in diameter, filled with cesium vapor and some inert gas, such as argon. The tube ends in the bulb B, 50 mm in diameter, one end of which terminates in the four-pin plug TS.

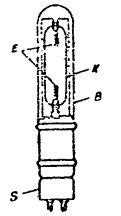

Fig.23 - Diagram of 100-Watt Cesium Lamp

The discharge takes place between the two spiral tungsten electrodes E coated with barium and strontium oxides. The distance between the electrodes is 76 mm.

The fact that the tube is filled with argon with an admixture of hydrogen (0.006%) facilitates ignition and increases the intensity of the luminescence of the cesium vapor. Under a pressure of 200 mm Hg, the lamp has its maximum resonant radiation in the region of the near infrared rays. With decreasing pressure, the resonant radiation diminishes, while with increasing pressure it shifts into the visible region of the spectrum, and the burning of the lamp becomes unstable. Figure 24 shows the radiation spectrum of the cesium lamp. The maximum radiation of the lamp corresponds to the wavelengths 0.86 and 0.89 μ.

A 100-watt cesium lamp has a power output in the infrared region of the spectrum equivalent to the output of a 700-watt incandescent lamp.

The cesium lamp has the very valuable property of permitting almost complete modulation of the current. The modulation characteristic given in Fig.25 shows that the modulation percentage, over the greater part of the audio-frequency range, is 90% and, at 10,000 cps, amounts to about 60-70%.

A 60-watt incandescent lamp is also modulated by an audio-frequency current up to 6000 cps. In view of the great thermal inertia, its percentage modulation at a frequency of 1000 cps is only a thousandth as great as in the cesium lamp.

STAT

Figure 26 shows a wiring diagram of the cesium lamp. The tungsten electrodes are heated to incandescence by current from the winding of the transformer T_2 (6 amp, 2.5 v) for one minute, after which a discharge takes place between them. The

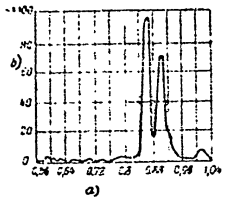

Fig.24 - Radiation Spectrum of the Cesium Lamp
a) Wavelength, μ; b) intensity of radiation, %

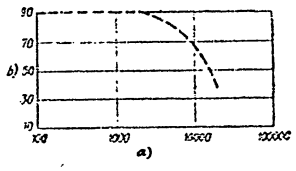

Fig.25 - Modulation Characteristic of the Cesium Lamp
a) Frequency, cps; b) Percentage modulation,%

300 volts alternating current for the power supply of the lamp are fed from the starting transformer T_2. After ignition of the lamp and after it has turned for

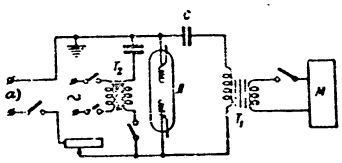

Fig.26 - Wiring Diagram of Cesium Lamp:
T_2 - Starting transformer; M - Modulator; L - Lamp; C - Capacitor of modulator; T_1 - Transformer of modulator
a) Direct current

one minute, the DC voltage is turned on and the current drops. Then the 300 volts AC and the heater voltage are turned off; 15 minutes later, the discharge in the lamp becomes steady (steady state), and a modulating voltage can be imposed on the lamp across the transformer T_1.

Section 28. Mercury Lamps

Mercury lamps are widely used in various fields of spectroscopy and infrared technology. The first patent for a mercury lamp (low-pressure) was issued in 1879 to

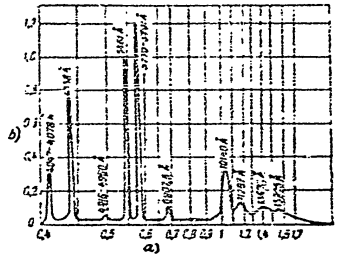

Fig.27 - Radiation Spectrum of an "IGAR-2" Type Mercury Lamp
a) Wavelength, μ; b) Intensity of radiation in relative units

the Russian scientist Professor Pep'yev.

The arc discharge in mercury vapor has certain peculiarities by comparison with the discharge in other vapors.

In mercury lamps, together with an electron current, an ion current passing from anode to cathode is generated. The density of the electron and ion currents depends on the velocity of the electrons and ions.

Since the velocity of electrons is considerably higher, the density of the electron current is also higher than that of the ion current. For this reason the total discharge current of the mercury arc is determined primarily by the electron current.

With increasing current density, the number of repeated collisions between the atoms, as well as their energy, increases "stepwise" or, as it is commonly expressed, "stepwise ionization" takes place.

For lamps with elevated pressure, the phenomenon of concentration of a luminous discharge column is characteristic - its constriction into a narrow "thread" of very great brightness ("threading").

Depending on the pressure of the mercury vapor filling the lamp, there are three forms of mercury-arc discharge, at low, high, and extreme mercury-vapor pressure. In this connection, mercury lamps are subdivided into lamps of low, high, and extreme pressure.

At low mercury-vapor pressure, not exceeding a few millimeters Hg, and low current density (about 4-5 amp/cm^2), the maximum radiation occurs in the ultraviolet region of the spectrum.

Table 20

Distribution of Radiation Energy over Spectrum of Low-Pressure Mercury Lamps (Bibl.7)

Power Input Watts	Spectral Distribution of Radiation Energy, %		
	Ultraviolet Region, 0.2-0.39 μ	Visible Region 0.29-0.75 μ	Infrared Region 0.76-4 μ
250	29.9	54.5	15.4
300	30.9	52.3	16.8
350	30.5	51	18.6
400	29.8	50.8	19.4

At high mercury-vapor pressure, the current density and concentrations of atoms and ions increase. Under these conditions, the phenomenon of threading of the discharge column takes place, and the resonance lines of radiation in the visible region of the spectrum are intensified: the yellow lines at wavelengths of 5791 and 5770 Å, and the green line at 5460 Å, as will be seen from Fig.27, which shows the radiation spectrum of the mercury lamp.

At extreme pressure, the current density is still greater, and the radiation in the infrared region of the spectrum increases.

Consequently, depending on the form of the discharge, the distribution of radiation energy over the spectrum also varies.

Table 20 gives data on the distribution of radiation energy over the spectrum of low-pressure mercury lamps.

Figure 28 shows the spectral distribution of radiation energy of three extreme-pressure mercury lamps, 4.5, 2, and 1 mm in diameter, respectively (Fig.28,a,b,c), at respective pressures of 20, 130, and 200 atm and potential gradients of 120, 500, and 800 watt/cm.

The curves are plotted from the data of measurements (Bibl.7) and show that with increased pressure the line spectrum changes into a continuous spectrum.

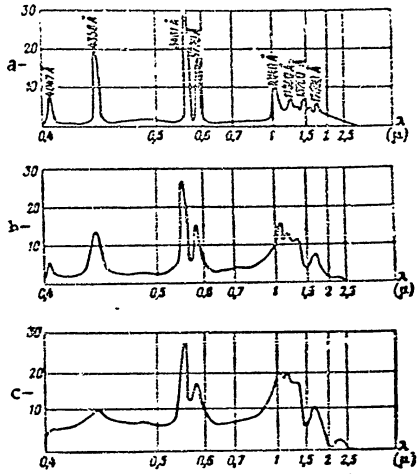

Fig.28 - Spectral Distribution of Radiation Energy for Three Extreme-Pressure Mercury Lamps:
a- Diameter of lamp 4.5 mm, pressure 20 atm, potential gradient 120 watt/cm;
b- Diameter of lamp 2 mm, pressure 130 atm, potential gradient 500 watt/cm;
c- Diameter of lamp 1 mm, pressure 200 atm, potential gradient 800 watt/cm
1) Radiation energy in relative units

Table 21 gives the spectral distribution of radiation energy (in %) of extreme-pressure mercury lamps.

Extreme-pressure lamps have a high efficiency.

For lamps at 200 atm pressure, the total radiation power amounts to about 75% of the power input, which indicates the great economy of the lamp. At a luminous

efficiency of 65 lm/watt and a power input of 710 watts, the lamp radiates a flux of 46×10^3 lm. To obtain a similar flux from a tungsten incandescent lamp would take

Table 21

Spectral Distribution of Radiation Energy of Extreme-Pressure Mercury Lamps (Bibl.7)

Lamp Data			Luminous Efficiency, lm/watt	Spectral Distribution of Radiant Energy, %		
Diameter mm	Gradient, watt/cm	Pressure, atm		$\lambda < 0.4\ \mu$	$\lambda = 0.4 + 0.7\ \mu$	$\lambda > 0.7\ \mu$
4.5	120	20	40	45	28	27
4.5	135	20	48	46	26	28
2	500	130	56	40	30	30
1	800	200	65	31	35	34

1700 watts, or 2.5 times as much power.

With increasing pressure, the radiation power in the infrared portion of the spectrum also increases. At a pressure of 200 atm, it reaches 34% of the total radiation of the lamp. For this reason extreme-pressure mercury-arc lamps are good radiators of short infrared rays.

Section 29. Extreme-Pressure Mercury Lamps

According to their design, extreme-pressure lamps (SVD) may be subdivided into three types: capillary and spherical with natural cooling, and water-cooled capillary.

This classification is based on the operating conditions of the lamp. The brightness of the radiation of mercury-arc lamps depends on the power consumed. This power is limited by the heat-resistant properties of the bulb, which is made of refractory quartz glass.

Extreme-pressure capillary mercury lamps with natural cooling are designed for a pressure of 20 atm and a power of 40 watts.

The capillary mercury lamp consists of a quartz capillary tube, of 2 mm inside diameter, 6 mm outside diameter, and 35-40 mm length. Two tungsten electrodes are inserted into the tube at the ends, and are separated from each other by a distance not exceeding 20 mm. The tube is filled with mercury vapor. As a result of the high pressure, the discharge column in the tube of the lamp is drawn into a narrow thread

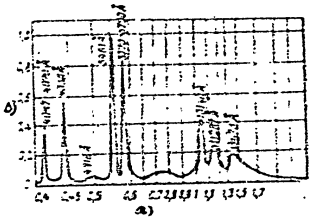

Fig. 29 - Radiation Spectrum of a SVD-250 Mercury Lamp
a) Wavelength, μ; b) Intensity of radiation in relative units

of a diameter not over 1 mm, thanks to which the high brightness of the radiation is obtained. Figure 29 shows the spectrum of radiation of the SVD-250 lamp.

The spherical lamp (Fig.30) consists of a spherical quartz bulb of 10 cm outside diameter and 4.5 mm inside diameter. The length of the tube is 40 mm, and the distance between the electrodes 15 mm. Special spirals placed on the electrodes are used for heating. At an energy consumption of 70 watts, the lamp has a luminous

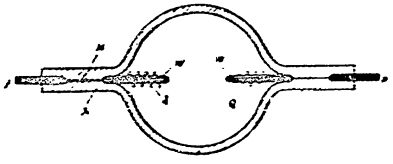

Fig. 30 - Arrangement of a SVD Spherical Lamp:
W- Tungsten electrodes; C- Spirals of oxide-coated tungsten; A- Quartz bulb; M- Molybdenum foil; P- Contacts of electrodes

efficiency of 50 lm/watt.

Table 22 gives the parameters of capillary and spherical extreme-pressure

STAT

mercury lamps with natural cooling.

The water-cooled capillary lamp is a quartz tube 150 mm long, placed in another quartz tube serving as a jacket for the coolant water. Table 23 gives the parameter

Table 22

Parameters of Super High Pressure Naturally-Cooled Capillary and Spherical Mercury Lamps (Bibl.8)

Type of Lamp	Ignition Voltage, v	Working Voltage, v	Current, Amp	Power, Watts	Heat-Up Time, min.	Brightness Sb	Luminous Flux, lm	Luminous Efficiency, lm/watt	Life, Hours
Capillary	180	115	0.4-0.75	80-100	4-4.45	1800-2000	3000-3600	33-36	500
Same	1500-2000	1250-1800	0.5-1.2	1000-1500	3-5	1500-3000	40,000-85,000	38	500
Spherical	-	70-90	6	300-500	10	10,000-25,000	12,000-20,000	40	100

of these lamps.

Section 30. Basic Data on the Theory of the Arc Discharge

Before discussing arc lamps in which the source of radiation is an electric arc, we will present basic information on the theory of the arc discharge.

Table 23

Parameters of Super-High Pressure Capillary Mercury Lamps, Water-Cooled (Bibl.9)

a	b	c	d	e	f	g	h	i	j	k	l	m
SP-500	12.5	2	6	75	500	1.5	1.3	420	30,000	33,000	60	500
SP-800	10	1	3	120	800	1.5	1.3	600	50,000	91,000	62	25
SVDV (NELZ)	-	-	-	100	1000	1.5-2.0	-	600-800	60,000	-	60	-

a) Type of lamp; b) Length of discharge, mm; c) Inside diameter of tube, mm; d) Outside diameter of tube, mm; e) Mercury-vapor pressure, atm; f) Power consumed, watts; g) Value of current, amp; h) Current, amp - AC; i) Current, amp - DC; j) Working voltage, v; k) Luminous flux, lm; l) Maximum brightness, sb; m) Luminous efficiency, lm/w; n) Life, hours.

An arc discharge develops from a glow discharge when the current density is increased to a value sufficient to heat the cathode to a temperature at which emission of electrons begins, i.e., at which thermoelectronic emission occurs. The high temperature is maintained by the bombardment of the cathode with positive ions. This form of discharge, called the thermal arc, is observed in electric arcs.

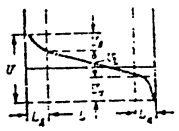

Fig.31 - Distribution of Potential in an Arc Discharge

If the cathode material has a low vaporization temperature (for instance, mercury), then vaporization takes place before the temperature necessary to start electron emission is reached, and at a certain pressure, a discharge occurs with a cold cathode. This is explained by the fact that the mean free path of electrons at high pressures is very short (about 10^{-5} cm) so that ionization takes place around the cathode. The positive space charge, formed as a result of ionization, is concentrated at a certain distance from the cathode, equal to the mean free path of the electrons. This space charge, together with the electrons, forms an electric layer with a potential gradient reaching 10^5-10^6 watt/cm. The discharge taking place is called an autoelectronic arc, or a cold-cathode arc.

Figure 31 shows the potential distribution in various parts of the arc.

The cathode-potential drop U_K is relatively small (10-15 v), which distinguishes the arc discharge from the glow discharge, in which the cathode-potential drop reaches 250-300 v. The length of the segment of the cathode-potential drop L_K for an arc discharge is negligibly small, shorter than the mean free path of the electrons, which, for a carbon arc in air, is 0.01 mm.

Near the anode, on the segment L_A, the anode-potential drop U_A is formed. The segment between the regions of the anode and cathode potential drops is called the luminous, or positive, column. In electric arcs, this segment is occupied by the flame of the arc. The potential drop U_L in the region of the positive column varies by a linear law.

The total potential difference between the electrodes of an arc is determined as the sum of the potential drops over the individual segments:

STAT

$$U_{arc} = U_K + U_A + U_L \qquad (101)$$

Let us consider the various types of arc lamps.

Section 31. The Simple Electric Arc

The electric arc was discovered in 1802 by the famous Russian scientist Professor V.V.Petrov.

Figure 32 gives the diagram of the simple arc. The arc discharge, or arc, is formed between two carbon or graphite electrodes. The cathode (5), heated to incandescence, is a source of electrons traveling toward the anode (1). As a result of bombardment by the electron stream, the anode is heated to white luminescence and a depression, the crater (3), at a temperature of up to 4000°K, is formed on it.

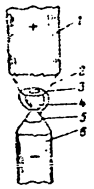

Fig. 32 - Diagram of Simple Arc:
1- Anode;
2- Cone of anode; 3- Crater
4 - Flame arc;
5 - Incandescent cathode;
6 - Cathode

This is explained by the fact that the electrons traveling from the cathode, impinging on the surface of the anode, give up their kinetic energy and disintegrate the anode.

The luminous properties of an arc are determined mainly by the temperature of the crater. The crater radiates about 85% of the luminous flux of the arc, the flame about 5%, and the cathode about 10%.

The anode, or positive electrode, is 20-40 mm in diameter and has an operating temperature of about 4200°K. The cathode, or negative electrode, is 9-20 mm in diameter and has a temperature of about 3100°K. An arc lamp can operate on either DC or AC. If an arc is fed with DC, the positive carbon burns considerably faster than the negative carbon. When an arc is fed by AC, the carbons burn down uniformly and no crater is formed in the anode, but the luminous flux obtained is smaller than with DC.

Table 24 gives the distribution of the luminous flux in the electric arc when fed with DC and AC.

The anode and cathode of the simple arc are usually made of carbon or have wicks enclosed in a hard shell of carbon. The wicks are made of a mixture of lampblack and waterglass. Electrodes with wicks burn more stably than carbon electrodes, since the softer mass of the wick, evaporating more strongly than the carbon shell,

Table 24

Distribution of Luminous Flux in an Electric Arc

Type of Current	Luminous Flux in % of Total Luminous Flux		
	Positive Electrode (Crater)	Negative Electrode	Flame of Arc
DC	85	10	5
AC	47.5	47.5	5

forms a gas cloud intensifying the ionization of the arc, thus facilitating ignition and maintaining the stability of the burning conditions. The rate of burning of the carbons under normal conditions is 1 mm/min.

The simple electric arc has what is called a descending characteristic - the voltage between the electrodes decreases with increasing current. To eliminate this

Table 25

Dependence of Luminous Intensity and Brightness of the Simple Arc on the Current Value (Bibl.9)

Intensity of Current, Amp	d_+ = 20 mm, d_- = 9 mm		d_+ = 28 mm, d_- = 14 mm		d_+ = 38 mm, d_- = 20 mm	
	I, cd	B, sb	I, cd	B, sb	I, cd	B, sb
60	5,200	15,000	4,000	12,500	-	-
80	8,000	17,200	8,000	-	-	-
100	11,000	19,000	11,000	14,500	8,300	14,800
120	14,500	20,500	-	-	12,000	15,000
140	-	-	16,000	17,000	14,800	15,400
160	-	-	-	-	16,200	15,600
180	-	-	22,500	20,000	20,000	15,700
200	-	-	-	-	22,500	15,800

phenomenon and stabilize the operation, an additional resistance is connected in

STAT

series with the circuit of the arc, thus making the characteristic assume an ascending slope and causing the arc to burn stably. The additional (ballast) resistor absorbs from 30 to 50% of the power of the arc.

The brightness of simple arcs reaches 18,000-20,000 sb with DC feed and about 12,000 sb with AC feed. The brightness of the arc is only slightly dependent on the length of the arc and the value of the current. With increasing current only the luminous area and luminous intensity increase. Table 25 gives data showing the dependence of the luminous intensity (I) and the brightness (B) of the simple arc on the value of the current at various diameters of the positive carbon (d_+) and of the negative carbon (D_-).

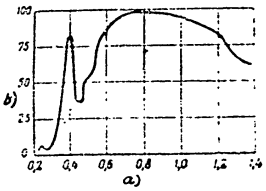

Fig. 33 - Radiation Spectrum of Simple Arc
a) Wavelength, μ; b) Luminous flux in relative units

As will be seen from Table 25, in the first pair of carbons, when the current increases, the luminous intensity increases by a factor of about 3 times, while the brightness increases by a factor of less than 1.5; in the second pair, the luminous intensity increases 5.5 times, and the brightness about 1.7 times; in the third pair, the luminous intensity increases 2.7 times, but the brightness hardly increases at all. The luminous efficiency of the arc is about 12-14 lm/watt at a current density of 15-17 amp/cm^2.

The brightness temperature of the crater is T_b = 3800°K, and the true temperature T_t = 4000°K.

At constant arc length, an increase in current from 8 to 60 amp, and an increase in current density in the positive carbon from 30 to 210 amp/cm^2, causes no change in the brightness of the crater. In ordinary arcs, therefore, the current density does not exceed 30 amp/cm^2. The brightness of the simple arc increases only with increasing pressure, since the vaporization temperature of carbon increases with increasing pressure.

The spectral distribution of radiation energy of simple arcs is shown in Fig. 33. The radiation maximum is in the region of 0.7-0.8 μ. Thus the ordinary arc is a good source of short-wave infrared rays.

Section 32. The High-Intensity Arc

The high-intensity arc differs from the simple arc by an electrode arrangement which allows the current density to be increased, and consequently improves the illumination characteristics of the arc.

The positive electrode of a high intensity arc consists of a hard compressed shell and a wick. The wick diameter is usually 50-65% of the shell diameter. The shell, as a rule, contains mineral additives, and consists of carbonblack, coke, or graphite, and 1% boric acid.

A shell mainly consisting of carbon black, is used at low current densities, while a graphite shell is used at high current densities.

The wick of the positive electrode consists of a 30-60% mixture of rare-earth fluorides (for instance fluorides of cerium, samarium, and lanthanum), mixed with carbon black or graphite, with about 4% boric acid added.

The luminous properties of the arc depends on the composition of the shell and the wick, and on the method of manufacturing the wick.

Wicks for high-intensity arcs are either tamped or inserted. A tamped wick is obtained by compressing a liquid wick mass into a pre-fired shell. In this case liquid potassium silicate is used as a binder. To obtain an inserted wick, the wick mass is passed through a round opening under pressure of some tens of atmospheres. Various powders can be used as binders in this case.

The negative electrode, like that in a simple arc, has a wick. The carbons for a high-intensity arc have a considerably greater brightness and luminous intensity than the carbons for a simple arc. The brightness of the carbons of a simple arc does not exceed 20,000 sb while that of the carbons in a high intensity arc may reach 80,000 sb. The respective maximum values of the luminous intensity are 22,500 candles for a simple arc and 110,000 candles (almost 5 times as great) for the high-intensity arc.

STAT

Figure 34 schematically shows a high-intensity arc. As shown in the diagram, the form of the flame and its direction are the same as in the simple arc, but a bright gas cloud beginning at the crater is formed in front of the anode. The flame from the cathode forces this cloud toward the anode, concentrating the gases in the depression of the crater. The brightness of the anode cloud is many times as great as that of the flame near the cathode.

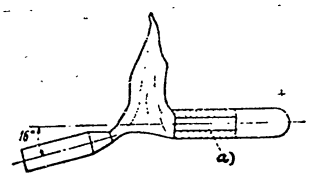

Fig.34 - Diagram of High-Intensity Arc
a) Solid wick

The crater formed in the positive electrode, as a result of its vaporization at high temperatures (about 5000°K) and as a result of ionic bombardment, is filled with the vapor of the rare-earth metals forming part of the composition of the wick of the positive carbon. The negative ions formed near the crater, under the action of the electric field, form a negatively charged layer which determines the boundaries of the flame near the anode.

The positive ions recombine with the electrons and negative ions emitted by the cathode; in this case energy is given off in the form of luminous flux. Thus, in contrast to the simple arc, in the high-intensity arc the pure thermal radiation of the crater is supplemented by the luminescent radiation of the cloud of incandescent vapor of the rare-earth elements contained in the positive electrode wick. Owing to this fact, the high-intensity arc is brighter than the simple arc.

The combustion products of the arc form a tongue of flame between the electrodes, which, in the form of the so-called "beard" is projected in the beam of a searchlight.

High-intensity arcs usually operate on DC, since their efficiency, when operated on AC, is lower.

The high-intensity arc has an ascending volt-ampere characteristic, which makes the use of an additional resistor unnecessary.

The curve 1 of the spectral energy distribution of the high-intensity arc, shown in Fig.35, indicates that this arc has no marked advantages over the simple arc (curve 3) as far as the distribution of radiated energy in the infrared portion of the spectrum is concerned.

This fact, as well as the necessity of using special devices for focusing and rotating the positive carbon about the axis, and the necessity of cooling systems,

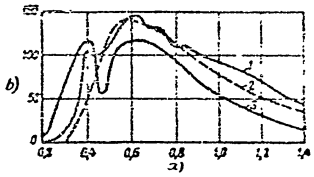

Fig.35 - Radiation Spectra:
1- Of high-intensity arc; 2- Of a black body at T = 5000°K
3- Of a simple arc
a) Wavelength, μ; b) Radiant flux in relative units

make the design of this arc lamp considerably more complicated.

High-intensity arcs are used in ordinary long-range searchlights. Such arcs are produced in special arc lamps whose design was first developed in 1874 by the famous Russian electrical engineer V.N.Chikolev.

The circuit of the arc lamp is given in Fig.36. The electromagnet (5), connected in series with the feed circuit of the electrodes, ensures instantaneous ignition of the lamp. The electromagnet (7), connected in parallel with the feed circuit, as the negative electrode burns away, automatically brings it closer to the positive electrodes, thus regulating the distance between the electrodes, and, consequently, the length of the arc. The electromagnet (6) serves to hold the crater of the positive electrodes in the focal plane of the projector.

In lamps without automatic ignition, the negative electrode is brought into contact with the positive electrode after which the electrodes are separated by the necessary length of the arc. In lamps with automatic ignition, when the power

STAT

supply is turned on, the electrodes are brought into contact by a spring attached to a lever connected to the armature of the electromagnet (5). When the power supply is turned on, a current flows through the winding of the electromagnet (5), and the electromagnet attracts the armature, connected over a lever with the shaft of a lead screw which separates the carbons by the distance necessary for arc formation. The electromagnet (7) periodically brings the carbons closer together, so that the arc does not go out when they burn down.

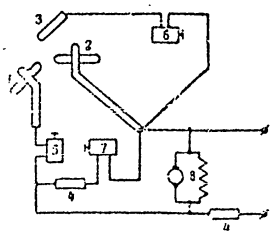

Fig. 36 - Circuit Diagram of the Arc Lamp:
1- Anode; 2- Cathode; 3- Additional electrode of red copper; 4- Resistors;
5, 6, 7- Electromagnet; 8- Motor actuating arc lamp

Section 33. Tungsten Arc Point Lamps

The tungsten arc lamp, because of the small size of the arc discharge, is called a point lamp. A characteristic peculiarity of lamps of this type is their high over-all brightness. Figure 37 gives an external view of the tungsten lamp.

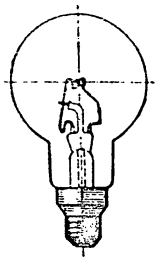

Fig. 37 - Layout of Tungsten Arc Lamp

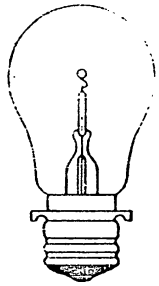

Fig. 38 - Layout of Point Arc Lamp with Conical Incandescent Body

The arc discharge originates at the instant of separation of the two tungsten electrodes, having the form of a sphere and hemisphere of a diameter of 1-6 mm, depending on the power of the lamp. The bulb of the lamp is filled with nitrogen or a mixture of helium and neon. When the voltage is turned off, the electrodes are in contact; at the instant the current is supplied, a high current passes through a bimetal plate. The plate, heated by the current, bends and separates the electrodes by the required distance.

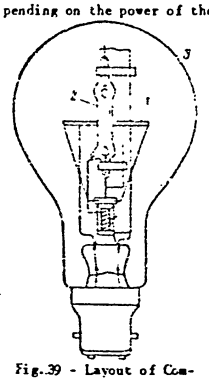

Fig. 39 - Layout of Combination Lamp:
1- Tungsten spiral;
2- Mercury lamp;
3- Bulb

The brightness of point lamps of 1 kw power is 2500 sb, at a luminous intensity of up to 4000 candles. The lamps may be fed by DC or AC.

Tungsten arc lamps with an incandescent body in the form of a sphere have proved to be inconvenient in operation, and this led to the necessity of developing an improved design of the tube with a conical incandescent body (Bibl. 10).

With an incandescent body of such form, its projection is completely filled by the luminous filaments.

The brightness of such a lamp, of 100 watts power and 12 v voltage, is equal to 1100-1510 sb, while the area of the projection on a plane perpendicular to the axis of the cone is only 0.11-0.158 cm^2. The life of the lamp is about 270 hours. The lamps can be made for various voltages from 5 to 40 volts, and in sizes of 30 to 3000 watts. The incandescent body is placed along, or perpendicular to, the axis of the bulb.

The principal advantages of this design of the point lamp are: its relatively great brightness, its use of either DC or AC, and the possibility of directly connecting it to the voltage source without a special connection circuit.

Figure 38 schematically shows an external view of the point lamp with a conical incandescent body.

The combination lamp developed by the Moscow electric lamp plant is a good source of near infrared rays (Bibl. 10a). The design of such a lamp is schematically shown in Fig. 39. It consists of a combination, in a single bulb, of an extreme-

pressure low-power mercury lamp and a tungsten incandescent lamp.

The tungsten spiral (1), which is the principal source of radiation in the

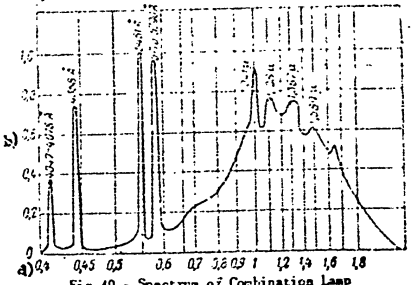

Fig. 40 - Spectrum of Combination Lamp
a) Wavelength, μ; b) Intensity of radiation in relative units

infrared region, is connected in series with the mercury lamp (2) and serves as a ballast resistor.

Figure 40 gives the curve of spectral energy distribution of the radiation of the combination lamp. As indicated by this curve, the lamp has a continuous spectrum in the near infrared region, with individual maxima of high intensity.

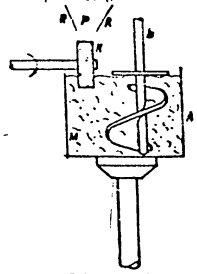

Fig. 41 - Schematic Diagram of Mass Radiator

Section 34. The Mass Radiator

In 1923, Professor A.A.Glagoleva-Arkad'yeva proposed a new and original source of infrared rays called the mass radiator. The mass radiator consists of a source radiating in the intermediate region of the spectrum lying between the shortest radio waves and the long infrared rays. Its design and principle of operation are explained in Fig. 41.

The glass vessel A is filled with the so-called vibrational mass M, consisting of a mixture of metal filings and machine oil.

The continuously rotating mixer P maintains uniformity of the mass. Within this mass, a small carbolite wheel (K) rotates and entrains the mass, causing a viscous coating (P) of metal filings to form on the surface of the wheel.

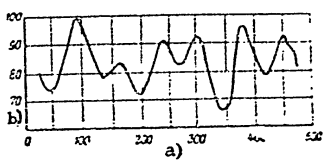

Fig. 42 - Radiation Spectrum of Mass Radiator
a) Wavelength, μ; b) Intensity of radiation, %

By means of the conductor-discharges (P), a high voltage is applied to the surface of the wheel across an inductor. The discharges between the conductors produce electric oscillations whose period is determined primarily by the size of the filings. Figure 42 gives the curve of the radiation spectrum of the Glagoleva-Arkad'yeva mass radiator.

Section 35. Extreme-Pressure Krypton-Xenon Lamp

Extreme-pressure 250- and 750-watt krypton-xenon lamps are of interest as radiators in the region of the near infrared. The 750-watt lamp is designed in the form of a quartz tube 36 mm in diameter with two vertically arranged tungsten electrodes. The upper electrode, which is the cathode, is coated with an oxide layer. The ignition of the discharge of the lamp is effected by means of a third electrode, of tungsten wire, placed perpendicular to the cathode and anode. The lamp is filled with a mixture of krypton and xenon under 25-30 atm pressure.

In the near infrared region, the lamp radiates a continuous spectrum, approaching the radiation of a black body at a temperature of 5200-5700°K, with individual intensity lines in the regions 0.76; 0.82; 0.84; 0.9 and 1 μ. With increasing atomic weight of the gas, the radiation maximum shifts toward the long-wave portion.

A pulsating discharge is one of the forms of non-stationary gas discharge, resembling a spark discharge. When high-capacitance high-voltage capacitors are discharged into a gas-discharge tube, an exceptionally great brightness, as high as

Table 26

Principal Electric and Illumination Data of Certain Gas-Discharge Lamps*

a	b	c	d	e	f	g	h	i	j	k
High-pressure mercury lamps:										
IGAR-4	250	125	4-4.25		-	3-8	7,000		28	
IGAR-3	400	125	5.6-6.2	0.3-07	-	3-8	14,000	30-80	35	500-2000
IGAR-2	500	125	7.5-8.2		-	3-8	16,000		32	
Extreme-pressure mercury lamps:										
SVD-125	125	190	0.7	-	25	-	4,500	-	36	-
NR-300	75	230	0.4	2-3	-	-	3,000	1,000-1,300	40	2000
NR-500	120	115	1.15	-	-	-	5,000	-	41.7	-
NR-4000	950	1800	0.56	-	-	-	40,000	-	42	-
Spherical extreme-pressure naturally-cooled mercury lamps:										
SVDSh-250	250	65-78	3.7-4.4	-	30-35	5-8	11,500	25,000	46	-
V-500	500	70-90	6	2-3	50	10	22,500	32,000	45	2000
SVDSh-1000	1000	220	-	-	-	-	34,000	13,000	34	-
Extreme-pressure mercury lamps, water-cooled:										
SVDV-1000	1000	600-800	1.5-2	-	100	-	60,000	-	60	-
SR-500	500	420	1.5	40	75	1	30,000	33,000	60	100-500
SR-800	800	600	1.5	200	120	1	50,000	91,000	62.5	25-500
Extreme-pressure MELZ combination mercury-tungsten lamps	300	220	1.35	-	-	4	5,500	-	18.5	1000-2000
Arc lamps with pure solid carbons:										
direct current	330-800	35-40	6	10-20	-	-	2,000-8,300	15,000-18,000	6-14	10-18
alternating current	200-1200	27-35	25		-	-	680-8,300	10,000	7	

a	b	c	d	e	f	g	h	i	j	k
Arc lamps with flame carbons										
direct current	310-770	55-80	75-200	-	-	-	7,300-23,300	60,000-80,000	23.6-30	2.5
alternating current	270-750	-	-	-	-	-	5,750-20,000	50,000	18.5-27.2	
Arc tungsten point lamp	220-250	45-50	5	-	-	1-2 sec	6,300	2,500	25.2	500-1000
Arc lamps with titanium carbide electrode	245-350	60-70	3-4.5	-	-	-	5,100-9,000	-	20.8-25.8	50-75
Searchlight arc lamps:										
sample	350-2880	44-48	8-60	10-30	-	-	2,900-25,000	4,200-12,200	10-12	-
high-intensity	8100-36,000	65-100	125-300	75-150	-	-	175,000-600,000	68,000-105,000	14-15	-

*Table 26 is based on data furnished by Ivanov (Bibl. 10 a)

a) Name and type of lamp; b) Power consumed, watts; c) Voltage in operating state, v; d) Current in operating state, amp; e) Current density, amp/cm^2; f) Pressure in lamp, atm; g) Heat-up time, min.; h) Luminous flux, lm; i) Brightness, sb; j) Luminous efficiency, lm/watt; k) Life, hours.

60×10^6 sb, may be obtained, with the flash of the lamp persistent about 10^{-5} sec.

One of the types of pulse lamps developed resembles the extreme-pressure krypton-xenon lamp. The difference is only in the interelectrode distance and the bulb diameter. A lamp of another type is made in the form of a tube of refractory glass or quartz, with an inside diameter of 1.5 to 10 mm. The ends of the tube are provided with cylindrical nickel electrodes, sometimes coated with a layer of barium or cesium. The distance between the electrodes, according to the voltage, may be as great as 1.5 m in high-power lamps.

Pulse lamps are usually charged with 90% krypton and 10% xenon, but the lamps may also be filled with helium and neon, thus shifting the radiation spectrum toward the longer wave portion.

In concluding this Chapter, we present a Table of the principal data of gas-discharge lamps (cf.Table 26).

CHAPTER V

PHOTOELECTRIC CELLS WITH EXTRINSIC PHOTOELECTRIC EFFECT

Section 36. Principal Types of Radiant-Energy Indicators

The conversion of radiant energy into other forms of energy (electrical, mechanical, chemical, or thermal) is accomplished in various ways. The instruments and devices serving to convert radiant energy and to record its conversion into some other form are called receptors or indicators of radiant energy.

Indicators that directly transform radiant energy into electric energy, using the photoelectric effect, are called photoelectronic indicators. This group of indicators includes photocells, photoelectric cathodes of electron-optical transducers, and electron multipliers.

Other indicators of radiant energy are thermocouples, bolometers, optico-acoustic and pneumatic indicators, which transform the energy into heat, thus heating a sensitive element.

The conversion of radiant energy into chemical energy is detected by photographic plates and luminous compositions, or luminophores.

Indicators of radiant energy are divided into selective and nonselective. An indicator is called selective if its sensitivity depends on the wavelength of the incident radiant flux. This group includes all photoelectric, chemical, and luminescent indicators. Nonselective indicators have a constant sensitivity in a definite, relatively wide region of the spectrum of infrared rays. Representatives of the group of nonselective indicators are, for instance, thermocouples and bolometers.

The technical types of photocells, in existence at present, use three forms of the photoelectric effect, extrinsic, intrinsic, and in the blocking layer.

STAT

Section 37. The Concept of the Extrinsic Photoelectric Effect

The emission of electrons by substances under the action of radiant energy flux incident on its surface is called the extrinsic photoelectric effect. Absorption of this additional energy causes the electrons to fly off the surface of the substance.

The simplest device for producing the extrinsic photoeffect consists of a metal plate (e.g., silver) negatively charged (photoelectric cathode), and a metal anode. If a galvanometer is connected in the circuit, a current appears in the circuit when the cathode is illuminated, caused by the electrons escaping from the surface of the photocathode and impinging on the anode.

Detailed studies of the extrinsic photoeffect were first conducted in 1888 by the prominent Russian physicist A.G.Stoletov, Professor at Moscow University, who termed this phenomenon the actino-electric effect. He made a valuable contribution to the study of the extrinsic photoeffect and has the distinction of having discovered the fundamental laws in this field.

Stoletov discovered the fundamental law of the extrinsic photoeffect namely, that the photocurrent is directly proportional to the radiant flux falling on the photocell. He also established the unipolarity and absence of inertia of the extrinsic photoeffect, as well as the dependence of the photocurrent on the applied voltage and the electrode spacing.

He established that, at a given pressure of the gas, the photocurrent has its maximum. This phenomenon of resonance of the photocurrent was denoted as "Stoletov effect".

The results of Stoletov's numerous studies of the extrinsic photoeffect formed the basis for all further research in this field.

In 1899 the electronic nature of the photoelectric current was demonstrated, and in 1899-1900 it was established that the electrons escaping from the illuminated surface of a metal possess energies of a few electron-volts, and that this energy depends on the frequency of the incident radiant flux, rather than on its intensity.

The great Soviet physicist, Academician A.F.Ioffe, made valuable studies on the nature of the photoelectric current. P.I.Lukirskiy and S.S.Prilezhayev, who first developed the classical method of quantitative verification of the fundamental equations of the photoeffect, rendered great services in the study of the extrinsic photoeffect, as have I.Ye.Tamm, P.V.Timofeyev, N.S.Khlebnikov, and other Soviet physicists.

Section 38. Structure of Solids

The photoelectric processes can be completely explained from the point of view of the quantum theory. For this reason we give below the principles of the quantum theory of the structure of solids, necessary for understanding the basic nature of photoelectric phenomena.

All solids are divided into three groups, according to their photoelectric properties:

Metals, with high electrical conductivity;

Semiconductors, with lower conductivities than metals;

Insulators (dielectrics) whose conductivity is close to zero.

All solids consist of atoms or molecules.

In a metal, the outer electrons of the atom, which are farthest from the nucleus, are weakly bound to the nucleus and are able to move freely within the metal, from one atom to another. These electrons are called free and are responsible for the conductivity of the metal.

The electrons bound to the nucleus (closer to the nucleus) cannot leave the atom. These electrons have no influence on the conductivity of the metal, since they cannot be displaced, even under the action of a powerful external electric field.

According to the quantum theory, confirmed by experiment, the electrons of an atom can exist only in a definite discrete set of stable states. The transition from one stable state to another can take place only by a jump. At the instant of such a transition, the atoms radiate or absorb energy of strictly determinate frequency.

The electrons in the atom move at various distances from the nucleus and possess various energy levels (beginning with the level of minimum energy), various values of the energy, and of the force of attraction to the nucleus. Each electron is in a state, and possesses an energy, not inherent to any other electron of the particular atom.

The energy levels form what are called sets of allowed energy levels, and only in them can electrons be found. The intermediate regions between the zones, in which

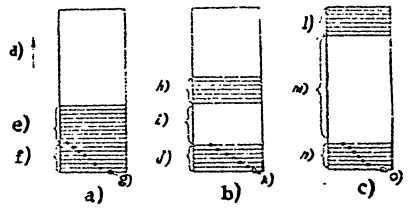

Fig. 43 - Schematic Diagram of Energy Levels of Electrons: a) In metals; b) In semiconductors; c) In insulators; d) Energy; e) Free allowed level; f) Lower allowed level; g) Nucleus; h) Free zone; i) Forbidden zone; j) Lower filled zone; k) Nucleus; l) Upper free zone; m) Forbidden zone; n) Lower filled zone; o) Nucleus

there can be no electrons, according to the quantum theory, are called forbidden zones.

The properties of solids are primarily determined by the energy levels of their electrons.

The energy levels of electrons (Fig. 43) are usually presented graphically in the form of a series of horizontal lines. The energy is plotted along the vertical.

As will be seen from Fig. 43 a, the lower forbidden zone of energy levels in metals is filled with electrons. Above this is a free zone of allowed energy levels. The free (external) electrons may pass from a low energy level to a higher one in the free zone, thus causing conductivity of metals.

The schematic diagram for semiconductors (Fig. 43 b) shows that the lower energy levels are likewise filled with electrons, but, in contrast to the situation in a metal, the free zone is separated from the lower region of forbidden energy levels. The width of the forbidden zone varies in different semiconductors. To make the transition from the lower filled zone to the upper free zone of allowed levels, the electron must overcome a potential barrier, determined by the width of the forbidden zone. To overcome this barrier, additional energy must be imparted to an electron. The quantity of energy necessary for an electron to overcome the barrier and to pass into the upper free zone, determines the degree of conductivity of a semiconductor.

In insulators (Fig. 43 c), the lower filled zone and the upper free zone are separated by so wide a forbidden zone that a transition of electrons is made impossible, even with a considerable additional energy. For this reason, the conductivity of insulators is practically equal to zero.

Thus the quantum theory successfully explains the phenomenon of conductivity in solids. As already pointed out, the transition of electrons from one level to another is accompanied by radiation (or absorption) of energy, i.e., by the phenomenon of the photoelectric effect, or luminescence.

Section 39. Fundamental Laws of the Extrinsic Photoeffect

Proportionality of the Photocurrent to the Value of the Incident Radiant Flux

The first law of the external photoeffect, discovered by A.G. Stoletov, establishes that a direct relation exists between the number of photoelectrons N escaping from the surface of a metal and the radiant flux Φ_i incident on it:

$$N = k\Phi_i \qquad (102)$$

The photocurrent i_{ph} arising in the photocell between the cathode and the anode, is directly proportional to the incident radiant flux Φ:

$$i_{ph} = s\Phi \qquad (103)$$

The proportionality factor s serves as a measure for the sensitivity of the photocell surface and is determined as the integral sensitivity of the photocell.

Fundamental Equation of Energy (First Quantum Relation)

According to the quantum theory of light, a radiant flux consists of discrete particles, or quanta, possessing a definite energy. The energy of a quantum of radiant flux, or photon, falling on the surface of a metal, is absorbed by one of the electrons on the energy level. If the electron has received sufficient energy from the photon, it is able to overcome the potential barrier at the boundary of the metal and escapes into the surrounding medium. The escaping photoelectrons have different velocities, since, having been at different energy levels and, consequently, at different distances from the surface of the metal, they traverse a different thickness of that metal and lose different quantities of energy when they strike a molecule.

Let U be the minimum positive energy at which, prior to irradiation, not a single electron can leave the surface of the metal. If, under the action of the radiant flux, an electron with a charge of e leaves the metal and impinges on some surface with zero potential (for example, on a grounded plate), then the work performed by it will be equal to Ue. If at the moment of leaving the surface, the photoelectron had the energy W, then the residual energy of the photoelectron on the surface of zero potential will be equal to

$$W - Ue$$

At W = Ue, a photoelectron will arrive at the surface of zero potential after it has expended all its initial energy of flight Ue, which is converted into kinetic energy of motion, equal to $\frac{mv^2}{2}$. Thus, in this case, all the potential energy allowing an electron to escape from the metal, will be equal to its kinetic energy of motion, i.e.,

$$W = \frac{mv^2}{2} = Ue \qquad (104)$$

where e and m = charge and mass of the photoelectron, respectively;

v = velocity of the photoelectron.

Hence,

$$v^2 = \frac{2Ue}{m} \qquad (105)$$

A measurement of the velocities of photoelectrons under different conditions allowed one of the fundamental laws of the photoeffect to be established: the velocities of photoelectrons escaping from a metal do not depend on the incident radiant flux but only on its frequency.

The relation between the velocity of the photoelectrons v and the frequency of the incident flux of radiant energy ν was determined on the basis of the quantum theory. When an atom absorbs the energy of a photon hν (where h is the Planck constant), then the liberated photoelectron must expend part of its energy to overcome the potential barrier at the boundary of the metal, in order to detach itself from that surface. This energy is called the work function of the photoelectron φ_0 and is expressed in electron-volts. Another part of the energy, however, is converted into the kinetic energy of this photoelectron $\frac{mv^2}{2} = Ue$.

According to the law of conservation of energy

$$\frac{mv^2}{2} = h\nu - e\varphi_0 \qquad (106)$$

or

$$Ue = h\nu - e\varphi_0 \qquad (107)$$

Equation (106) may be written in the form

$$h\nu = \frac{mv^2}{2} + e\varphi_0 \qquad (108)$$

Equation (108) is the fundamental equation of the extrinsic photoeffect and is sometimes called the first quantum relation.

If all the energy of the absorbed photon is expended in overcoming the potential barrier, and the velocity of the escaping photoelectrons is equal to zero, then

$$e\varphi_0 = h\nu_0 \qquad (109)$$

STAT

where ν_0 is the limiting frequency at which the electrons will leave the surface of the metal at zero velocity.

To the frequency ν_0 corresponds the wavelength λ_0, which is called the long-wave, or red, boundary of the photoeffect. The term "red boundary" is explained by the fact that, at longer wavelengths (in the direction of the red portion of the spectrum), no photoelectronic emission takes place.

From eq.(109) we obtain

$$\varphi_0 = \frac{h\nu_0}{e} = \frac{hc}{e} \cdot \frac{1}{\lambda_0} \qquad (110)$$

where c = speed of light;

λ_0 = long-wave (red) boundary of photoeffect.

Hence

$$\lambda_0 = \frac{c}{\nu_0} = \frac{hc}{e\varphi_0} = \frac{1236}{\varphi_0} \qquad (111)$$

It follows from eq.(111) that, at decreasing work function, the long-wave boundary shifts toward the red and infrared portions of the spectrum. At decreasing wavelength, the energy of the photon $h\nu$ increases, and, consequently, so does the yield of photoelectrons (photoelectric emission), but only up to a certain limit, after which the emission drops off again. This is explained by the fact that, at increasing frequency ν, the number of photons of the radiant flux with an energy W equal to $\frac{W}{h\nu}$ decreases and, consequently, the photocurrent also decreases. To reduce the work function, the absorption may be increased by depositing a monomolecular layer of atoms of an electropositive metal on the surface of the principal metal. In this case, between the principal metal and the surface layer of adsorbed atoms an intermediate layer is formed, usually in the form of an oxide of the principal metal. By varying the absorption, a different work function may be obtained so that the long-wave boundary may be modified. At small values of the coefficient of adsorption, which are characteristic of a pure metal, there exists the so-called normal photoeffect, in which the sensitivity increases exclusively with decreasing wavelength. At increasing coefficient of absorption, the selective photoeffect takes place: the photocurrent has a maximum in the spectral band of absorption of light by the adsorbed atoms of the electropositive metal.

The value and position of the selective maximum depends on the thickness of the intermediate layer and of the layer of electropositive metal, as well as on the valence of the metal.

The wavelength of the selective maximum may be determined by the empirical formula

$$\lambda_{max} = \frac{2\pi c}{\sqrt{\frac{e^2}{mr^2}}} \qquad (112)$$

where r = radius of electron, m = mass of electron.

The calculation results obtained from eq.(112) differ little from the experimental data.

The Quantum Equivalent

The number of electrons per unit of absorbed radiant energy increases by the law of the quantum equivalent (the second quantum relation), according to which one absorbed photon of radiant energy must liberate one photoelectron.

Assume that, in liberating N photoelectrons, forming a photocurrent, the radiant energy W, with a frequency of ν, incident on the surface of the photoelectric cathode, is absorbed.

Then the number of photoelectrons leaving the cathode on absorption of this energy will be equal to

$$N = \frac{W}{h\nu} \qquad (113)$$

where h = Planck's constant.

If each of the N absorbed photons liberates one photoelectron, then

STAT

$$N = \frac{W}{h\nu} = n \qquad (114)$$

It follows from eq.(114) that the number of photoelectrons liberated cannot be greater than $\frac{W}{h\nu}$.

Table 27

Energy of Photons (Quanta) and Quantum Equivalent

Wavelength, μ	Energy of Photons		Quantum Equivalent	
	ergs	volts	Number of electrons/erg	ma/watt
0.6	3.31×10^{-12}	2.06	3.02×10^{11}	484
0.75	2.65×10^{-12}	1.65	3.78×10^{11}	605
1.0	1.99×10^{-12}	1.24	5.04×10^{11}	807
1.5	1.32×10^{-12}	0.83	7.56×10^{11}	1210
2.0	0.99×10^{-12}	0.62	10.08×10^{11}	1614

If only a part η of the absorbed photons liberate photoelectrons, then

$$N = \eta n \qquad (115)$$

The photocurrent per unit energy absorbed is determined by the relation

$$i = \eta \frac{e}{h\nu} \cdot \frac{x}{d} = \eta \frac{e\lambda}{hc} \cdot \frac{x}{c} \qquad (116)$$

where d = electrode spacing of the photocell;

x = distance traveled by the photoelectrons.

Table 27 gives the values of the energy of photons (quanta) and of the quantum equivalent, for a few wavelengths.

The law of the quantum equivalent, in the general form, characterizes the intensity of the photoeffect.

On the basis of the law of the quantum equivalent, the quantum yield may be calculated if the spectral sensitivity of the photocell in absolute units is known.

Section 40. Long-Wave Boundary and Work Function

If the wavelength of a luminous flux incident on the surface of a photoelectric cathode is beyond the limits of the long-wave (red) boundary, then the energy of the light quanta becomes insufficient to enable the photoelectrons to leave the surface of the metal. This value of the energy determines the threshold of the photoeffect.

The work function for various metals is different. It depends on the position of the metal in the periodic system of the elements. The electron theory of metals permits an approximate determination of the law governing the work function φ_0 in pure metals on the basis of the quantative relation between the atomic weight M, the atomic number of the element Z, and the density of the substance D:

$$\varphi_0 = C \left(\frac{ZD}{M}\right)^{\frac{1}{3}} \qquad (117)$$

where C = factor of proportionality.

Table 28 gives the long-wave boundaries and values of the work function of the electrons for the most important pure metals.

The alkali and alkaline earth metals, particularly cesium, have the smallest work functions while combinations of cesium with cesium oxide have the smallest work function of all, amounting to about 1.0-0.7 v. This is the reason why a cesium surface is selected as the surface layer of photocathodes sensitive to both visible and infrared rays. Photocathodes of this type are used in so-called cesium photocells.

Section 41. The Contact Potential Difference

If two grounded surfaces having a different work function are placed in a vacuum and a radiant flux is directed onto them, then the photoelectrons emitted by the surface with the smaller work function will be concentrated on the surface with the higher work function.

As a result, the latter surface will be negatively charged with respect to the former, and an electric field will form in the photocell between the anode and

cathode, possessing different work functions. The potential difference, formed in this case on the surfaces, is called the contact potential difference and is equal

Table 28

Long-Wave Boundaries and Work Functions of Electrons of Pure Metals

Metal	λ_0 mμ	φ_e volts	Metal	λ_0	φ_e volts
Lithium	510-540	2.42-2.28	Thorium	336-370	3.68-3.34
Sodium	583-600	2.11-2.05	Germanium	255	4.85
Potassium	612-710	2.01-1.74	Tin	281-350	4.31-3.52
Rubidium	810	1.52	Lead	298-355	4.14-3.48
Cesium	630-900	1.96-1.87	Vanadium	326	3.78
Copper	266-303	4.63-4.07	Tantalum	297-315	4.15-4.92
Silver	258-268	4.78-4.61	Arsenic	236	5.23
Gold	252-260	4.9 -4.74	Antimony	307	4.02
Beryllium	374-399	3.17-3.3	Bismuth	278-330	4.44-3.74
Magnesium	330-450	3.74-2.74	Chromium	330	3.74
Calcium	385-510	3.2 -2.42	Molybdenum	258-297	4.33-4.15
Strontium	550	2.24	Tungsten	250-273	5.26-4.52
Barium	540-650	2.28-1.9	Selenium	220-267	4.62-5.61
Zinc	302-346	4.08-3.57	Manganese	328	3.76
Cadmium	305-330	4.05-3.75	Radium	248	4.97
Mercury	260-273	4.75-4.52	Iron	259-315	4.77-3.92
Aluminum	298-439	4.14-2.81	Cobalt	290-315	4.25-3.92
Gallium	291-300	4.2 -4.12	Nickel	246-336	5.01-3.68
Thallium	335-360	3.68-3.43	Rhodium	251	4.92
Titanium	313	3.95	Palladium	249-200	4.97-4.31
Zirconium	322-338	3.84-3.73	Platinum	185-280	6.67-4.4

to the difference between the work functions taken with reverse sign:

$$U_{p.d} = -(\varphi_c - \varphi_A) \qquad (118)$$

The maximum potential entering into eq.(107) is equal to the negative anode potential only where the work functions of the anode and cathode are equal. If, however, they are not equal, then the quantity $eU_{p.d}$ is added.

The measured maximum potential is thus

$$U_m' = \frac{h\nu}{e} - \frac{h\nu_0}{e} - U_{p.d} = \frac{h\nu}{e} - \varphi_c + \varphi_c - \varphi_A = \frac{h\nu}{e} - \varphi_A \qquad (119)$$

This equation shows that the quantity U_m' depends on the frequency ν and the work function of the anode φ_A, but does not depend on the work function of the cathode φ_c.

Section 42. The Total Photoelectric Emission

If a radiant flux emitted by a body at a temperature T strikes the surface of a photocathode, the total photoelectric emission can be determined from the equations

$$i_{ph} = A_{ph}T^d e^{-\frac{h\nu_0}{kT}} \qquad (120)$$

$$i_{ph} = A_{ph}T^d e^{-\frac{e\varphi}{kT}} \qquad (121)$$

where A_{ph} = constant of photoelectronic emission;

k = Boltzman constant, equal to 1.372×10^{-16} erg-deg;

d = an exponent (about 2);

e = the charge of the electrons;

e = the base of natural logarithms, equal to 2.718282.

Denoting $\frac{h\nu_0}{k} = \frac{e\varphi}{k}$ by the letter b, we obtain the formula

$$i_{ph} = A_{ph}T^d e^{-\frac{b}{T}} \qquad (122)$$

From this formula, the work function of photoelectronic emission can be determined if the value of the emission current has been measured.

Section 43. The Extrinsic Photoeffect in Complex Photocathodes

A metal plate or layer of pure metal on a glass base, with the surface of the metal oxidized and a layer of adsorbed atoms of an electrically positive metal on that surface, is called a complex photocathode.

In their electrical properties, coated photocathodes belong to the group of

STAT

semiconductors, since they have a negative temperature coefficient of resistance (i.e., their resistance decreases with increasing temperature).

The electrons of the lower filled zone (cf. Fig. 43,b) play the principal role in the formation of photoelectrons (photoelectronic emission). This follows from the fact that photoelectrons are formed when an electron absorbs the energy of a photon of a radiant flux, and therefore the maximum effect should be given by a zone where the greatest number of electrons is concentrated, i.e., the lower electron-filled zone.

In addition, the atoms of an alkali metal adsorbed on the surface of the photocathode participate in the formation of the photoelectronic emission.

In emissive photocells designed for operating in the infrared region of the spectrum, coated oxygen-cesium photocathodes are used, which consist mainly of three components: a metal base (substratum) of silver, an intermediate layer of cesium oxide, and a thin layer of atoms of the alkali metal cesium.

Such photocathodes, with the chemical formula [Ag] – O, Cs or, with a thicker intermediate layer, [Ag] – Cs_2O – Cs, have a long-wave boundary between 0.8 and 1.1μ and a maximum sensitivity around 0.62 μ, i.e., they possess sensitivity to the short-wave portion of the infrared spectrum.

At present, more sensitive oxygen-cesium cathodes are being built, in which the intermediate layer consists of cesium oxide (Cs_2O) with atoms of cesium and silver disseminated in it. The structure of such photocathodes may be represented by the formulas [Ag] – Cs_2O, Cs – Cs and [Ag] – Cs_2O, Cs, Ag – Cs.

Table 29 gives the values of the long-wave boundary λ_o and the spectral maximum λ_{max} for different oxygen-cesium photocathodes.

The possibility of constructing photocathodes from alloys must be pointed out. It has been found that photocathodes of high photoelectric sensitivity can be made from alloys of cesium with a metal of very low conductivity (for instance, Sb, Bi, Pb, Tl). Such photocathodes have a peculiar property: The metal of the base has no influence on their spectral sensitivity and modifies only the integral sensitivity.

Section 44. Types of Emissive Photocells

Depending on the filling of the tube and the design of the electrodes, emissive photocells can be divided into several groups. According to the filling of the tube,

Table 29

Long-Wave Boundary and Spectral Maximum of Coated Oxygen-Cesium Photocathodes

Cathode	λ_o μ	λ_{max} μ
[Ag] – O, Cs	0.8	0.35
[Ag] – Cs_2O – Cs	0.9 – 1.1	0.62
[Ag] – Cs_2O, Cs – Cs	1.1 – 1.2	0.7 – 0.8
[Ag] – Cs_2O, Cs, Ag – Cs	1.2 – 1.3	0.75 – 0.85

they may be divided into two groups: vacuum and gas-filled. In the tube of photocells of the former group, a high vacuum of 10^{-5} mm Hg is created. The tubes of photocells of the second group are filled with an inert gas.

In the design and arrangements of the electrodes, both groups are divided into photocells with a central anode, with a central cathode, with parallel or with symmetric electrodes.

Of all emissive photocells, only those with coated oxygen-cesium photocathode are indicators of infrared rays. We will, therefore, consider only these cells in the following.

Section 45. Principal Characteristics of Emissive Photocells

Emissive photocells have the following principal characteristics:

Integral sensitivity, representing the ratio of the photoelectric current in the circuit of the photocell to the power of the radiant energy incident on the photocathode, at a definite radiator temperature.

Integral sensitivity is expressed in $\frac{\text{amperes}}{\text{watts}}$ (amp/w). For the visible part of the spectrum, integral sensitivity is usually expressed in $\frac{\text{microamperes}}{\text{lumens}}$ (μ amp/lm).

STAT

Spectral sensitivity, determining the dependence of integral sensitivity, expressed in absolute or relative units, on the wavelength (frequency) of the incident radiation. The graph of spectral sensitivity is called the spectral characteristic of the photocathode.

Luminous characteristic, showing the dependence of the photocurrent on the incident radiant (luminous) flux at constant applied voltage.

Volt-ampere characteristic, showing the dependence of the photocurrent on the applied voltage.

Dynamic (or frequency) characteristic, determining the dependence of the variation in photocurrent or in sensitivity on the modulation frequency of the incident radiant flux.

Sluggishness or inertia, characterizing the time after which the photocurrent reaches its maximum value, measured from the beginning of irradiation of the photocathode surface by a constant radiant flux.

Threshold sensitivity, or energetic threshold, determining the minimum value of the power radiated in watts, which can be registered by the photocell.

Section 46. The Integral Sensitivity of Photocells

The integral sensitivity is due to the distribution of energy in the spectrum of the radiation source, since a radiant flux from sources at different temperatures produces a photocurrent of different value.

Quantitatively, the integral sensitivity is expressed as the area bounded by the curve obtained on multiplying the values of the spectral sensitivity of a photocell by the value of the energy for the spectrum of the radiation source.

In this way, to determine the integral sensitivity of a photocell when irradiated by a source of non-monochromatic radiation, it is necessary to construct the spectral sensitivity curve of the photocell expressed in absolute units, and the curve of energy distribution of the radiation source at a definite temperature, likewise in absolute units.

In its general form, a photocurrent is defined by the expression

$$i_{ph} = \eta \int_0^\infty S_\lambda f(\lambda,T)\,d\lambda \qquad (123)$$

where $\eta = \frac{N_a}{N_c}$ is the proportionality factor characterizing the electric properties of the photocell; (N_c = number of electrons emitted by cathode; N_a = number of electrons reaching the anode);

S_λ is the spectral sensitivity in amp/watt;

$f(\lambda,T)$ is the spectral energy distribution of the given radiator.

Since the quantities S_λ and η are strictly constant for a given photocell, they may be combined into a single parameter σ_λ, which is called the spectral efficiency of a photocell:

$$i_{ph} = \int_0^\infty \sigma_\lambda f(\lambda,T)\,d\lambda \qquad (124)$$

If the value of the photocurrent is related to the unit of incident energy, the lumen, then the integral sensitivity may be expressed by the formula

$$\varepsilon = \frac{\int_0^\infty \sigma_\lambda f(\lambda,T)\,d\lambda}{\frac{1}{M}\int_0^\infty K_\lambda f(\lambda,T)\,d\lambda} \qquad (125)$$

where $\frac{1}{M} = 670$ is the luminous equivalent of the radiant flux;

K_λ is the spectral visibility factor;

The numerator in eq.(125) is usually expressed in units of current, for instance in microamperes (μ amp) or in amperes (amp), while the denominator is expressed in units of radiant flux, usually in watts (w).

Since it is difficult to determine the value of σ_λ, the simpler formula

$$\varepsilon = \frac{I_{ph}r^2}{SI_a} = \frac{I_{ph}}{ES} = \frac{I_{ph}}{\Phi} \qquad (126)$$

is usually used for calculating the integral sensitivity.

Where I_{ph} = maximum photocurrent; for a vacuum photocell, the saturation current;

Φ = incident radiant flux in watts;

E = illumination in w/cm^2;

S = illuminated area of photocells in mm^2;

r = distance from radiation source to photocell in m;

I_s = luminous intensity of source in w/ster.

The values of the integral sensitivity of a few photocells produced in USSR are given in Table 30. The letters TsV denote oxygen-cesium vacuum photocells; the letters TsG, gas-filled photocells.

Table 30

Integral Sensitivity of a Few Photocells

Type	Integral Sensitivity, μ amp/lm	Useful Life, Hours
TsV-1	20	200
TsV-2	20	200
TsG-1	75	700
TsG-2	150	700
TsG-3	150	700
TsG-4	150	700

The data of Table 30 show that the integral sensitivity of vacuum photocells is considerably less than that of gas-filled photocells.

The integral sensitivity of gas-filled cells is increased by filling the tube with an inert gas, which leads to an increase of the photocurrent, due to an ionization of the gas by the photoelectrons moving from the photocathode to the anode.

Section 47. Spectral Characteristic of Photocells

The spectral characteristic is very important for proper selection of a photocell and a radiator. The maximum efficiency of a system photocell-radiator is obtained when the spectral sensitivity of the photocell corresponds to the spectral energy distribution of the radiator.

The determination of the spectral sensitivity in absolute units involves great difficulty, since up to now there is no satisfactory mathematical formula for calculating it. The spectral characteristic is therefore usually constructed in relative units. In this case, the greatest of the maxima is conventionally taken as 100%.

A cesium photocell has its maximum spectral sensitivity at 0.78 μ, while the

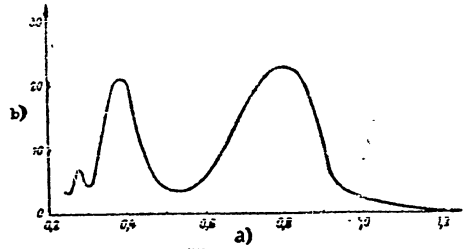

Fig. 44 - Spectral Sensitivity of a Cesium Photocell with Coated Cathode
a) Wavelength, μ, b) Photocurrent in relative units

red boundary of its spectral characteristic in the infrared region runs up to 1.2 μ.

Figure 44 gives the spectral sensitivity curve of a cesium photocell with coated cathode. As will be seen from the diagram, the spectral characteristic of a coated cesium photocathode has several maxima, which is explained by the complex chemical structure of the photocathode. The uniformity of the coating layer and the thickness of the intermediate layer are very important for the characteristic. When the thickness of the intermediate layer increases, the steepness of the maximum rises, but this leads to the phenomenon of photocathode "fatigue", which will be considered below.

The cesium photocell, as will be seen from the diagram, is rather sensitive to radiations of wavelengths up to about 0.9 μ, but its sensitivity drops sharply as the wavelength increases further.

STAT

Section 48. Gas Amplification

As pointed out above, the increase in integral sensitivity, or photocurrent, of a gas-filled photocell is accomplished by the ionization of a small amount of inert gas introduced into the tube. The process of gas amplification in general outline, is as follows:

When a radiant flux is incident on the surface of a gas-filled photocell, then the liberated photoelectrons, on their path from the cathode to the anode, collide

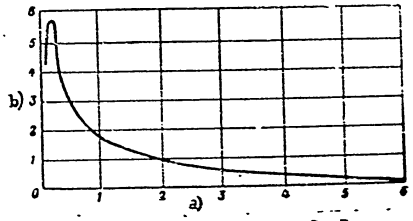

Fig. 45 - Relation of Photocurrent to Gas Pressure
a) Pressure, mm Hg; b) Photocurrent, μ amp

with neutral gas molecules. When an electron collides with a molecule, it becomes ionized, i.e., a positive ion and an electron are formed. As a result, two electrons will move toward the anode, while the positive ion will move toward the cathode. Successive collisions of electrons with the molecules of the gas lead to an avalanche of electrons, i.e., to an increase in total photocurrent. The photocurrent is also increased owing to bombardment of the photocathode surface by positive ions. This might increase the photocurrent by a factor of 5 to 7. Further increase leads to a rapid disintegration of the cathode.

The ratio of the current intensity I_{ph} (produced by the ionization) to the strength of the primary photocurrent I_0, is called the amplification factor:

$$\delta = \frac{I_{ph}}{i_0} \qquad (127)$$

The gas amplification factor depends on the design of the photocell, the kind of gas, and its pressure.

The gas charging the photocell must not interact with the photosensitive layer of the photocell nor with the glass of the tube. The ionization potential of the gas must be low, so as to facilitate ionization. The inert gases meet these requirements.

Photocells are most often filled with argon, which is the cheapest gas and easily obtainable.

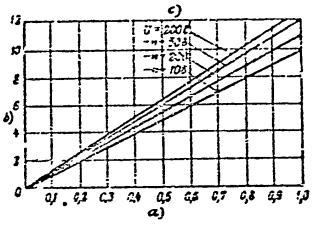

Fig. 46 - Luminous Characteristics of Vacuum Oxygen-Cesium Photocell at Various Voltages
a) Luminous flux, lm; b) Photocurrent, μ amp; c) U = 200 volts

The pressure of the gas in the photocell is about 0.2 mm Hg. When the gas pressure is decreased, the collision probability between electrons and molecules diminishes, since the distances between them increase.

With increasing pressure, on the other hand, the electrons may collide with molecules without imparting sufficient energy for ionization.

Figure 45 gives the curve of relation between photocurrent and gas pressure. At a pressure of 0.2 mm Hg, the so-called "Stoletov maximum" is obtained. Its position is determined by the length of the mean free path of the electron between two collisions, and depends on the design of the photocell.

Gas amplification also has its unfavorable properties: the linearity of the luminous characteristics is destroyed and sluggishness of the photocurrent results.

Section 49. Luminous Characteristics of Photocells

Luminous Characteristics of Vacuum Photocells

Equation (103) expresses the proportionality of photocurrent to the luminous flux incident on the surface, or illumination. This linear relation is valid only

for relatively small luminous fluxes.

Figure 46 gives the luminous characteristics of a vacuum oxygen-cesium photocell at various voltages. The curve shows that, at an insignificant luminous flux, the linear relation i = f(F) holds strictly, regardless of the voltage.

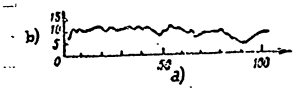

Fig. 47 - Distribution of Sensitivity of an Oxygen-Cesium Cathode along its Surface
a) Distance along surface, mm; b) Sensitivity

With increasing luminous flux the linear relation is disturbed due to the formation of charges on the walls of the tube and the formation of a space charge, as well as due to the influence of "fatigue".

It must be borne in mind that a photocathode is not uniformly sensitive at various points of its surface.

Figure 47 shows the curve of variation in sensitivity for various points of an oxygen-cesium cathode, obtained by N.S.Khlebnikov and N.S.Zaytsev. The curve shows irregular distribution of sensitivity along the surface of the photocell.

Luminous Characteristics of Gas-Filled Photocells

In gas-filled photocells, the relation of photocurrent and luminous flux is likewise nonlinear.

The luminous characteristics of a gas-filled photocell, taken at various voltages (Fig. 48), show that, at increasing applied voltage, the nonlinearity of the characteristics increases. This has to do with the increased ionization and the approach to a state of independent gaseous discharge with increasing voltage.

At small luminous fluxes (up to 0.1 lm), the linear dependence i = f(F) holds rather strictly for gas-filled photocells.

Section 50. Volt-Ampere Characteristics of Photocells

Volt-Ampere Characteristics of Vacuum Photocells

In vacuum photocells of any design the volt-ampere characteristic reaches saturation at some definite anode voltage. Figure 49 shows the volt-ampere characteristics of an oxygen-cesium vacuum photocell at various luminous fluxes. The

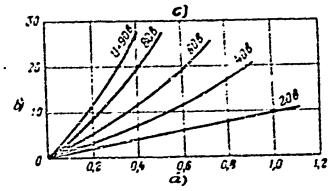

Fig. 48 - Luminous Characteristics of a Gas-Filled Photocell at Different Voltages
a) Luminous flux, lumen; b) Photocurrent, μ amp; c) U = 90 volts

curves show that the saturation current is reached at a plate voltage from 50 to 100 volts.

In photocells with a central cathode, saturation sets in at a low voltage, since all electrons rapidly reach the surface of the anode, which surrounds the cathode. In photocells with a central anode, saturation is reached at a higher voltage (50-100 v), since the electrons leave the surface of the cathode in all directions and therefore the electric field must be relatively powerful to direct the electrons toward the anode.

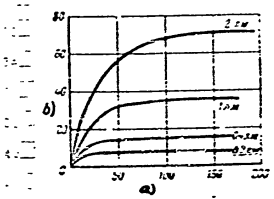

Fig. 49 - Volt-Ampere Characteristics of an Oxygen-Cesium Vacuum Photocell at Various Luminous Fluxes
a) Voltage, volts; b) Photocurrent, μ amp

With increasing luminous flux, the saturation current, and the corresponding plate voltage corresponding to it, increase.

Volt-Ampere Characteristics of Gas-Filled Photocells

In contrast to the volt-ampere characteristics of vacuum photocells, the volt-ampere characteristics of gas-filled photocells do not reach saturation (Fig. 50).

The photocurrent increases with increasing anode voltage. At a voltage above 320 v, a transition of the nonindependent gas discharge to an independent takes place. The

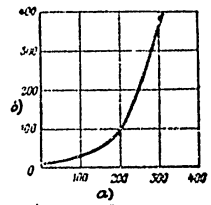

Fig. 50 - Volt-Ampere Characteristic of a Gas-Filled Photocell
a) Voltage, v; b) Photocurrent, μ amp

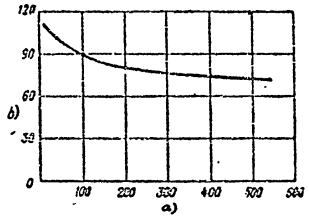

Fig. 51 - Relation of Ignition Potential and Illumination
a) Illumination, lux; b) Ignition potential U_i, volts

latter is characterized by luminescence of the gas in the photocell, with the value of the current not depending on the luminous flux and being determined only by the value of the external resistance in the circuit. The voltage at which the nonindependent discharge changes to an independent is called the ignition potential of independent discharge. The ignition potential decreases with increasing illumination (Figure 51) and with the gas pressure (Fig. 52).

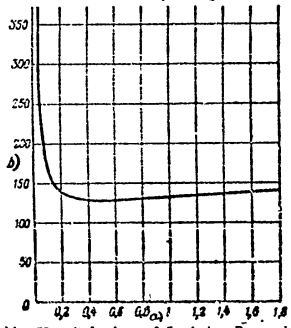

Fig. 52 - Relation of Ignition Potential to Gas Pressure
a) Pressure, mm Hg; b) Ignition potential U_i, volts

In the region of the ignition potential of the independent discharge, the operation of the photocell is unstable, its sluggishness increases, and its "fatigue" grows. The working point on the volt-ampere characteristic must therefore be selected around 240-250 v; at this voltage, the photocell will operate stably.

Section 51. Frequency Characteristics and Sluggishness of Photocells

The frequency characteristic permits judging the suitability of a photocell for operation with a modulated flux.

Vacuum photocells are inertialess in the range from audio frequencies to frequencies of the order of 2×10^3 cps. The region of frequencies at which sluggishness begins to appear depends on the velocities of the electrons in the inter-

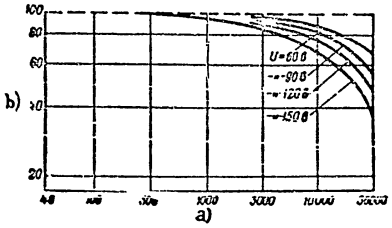

Fig. 53 - Frequency Characteristic of an Oxygen-Cesium Photocell Filled with Argon at Various Voltages
a) Frequency ν, cps; b) Photocurrent, %; c) U = 60 volts

electrode space. Since there is no gas in a vacuum photocell, the electrons travel to the anode without colliding with molecules. Their velocity is very high, and the transit time is about 10^{-8} sec. Until the frequency of modulation of the incident light becomes comparable with the velocities of the electrons, a vacuum photocell may be considered free of sluggishness.

Gas-filled photocells, at working voltages below the ionization potential, are also inertialess. Only when the voltage becomes higher than the ionization potential does the phenomenon of sluggishness occur, due to the formation of positive ions.

The sluggishness of a photocell can be determined by the fact that an instantaneous or intermittent irradiation of the photocell by a radiant flux of certain frequencies, will not result in an instantaneous rise of the photocurrent to its normal value; also, when the cell is darkened the photocurrent does not drop instantly but only after a certain interval of time.

This delayed drop in photocurrent is due to recombination, a process which takes a certain time. In addition, when a photocell is irradiated, not only ions but also metastable atoms, which persist for a period of about 10^{-3} sec, are formed. These atoms are able to ionize the admixtures of foreign gas, always present in the tube, whose ionization potential is usually lower than the ionization potential of the principal gas. This additional ionization also affects the time of the current drop.

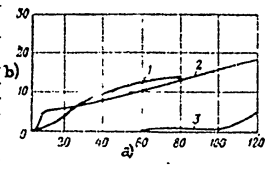

Fig. 54 - Relation of Sluggishness of Gas-Filled Photocells to the Applied Voltage and Type of Gas: 1- Filled with neon; 2- Filled with helium; 3- Filled with argon
a) Applied voltage, volts;
b) Sluggishness d, %

Figure 53 shows the frequency characteristics of an oxygen-cesium photocell filled with argon, for various values of the applied voltage. As indicated by the diagram, an increase in voltage leads to a sharper downtrend of the curve, which is explained by the increase in ionization, i.e., by the increase in the number of positive ions.

The sluggishness is defined as the ratio of the amplitude difference of the AC voltages A_{v1} and A_{v2} at the output of the photocell (or amplifier) when the frequency varies within the limits from ν_1 to ν_2, to the amplitude of the voltage A_{v1}:

$$d = \frac{A_{v1} - A_{v2}}{A_{v1}} 100\% \qquad (128)$$

where ν_1 = frequency at which the photocell is inertialess;

ν_2 = frequency for which the sluggishness of the photocell is being determined.

The value of d depends on the voltage applied to the photocell, and on the kind of gas filling the tube.

Figure 54 gives curves showing this relation. The values of d are plotted in percent on the ordinate, and the applied voltage on the abscissa. Curves 1, 2, and 3 are constructed for photocells filled respectively with neon, helium, and argon. For argon the value of d is greatest and is, therefore, most often used for filling photocells.

Section 52. Photoelectric "Fatigue" of Photocells

The reduction in sensitivity of a photocell (decrease in photocurrent) on prolonged irradiation of the photocathode, is called "fatigue" of a photocell.

Fatigue is due to the fact that the number of adsorbed atoms formed on the surface of the photocathode, and consequently also the value of the photocurrent, decrease on prolonged irradiation. The same phenomenon is produced by bombardment of the photocathode by the ions of the gas filling the photocell tube.

Vacuum photocells are also subject to fatigue produced by the liberation of gas by the inside walls, the presence of residual gases, and the infiltration of gas through the leads.

Photocells with solid cathodes of pure metal have relatively low fatigue, but their sensitivity is also low. Photocells with coated cathodes are highly susceptible to fatigue.

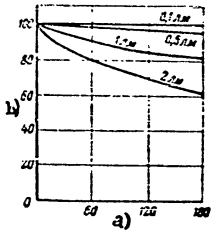

Fig. 55 - "Fatigue" of an Oxygen-Cesium Photocell at Various Luminous Fluxes
a) Time, hours; b) Sensitivity, %

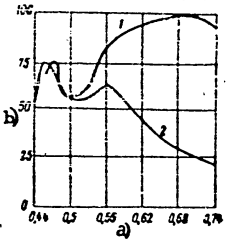

Fig. 56 - Spectral Sensitivity of an Oxygen-Cesium Photocell:
1- Before fatigue; 2- After fatigue;
a) Wavelength, μ; b) Sensitivity, %

Figure 55 gives curves showing the decrease in sensitivity of a vacuum oxygen-cesium photocell (fatigue) at various luminous fluxes. The greatest fatigue of coated photocathodes is caused by short-wave rays, particularly ultraviolet rays, and the least, by infrared rays.

In time, the spectral sensitivity of photocells changes. For example, a comparison of the spectral characteristic of an oxygen-cesium photocell (Fig.56) before the onset of fatigue (Curve 1) with its same characteristic after fatigue (Curve 2) shows that a particularly sharp drop in sensitivity takes place on transition to the infrared region. This is confirmed by the curves in Fig. 57, which show that, after fatigue, the sensitivity to infrared rays decreases considerably faster than the sensitivity to visible rays.

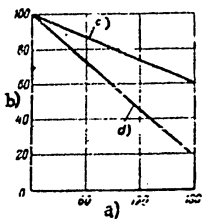

Fig. 57 - Influence of Fatigue on Spectral Sensitivity
a) Time, hours; b) Sensitivity, %; c) Visible rays; d) Infrared rays

Section 53. Sensitivity Threshold of Photocells

For each photocell there exists an upper limit of illumination. If the illumination exceeds this limit, then the photocell operates unstably and its life is considerably shortened.

Besides the upper limit of illumination, a photocell also has a sensitivity threshold, which is determined primarily by the noise level in the photocell-power supply circuit.

We know from statistical physics that, even in the stationary state, a number of parameters such as temperature, electric current, voltage and certain others, are not strictly constant, but continuously fluctuate about their mean values. Such fluctuations of the properties with respect to their mean values (fluctuations) produce random voltages ("hum") in the circuit of a photocell, restricting the lower limit of illumination. The minimum illumination must be such that the resultant output voltage will exceed the noise level by not less than 1.5 to 2 times.

The electrical circuit of photocell-external load contains certain noise sources.

Part of the electrons move toward the anode at random, rather than in a linear manner. This accelerates the variation in their number in unit time, causing fluctuations in the anode current, which are also called noise. The phenomenon of fluctuations in current, known as shot effect, is one of the noise sources. In zones of saturation current, the noise current i_n of a photocell due to the shot effect, is determined by the formula

$$i_n^2 = 2eI\Delta f \qquad (129)$$

where I = saturation current, in amp;

Δf = width of amplification frequency band in cycles;

e = charge of an electron.

It follows from this formula that the noise current at saturation current is the same for equal frequency intervals, provided that the fluctuation period is small by comparison with the transit time of the electrons.

A second source of noise is the so-called flicker effect, observed mostly in coated cathodes and at high value of the photocurrent.

This effect is produced by fluctuations in the photocurrent due to increased electron density. In vacuum photocells, with their low photocurrents, the flicker effect is weak.

A third source of noise is the external load in the photocell circuit. As a result of the chaotic thermal motion of the electrons at the ends of the resistor, an alternating electromotive force (emf) arises.

The voltage of this thermal noise or thermal agitation is determined by the formula

$$e_t^2 = 4KTR\Delta f \qquad (130)$$

and the current of the thermal noise by the formula

$$i_t^2 = 4KT\frac{\Delta f}{R} \qquad (131)$$

where K = Boltzmann constant;

T = absolute temperature;

Δf = width of frequency band of the amplifier;

R = load resistance.

The threshold of sensitivity is determined by the leak current and the dark current. The leak current in emissive photocells amounts to 10^{-12} amp, and the dark

current to about 10^{-15} amp. Consequently, the sensitivity threshold is practically determined by the leak current (if it is not compensated).

Figure 58 shows the characteristic curve of the relation between the amplitude of the noise voltage and the applied voltage for a gas-filled photocell.

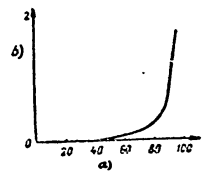

Fig. 58 - Relation between the Amplitude of Noise Voltage and the Applied Voltage for a Gas-Filled Photocell
a) Applied voltage, v;
b) Amplitude of noise voltage, v

To evaluate the noise level, the voltage obtained at the amplifier output, or the so-called distortion voltage, is used. This should be several times lower than the output voltage of the useful signal.

Section 54. Voltage Sensitivity

The potential difference U, generated across the external resistor connected in series with the photocell on irradiating the photocell by unit radiant flux is called the voltage sensitivity φ. Thus $\varphi = \frac{dU}{d\Phi}$.

The sensitivity of a photocell to voltage depends on its integral sensitivity ε and on the value of the external load resistance R. The maximum voltage sensitivity is obtained when the external resistance equals the internal resistance of the irradiated photocell.

The voltage drop across the load resistance R is equal to

$$U = i_{ph}R = \varepsilon \Phi R \qquad (132)$$

since, according to eq.(103), the photocurrent $i_{ph} = \varepsilon\Phi$.

By differentiating eq.(132) with respect to Φ, we find the following formula for the voltage sensitivity

$$\varphi = \frac{dU}{d\Phi} = R\left(\varepsilon + \Phi \frac{d\varepsilon}{d\Phi}\right) \qquad (133)$$

For a gas-filled photocell

$$\varphi = \frac{dU}{d\Phi} = \frac{R\varepsilon}{1 + R\Phi \frac{d\varepsilon}{de}} \qquad (134)$$

where $e = E - i_{ph}R$.

For a vacuum photocell operating under saturation conditions, we have

$$\varphi = \frac{dU}{d\Phi} = R\varepsilon \qquad (135)$$

Section 55. Current Sensitivity

Current sensitivity is the magnitude of the photocurrent produced on irradiation of a photocell by unit monochromatic radiant flux:

$$\gamma = \frac{i_{ph}}{\Phi} \text{ amp/watt}$$

The value of the photocurrent depends on the ratio of the number of electrons reaching the anode (N_a) to the number of electrons leaving the cathode (N_c). The photocurrent is greatest when the values of N_a and N_c are equal; consequently, the current sensitivity reaches its maximum value under the condition that all the energy of the radiant flux is absorbed by the photocell and that all the photoelectrons leave the surface of the cathode.

Section 56. Design of Emissive Photocells

Photocells with a central cathode are used rarely, and only when a saturation current must be obtained at low voltage.

The design of a photocell with central cathode is schematically shown in Figure 59. The anode A consists of a small grid covering the inner glass wall of the tube. The anode must be transparent and must pass the maximum possible amount of radiant energy to the cathode. The cathode K has various shapes, most often that of a metal plate or sphere, coated with a photosensitive layer.

A photocell with central anode has a cylindrical or spherical tube (Fig.60). A photosensitive layer applied to the inner surface of the tube serves as the

hode K. The anode A has the form of a rod (in cylindrical photocells), of a ere, or a loop (in spherical photocells). Anodes in the form of wires, r... s, or

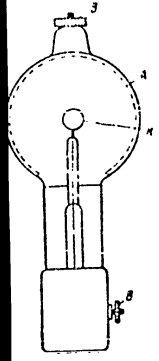

.59 - Photocell with Central Cathode; Anode; K- Cathode; Terminals of anodes and cathode

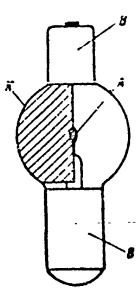

Fig. 60 - Photocell with Central Anode; A- Anode; K- Cathode; B- Leads of anode and cathode

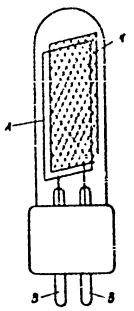

Fig. 61 - Photocell with Plane-Parallel Electrodes; A- Anode; K- Cathode; B- Lead-Out Pins

ds of nickel or copper are also often used. This eliminates the influence of the rges formed on the nonconducting part of the inner surface of the tube. These

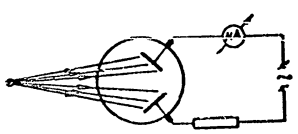

Fig. 62 - Photocell with Symmetric Electrodes

rges are generated as a result of the fact that part of the photoelectrons fly t the anode and settle on the surface of the tube not covered by a photosensitive layer (the light-admitting window).

A photocell with plane-parallel electrodes (Fig. 61) has electrodes in the form of flat plates arranged parallel to each other. A peculiarity of photocells of this type is the uniformity of the electric field between the electrodes. This produces favorable operating conditions for the photocathode.

A photocell with symmetric electrodes (Fig. 62) has electrodes of the same dimensions and photosensitivity. Under uniform irradiation of both electrodes, the resistance of the photocell circuit decreases. The advantage of these photocells is their ability to pass alternating current; all other photocells, when connected in an AC circuit, pass current only in one direction.

STAT

CHAPTER VI

PHOTOCELLS WITH INTRINSIC PHOTOEFFECT (PHOTORESISTANCE)

Section 57. Intrinsic Photoeffect in Semiconductors

The increase in electric conductivity of a substance under the action of incident radiant energy at constant temperature is called the intrinsic photoeffect. The intrinsic photoeffect is observed in dielectrics and semiconductors. Only in semiconductors does this effect become so pronounced in the visible region, and particularly in the infrared region, of the spectrum that it can be utilized for practical purposes.

Table 31

Classification of Substances According to Electrical Properties

Substance	Resistance per cm^3 ohms	Carrier of Electricity	Temperature Coefficient
Metals	$< 10^{-4}$	Electrons	"+"
Semiconductors:			
electrolytes	$> 10^{-4}$	Ions	"+"
crystals	$< 10^{10}$	Electrons and ions	"−"
Dielectrics	$> 10^{10}$	-	"−"

In their electric properties, semiconductors are substances intermediate between metals and dielectrics. There is no sharp boundary between these three groups, but it is customary to classify them according to the value of their resistances (see Table 31).

Semiconductors are substances having a resistance not less than 10^{-4} and not more than 10^{10} ohms/cm^3.

In semiconductors, as already stated (cf. Fig. 43 b), the forbidden zone is of small width, and when the energy of a photon is absorbed, electrons may pass from the lower filled zone to the upper free zone. An electron that has passed into the upper zone leaves behind it a vacant place, having a positive charge. Such a place is called "a positive hole". Its charge is numerically equal to the charge of an electron.

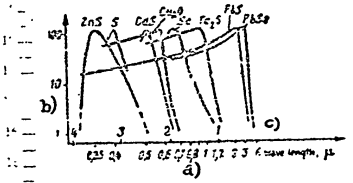

Fig. 63 - Relation of Spectral Sensitivity of Certain Semiconductors and Energy of the Quanta
a) Wavelength, μ; b) Sensitivity in relative units; c) Energy of quanta, in electron-volts

Consequently, to each electron passing into the upper zone there must correspond a "positive hole" in the lower zone. This occurs in semiconductors only at high temperatures, when the passage of electrons from zone to zone is facilitated.

At room temperature, the conductivity of semiconductors is explained by the presence of impurities, which disturbs the electric fields linking the atoms in the crystalline structure of the semiconductor. The presence of impurities leads to the appearance in the forbidden zone of allowed energy levels called "Tamm levels" after the Soviet scientist who investigated this phenomenon. In outline, the mechanism of the intrinsic photoeffect is as follows: On absorption of the energy of quanta of a radiant flux by the atoms of a semiconductor, electrons are liberated from the crystal lattice and, under the action of the applied voltage, move in the direction of the electrode having the positive potential. As a result, a primary electronic photocurrent is produced.

The positive charges move toward the electrode having the negative potential. The current produced by their motion is called secondary. The sharply increased sensitivity of semiconductors to infrared rays, by comparison with photocathodes

STAT

operating on the principle of the extrinsic photoeffect, is explained by the fact that in semiconductors the energetic distance between a field and a free zone is small, since all the process takes place inside the substance. Naturally, a smaller amount of energy is required to displace an electron from zone to zone than to overcome the potential barrier and cause the electron to fly beyond the surface, in the external photoeffect.

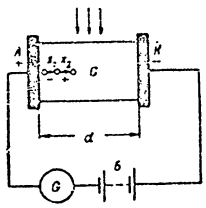

Fig.64 - Schematic Process of Internal Photoeffect

Of all semiconductors with photoelectric effect, the minerals are of greatest interest, for example silver blende or argentite (Ag_2S), lead blende or galena (PbS), molybdenum blende or molybdenite, bismuth blende or bismuthinite (Bi_2S_3), and inorganic compounds, for example a mixture of thallium sulfide and thalium oxide, a selenium-tellurium alloy.

Figure 63 shows the relation of the spectral sensitivity of certain semiconductors to the energy of the quanta (or to the radiation wavelength). The diagram shows that semiconductors possess high sensitivity to infrared rays of wavelengths up to 5-6 μ.

Section 58. Currents of the Intrinsic Photoeffect

The photoelectric process in semiconductors begins under the action of a radiant flux which causes generation of the primary electronic photocurrent i_p, arising as a result of the motion of the electrons liberated by the quanta of the radiant flux.

The process taking place in the internal photoeffect is demonstrated in Fig.64, which shows a semiconductor C, placed between two electrodes A and K. The voltage on the electrodes is imposed by the battery B. The galvanometer G serves to measure the current arising on irradiation of the semiconductor.

The absorption of the energy of the radiant flux by the crystal leads to the formation of positive charges which are displaced, under the action of the applied field, toward the electrode K, by a distance x_2, and to the formation of negative charges, which are displaced toward the electrode A by a distance x_1. On motion of the charges toward the electrode A, a primary current is produced, while on their motion toward the electrode K, a secondary current is generated. On the electrodes there arises the charge

$$Q = \frac{eN}{d}(x_1 - x_2) \qquad (136)$$

where d = electrode spacing;

x_1 = distance by which the negative charge is displaced;

x_2 = distance by which the positive charge is displaced;

N = number of electrons liberated.

If, in unit time, N' moving charges are formed, then the primary photocurrent will be

$$i_a = \frac{eN'}{d}(x_1 + x_2) \qquad (137)$$

It has been found that the primary photocurrent arises about 10^{-4} sec after the beginning of irradiation, i.e., its sluggishness is low. The primary current is strictly proportional to the radiant flux and, at increasing applied voltage, approaches the saturation current as its limit. A comparison of primary photocurrent in the saturation region with the energy of the absorbed radiation shows that the law of the quantum equivalent is valid here: In the region of saturation, each absorbed quantum of energy hν causes the appearance of one photoelectron.

In addition to the primary current there is also a secondary current whose nature has not been established exactly. It is assumed to result from the disturbance of the crystalline structure of the semiconductor by the passage of the primary current, which reduces the resistance of the semiconductor. The magnitude of the secondary current is usually greater than that of the primary current, and it has a greater inertness. Not being produced as a direct result of irradiation, this current is not proportional to the incident radiant flux, but depends strongly in magnitude on the applied voltage and the temperature of the semiconductor.

If the semiconductor element is supplied with an external voltage U, then, the

liberation of electrons from their places causes a dark electronic current to flow from the disturbed crystal structure, in the absence of irradiation:

$$i_d = j \frac{q}{l} U \tag{138}$$

where j = electric conductivity;

q = surface of electrodes;

l = electrode spacing.

When a semiconductor is irradiated, the conductivity G is increased, which may be determined from the expression

$$G = ne\tau v \tag{139}$$

where e = charge of the electron;

τ = mean duration of excited state of an atom;

v = velocity of the electron;

n = number of places in disordered structure.

The current increment Δi which appears on irradiation is calculated by the formula

$$\Delta i = \frac{ne\tau v}{ql} \frac{q}{l} U = \frac{ne\tau v}{l^2} U \tag{140}$$

From eq.(140) the following conclusions may be drawn:

The dark current i_d and the increment of photocurrent on irradiation obey Ohm's Law;

The photocurrent is proportional to the number of places with a disordered crystal structure;

The photocurrent is inversely proportional to the square of the distance between the electrodes.

The photocurrent i_{ph}, corresponding to the incident radiant flux, is defined by the formula

$$i_{ph} = \Delta i - i_d \tag{141}$$

The principal portion of the current Δi is formed by the secondary current, so that the current Δi is not proportional to the incident radiant flux.

The value of the photocurrent i_{ph} is determined as a function of the incident radiant flux by the formula

$$i_{ph} = \alpha \sqrt{\Phi} \tag{142}$$

where α = the proportionality factor;

Φ = radiant flux.

It follows from eq.(142) that the photocurrent increases proportionally to the square root of the radiant flux.

In this case, eq.(141) and eq.(142) give the additional current

$$\Delta i = i_d + \alpha \sqrt{\Phi} \tag{143}$$

The relation between the photocurrent and the time of illumination is expressed by the formula

$$i_{ph} = \Delta i - i_d (1 - e^{-kt}) \tag{144}$$

where k = an expirical coefficient;

t = time from beginning of irradiation during which the photocurrent reaches its limiting value;

e = base of natural logarithms.

If a semiconductor is connected in series with a battery and a measuring instrument, as shown in Fig.64, then the photocurrent

$$i_{ph} = U(G_d + \beta \sqrt{\Phi}) \tag{145}$$

where U = voltage of the battery;

G_d = dark conductivity;

$\beta \sqrt{\Phi}$ = increment of conductivity on irradiation;

β = constant coefficient.

STAT

Using eq. (143), the integral sensitivity may be determined as

$$\varepsilon = \frac{di}{d\Phi} = \frac{\alpha}{2\sqrt{\Phi}} \qquad (146)$$

The conductivity increment per unit flux, on irradiation, is

$$x = \frac{d(\beta\sqrt{\Phi})}{d\Phi} = \frac{\beta}{2\sqrt{\Phi}} \qquad (147)$$

Equation (145) yields the integral sensitivity

$$\varepsilon = \frac{di}{d\Phi} = \frac{U\beta}{2\sqrt{\Phi}} \qquad (148)$$

If the load resistance R, commensurable in value with the resistance of the photocell, is connected in the circuit of phe photocell, then ε diminishes.

Section 59. Characteristics of Photocells with Intrinsic Photoeffect

The principal characteristics of photocells of this group, as for photocells extrinsic-photoeffect, are spectral characteristic, integral sensitivity, threshold of sensitivity, frequency, volt-ampere, luminous characteristics, voltage sensitivity, and current sensitivity. There is, however, a difference in the definition of characteristics such as integral sensitivity and sensitivity threshold.

For photocells with intrinsic photoeffects, the integral sensitivity ε can be defined as the decrease in the resistance of the semiconductor R_c under the action of irradiation by a definite radiant flux Φ at a given radiator temperature, related to the resistance R_d of the nonirradiated semiconductor

$$\varepsilon = \frac{R_d - R_c}{R_d} 100\%/\Phi \qquad (149)$$

Such an expression for the integral sensitivity is more accurate, since the sensitivity there is defined as a quantity independent of the connection conditions.

The sensitivity can also be defined as the ratio of the amplitude of the alternating signal U, arising on the input resistor of the amplifier, to the value of the luminous flux Φ causing this signal. In this case, the sensitivity is expressed in volts per watt (v/w).

The threshold sensitivity characterizes the minimum radiant flux which produces, in the photocell circuit, an electric signal 2-3 times greater in value than the signal due to the inherent noise of the photocell, caused by the discrete nature of electricity.

The noise voltage may be found from the expression

$$U_n = \sqrt{4kTR\Delta f} \qquad (150)$$

where k = Boltzmann constant;

T = absolute temperature;

R = resistance;

Δf = width of pass-band of amplifier.

The threshold sensitivity is less, the lower the noise level becomes.

In addition, photocells with intrinsic photoeffects are characterized by the temperature dependence, indicating the influence of the temperature on the photocell characteristic.

Section 60. Types of Photoresistance Cells

Photocells with intrinsic photoeffect are usually called photoresistors, since this term characterizes the basic process taking place in such cells, namely the variation in resistance under the action of a radiant flux. All photoresistors are sensitive to infrared rays. At present, selenium, selenium-tellurium, thallium-sulfide, lead-sulfide, lead-selenide and lead telluride photoresistors are used in technology. Let us consider the peculiarities and characteristics of each of these photoresistors.

Section 61. Selenium Photoresistors

The first model of a selenium photoresistor was built in 1876. It consisted of two wires, spirally wound on sheet mica (Fig. 65 a). To impart photosensitivity to the selenium cell, molten selenium was poured on the mica and wire, which were

then heated for several hours at 200°C.

Wire resistors with an unglazed porcelain core were built later. The surface of the core had a double screw thread on which two platinum or iridium wires were

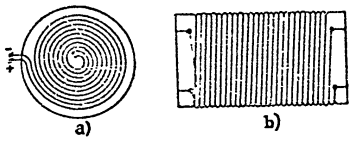

Fig.65 - Wire Photoresistors:
a) Wound on sheet mica; b) With a porcelain core

spirally wound (Fig.65,b). The spaces between the wires were coated with molten selenium.

Photoresistors of the condenser type (Fig.66) were built later, with more success, using a design resembling that of conventional mica capacitors. Plates of

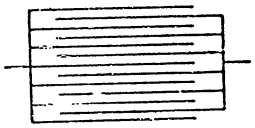

Fig.66 - Condenser Photoresistor

Fig.67 - Engraved Photoresistor

metal foil, connected by a "comb" and covered with selenium, were pressed on the surfaces of mica plates of such photoresistors. The drawbacks of such photoresistors lie in their high capacitance and in the dependence of the photocurrent on the modulation frequency of the incident irradiation.

The etched selenium photoresistor (Fig.67) is an improved design. The electrodes (E_1 and E_2) are prepared by precipitating a thin film of gold on a glass or graphite plate. The narrow strips of gold removed by a sharp tool, form a grid. The space between the electrodes is filled with a thin layer of selenium. The advantage of this photocell over the ones described above consists in their increased sensitivity and lower capacitance.

The comb construction of selenium and other photoresistors (Fig.68) is widely used. This design consists of the glass plate (1), on which a gold grid has been applied by heating, or on which the grooves (2) in the form of interlinked "combs" have been etched. The distance between the grooves is 0.1 mm, and their length 10 cm. The depressions of the grooves are filled with gold, graphite, or other conducting substance, covered with a layer of selenium about 2.5×10^{-3} cm in thickness. The plate with the electrodes is inserted in a tube. In building photoresistors, the selenium surface is first

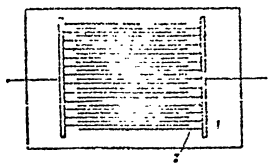

Fig.68 - The Comb-Type Photoresistor:
1- Glass plate; 2- Grid-lines

formed in vacuo; during the firing process, an inert gas is introduced into the tube. This considerably increases the stability of operation of the photoresistor*, while the temperature fluctuations are reduced.

The sensitivity of a photoresistor is expressed in percent [cf.eq.(142)], or in amperes per watt of incident radiant flux. When the resistance varies from the dark resistance (R_d) equal to a few megohms, to the light resistance (R_c) equal to a fraction of a megohm, the sensitivity of the photoresistor varies by tens of percent.

The determination of sensitivity in terms of percentage fluctuation in resistance is not always useful. It is incorrect to determine the sensitivity in microamperes per lumen, since the photoresistances react to a radiant flux over a wide spectral range, and not merely to the luminous flux. For this reason, in measuring sensitivity in absolute units, the sensitivity is expressed by the ratio of the photocurrent strength (amp) to unit power of incident radiant flux (watt).

Spectral Sensitivity. The distribution of the spectral sensitivity of a

* Apparently the instability in the operation of photoresistors is due to the action of oxygen (both during manufacture and during operation). For this reason, the forming of the selenium surface in vacuo and the filling of the bulb with an inert gas favor increased stability.

STAT

selenium photoresistor is shown in Fig.69. The diagram shows that, at low illumination (Curve b), there are no pronounced maxima of sensitivity; at illuminations of

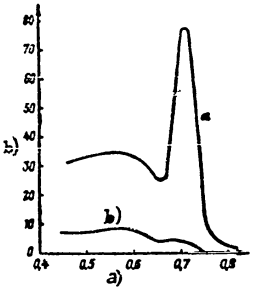

Fig.69 - Distribution of Spectral Sensitivity of Selenium Photoresistors
a- At high illumination; b- At low illumination
a) Wavelength, μ; b) Photocurrent in relative units

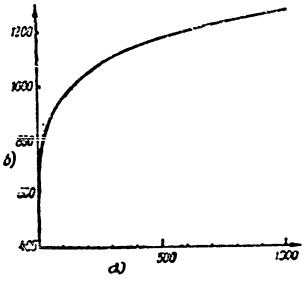

Fig.70 - Relation of Photocurrent of Photoresistor and Illumination
a) Illumination, lux; b) Total photocurrent, μ amp

over 100 lux (Curve a), there is a sharp maximum in the region $\lambda = 0.7$ μ and a weak maximum in the region $\lambda = 0.5$-0.6 μ.

Luminous Characteristics. In photoresistors, only the primary component of the photocurrent depends linearly on the illumination. When a secondary current arises, this proportionality no longer applies. This is illustrated in Fig.70, in which the total photocurrent i is plotted as a function of the illumination E.

The total photocurrent is related to the illumination by the equation

$$i = CE^x \qquad (151)$$

where C = a constant;

x = an exponent depending on the properties of the photoresistor and the wavelength of the incident light.

The relation between the increment in conductivity (reduction of resistance) and the illumination is expressed by the formula

$$\Delta G = \frac{1}{R_c} - \frac{1}{R_d} = \beta E^x \qquad (152)$$

For a selenium photoresistor, the exponent x in this formula is about 0.5, whence

$$\Delta G = \frac{1}{R_c} - \frac{1}{R_d} = \beta \sqrt{E} \qquad (153)$$

i.e., the increase in conductivity is proportional to the square root of the illumination or luminous flux.

The curve shown in Fig.71 confirms the relation expressed by eq.(152). The difference between the light and dark conductivity $\Delta G = \frac{1}{R_c} - \frac{1}{R_d}$ is laid off on the ordinate and the illumination in lux on the abscissa.

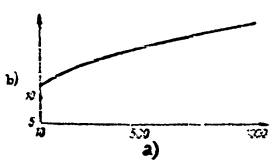

Fig.71 - Relation of Conductivity of Photoresistor to Illumination
a) Illumination, lux; b) Conductivity ΔG, $\frac{1}{\text{ohm}}\ 10^{-6}$

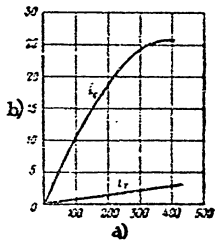

Fig.72 - Volt-Ampere Characteristic of Photoresistor:
i_d- Dark current; i_c- Current under illumination
a) Voltage, v; b) Photocurrent, μ amp

Volt-Ampere Characteristic. The photocurrent depends not only on the illumination but also on the applied voltage. Figure 72 shows the volt-ampere character-

istics for the dark current (i_d) and the light current (i_c).

The dependence of the dark resistance R_d and the light resistance R_c on the applied voltage U is shown in Fig.73.

Frequency Characteristic. All photoresistors have inertia, meaning that the photocurrent, on illumination or darkening, does not change instantaneously but with

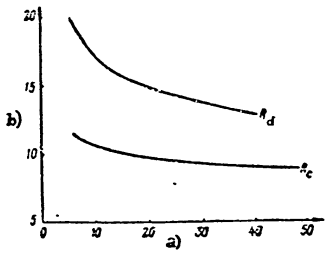

Fig.73 - Relation of the Dark Resistance R_d and the Light Resistance R_c to the Applied Voltage
a) Voltage, v; b) Resistance, ohm × 10^{-3}

a certain lag. The time necessary for the photocurrent to reach a value equal to 95% of the maximum photocurrent is usually taken as a criterion for the sluggishness. The sluggishness at decreasing photocurrent differs from the sluggishness at rising current; usually the time of rise is shorter than the time of drop.

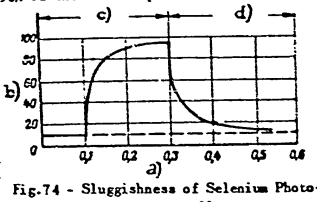

Fig.74 - Sluggishness of Selenium Photocells
a) Time, sec; b) Photocurrent, %; c) Light; d) Darkness

Figure 74 gives the sluggishness curve of a selenium photoresistor, indicating that the time of rise of the photocurrent, from the instant of illumination, amounts to about 0.2 sec.

If a selenium photoresistor is irradiated by a modulated radiant flux, the sluggishness increases with increasing modulation frequency f. The curve in Fig.75 shows that, at 3000 cps, the sensitivity of a photoresistor is only 10% of the initial sensitivity measured at a frequency of 40 cps.

The frequency dependence limits the application of selenium photocells in the high-frequency region.

Temperature Characteristic of Conductivity. The value of the resistance depends on the temperature, and this dependence differs in different types of photo-

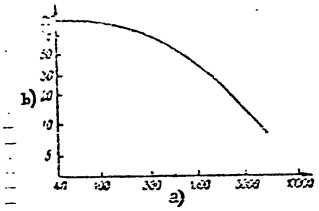

Fig.75 - Frequency Characteristic of Selenium Photoresistor
a) Modulation frequency of radiant flux, cps; b) Sensitivity, %

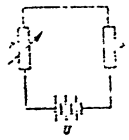

Fig.76 - Equivalent Circuit of Photoresistor

resistors, being determined by the state of the semiconductor layer. For some types, the dark and light conductivity decreases until the low-temperature zone is reached, while in other types the maximum of light and dark conductivity occurs at 0°C.

The sensitivity of photoresistors rises with decreasing temperature, but in this case their frequency characteristic also becomes less favorable.

Voltage Sensitivity. Using the equivalent circuit (Fig.76) of the photoresistor r, connected in series with the voltage source U and the external load R, the voltage sensitivity of a photoresistor can be determined.

The voltage drop across the external load is determined by the formula

$$U_R = iR = \frac{UR}{R + r} \qquad (154)$$

By differentiating eq.(154) with respect to r, we get

$$\frac{dU_R}{dr} = -\frac{UR}{(R + r)^2}$$

We recall that the variation in conductivity under illumination is proportional to the square root of the illumination. The total conductivity

$$G = G_d + G_c$$

where G_d = dark conductivity;

G_c = conductivity under illumination.

Since

$$G = \frac{1}{r}$$

it follows that

$$\frac{1}{r} = r_d + \beta\sqrt{\Phi}$$

where β = a constant;

Φ = radiant flux.

Hence

$$r = \frac{G_d}{1 + G_d\beta\sqrt{\Phi}} \qquad (155)$$

By differentiating eq.(155), we get

$$dr = \frac{G_d^2\beta}{2\sqrt{\Phi}(1 + G_d\beta\sqrt{\Phi})^2}\,d\Phi \qquad (156)$$

At R = r, the value of $\frac{dU_R}{dr}$ is maximum.

Using eq.(155), we find the voltage fluctuation

$$\frac{dU_R}{dr} = -\frac{U(1 + G_d\beta\sqrt{\Phi})}{4G_d}$$

On the basis of eq.(156), let us determine the voltage sensitivity.

$$\frac{dU_R}{d\Phi} = \frac{UG_d\beta}{8\sqrt{\Phi}(1 + G_d\beta\sqrt{\Phi})} \qquad (157)$$

where $\frac{dU_R}{d\Phi}$ is expressed in v/w.

The curve shown in Fig.77 gives an idea as to the voltage sensitivity of a selenium photoresistor at low radiant fluxes. The curves decline sharply at a luminous flux above 0.1 lumen.

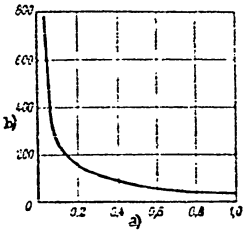

Fig.77 - Voltage Sensitivity of Selenium Photoresistors
a) Luminous flux, lumen; b) voltage sensitivity, v/lm

Section 62. Thallium Sulfite Photoresistors

In 1917, thallium sulfide photoresistors were developed. These consisted of a compound of thallium and sulfur, plus oxygen. Such photoresistors, which were given the name "thallofides", possessed high sensitivity to infrared rays. The technique of their manufacture, in general outlines, is as follows:

Thallium is boiled in sulfuric acid and the solution evaporated to give thallium sulfate. On electrolytic purification, metallic thallium is formed, which is dissolved in water. On treatment with hydrogen sulfide, thallium sulfide is precipitated, which, after heat treatment, becomes sensitive to radiant energy. The resultant thallium sulfide powder is applied to a quartz plate. To protect the photolayer from atmospheric influences, the photoresistor is placed under a vacuum.

The sensitivity of thallofide, determined from eq.(149), at an illumination of one lux, is as high as ~ 30% if the dark resistance of this thallofide is about 2-8 megohms.

The threshold sensitivity to luminous flux in modern thallofides is 4×10^{-7} to 8×10^{-8} lumens and to a radiant flux, 3×10^{-8} to 6×10^{-9} watts.

Figure 79 shows the relation between the threshold sensitivity of thallofide and the intensity of the applied voltage. The diagram indicates that the threshold

STAT

sensitivity of thallofide increases with the applied voltage.

The sensitivity of thallofide decreases with increasing illumination E; the curve in Fig.79, which shows the relation of sensitivity and illumination, confirms this statement.

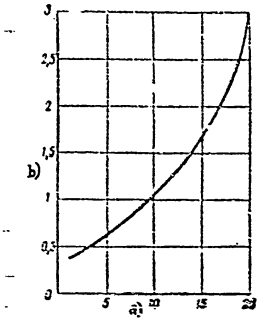

Fig.78 - Relation between Threshold Sensitivity of a Thallofide and the Voltage
a) Voltage, v; b) Threshold sensitivity in relative units

The spectral characteristic of sensitivity of a thallofide is given in Fig.80. The characteristic has two sharp maxima: at $\lambda \approx 0.5$ μ and at $\lambda = 1.05$ μ.

These maxima are inherent in all thallofides, but are somewhat shifted depending on the method used in preparing the thallofide. The long-wave boundary of sensitivity reaches 1.3-1.4 μ.

The volt-ampere characteristics of thallofide are nonlinear. Figure 81 gives the curves of the dependence of the dark current i_d on the applied voltage U, taken for three different thallofides (Curves 1, 2, 3). At increasing voltage, the steepness of the characteristics rises. In the range of 10-15 v applied voltage, the relation of the dark current to the voltage is close to linear.

The luminous characteristics of a thallofide, taken at voltages of 4, 10, and 20 volts and illuminations up to 100 lux, are given in Fig.82. The curves of Figure 82 show that, at increasing illumination, the photocurrent i_c increases nonlinearly, since the slope of the curve varies with the applied voltage U. It has been experimentally established that the photocurrent of thallofide reaches its maximum value 1×10^{-3} to 1.5×10^{-3} sec after the beginning of irradiation.

The frequency characteristics, taken in the dynamic state for an obsolete (Curve 1) and a modern (Curve 2) thallofide, are given in Fig.83. The diagram indicates that the sensitivity of the old specimens of thallofide was more dependent on the frequency of the incident light, and that this type could not be used at frequencies higher than 1000 cps. The sensitivity of modern specimens of thallofide

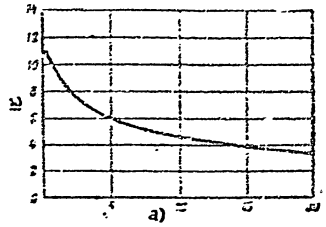

Fig.79 - Relation of Sensitivity of a Thallofide to Illumination
a) Illumination, lux; b) Sensitivity in arbitrary units

depends less on the frequency, and at 10,000 cps amounts to about 30% of maximum sensitivity.

The temperature characteristic of a thallofide is shown in Fig.84. It follows from this diagram that the sensitivity decreases with increasing temperature.

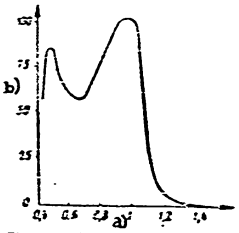

Fig.80 - Spectral Characteristic of Sensitivity of a Thallofide
a) Wavelength, μ; b) Sensitivity, %

Figure 85 shows curves indicating the relation of the noise level or dark noise voltage U_{da} on the applied voltage U. The noise voltage increases nonlinearly with increasing voltage. Curves 1 and 2 correspond to the high-resistance photoresistors (1, 9.8 megohms, and 2, 14.5 megohms); they are almost linear and are characterized by a low noise level. Curves 3 and 4 correspond to low-ohmic photoresistors (3, 2.57 megohms and 4, 2.54 megohms); they have a relatively high noise level and a nonlinear dependence. Thus the higher-resistance resistors have an intrinsically lower noise level.

The curves of Fig.86, taken for different voltages U (2.4 and 6 v), show the

relation of the noise level U_n of a thallo..ide to the illumination. The curve indicates that the noise level sharply rises with the illumination and with the applied voltage.

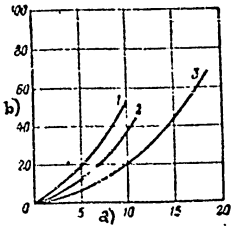

Fig.81 - Volt-Ampere Characteristics of Dark Current for Three Thallofides
a) Voltage, v; b) Dark current, μ amp

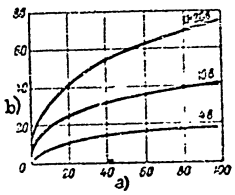

Fig.82 - Relation of Photocurrent of a Thallofide to Illumination at Various Voltages
a) Illumination, lux; b) Photocurrent under illumination, μ amp

Section 63. Tellurium-Selenide Photoresistors

In 1929, an alloy of selenium with tellurium was proposed as a photosensitive layer. The basis for this was the fact that the selective maximum in alkali metals shifts toward the long-wave range with increasing atomic weight. The higher the atomic weight of a metal, the lower the work function of the electrons. Consequently, the photosensitivity of selenium can be shifted toward the longer-wave infrared rays by adding to the selenium a small amount of tellurium, which has a higher atomic weight.

Tellurium-selenide photoresistors were first built in 1931. The difficulty in their manufacture was the fact that the conductivity changed at a layer thickness of 5×10^{-5} mm (the depth of penetration of light) and the resistivity of the alloy dropped with increasing tellurium content. In this case, the shunting effect of the deep layers took effect. In addition, the preparation of an alloy of selenium and tellurium was made difficult by the difference between the melting points of selenium (220°) and tellurium (453°), and by the difference in the vapor pressure.

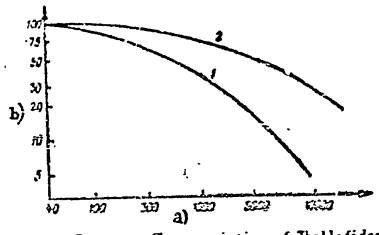

Fig.83 - Frequency Characteristics of Thallofides
1- Thallofide, obsolete model; 2- Thallofide, modern model
a) Modulation frequency, kc; b) Sensitivity, %

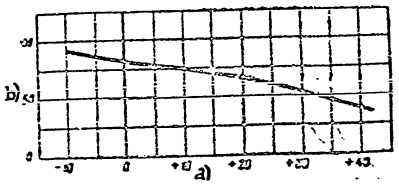

Fig.84 - Temperature Characteristic of Thallofide
a) Temperature, °C; b) Sensitivity, %

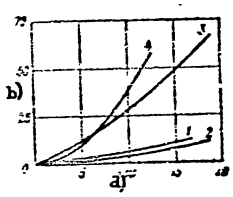

Fig.85 - Relation between Noise Level of Thallofide and Applied Voltage
a) Applied voltage, v; b) Noise voltage, μv

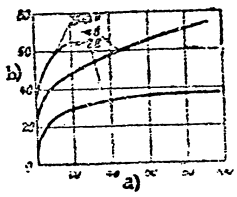

Fig.86 - Relation between Noise Level of Thallofide and Illumination
a) Illumination, lux; b) Noise voltage, μv

STAT

At first the tellurium-selenide layers were applied by cathode sputtering. Later, such photoresistors were made, with completely satisfactory parameters, by means of vapor-deposition.

The spectral sensitivity of a tellurium-selenide photoresistor is given in figure 87. The maximum sensitivity lies in the region 0.7-0.8 μ. The sensitivity of photoresistors at an illumination 100 lux is 100-250 μ amp/lumen, and the variation in conductivity under the action of irradiation reaches 30-50%. The basic disadvantage of tellurium-selenide photoresistors is their low sensitivity in the spectral region near 1.0 μ and the low value of the red boundary, amounting to 1.2-1.3 μ.

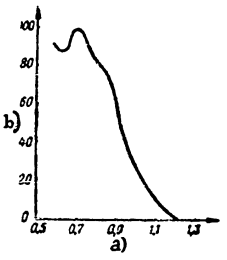

Fig.87 - Spectral Sensitivity of Tellurium-Selenide Photoresistor
a) Wavelength, μ; b) Sensitivity, %

Section 64. Lead Sulfide Photoresistors

In these photoresistors, the layer sensitive to radiant flux is formed by a synthesized lead sulfide.

The technique of building lead sulfide photoresistors is as follows:

A lead sulfide layer about 1 μ thick is deposited on a glass base. Such a layer can be obtained by two methods: either by dissolving ammonium sulfide in lead-containing compounds (the "wet" method) or by distilling in vacuo (the "dry" method). In both cases, the lead sulfide layer deposited on the base is subjected to an oxygen atmosphere to obtain a particularly sensitive surface. Then two thin, almost transparent layers of gold, forming the electrodes are applied to each side of the photoresistor. The photoresistor is placed in a casing with a window of quartz or other material permeable to infrared rays. To make the photoresistor highly sensitive it must be cooled to low temperatures, which considerably complicates the design of the body of the photoresistor.

The threshold sensitivity of a photoresistor depends on the electrode spacing (Fig.88). The smaller this spacing, the smaller a radiant flux can be detected by the photoresistor.

Figure 89 gives the spectral characteristics of a photoresistor at various temperatures of the sensitive surface of the photolayer. The curves show that the maximum of spectral sensitivity and the long-wave boundary are shifted toward the longer-wave range with decreasing temperature of the photolayer.

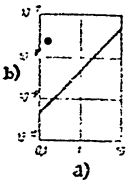

Fig.88 - Relation of Threshold Sensitivity of Lead Sulfide Photoresistor to Electrode Spacing
a) Interelectrode distance, cm, b) Threshold sensitivity, watt

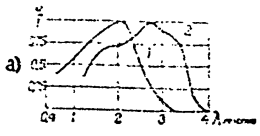

Fig.89 - Spectral Characteristics of Lead Sulfide Photoresistors
1- At a temperature of the photolayer + 20°C;
2- At a temperature of the photolayer -185°C
a) Sensitivity in relative units

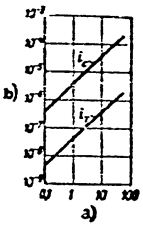

Fig.90 - Volt-Ampere Characteristics of the Dark Current i_d and the Photocurrent i_c for a Lead Sulfide Photoresistor
a) Voltage, v; b) Current, amp

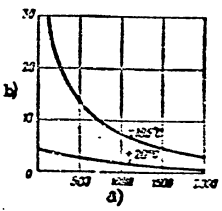

Fig.91 - Frequency Characteristics of Lead Sulfide Photoresistor at Various Temperatures
a) Frequency modulation, cps; b) Sensitivity in relative units

Figure 90 gives the volt-ampere characteristics of the dark current i_d and the photocurrent i_c at various voltages U. Both characteristics are linear. The dark current of this photoresistor reaches high magnitudes.

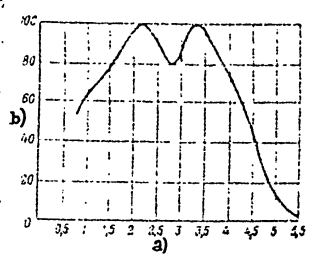

Fig.92 - Spectral Sensitivity of Lead Selenide Photoresistor
a) Wavelength, μ; b) Sensitivity, %

Frequency characteristics, plotted for room temperature (+ 20°C) and the temperature of liquid air (-185°C), are given in Fig.91. The modulation frequency in cycles is plotted on the abscissa and the sensitivity in relative units on the ordinate.

The diagram indicates that the temperature has a strong influence on the slope of the frequency characteristic. At room temperature, the sensitivity varies little with the frequency modulation; at the temperature of liquid air, however, this dependence is very pronounced, particularly in the region of low and medium modulation frequencies (up to 2000 cps). For frequencies above 2000 cps, the sensitivity is low. The inertia of the photoresistor is about 3×10^{-4} sec.

Section 65. Lead-Selenide Photoresistors

Photoresistors of lead selenide, like those of lead sulfide, are built by two methods, the "dry" and the "wet". In the former case, an alloy of selenium and lead is vapor-deposited on a plate with electrodes and is then treated in oxygen to obtain a photosensitive layer. In the latter case a film of lead selenide is precipitated on a plate with electrodes from a solution of lead acetate, and a layer of selenide is precipitated on this film from a solution of selenourea.

To increase the sensitivity, the photoresistor is heated for several hours at a temperature of 350-500°C.

The spectral characteristic of sensitivity of the photoresistor is given in Fig.92. The curve has two maxima, at 2.3 μ and at about 3.4 μ. The long-wave boundary runs up to 5.5 μ.

Table 33 (Chapter VII) gives the principal parameters of lead-selenide photoresistors. Because of their high sensitivity near wavelengths of 1-6 μ, lead sulfide and lead-selenide photoresistors are widely used today in various fields of infrared technology.

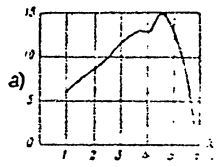

Fig.93 - Spectral Characteristic of a Lead-Telluride Photoresistor
a) Yield in relative units

Section 66. Lead-Telluride Photoresistors

A known process of preparing lead-telluride photoresistors consists in vapor-depositing a mixture of tellurium and lead on a glass plate with platinum electrodes or a ceramic plate with compressed carbon electrodes.

The lead-telleride film is sensitized by heating it in oxygen at a pressure of 10-100 mm Hg, which reduces the dark conductivity at room temperature by a factor of about 100.

Figure 93 gives the spectral characteristic of a lead-telluride photoresistor at - 186°C. The maximum sensitivity lies at $\lambda = 4.5$ μ, and the long-wave boundary extends to $\lambda = 5.8$-6 μ. With increasing temperature, the sensitivity of a lead-telluride photoresistor decreases, accompanied by a certain leftward shift of the maximum.

CHAPTER VII

BARRIER-LAYER PHOTOELECTRIC CELLS (BLOCKING-LAYER OR PHOTOVOLTAIC)

Section 67. The Photoeffect in the Barrier Layer

The photoeffect in the barrier layer has been detected in solids and liquids. It was first observed in 1888 by the Russian Physicist V.A.Ul'yanin, Professor at Kazan' University. The thin layer (10^{-5} to 10^{-6} cm), formed between a semiconductor and a conductor, is called a barrier layer. This layer has a high resistance and possesses the property of unilateral conductivity. When a radiant flux is incident on a semiconductor, the barrier layer passes the formed photoelectrons only in one direction and prevents their motion ("blocks" or bars it) in the opposite direction. A barrier-layer photocell (or blocking-layer photocell) consists of a conductor and semiconductor, with a barrier layer between them.

The electrons formed under the action of the radiant energy are displaced toward one side of the barrier layer, as a result of which a potential difference is formed between the surfaces of this layer, producing a current in the external circuit. Thus barrier-layer photocells require no external voltage source.

A peculiarity of the photoeffect in the barrier layer is the direct conversion of radiant energy into electric energy; for this reason such photocells are sometimes called photovoltaic.

The generation of photoelectrons in a semiconductor takes place in the same way as in the intrinsic photoeffect, so that barrier-layer photocells possess high sensitivity to radiation of the near infrared region of the spectrum.

The photoeffect in the barrier layer is either of the rear-wall or front-wall type.

The Back-Effect Photocell

Figure 94 gives a schematic diagram of a barrier-layer rear-wall photocell. The photocell consists of the layer of metal a (the substratum) to which a thin film of semiconductor (b) is applied; a metal grid electrode (c) is placed on top of the semiconductor.

On irradiation of the photocell by a flux of radiant energy, an emf arises on the boundary between the semiconductor and the metal. This boundary forms the barrier layer (d), which passes electrons only in one direction, from the metal to the semiconductor.

The Front-Effect Photocell

Figure 95 is a diagram of a barrier-layer photocell with front photoeffect. The photocell consists of the metal base (a), a thick layer of semiconductor (b), and

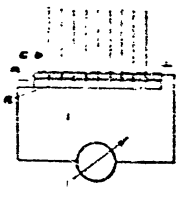

Fig. 94 - Diagram of Back-Effect Barrier-Layer Photocell
a) Base; b) Semiconductor; c) Electrodes; d) Barrier layer

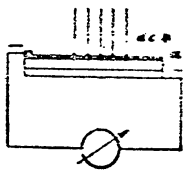

Fig. 95 - Diagram of Front-Effect Barrier-Layer Photocell
a) Base; b) Semiconductor; c) Electrodes; d) Barrier layer

the upper semitransparent metal electrode (c). The barrier layer (d) is formed on

the boundary between the semiconductor and the upper metal electrode. On irradiation of the photocell, the radiant flux penetrates to a certain depth into the semiconductor (without reaching the lowest metal layer) and liberates electrons which pass through the barrier layer to the upper electrodes. Thus, in contrast to back-effect photocells, the electrons in this case move in the direction from the semiconductor to the metal.

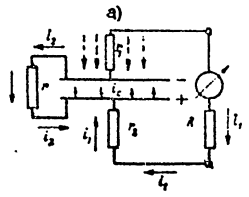

Fig.96 - Equivalent Circuit of a Barrier-Layer Photocell
a) Radiant flux

Section 68. Equivalent Circuit of Barrier-Layer Photocells

Figure 96 gives an equivalent circuit for a barrier-layer photocell.

The total resistance R_{ph} of the photocell comprises the resistance r of the barrier layer, the resistance r_1 of the semiconductor, and the resistance r_2 of the transparent electrode and the contacts

$$R_{ph} = r + r_1 + r_2 \qquad (158)$$

The photocurrent i_c, arising under the action of the radiant flux, is equal to the sum of the current i_1 in the external circuit, and the leakage current i_2:

$$i_c = i_1 + i_2 \qquad (159)$$

At open circuit, we have

$$i_c = i_2 \qquad (160)$$

The electromotive force arising across the electrodes of the photocell will be equal, at open circuit, to

$$E_{ph} = i_{ph}(r_1 + r_2) \qquad (161)$$

The photocurrent in the external circuit increases with diminishing external load R.

Photocells of this type are also characterized by an efficiency η. This efficiency η is the ratio between the maximum power output of the photocell and the power of the flux striking the surface S of the photocell. At a linear volt-ampere characteristic, the efficiency may be calculated by the formula

$$\eta = \frac{\pi i_{ph} E r^2}{4S} \qquad (162)$$

where i_{ph} = photocurrent;

E = emf of the photocell;

r = distance from radiation source to photocell;

Φ = radiant flux;

S = area of the photocell.

Section 69. Design of Barrier-Layer Photocells

Barrier-layer photocells are almost the same in design. Figure 97 gives a schematic design of a typical barrier-layer photocell. The photocell consists of an ebonite or textolite case (1), a protective glass (2), an upper grid or thin solid electrode (3), the semiconductor layer (4), and the metal base (5) (lower electrode).

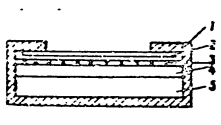

Fig.97 - Arrangement of a Barrier-Layer Photocell: 1- Casing; 2- Protective glass shield; 3- Electrodes; 4- Semiconductor; 5- Base

Of the group of barrier-layer photocells, only photocells sensitive to infrared rays will be discussed below, including cuprous oxide (cuprox) back-effect photocells, silver-sulfide, lead-sulfide, and thallium-sulfide photocells.

Section 70. The Cuprous Oxide Back-Effect Photocell

The process of manufacturing cuprous oxide back-effect or rear-wall photocells is very simple. On a lead plate attached to a copper plate about 1 mm, oxidized in

an oven at a temperature of 1000°C, a layer of cuprous oxide (Cu_2O) about 0.1 mm thick is formed. The plate is cooled slowly to 600°C under exclusion of oxygen. A metal wire mesh or grid, serving as the second electrode, is attached to the layer of cuprous oxide.

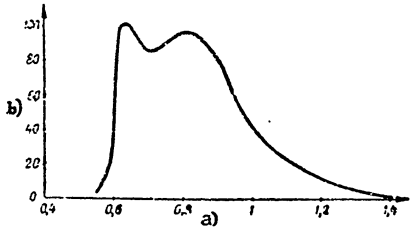

Fig.98 - Spectral Characteristic of Cuprous Oxide Photocell
a) Wavelength, μ; b) Photocurrent in relative units

The spectral characteristic of a cuprous oxide back-effect photocell (Fig.98) has two sensitivity maxima. The first maximum occurs at a wavelength of about 0.615 μ. With decreasing temperature, this maximum shifts slightly toward the short-wave portion. The second maximum corresponds to λ = 0.8 μ and likewise depends on the temperature. The integral sensitivity of a cuprous oxide back-effect photocell is equal to 100-200 μ amp/lm.

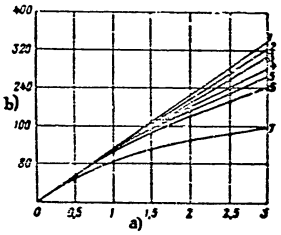

Fig.99 - Volt-Ampere Characteristics of a Cuprous Oxide Photocell
a) Luminous flux, lumen; b) Photocurrent, μ amp

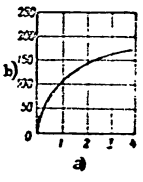

Fig.100 - Relation between Photoelectromotive Force and Luminous Flux for a Cuprous Oxide Photocell
a) Luminous flux, lumen; b) Photoelectromotive force, mv

Figure 99 shows a family of volt-ampere characteristics, indicating the dependence of the photocurrent on the value of the radiant flux and the resistance of the external load. Curves 1, 2, 3, 4, 5, 6 and 7 were taken, respectively, at external circuit resistances of 3, 100, 200, 300, 400, 500, and 1000 ohms. The diagram in Fig.99 shows that, at low flux and low external resistance, the photocurrent is directly proportional to the flux. With increasing external resistance, this proportionality no longer holds.

Figure 100 shows the relation between the photoelectromotive force generated by the photocell and the magnitude of the incident flux. The diagram indicates that the photoelectromotive force depends logarithmically on the light flux and increases with it.

The frequency characteristic of a cuprous-oxide photocell is shown in Fig.101. Since cuprous-oxide photocells have a natural capacitance, their sensitivity drops at high modulation frequency. Figure 101 indicates that, at a modulation frequency of 10,000 cps, the sensitivity decreases to 60% of the maximum.

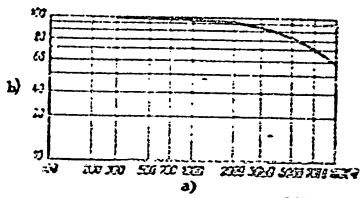

Fig.101 - Frequency Characteristic of a Cuprous Oxide Photocell
a) Modulation frequency, cps; b) Sensitivity, %

The photocurrent and emf arising under irradiation are highly temperature-dependent. The temperature coefficient of the photocurrent in the external circuit in the temperature interval from T_1 to T_2 is determined by the formula

$$\alpha = \frac{i_1 - i_2}{i_1(T_1 - T_2)} \qquad (163)$$

where i_1 = photocurrent at the temperature T_1;

i_2 = photocurrent at the temperature T_2.

The temperature coefficient in the interval from -20 to + 80°C fluctuates from -0.0086 to -0.0016.

Figure 102 shows the relation between the value of the short-circuit current of a cuprous-oxide photocell and the applied voltage, for various temperatures.

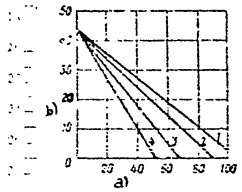

Fig. 102 - Relation of Short-Circuit Current of Cuprous-Oxide Photocell to Voltage
a) Voltage, mv; b) Short-circuit Current, μ amp

The power output of the photocell to the external circuit reaches a maximum when the resistance of the external circuit equals the internal resistance of the photocell.

To increase the power output, the surface of the photocell can be increased. The power delivered by a cuprous oxide photocell is equal to 2.9-3.03 μ watt.

The main disadvantage of cuprous oxide photocells is their instability of operation, due to the inconstancy of the parameters.

At present, cuprous-oxide photocells are rarely used and have been replaced by improved types in which sulfur compounds are used.

Section 71. The Silver-Sulfide Photocell (FESS)

Silver-sulfide photocells, developed by the Physics Institute of the Ukrainian Academy of Sciences, use a layer of silver sulfide as the semiconductor.

The integral sensitivity of silver-sulfide photocells, determined by means of an incandescent electric lamp with a filament temperature of 2400°K, equals 2000-5000 μ amp/lumen. The maximum sensitivity is in the infrared region.

The spectral characteristics given in Fig. 103 show that the photocell has its maximum sensitivity at λ = 1.0-1.1 μ, and that it is sensitive to rays of wavelengths from about 0.5 to 1.35 μ.

The volt-ampere characteristics shown in Fig. 104 are taken at room temperature (15°C), at illumination of 50 and 100 lux. At an illumination of 50 lux, the curve

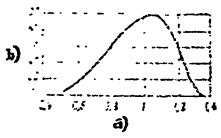

Fig. 103 - Spectral Characteristic of a Silver-Sulfide Photocell (FESS)
a) Wavelength, μ; Sensitivity, % b)

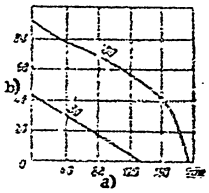

Fig. 104 - Volt-Ampere Characteristics of FESS
a) Voltage, mv; b) Photocurrent μ amp

of photocurrent versus voltage drop in the external circuit is linear. With increasing illumination, this linearity no longer holds.

The dependence of the photocurrent and of the photo-emf on the illumination is shown by the curves given in Fig. 105. The maximum value of the emf (Curve 2) at

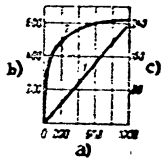

Fig. 105 - Relation between Photocurrent (Curve 1) or Photoelectromotive Force (Curve 2) and Illumination, for FESS
a) Illumination, lux; b) Photocurrent, μ amp; c) Photoelectromotive force, mv

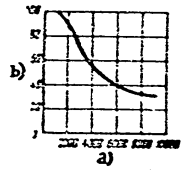

Fig. 106 - Frequency Characteristic of FESS
a) Modulation frequency, cps; b) Sensitivity, %

room temperature and an illumination of 1000 lux is 250 mv. The photocurrent

(Curve 1) is directly proportional to the illumination and reaches 600 μ amp at 1000 lux. The internal resistance of photocells having an area of 2 cm^2 varies from 1000 to 6000 ohms.

The frequency characteristic given in Fig. 106 shows the relation of the sensitivity of FESS to the frequency. The diagram shows that the sensitivity of the photocells decreases, from about 1000 cps. It is suggested to use such photocells at frequencies not exceeding 4000 cps, since the sensitivity is less than 60% of maximum at higher modulation frequencies.

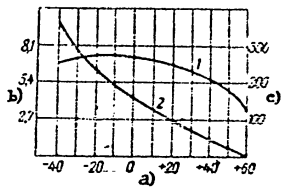

Fig. 107 - Relation of Photocurrent (Curve 1) and Photoelectromotive Force (Curve 2) to Temperature, for FESS
a) Temperature, °C; b) Photocurrent, amp × 10^{-5}; c) Photo emf, mv

The relation of photocurrent and photoelectromotive force to the temperature is shown in Fig. 107. The photocell operates normally at a temperature from -60 to + 40°C. Outside this temperature range, the photocurrent and emf decrease considerably.

The power given off by the photocell to the external circuit will reach a maximum as soon as the spectral characteristic of the radiation source corresponds to the spectral characteristic of the photocell. Figure 108 gives the spectral characteristics of an incandescent lamp at a filament temperature of 2870°K (Curve 1) and of the photocell (Curve 2). The areas of these curves are superimposed on one another over part of the range (hatched in the diagram), making the photocell useful as an indicator of luminous flux if the radiator is an incandescent lamp.

The efficiencies of a silver-sulfide photocell (cf. eq. 162) as a function of the illumination are given in Table 32.

The photocurrent and the efficiency of silver-sulfide photocells increase with time. The photocurrent rises considerably during the first two months of operation and the emf increases most in the 5th to 6th month. This increase is explained by the gradual improvement in the formation of the barrier layer.

Section 72. The Thallium-Sulfide Photocell

Thallium-sulfide photocells were first developed in 1938 by the Soviet physicist B.T. Kolomiyts under the direction of Academician A.F. Ioffe. The design of the photocell is schematically shown in Fig. 109.

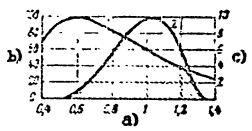

Fig. 108 - Spectral Characteristics of Radiation of a Source at T = 2870°K (Curve 1) and of an FESS Photocell (Curve 2)
a) Wavelength, μ; b) Sensitivity of Photocell, %; c) Intensity of radiation in relative units

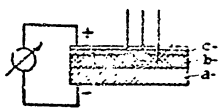

Fig. 109 - Design of a Thallium Sulfide Photocell:
a- Base; b- Semiconductor; c- Barrier

To construct such a photocell, a semiconductor (b) is vapor-deposited on the iron plate or base (a); the conductor consists of a mixture of thallium sulfide and tellurium. To obtain a photosensitive layer, the conductor must be oxidized. On the oxidized film (representing the barrier layer c), the upper semiconductor gold electrode (d) is deposited by cathode sputtering and is then coated with varnish to protect it from moisture. The photocell is placed in a tube filled with hydrogen at a pressure of up to 400 mm Hg, which helps to prolong the life of the photocell.

Table 32

Efficiency of Silver-Sulfide Photocells

Illumination, lux	10	50	100	1000
Efficiency, %	0.034	0.2	0.34	0.38

The integral sensitivity of thallium-sulfide photocells runs on the average up to 4000-6000 μ amp/lm at 2800°K color temperature of the radiator.

The spectral characteristic (Fig.110) covers a rather wide range of wavelengths, which is about the same as the characteristic of a thallofide photoresistor. The

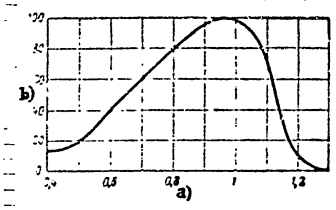

Fig.110 - Spectral Characteristic of a Thallium-Sulfide Photocell
a) Wavelength, μ; b) Sensitivity, %

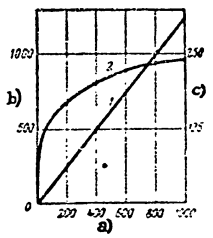

Fig.111 - Relation of Photocurrent (Curve 1) and Photoelectromotive Force (Curve 2) to Illumination, for a Thallium-Sulfide Photocell
a) Illumination, lux; b) Photocurrent, μ amp; c) Photo-emf, mv

maximum sensitivity is in the region of about 1 μ, and the long-wave boundary reaches 1.3 μ.

The photocurrent and photo-emf are plotted in Fig.111 as a function of the illumination. The curves are similar to the corresponding curves of other barrier-layer photocells.

The frequency characteristic of the photocell is shown in Fig.112. At a frequency of 5000 cps, the sensitivity is about 80% of the maximum frequency of the photocell (the sensitivity at a frequency of 50 cps being taken as 100%).

Section 73. The Galena Photocell

Figure 113 schematically shows the design of a photocell with a natural crystal of galenite (lead glance). In the body (1) of the photocell, the crystal (3) is held by the electrodes (2). The grid electrode (4) is placed on the surface of the crystal. The upper part of the body is provided with a window (5) of an optical

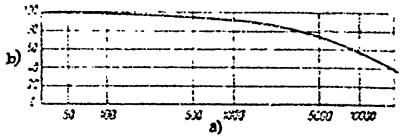

Fig.112 - Frequency Characteristic of a Thallium-Sulfide Photocell
a) Modulation frequency, cps; b) Sensitivity, %

material transparent to infrared rays.

The technology of manufacture for such photocells is about as follows:

The surface of the galena is ground and polished. On the polished surface, first heated in vacuo, a layer of lead is deposited (by evaporation) and a molybdenum

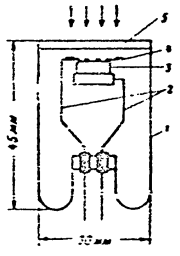

Fig.113 - Design of a Galena Photocell:
1- Body; 2- Electrode; 3- Galena crystal;
4- Grid electrode; 5- Window

or tungsten grid (electrode) is pressed into it. A second electrode serves as the base to which the galena is attached. The photocell is then reheated, making it sensitive to a radiant flux, which produces a photocurrent in it, directed from the crystal to the grid. To eliminate the influence of the atmosphere, the photocell is

STAT

placed in a casing, within which a vacuum of about 10^{-8} mm Hg is produced.

The spectral characteristic of this photocell is analogous to the characteristic of a lead-sulfide photoresistor. It has a smooth region of rise and reaches a maximum at $\lambda = 2.5\ \mu$, after which it drops rather sharply.

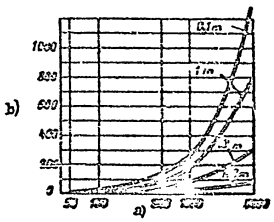

Fig.114 - Dependence of Photocurrent on the Illumination for a Galena Photocell
a) Illumination, lux; b) Photocurrent, μ amp

Figure 114 shows the relation between photocurrent and illumination, at various external loads (0.1; 1, 10, 100 ohms). This relation is nonlinear, becoming almost linear at low illumination or very low external load (close to zero).

The frequency characteristic of galena photocells shows that, within a wide frequency range from 300 to 40,000 cps, these photocells are practically inertialess.

Section 74. Comparison of Parameters of Various Photocells Sensitive to Infrared Rays

Table 33 gives the principal parameters of various photocells. By comparing these parameters, the following conclusions may be drawn:

The internal resistance of the photoresistors reaches 10^6 ohms and more, and that of emissive photocells, 10^{11} ohms. Photocells are therefore useful for amplifying circuits.

The group of barrier-layer (blocking-layer) photocells has a smaller internal resistance than the first two groups (10^2-10^3 ohms).

A comparison of the maximum sensitivity and long-wave boundary of various photocells shows that photoresistors have their maximum sensitivity and sensitivity

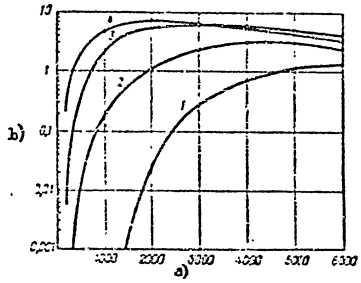

Fig.115 - Efficiency of Various Photocells:
1- Selenium; 2- Thallofide; 3- Lead sulfide; 4- Lead selenide;
a) Black-body temperature, °K; b) Efficiency, %

threshold in a longer-wave portion of the spectrum than the other photocells.

The sensitivity threshold of photocells ranges from 10^{-6} to 10^{-9} lumen, or 10^{-7} to 10^{-16} watt, at 2400°K color temperature of the radiator. The maximum sensitivity threshold is exhibited by lead-sulfide photoresistors, whose sensitivity is about 5 times as great as that of the thallofide photoresistors.

With respect to inertia, the emissive photocells have the advantage, since they have the smallest inertia (about 10^{-9} sec for vacuum photocells of this type). The sluggishness of photoresistors is of the order of 10^{-4} sec.

Figure 115 gives curves indicating the variation in the efficiency of various photocells with any variation in the temperature of the radiator (black-body). Photocells sensitive to the longer-wave portion of the spectrum have the highest efficiency (cf. Table 33).

Figure 116 gives the curve of threshold sensitivity for a few photocells at various temperatures of the radiation source. At temperatures of a few thousand

STAT

Table 33

Basic Parameters of Various Photocells

Type of Photocell	Character of Photoeffect	Internal Resistance, Ohm	Wavelength, μ: At Maximum Sensitivity, λ_{max}	Wavelength, μ: Long-Wave Boundary λ_0	Sensitivity: Integral, μ amp/lm	Sensitivity: Threshold at T_c = 2400°K: lumen	Sensitivity: Threshold at T_c = 2400°K: watt	Sluggishness sec
Cesium vacuum	Extrinsic photoeffect	10^{11}	0.85	1.3	20-40	1×10^{-6} - 5×10^{-7}	8×10^{-8} - 4×10^{-8}	10^{-9}
Cesium gas-filled	Same	-	-	-	150-300	2×10^{-7}	1.6×10^{-8}	10^{-6}
Selenium	Intrinsic photoeffect	3×10^{6}	0.7	0.9	-	-	-	3×10^{-1}
Thallium sulfide (thallofide)	Same	2×10^{6} - 10^{7}	1.05	1.4	-	4×10^{-7} - 8×10^{-8}	3×10^{-8} - 6×10^{-9}	1×10^{-3}
Lead sulfide	Same	$\sim 10^{6}$	2.4	3.5	-	2×10^{-8} - 1×10^{-9}	1.6×10^{-9} - 8×10^{-10}	10^{-4}
Lead selenide	Same	$\sim 10^{6}$	3.4	5.5	-	-	-	-
Cuprous oxide	Barrier-layer	4×10^{2}	0.6	1.4	100-200	-	-	-
Silver sulfide	Same	10^{3} - 4×10^{3}	1 - 1.1	1.35	2000-5000	-	-	-
Thallium sulfide	Same	10^{3}	0.96	1.3	5000-8000	-	-	-
Lead sulfide	Same	10	2.4	3.5	-	2×10^{-4} - 2×10^{-7}	1.6×10^{-7} - 1.6×10^{-8}	10^{-5}

degrees, the threshold sensitivity varies little and is very high, i.e., the photocells are sensitive to a very small radiant flux (as low as 2×10^{-9} watt). With

Fig. 116 - Threshold Sensitivity of a Few Photocells:
1- Selenium; 2- Thallium sulfide; 3- Lead sulfide
a) Black-body temperature, °K; b) Threshold sensitivity, watt; c) Eye

decreasing temperature, beginning at 3000-2000°K, the threshold sensitivity drops sharply: The photocells become sensitive only to high values of the radiant flux. For comparison, the curve of threshold sensitivity of the eye is given in Fig. 116.

CHAPTER VIII

A FEW TYPES OF SELECTIVE INDICATORS OF INFRARED RAYS

Section 75. Electron Multipliers

In 1934 the Soviet scientist L.A.Kubetskiy proposed the construction of a new type of photocell, the electron multiplier, or multistage secondary-electron amplifier.

This instrument combines the conversion of the energy of a radiant flux into photocurrent and the amplification of that photocurrent. The photoeffect of an irradiated coated oxygen-cesium photocathode is used for the conversion of radiant energy into electric energy, while the secondary electronic emission is used for amplification of the photocurrent.

The phenomenon of secondary emission consists in the liberation of secondary electrons from the surface of a body under the impact of electrons of sufficient energy. The number of such secondary electrons (N_2) may be several times as great as the number of primary electrons (N_1). The ratio

$$\sigma = \frac{N_2}{N_1} \qquad (164)$$

is called the coefficient of secondary emission.

Bodies having the smallest work function of the primary electrons, for example cesium and its compounds, possess the greatest secondary emission. Electron multipliers use multiple amplification of the secondary electron current, which successively increases through a few stages of the instrument.

Figure 117 shows a schematic diagram of the electron multiplier. The multiplier consists of the photocathode K, several electrodes S_1, S_2...S_7 with secondary emission, and the anode (collector) A. The electrodes S_1...S_7 are supplied with successively increasing potentials.

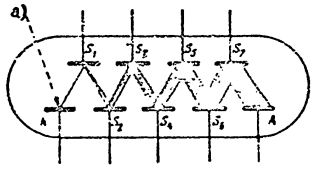

Fig.117 - Schematic Diagram of Electric Multiplier:
K- Photocathode; A- Anode; S_1-7- Electrodes;
a) Radiant flux

The radiant flux falling on the photocathode K, liberates primary electrons which, under the action of the accelerating field, impinge on the primary electrode S_1 and "dislodge" secondary electrons from it. Each primary electron "dislodges" a few secondary electrons (average 3 to 10, depending on the coefficient of secondary emission). The electrons escaping from the electrodes S_1 impinge on the following electrode S_2 and there "dislodge" a still larger number of secondary electrons. The repetition of this process in each pair of electrodes creates, in the circuit of the anode A, a current millions of times higher than the primary photocurrent.

The magnitude of the photocurrent I at the multiplier output is determined by the equation

$$I = I_0 \sigma^n \qquad (165)$$

where I_0 = primary electron current from the photocathode surface;

σ = coefficient of secondary emission of the electrodes;

n = number of electrodes.

To obtain maximum yield under multiple amplification, the electrons must be concentrated in such a way that, if possible, all electrons leaving the preceding electrode strike the following one. This is done by means of electrostatic or electromagnetic focusing. Soviet scientists have developed various designs of electron multipliers (Bibl.11).

The special feature of the electron multiplier design, developed by

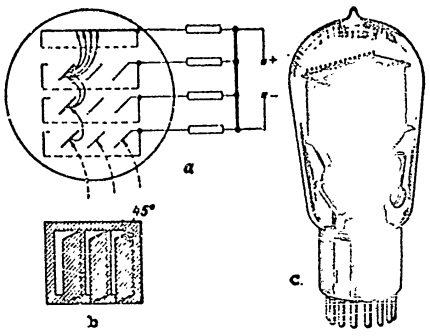

Fig. 118 - Electron Multiplier Designed by S.A.Vekshinskiy
a- Principle of operation; b- Construction of plate;
c- General view;
a) Light; b) Anode; c) Cathode

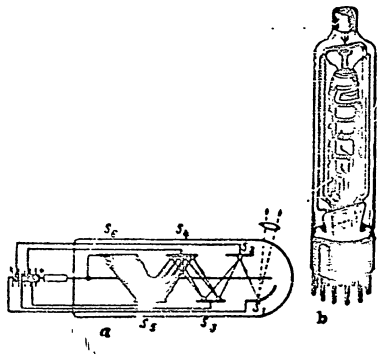

Fig. 119 - Electron Multiplier Designed by P.V.Timofeyev
a- Principle of operation; b- General view;
a) Light

L.A.Kubetskiy, is that all the electrodes are deposited in the form of thin annular layers on the inner surface of a glass tube. The oxygen-cesium photocathode is likewise deposited on the surface of the tube. To accelerate the electrons and focus the electron beams, voltage is imposed on the electrodes from various points of a potentiometer fed by a voltage source.

A schematic diagram of the electron multiplier with electrostatic focusing (Bibl. 12), designed by S.A.Vekshinskiy, is shown in Fig. 118 a. The glass tube con-

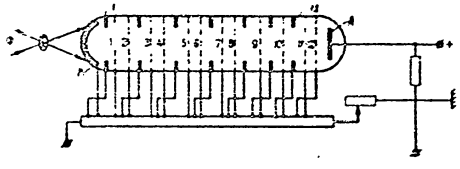

Fig. 120 - Schematic Diagram of a "Grid-Controllance"
k- Photocathode; $D_1,\ldots D_{12}$- Diaphragms; A- Anode

tains metal plates with slits in louver form (Fig. 118, b). The plates are coated with cesium and are arranged parallel to one another. The potential difference between any adjacent pair of plates is equal to 200 volts. The increasing electron flux penetrates successively through the openings in the plates, until it reaches the last plate (anode) which has no opening.

The sensitivity of the multiplier is 6-8 amp/lm at 10-12 stages of amplification.

Figure 119 shows the scheme of the electron multiplier designed by Professor P.V.Timofeyev (Bibl. 12).

The electrodes of the multiplier $S_1\ldots S_6$ are arranged in checkerboard design. In front of each electrode is a metal grid connected with the next electrode. The electrons leaving the electrode enter the accelerating field produced by the grid. The potential of each grid is 150 volts higher than that of the preceding one. In the Timofeyev multiplier the electrons show little scattering, due to the high accelerating field, thus ensuring high values for the amplification factor.

STAT

Figure 120 schematically shows the arrangement of a "grid-controllance" multiplier (with grids). Inside the tube, grid metal electrodes (1,2,3...12) are arranged in succession. Each successive grid has a higher potential than the preceding one. The photoelectrons escaping from the photocathode K, under the action of the radiant flux Φ, impinge on the grid (1), dislodge secondary electrons there, and are attracted to the grid (2) under the action of the electric field produced by this grid. The electron stream, increasing in volume as it passes each grid, is collected on the anode A.

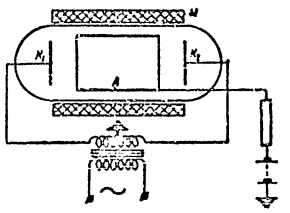

Fig. 121 - Scheme of Dynamic Electron Multiplier with Longitudinal Magnetic Field:
K_1 and K_2 - Cathode; A- Anode cylinder; M- Electromagnetic coil

The angular diaphragms $D_1 \ldots D_{12}$, located between the grids, are used to focus the electron stream. The electrostatic fields produced by the diaphragms play the part of electronic lenses, focusing the electron beam.

Figure 121 shows a schematic diagram of the dynamic electron multiplier with longitudinal magnetic field. The high-frequency alternating field, of frequency up to 10^6 cycles, produced by the power supply system, acts on the cathodes K_1 and K_2. Between the cathodes, a cylindrical anode (collector) is installed. The coil M, fed with direct current, produces a longitudinal focusing magnetic field. The anode is supplied with a positive potential from an auxiliary battery; the negative pole of the battery and the center point of the cathodes are grounded. The electrons leaving the cathode K_1 in the direction of the anode, do not strike this cathode because of the focusing action of the magnetic field of the coil. They reach the opposite cathode K_2 if the electric parameters are such that the electrons are able to traverse the distance between the cathodes during the time of one half-period of the high frequency. During this time, the direction of the high-frequency field does not change, so that the electrons remain under the action of an accelerating field. On reaching the opposite cathode K_2, they detach secondary electrons from it; these secondary electrons, under the action of the field with a changed sign (the following half-period), travel in the opposite direction and, striking the cathode K_1, dislodge secondary electrons there, which again travel toward the cathode K_2, and so on. When the number of electrons increases to a certain value, some of the secondary electrons begin to impinge on the anode, producing an increasing current in the amplifier circuit.

In order to obtain an amplification factor $\sigma > 1$, a high-frequency voltage of the order of 50 v can be imposed on the cathodes. Since the transit time of the electrons at a frequency of 10^6 cycles is about 10^{-8} sec, the distance between the cathodes must not exceed 6 cm. The limit of rise of the current is determined by the space charges formed.

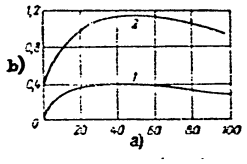

Fig. 122 - Relation of Output Current and Voltage under Secondary Electron Emission
a) Voltage, v; b) Output current, ma

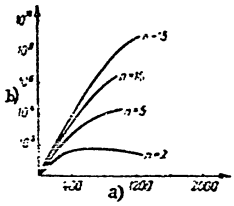

Fig. 123 - Relation of Amplification Degree to Number of Stages n and to Value of the Applied Voltage
a) Voltage, v; b) Degree of amplification

The dynamic electron multiplier, according to its schematic diagram, is a photoelectronic amplifier of current, but it may also be used as a multiplier, if a photoelectric cathode, producing primary electrons when struck by a radiant flux, is introduced in it.

Electron multipliers are evaluated by the same basic characteristics as photocells.

The threshold sensitivity of modern electron multipliers is determined by the

level of inherent noise. In practice a multiplier reacts to a very insignificant radiant flux, which is one of its principal advantages. For example, an eight-stage

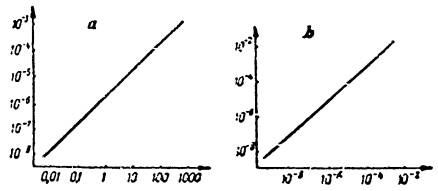

Fig. 124 - Luminous Characteristics of Three-Stage Electron Multipliers
a- Relation of output current and illumination; b- Relation of output current and radiant flux
a) Illumination, lux; b) Output current, amp; c) Radiant flux, lumen

multiplier has a threshold sensitivity of about 15×10^{-7} amp/lm. The integral sensitivity of a fifteen-stage multiplier is as high as 10 amp/lm.

Figure 122 gives curves relating the output current to the applied voltage for a low-voltage multiplier, designed by P.V.Timofeyev. Curve I is taken at a flux of $F = 5 \times 10^{-4}$ lm, and Curve 2 at $F = 1.4 \times 10^{-3}$ lm. The diagram indicates that the current rises up to a voltage of 50 v but, on further increase in voltage decreases slightly.

The degree of amplification, as a function of the number of stages n and of the applied voltage, is illustrated by the curves in Fig. 123. At fifteen stages, the degree of amplification reaches 10^9.

The spectral characteristics of electron multipliers are determined by the type of photocathode and do not differ from the characteristics of emissive photocells which have the same type of photocathode.

The luminous characteristics of the three-stage electron multiplier given in Fig. 124 show that, at a small number of stages, the amplification of the photocurrent is proportional to the illumination or to the luminous flux.

In multistage electron multipliers, the photocurrent in the final stages reaches high values and the space charges formed affect the focusing adversely. This disturbs the strict proportionality between photocurrent and illumination (or radiant flux).

Figure 125 gives the frequency characteristic showing the dependence of the photocurrent, in relative units, on the modulation frequency of the incident radiant flux. The diagram shows that the characteristic is linear over the segment of 1-10 megacycles. At higher frequencies, a smooth decline begins, which becomes steep above 50 megacycles.

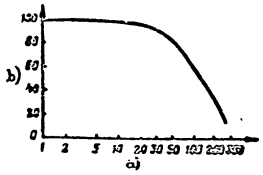

Fig. 125 - Frequency Characteristic of Electron Multipliers
a) Modulation frequency, megacycles; b) Photocurrent, %

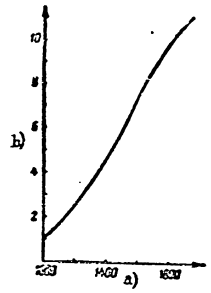

Fig. 126 - Noise Voltage of Electron Multiplier
a) Applied voltage, v; b) Noise voltage, μ amp

Like emission phototubes, electron multipliers show no perceptible temperature dependence in the interval from -40 to + 50°C. At temperatures above + 50°C, the photocathode begins to disintegrate.

The stability of operation of electron multipliers depends in general on the quality of the electrodes emitting the secondary electrons. In time, the electrodes "age", even when operating under normal load (about 0.5 watts/cm^2). The "aging" shows in a decrease of the secondary emission factor. For example, the sensitivity of a fifteen-stage multiplier (about 10 amp/lm) drops by about 20%, after 2000 hours of operation.

Electron multipliers have an insignificant noise current (Fig. 126). For example, at a feed voltage of 1800 v, the noise voltage slightly exceeds 10 μ asp. The noise in a multiplier is classified, according to origin, into noise produced in the photocathode, noises due to the influence of secondary emission, and noises of the output load.

Section 76. Luminophores, Sensitive to Infrared Rays

Under the action of radiant energy, many substances begin to radiate visible light themselves. This phenomenon is called photoluminescence. If the luminescence is interrupted immediately after stoppage of irradiation, the phenomenon is called fluorescence; if, after stoppage of irradiation, the luminescence persists for a certain time, it is called phosphorescence.

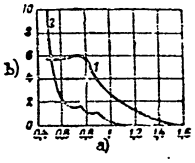

Fig. 127 - Relation of Luminous Discharge (1) and Quenching (2) to the Wavelength, for the Luminophore CaSBi
a) Wavelength, μ; b) Sensitivity in relative units

Luminescent substances are called luminophores.

The bases for luminophores are inorganic substances, such as the sulfides of alkali metals. On addition of certain metals, or activators, these substances phosphoresce under irradiation. The principal substances and metals (activators) are usually indicated in the designation of a luminophore. For example, CaSBi indicates a luminophore of calcium sulfide, with bismuth as activator.

Luminophores are excited only under irradiation by a short-wave luminous flux, for example gamma rays, X-rays, and ultraviolet rays, visible light, and near infrared rays, and luminophores can be excited only by the radiant energy they absorb.

The process of excitation of a luminophore under the action of radiant energy takes place within the atoms or molecules of the substance, without the occurrence of electronic emission. An electron of the luminophore leaves the center of excitation, which consists of a complex of molecules of the principal substance containing the atoms of the activator, and returns to it after a certain interval of time, sometimes measured in tens of hours. When the electron returns to its previous energy level, part of the energy received by the electron is radiated in the form of radiant energy. Thus luminescence is characterized by an accumulation of energy in the luminophore during the period of transition of the electrons to higher energy levels. This accumulated energy is called the light sum.

At low temperatures, a luminophor does not radiate, and the light sum remains constant. With increasing temperature, the light sum decreases, i.e., radiation begins.

Under the action of infrared rays, two phenomena may occur in luminophores: accelerated luminescence or flare-up and quenching of luminescence. Accelerated luminescence is accelerated radiation of the light sum accumulated by the luminophore, while quenching is the interruption of luminescence.

According to research done by Academician S.I.Vavilov, accelerated luminescence is due to the heating of the excited centers of luminescence by the energy of the quanta of infrared rays absorbed, thus encouraging the return of the electrons to their former energy levels and, consequently, also encouraging radiation. The reduction in the light flux of a luminophore has two forms: accelerated luminescence, when the accumulated light sum, under the action of long-wave radiation, is rapidly radiated in the form of luminous flux; and quenching, in which part of the light sum is transformed into heat and cannot be radiated. In this case, quenching and accelerated luminescence occur simultaneously.

The incident radiant flux is absorbed by a luminophore; the absorption bands due to quenching exist only in an excited luminophore, and the degree of absorbing is proportional to the degree of excitation.

The process of quenching is explained by the drop in the emissivity of luminophores at temperatures above 200°C; this emissivity is completely lost at a temperature of 500°C. For this reason, if the temperature of a luminophore does not rise above 200°C in the process of absorbing a quantum of long-wave rays, only accelerated luminescence takes place; however, if the temperature exceeds 500°C, the accelerated

luminescence stops and only quenching takes place.

In the temperature range from 200 to 500°C, simultaneous accelerated phosphorescence and quenching are possible. The ratio of accelerated luminescence to quenching, for a given luminophore, is determined by the wavelength of the luminous flux incident on it. Figure 127 gives the curves of the wavelength-dependence of accelerated luminescence (Curve 1) and quenching (Curve 2) for the luminophore CaSBi.

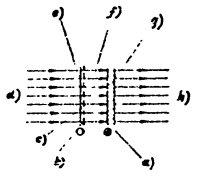

Fig. 128 - Principle of Construction of an Electron-Optical Transducer
a) Fluorescent screen anode; b) Semitransparent photocathode; c) Electrons; d) Infrared rays; e) Infrared image; f) Electron image; g) Visible image; h) Visible rays

The diagram shows that quenching and accelerated luminescence occur not only under the action of infrared rays but also under the action of visible and ultraviolet rays of the spectrum, in which case visible rays quench luminescence much more than do infrared rays. Consequently, the action of the short-wave radiation induces excitation and quenching at the same time.

In its relative value, accelerated luminescence due to infrared rays predominates over the quenching by rays of shorter wavelengths. The ratio between accelerated luminescence and quenching depends on the temperature of the luminophore. At low temperatures, the accelerated luminescence is more pronounced, while at high temperatures quenching is predominant.

Infrared rays longer than 1.2 μ produce only accelerated luminescence since their energy is insufficient to heat the luminophore to temperatures above 200°C, at which weakening of its emissivity begins.

The substances which can yield the greatest effect in the infrared region are the sulfides, selenides, and tellurides of cadmium and of certain other metals.

Luminophores sensitive to infrared rays may serve as indicators of infrared rays.

Section 77. Electron-Optical Transducers

The usual photoelectric instruments that pick up radiant energy, transform it into electric energy, or change their own conductivity. In some cases, the radiant energy of some portion of the spectrum must be converted into the energy of another portion, e.g., ultraviolet or infrared rays are converted into visible rays. For this purpose the so-called electron-optical transducers may be used.

Figure 128 illustrates the principle of construction of the electron-optical transducer. The transducer consists of a semitransparent photocathode and screen coated with a fluorescent substance and serving as the anode. The infrared rays, falling on the photocathode, induce the emission of electrons. These electrons accelerate their motion in the electric field produced between the cathode and anode and, by bombarding the anode, cause it to glow. In this way the infrared rays striking the cathode are converted into visible radiation of the screen.

The intensity of luminescence of the fluorescent screen depends on the intensity of the flux and the velocities of the electrons bombarding the screen. For this reason, the intensely irradiated areas of the photocathode cause a bright luminescence on the screen, while the less intensely irradiated regions produce a weaker luminescence. Thus, by projecting on the cathode an image of an object in infrared rays, a visible image of this object is obtained on the screen. The image will be undistorted if the distribution of the electron fluxes produced by various parts of the photocathode (the electron image), is not distorted along its path from the photocathode screen.

Special electron-optical focusing systems are used for focusing the electron beams between the photocathode and the screen. According to the type of such systems, transducers are subdivided into the following groups:

groups with uniform distribution of the electric field between the photocathode and the screen;

groups with electrostatic focusing;

groups with magnetic focusing;

groups with combined electrostatic and magnetic focusing.

The method of focusing by means of a uniform electric field, similar to the field of a plane capacitor, is the simplest but requires the distance between photocathode and screen to be small. With such focusing, an erect image is obtained on the screen.

The electrons emitted by the irradiated points of the photocathode move toward the anode screen in parabolic paths. Impinging on the screen, they yield an image no longer in point form, but in the form of a certain circle of confusion. If the electric field is sufficiently strong, the diffusion is so slight that the image is still distinct. However, close spacing of the electrodes and the intensification of the field between them is limited by the difficulty of manufacturing a uniform cathode, by the increased photoemission from the cathode under the action of the light radiated by the screen, and also by the intensified luminous background of the screen, produced by the increase in the autoelectronic and dark emissions of the cathode*.

An electrostatic system of focusing electron beams consists of metal diaphragms with apertures (electrodes). The electrostatic fields produced between the electrodes, due to their potential difference, have the same effect on the electron beams as glass lenses have on light rays. Such electrostatic fields are called electronic, or electrostatic, lenses.

A focusing system of electrostatic lenses has several advantages over the former type of focusing system: possibility of turning the image, which makes optical turning of the system unnecessary; better quality of the image; and possibility of using more powerful electric fields for accelerating the motion of the electrons.

Magnetic focusing is effected by means of magnetic fields ("magnetic lenses"), produced by permanent magnets or electromagnets. Systems of this type are widely used in electron microscopes.

To obtain maximum effectiveness of transduction, the fluorescent screen must

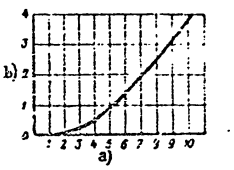

Fig. 129 - Relation between Amplification Factor and Accelerating Potential
a) Accelerating potential, kv; b) Amplification factor

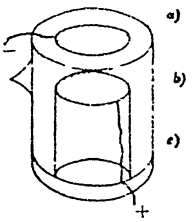

Fig. 130 - Electron-Optical Transducer of the Contact Type
a) Semitransparent photocathode; b) Fluorescent screen anode; c) Casing

meet the following basic requirements:

it must be a highly efficient transducer of electronic energy into visible radiation and must have a spectral composition corresponding to the spectral sensitivity of the eye;

it must have a fine-grained structure, permitting a high resolving power;

it must have negligible sluggishness and high luminous efficiency.

The irradiation sources of the photocathode generally have broad radiation spectra; therefore the radiant flux is passed through a special infrared filter to cut off the visible and ultraviolet rays.

The electron-optical transducer is able not only to transform invisible radiation into visible but also to increase the brightness of the image obtained on the screen. The intensification of the brightness of the image on the screen of the transducer, relative to the brightness on the photocathode is characterized by the amplification factor. Despite the low efficiency of the photocathode and the

* The dark emission is caused by the unirradiated photocathode being struck by long-wave infrared radiation, due to the temperature of the medium surrounding the transducer.

STAT

fluorescent screen, amplification still occurs because of the energy acquired by the electrons during their ... vel in the electric field between the anode and photocathode. Figure 129 gives the curve of the relation between the amplification factor and the accelerating potential (the potential between the anode and photocathode).

Figure 130 shows one of the first designs of an electron-optical transducer. The

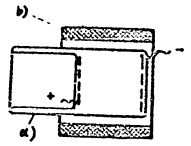

Fig. 131 - Electron-Optical Transducer with Magnetic Focusing
a) Body of transducer; b) Magnetic focusing coil

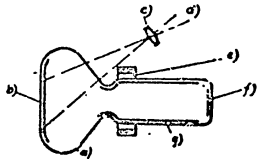

Fig. 132 - Electron-Optical Transducer with Solid Photocathode
a) Body; b) Photocathode; c) Lens; d) Infrared rays; e) Focusing coil: f) Anode (screen); g) Accelerating electrode

body of the transducer consists of a double-wall glass jar with a flat double bottom. Inside the body, a high vacuum of about 10^{-6} mm Hg is created. The inner surface of the bottom of the inner glass is coated with the translucent layer of the photocathode, while the bottom of the inner jar carries the fluorescent screen (anode). The constant voltage applied between anode and cathode is 3-10 kv.

If the photocathode is sensitive to infrared rays (for instance, an oxygen-cesium cathode), the electron-optical transducer will transform an invisible image into a visible one.

The sharpness of the image is increased and the resolving power of the instrument is raised, in some designs, by magnetic focusing (Fig. 131). Other designs use a solid photocathode, irradiated from inside (Fig. 132), which increases the sensitivity of the instrument. A transducer with a solid photocathode in addition to the magnetic focusing coil for accelerating the motion of the electrons, also uses an electrostatic field produced by a special accelerating electrode.

Figure 133 a schematically shows an electron-optical transducer with electrostatic focusing systems, consisting of several electrostatic lenses. Figure 133 b

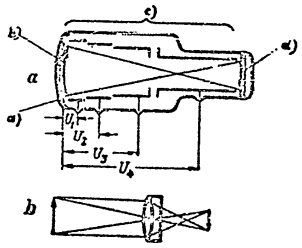

Fig. 133 - Electron-Optical Transducer with Focusing System of Several Electrostatic Lenses:
a- Schematic arrangement; b- Simplified optical analogy;
a) Photocathode; b) Image of object in infrared rays; c) Electrostatic lenses; d) Fluorescent screen anode

shows an optical system whose action on light rays is analogous to the action of an electrostatic focusing system on electron beams.

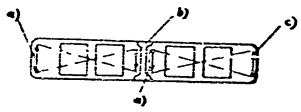

Fig. 134 - Two-Stage Electron-Optical System with Semi-transparent Photocathodes
a) Photocathode; b) Screen of first transducer; c) Screen of second transducer

In a multistage electron-optical system (Fig. 134), two or more electron-optical transducers are connected in series. The image obtained on the screen of the first transducer is transmitted to the photocathode of the following transducer, etc. The electrodes of all transducers can be fed in parallel from a common source.

Occasionally, secondary electronic amplification is used to increase the sensitivity. In this case, the electrons emitted by the photocathode are first focused on an electrode yielding a secondary electron emission; the secondary electrons are then directed onto a fluorescent screen. The principal disadvantages of systems with secondary-electron amplification is the poor image quality and the complex design.

CHAPTER IX

NONSELECTIVE INDICATORS OF INFRARED RAYS

Section 78. Types of Nonselective Indicators

Indicators of radiant energy in which photoeffect and luminescence are utilized, have sensitivity only in the short-wave portion of the infrared spectrum, up to wavelengths of 5-7 μ. They are, therefore, unsuitable for measuring radiant energy in the longer-wave portion of the infrared spectrum.

For this reason, so-called nonselective indicators are used in practice. Their sensitivity remains constant over a certain, rather wide portion, of the spectrum. Thermal indicators, based on the principle of transformation of the energy of infrared rays into thermal energy, may be used as such indicators for the infrared region. To produce a thermal indicator without selectivity, the surface of its sensitive element must have an absorption factor that is constant for a given portion of the spectrum. Platinum black, carbon black, and other substances with a high coefficient of absorption for infrared rays, are generally used as coatings for the sensitive elements of thermal indicators.

The following types of thermal indicators are used in practice: thermocouples, bolometers, thermistors, optico-acoustic and pneumatic indicators, radiometers, and microradiometers. Since the principle of operation of a number of thermoindicators is based on utilization of thermoelectric phenomena, we will first review the fundamental laws of thermoelectricity.

STAT

Section 79. Fundamental Laws of Thermoelectricity

When a junction of two different metals or alloys is heated, a thermoelectromotive force (temf) is produced. In a closed circuit, consisting of two different metals or alloys coupled to each other, different temperatures of the junctions cause a temf to arise which produces an electric current in the circuit. The value of the temf depends on the type of metals coupled and their temperature difference.

The electron theory of metals explains the formation of temf by the variation in the concentration of free electrons, due to the temperature difference: The electrons move from the more heated portions to the cooler portion.

According to this theory, the value of the temf becomes

$$E_T = \frac{K}{e} \ln \frac{N_A}{N_B} (T_2 - T_1) \qquad (166)$$

where K = Boltzman constant, equal to 1.38×10^{-16} erg/deg;

e = charge of an electron;

N_A and N_B = number of free electrons in 1 cm^3 of the thermocouple material;

T_1 and T_2 = temperatures of the junctions.

At minor temperature differences between the junctions, it may be assumed that

$$E_T = a(T_2 - T_1) \qquad (167)$$

where a = a coefficient characterizing the properties of the junction;

T_1 and T_2 = temperatures of the junctions.

In a circuit consisting of several different metallic conductors, a temf is created if the temperature of the junctions differs. When the circuit is broken, the temf becomes equal to the algebraic sum of the emf of all the junctions. Two different conductors, coupled together, form a thermocouple.

Connecting a new conductor in the circuit of a thermocouple does not change its emf if the terminals of the conductor have the same temperature. The thermoelectromotive force of a given thermocouple, corresponding to any temperatures of the two junctions, will not change if a series of other metals, at the same temperature as any junction, are inserted between the elements of that junction.

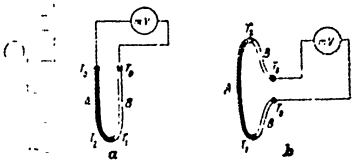

Fig. 135 - Connection Diagram of Electric Measuring Instrument to Thermocouple: a- To the junction of the thermocouple; b- To one of the electrodes of the thermocouple

Figure 135 shows an extremely simple circuit for connecting an electric measuring instrument to a thermocouple. The connection of the lead wires to the thermocouple does not change its temf if the temperature of the terminals of these leads is the same. Usually lead wires are used, which differ little in their thermoelectric properties from the wires of the thermocouple.

The direction of current in a thermocouple depends on the combination of its materials. For example, in a thermocouple consisting of bismuth (Bi) and antimony (Sb), when the junction is heated, the thermocurrent flows from the bismuth to the antimony. In a closed thermocouple with two junctions (Fig. 136), the thermocurrent likewise flows from the bismuth to the antimony in the junction having the higher temperature.

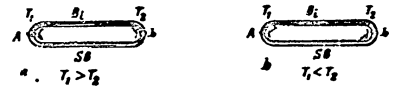

Fig. 136 - Direction of Currents in the Thermocouple Bismuth-Antimony at Various Temperatures of the Junctions

Figure 136 a shows the direction of the current for the case when the temperature T_1 of the junction A is higher than the temperature T_2 of the junction B; however, if the temperature of the junction B is higher than that of the junction A

(Fig. 136 b), the current will have the opposite direction.

All materials used for thermocouples may be arranged in a series in which each given material is more positive than the preceding one. It is customary to consider the material toward which the current flows in the heated junction as the more positive material.

The thermoelectric series given below consists of pure metals, a few alloys, and nonmetallic conductors and semiconductors: (-) bismuth; copel; constantan; an alloy of gold, platinum, and palladium; cobalt; nickel, alumel; potassium; palladium; sodium; mercury; platinum; carbon; aluminum; magnesium; tin; lead; tantalum; cesium; platinorhodium, rhodium; iridium; zinc; silver; tungsten; copper; brass; gold; manganin; cadmium; platinoiridium; molybdenum; iron; nichrome; chrome; antimony; silicon; tellurium; selenium (+).

Materials used for thermocouples are characterized by the magnitude of the temf induced by them in a couple with pure platinum.

Table 34 gives the values of the temf developed by various substances in a couple with platinum, together with the values of the temperature coefficients, the resistivities, and a few other physical constants of these thermocouples.

The temf of any couple (per 1°C), composed of the materials shown in this Table, is equal to the difference of the temf of thermocouples made of these materials in platinum couples.

Table 34

Name of Material	Symbol or Composition	Thermoelectromotive Force (in Couple with Pure Platinum) μv/°C	Temperature Coefficient, %	Resistivity, ohm mm^2 / m	Specific Heat, cal/degree	Thermal Conductivity at 18°C c.i. / cm-sec-deg	Specific Gravity, g/cm³	Melting Point, °C
Aluminum	Al	+ 4.0	0.43	0.025-0.0278	0.2-0.225	0.5	2.6	658
Alumel	95% Ni + 5% Al, Si, Mg	-10.2 ÷ -13.8	0.14	0.33-0.35	-	-	8.5	1450
Bismuth	Bi	-58.4 ÷ -78.0	0.454	1.1-1.40	0.03-0.033	0.024	9.8	270
Tungsten	W	+ 7.9	0.44	0.055-0.0612	0.034	0.23	19.1	3387
Iron (pure)	Fe	+ 18	0.621-0.637	0.09	0.105-0.16	0.165-0.16	7.85	1528
Gold	Au	+ 8	0.397	0.022	0.031	0.74	19.25	1063
Iridium	Ir	+ 6.5	0.393	0.053	0.032	0.14	22.42	2350
Cadmium	Cd	+ 9	0.42	0.076	0.054-0.062	0.22	8.64	321
Cobalt	Co	-16.8 ÷ -17.6	0.566-0.656	0.097	0.104	0.16	8.8	1473
Constantan	60% Cu + 40% Ni	-35	0.004	0.45-0.5	0.098	0.054	8.9	1220-1280
Copel	56% Cu + 44% Ni	-46	0.01	0.49	-	-	8.85	1250
Silicon	Si	+ 440	-	-	0.196	-	-	-
Brass	Cu (ca. 55%) + Zn (ca 45%)	+ 11	0.2	0.08	0.093	0.26	8.4	900
Magnesium	Mg	+ 4.1	0.39	0.0454	0.24	0.38	1.74	644
Manganin	84% Cu + 13% Mn + 3% Ni + 1% Fe	+ 8	0.0006	0.42	0.096	0.5	8.4	910
Copper (pure)	Cu	+ 7.6	0.433	0.0156-0.0168	0.091-0.094	0.85-0.94	8.95	1083
Molybdenum	Mo	+ 1.2	0.435	0.044-0.048	0.065-0.072	-	9.0	3000

Section 80. Characteristics of Thermocouples

The most widely used type of thermal indicator is the thermocouple.

Thermocouples are characterized by the following basic parameters: sensitivity, efficiency, sluggishness, and resistance.

The sensitivity is usually evaluated by the ratio of the temf of the thermocouple to the radiant flux incident on it. The absolute sensitivity of a thermoelement may be expressed in volts per watt (v/w), in microvolts per microcalory per second (μv/μ cal-sec), or in other units of voltage and radiant energy.

STAT

Name of Material	Symbol or Composition	Thermoelectromotive Force (in Couple with Pure Platinum) μv/°C	Temperature Coefficient, %	Resistivity, ohm mm^2 / m	Specific Heat, cal/deg·hour	Thermal Conductivity at 18°C cal / cm·sec·deg	Specific Gravity, g/cm^3	Melting Point, °C
Nickel	Ni	-15 ÷ -15.4	0.621-0.634	0.118-0.138	0.105-0.130	0.14	8.75	1455
Nichrome	80% Ni + 20% Cr	+ 15 ÷ + 25	0.014	0.95-1.05	-	-	8.2	1400
Tin	Sn	+ 4.3	0.44	0.143	0.052-0.056	0.155	7.4	232
Palladium	Pd	-5.7	0.35	0.17	0.06	0.168	11.5	1553
Platinum (pure)	Pt	0.00	0.394	0.098 + 0.106	0.032 + 0.033	0.167	21.3	1779
Platoiridium	90% Pt + 10% Ir	+ 13	0.115 + 0.126	0.23 + 0.25	-	-	-	-
Platinorhodium	87% Pt + 13% Rh	+ 6.46	0.167	0.19	-	-	-	≈ 1800
Rhodium	Rh	+ 6.4	0.443	-	0.058	-	-	967
Mercury	Hg	+ 0.4	0.096	0.943	0.033	0.020	13.6	-38.7
Lead	Pb	+ 4.4	0.411	0.227	0.031	0.084	11.3	327
Selenium	Se	+ 935	-	10^6 + 10^7	10^6 + 10^7	0.045	4.27	-
Silver	Ag	+ 7.2	0.41	0.0147	0.056	1.1	10.5	960.5
Alloy	60% Au + 30% Pd + 10% Pt	-23.1	0.02	0.34	-	-	-	1430
"	95% Rh + 5% Sn	+ 51	-	2.75	-	-	9.45	-
"	97% Rh + 3% Sb	- 70	-	1.74	-	-	9.62	-
"	90% Rh + 10% Sb	+ 75		1.00	-	-	8.89	-
"	99.6% Ta + 0.4% Bi	+ 195	-	29.2	-	0.005-0.008	6.26	-
"	99.1% Ta + 0.9% Sb	+ 140	-	23	-	0.005-0.008	6.32	-
"	98.5% Ta + 1.5% S	+ 580	-	35.10^3	-	0.0035-0.007	6.1	-
"	50% Sb + 50% Cd	+ 141	-	-	-	-	7.85	-
Alloy	51.7% Sb + 48.3% Cd	+ 312	-	-	-	-	7.8	-
"	65% Sb + 35% Cd	+ 110	-	7.9	-	0.0035-0.01	7.35	-
"	75% Sb + 25% Cu	+ 115	-	6.9	-	0.0035-0.01	7.15	-
Antimony	Sb	+ 48.6	0.47	0.417	0.05	0.054	6.67	630.5
Tantalum	Ta	+ 5.1	0.15	0.065	0.033	0.07-0.20	16.6	2800
Tellurium	Te	+ 375 ÷ + 440	0.38	0.35 + 2.5	0 048	0.0025-0.0043	6.24	302-452
Carbon	C	+ 3	-0.08	10	0.238	0.037	-	-
Chromel	90% Ni + 10% Cr	+ 27.1 ÷ + 31.3	0.05	0.7	-	0.048	8.7	1450
Chromel P	90% Ni + 10% Cr	> 40	-	0.75	-	0.047	-	-
Zinc	Zn	+ 7	0.39	0.062	0.091-0.095	0.27	6.86	419.5

STAT

However, such an evaluation does not take the size of the working area of the thermocouple into consideration. A thermocouple is therefore sometimes characterized by its relative sensitivity, which equals the ratio of the emf of the thermocouple to the density of the energy incident on its working area. In this case, the sensitivity is determined by the value of the emf developed by the thermoelectric cell under the action of the radiant energy incident on it.

The relative sensitivity is expressed, for example, in volts per watt per square millimeter (v-mm^2/w) or in microvolts per microcalory per second per square millimeter (μv-sec-mm^2/μ cal). In some cases, a thermocouple is characterized by the effective sensitivity, which means the ratio of the absolute sensitivity to its effective area (v/w-mm^2 or μv/μ cal-sec-mm^2).

It is common practice to evaluate a thermocouple by its absolute sensitivity in cases where it is irradiated by a concentrated flux whose cross section is less than the working (irradiated) area of the thermocouple. If the thermocouple, however, is in a diffused flux whose cross section is larger than the size of the instrument, it is preferable to use the relative sensitivity.

The sensitivity of a thermocouple depends on the material of the thermolayers and on the dimensions and shape of the working surface. The dimensions and shape of the working surface of a thermocouple are selected in accordance with its purpose.

The minimum radiant energy at which the signal at the output of a thermocouple is greater than the noise signal or equal to it is called the threshold of sensitivity of that thermocouple.

The sensitivity threshold of a thermocouple is limited by the voltage fluctuations due to the thermal agitation of the electrons, or to temperature fluctuations. The generated emf determines the sensitivity threshold of the thermocouple. The sensitivity threshold likewise depends on the resistance of the thermocouple, its specific heat, and its inertia or sluggishness. The value ranges from 10^{-8} to 10^{-13} watts.

The efficiency of a thermocouple is determined as the quantity of radiant energy, incident on the thermocouple, that is converted into electrical energy. The efficiency of thermocouples is very low (not exceeding fractions of a percent).

The inertia of a thermocouple depends on the rate of rise or fall of the thermal emf. The more rapidly the emf of a thermocouple reaches values corresponding to the energy incident on it, the smaller will be its inertia.

The thermal emf gradually increases to its final value, corresponding to the radiant flux striking the photocell. For this reason, the inertia is determined by the time τ taken by the thermocouple to develop an emf equal to 50, 90, or 95% of the total (final) emf, which is denoted by $\tau_{0.5}$, $\tau_{0.9}$, or $\tau_{0.99}$, respectively. The inertness values of different thermocouples range from hundredths of a second to a few seconds.

The resistance of a thermocouple depends on its material and design. The value of the thermocouple inherent noise and the selection of the measuring instrument to which the thermocouple is connected, are determined by the resistance.

Section 81. Design of Thermocouples

The parameters of a thermocouple depend mainly on its design. The sensitivity of a thermocouple rises with diminishing heat losses. In designing thermocouples, therefore, efforts are made to reduce the mass and thermal yield of the thermocouple. For this purpose, the thermocouple is placed in a vacuum, which almost completely eliminates the losses through the gas, and might increase the sensitivity by a factor of 20-40 (but it must be borne in mind that the inertia of the thermocouple is also increased in this case). The significance of vacuum for increasing the sensitivity was first established by the noted Russian scientist, Professor P.N.Lebedev.

If a thermocouple is mounted in a tube, the material of the tube or the window of the body must be transparent to infrared rays in the working region of the spectrum. The working areas of thermocouples are covered by substances with a good ab-

STAT

sorption for these rays, such as metallic black, carbon black, or magnesia.

Let us consider the construction of a few types of thermocouples.

The first thermocouple, in the form of a thermopile was built in 1835. It consisted of 28 pairs of bismuth and antimony plates, stacked and connected in series.

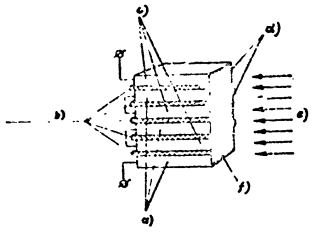

Fig.137 - Thermopile of Bismuth and Antimony (in all, 25 Junctions Each 2 × 2 mm; Total Area 100 mm²)
a) Antimony; b) Insulating plates; c) Bismuth; d) Working space; e) Luminous flux; f) Absorbing layer

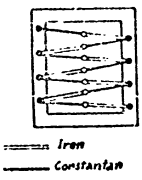

Fig.138 - Iron-Constantan Thermopile (20 Junctions in all)

The design of this thermopile is shown (for three pairs of plates) in Fig.137. The thermopile produced a sufficient emf, but had a low specific sensitivity, since its working area was very large (100 mm²). In addition, due to the large mass of the plates, the inertia of the thermopile was high (14 sec). Mechanically, the thermopile was of low strength.

Later, in 1898, a thermopile was built of 20 iron-constantan thermocouples. The thermocouples consisted of thin iron and constantan wires, joined by silver (Fig.138). To increase the working area of the thermocouple, sheets of metal foil covered with carbon black were soldered to the junction points. All junctions were on a single vertical line. This thermopile was used for spectrometry. Its sensitivity was lower than that of the thermopile described above.

The next step in the perfection of thermocouples was taken in 1902, when P.N.Lebedev first placed a thermocouple in a vacuum, thereby considerably raising the sensitivity of the thermocell. The investigations by Lebedev showed that it was of great practical importance to place the thermocouples in a vacuum when using fine wires, where the heat losses due to the thermoconductivity of the wires are small in comparison to the radiation losses.

At first thermoelements and thermopiles were made of thin wires or plates of tellurium, bismuth, antimony, silver, iron, constantan, and certain other metals. The first thermoelectric cells had relatively large mass and sluggishness. The working spaces of thermoelements, intended for spectrometry, were made in the form of piles, and those for measuring a diffuse radiant flux in the form of a plane square. In many designs, a special plate absorbing the energy of the radiant flux was soldered to the thermocouple.

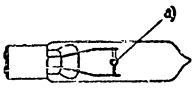

Fig.139 - Ribbon Vacuum Thermoelement
a) Thermojunction

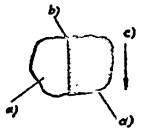

Fig.140 - Thermo-Foil
a) Constantan; b) Thermojunction; c) Direction of rolling; d) Iron

The object of reducing the mass of the electrodes and the working space of the thermoelement led to the construction of the so-called strip thermoelements.

The thermocouples of such thermoelements are made of strip thermofoil. The vacuum thermoelectric cell shown in Fig.139 uses thermofoil of manganin-constantan about 1 μ in thickness.

A thermofoil is made of two different metals. First, two relatively thin wires are soldered together, e.g. iron and constantan or manganin and constantan; these are then rolled perpendicularly to the axis of the wires (Fig.140). As a result, a very thin foil 0.5 to 1 μ thick is obtained, from which strips of any desired

STAT

width and shape are cut.

Thermobatteries (Fig.141), or thermopiles, are sometimes assembled of thermofoil. A thermobattery consists of many junctions which need not all be irradiated by the incident radiant flux. The irradiated junctions are called working junctions, the unirradiated, free junctions.

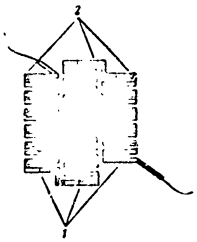

Fig.141 - Thermobattery of Thermofoils:
1- Working junction; 2- Free junctions

Thermocouples can also be made by an electrolytic method. In this case, thin layers of two materials are alternately deposited through a stencil on a polished plate, in such a way that the different metals partly overlap. From the film so obtained, strip thermocells or thermopiles are made. The thickness of the strips is 0.1 μ.

In addition, thermocells are made by the method of cathode sputtering and by the method of vacuum deposition.

The former method is based on the fact that, when an electric discharge takes place in gases, the positive ions gradually destroy the cathode. The sputtered material is deposited in the form of a thin film on the surface surrounding the cathode. The degree of sputtering depends on the cathode material and also on the discharge current and voltage as well as on the nature of the gas in which the discharge takes place. To obtain a film for a thermocouple, the material to be sputtered and the plate on which it is to be deposited are placed in a tube containing a rarefied gas, and a discharge is induced. The plate is then covered with a thin film of sputtered material, about 0.1 μ thick.

The second method consists in an evaporation of metal in vacuo. The metal, heated in an electric furnace to the temperature of vaporization, is placed in a vacuum; above or below the metal, a mica plate or celluloid film, covered with a stencil is placed, on which the vaporized metal is deposited. The two metals forming the thermocouple are deposited on the plate through the stencil in such a way that a thermoelement or thermopile is obtained. The thickness of the metal layers obtained by this method is very small.

Bismuth, antimony, tellurium, nickel, copper, and certain other metals are conventional materials for thermocouples; sometimes alloys, which produce a higher thermoelectromotive force, are used.

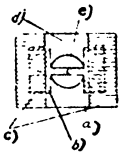

Fig.142 - Foil Thermoelement
a) Bismuth; b) Tellurium; c) Gold; d) Mica; e) Celluloid

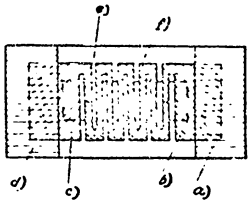

Fig.143 - Foil Thermopile
a) Gold; b) Bismuth; c) Tellurium; d) Gold; e) Celluloid; f) Mica

Contact with the electrodes of a thermocouple is effected through a layer of gold deposited by the same method at the ends of the electrodes. Leads are soldered to the gold layer by low-melting solders.

In some cases, clamps are used for making the contacts.

The foils on which metallic layers are deposited have a thickness of 10^{-5} - 10^{-6} cm (0.1-0.01 μ), while metal layers deposited on these films are 10^{-6} - 5×10^{-6} cm (1-0.05 μ) thick. The sensitivity of thermoelements produced by such methods is very high, and their inertia is insignificant.

Thermoelements of this type were made with one junction (Fig.142) or in the form of a thermopile with several junctions (Fig.143). The thickness of the celluloid base was 3×10^{-6} cm, and the thickness of the metal layer applied was 5×10^{-5} cm. The total thickness of the center portion of the thermoelements was about 10^{-5} cm, i.e., about 10 times less than the thickness of strip thermocouples.

The sensitivity of these thermoelements (with amplifier) was as high as 2 × × 10^{-10} cal/sec-cm^2, i.e., 30 to 40 times as high as that of strip thermoelements (cf. Fig. 139).

In some thermoelements, alloys of different metals which yield a higher thermoelectromotive force are used for the thermocouples.

Such alloys include alloys of bismuth, antimony, and tin, e.g., an alloy of bismuth with 5% tin (95% Bi + 5% Sn) or of bismuth with 3% antimony (97% Bi + 3% Sb); the thermoelectromotive force of thermoelements made of these alloys is as high as 120 μv/deg.

Of such alloys, foils or very fine wire (thickness down to 15 μ) are usually prepared and are soldered to a plate of thin metal foil, serving as the receptor of radiant energy.

In addition to metals and their alloys, certain semiconductors possessing a high temf are sometimes used in making thermoelements; these include, for example, selenium, whose temf is equal to almost 1000 μv/deg.

M.A. Levitskaya developed a thermoelement in which one electrode was made of an alloy of selenium with copper and the other of pure copper. Selenium has a very high resistance, but compounds of electrically conducting metals with selenium may have a rather high electric conductivity and are useful as thermoelements. The thermoelectromotive force of this thermocouple, equal to 250 μv/deg is several times as great as that of other thermocouples.

Table 35 gives the data of a few thermoelements.

Table 35

Data of Several Thermoelements

Type of Thermoelements	Year Built	Material of Thermocouple	Temf, μv/deg	Number of Junctions	Receptor Area and Thickness, mm	Resistance, ohm	Sensitivity, μv/lm	Sluggishness, sec	Remarks
Thermopile of bismuth and antimony	1835	Bismuth-antimony	-	25	10 × 10	0.5?	1	11	
Iron-constantan pile	1858	Iron-constantan	53	20	20 × 3.14 × 0.25	3.5	4	2	
Lebedev thermoelement	1902	Same	-	-	-	-	-	-	First Lebedev vacuum thermoelement
Levitskaya-Lukomskaya thermoelement	1922	Tellurium-bismuth	360	1	3 × 0.25	10	-	-	
Strip thermoelement	1925	Manganin-constantan	40	1	1 × 1	10-20	3.5	2-3	
Lee-Leertis thermoelement	1947	Alloys of bismuth with antimony and bismuth with tin	-	1-4	0.5-4 mm^2	5-12.5	3.5-6.5	0.03-0.04	Operates with modulation of radiant flux at f = 5 cps

Section 82. Bolometers (Bibl. 13)

An indicator of radiant energy whose action is based on the variation in resistance of the sensitive element, when heated by the absorption of a radiant flux, is called a bolometer.

Bolometers, like elements, are widely used in infrared technology. A bolometer will measure variations in temperature as small as 10^{-7}°C and in voltage down to

STAT

The sensitivity of these thermoelements (with amplifier) was as high as 2 × × 10^{-10} cal/sec-cm^2, i.e., 30 to 40 times as high as that of strip thermoelements (cf. Fig. 139).

In some thermoelements, alloys of different metals which yield a higher thermoelectromotive force are used for the thermocouples.

Such alloys include alloys of bismuth, antimony, and tin, e.g., an alloy of bismuth with 5% tin (95% Bi + 5% Sn) or of bismuth with 3% antimony (97% Bi + 3% Sb); the thermoelectromotive force of thermoelements made of these alloys is as high as 120 μv/deg.

Of such alloys, foils or very fine wire (thickness down to 15 μ) are usually prepared and are soldered to a plate of thin metal foil, serving as the receptor of radiant energy.

In addition to metals and their alloys, certain semiconductors possessing a high temf are sometimes used in making thermoelements; these include, for example, selenium, whose temf is equal to almost 1000 μv/deg.

M.A. Levitskaya developed a thermoelement in which one electrode was made of an alloy of selenium with copper and the other of pure copper. Selenium has a very high resistance, but compounds of electrically conducting metals with selenium may have a rather high electric conductivity and are useful as thermoelements. The thermoelectromotive force of this thermocouple, equal to 250 μv/deg is several times as great as that of other thermocouples.

Table 35 gives the data of a few thermoelements.

Table 35

Data of Several Thermoelements

Type of Thermoelements	Year Built	Material of Thermocouple	Temf, μv/deg	Number of Junctions	Receptor Area and Thickness, mm	Resistance, ohms	Sensitivity, μv/μw	Sluggishness, sec	Remarks
Thermopile of bismuth and antimony	1835	Bismuth-antimony	-	25	10 × 10	0.55	1	11	
Iron-constantan pile	1898	Iron-constantan	53	20	20 × 3.16 × 0.25	3.5	4	2	
Labedev thermoelement	1902	Same	-	-	-	-	-	-	First Labedev vacuum thermoelement
Lavitskaya-Lukomskaya thermoelement	1922	Tellurium-bismuth	240	1	3 × 0.25	10	-	-	
Strip thermoelement	1925	Manganin-constantan	40	1	1 × 1	10-20	3.5	2-3	
Low-inertia thermoelement	1947	Alloys of bismuth with antimony and bismuth with tin	-	1-4	0.5-4 mm^2	5-12.5	3.5-6.5	0.03-0.04	Operates with modulation of radiant flux at f = 5 cps

Section 82. Bolometers (Bibl. 13)

An indicator of radiant energy whose action is based on the variation in resistance of the sensitive element, when heated by the absorption of a radiant flux, is called a bolometer.

Bolometers, like elements, are widely used in infrared technology. A bolometer will measure variations in temperature as small as 10^{-7}°C and in voltage down to

10^{-10} v and detect a radiant flux of powers down to 10^{-10} watt.

The element of a bolometer sensitive to radiant flux (the receptor area) is made of thin layers of various metals, semiconductors and dielectrics, the layers of

Table 36

Characteristics of Certain Materials Used in Making Bolometers

Material	Resistivity at 0°C, ohms-cm	Resistivity at 18°C, ohms-cm	Temperature Coefficient of Resistance α of Thin Layers at 18°C, 1/deg
Platinum	9.8×10^6	10.5×10^6	+ 0.0039
Gold	2.06×10^6	2.21×10^6	+ 0.004
Nickel	6.6×10^6	7.35×10^6	+ 0.0063, + 0.0067
Iron	8.9×10^6	9.9×10^6	+ 0.0065
Tungsten	4.89×10^6	5.32×10^6	+ 0.0046
Bismuth	109×10^6	118×10^6	- 0.0045
Antimony	36.3×10^6	39.8×10^6	- 0.0047
Tellurium	15.9×10^6	17.5×10^6	- 0.005
Copper oxide	3.3×10^{10}	-	- 0.033
Oxides of Manganese, nickel, and cobalt	3×10^9	-	-0.06, -0.05

the material ranging in thickness from fractions of a micron to several microns. The sensitivity of a bolometer depends on the value of the thermal coefficient of resistance of the material of the element, so that better results are obtained by using substances with a high temperature coefficient of resistance.

Table 36 gives comparative data for a few materials used in making the sensitive elements of bolometers.

The bolometer usually operates on a bridge circuit fed by DC or AC, when connected to one of the arms of the bridge as shown in Fig.144.

In this diagram, R_x denotes the resistance of the sensitive element of bolometer; R_1, R_2, R_3 are the resistances of the remaining arms of the bridge; I is the total current; I_1 the current flowing through the bolometer; I_2 the current through the resistor, Y the amplifier; R_g the resistance of the measuring instrument.

If the sensitive element is not irradiated, the bridge is in equilibrium, and the pointer of the measuring instrument connected to the output of the amplifier

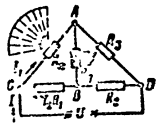

Fig.144 - Bridge Circuit of Connecting Bolometer

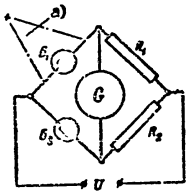

Fig.145 - Compensation Bridge Circuit of Connecting Bolometer
a) Flux measured

does not deflect. On irradiation of the element, its resistance R_x varies, the balance of the bridge is disturbed, and a current fixed by the measuring instrument appears. The sensitivity of the bolometer depends on the value and direction of the feed current.

A circuit with one bolometer, as shown in Fig.144, is subject to the influence of fluctuations in the ambient temperature and in the temperature of the feed source, which may lead to unbalancing of the bridge, even without irradiating the bolometer. To exclude this influence, a compensation bridge circuit with two bolometers is used, connected as shown in Fig.145. When the ambient temperature varies, both bolometers have the same variation in resistance, so that the balance of the bridge is not disturbed. When the feed voltage fluctuates, the change in the current produces the same change in the resistance of both bolometers, and the balance of the bridge is maintained. The measured radiant flux is focused on one bolometer, whose resistance varies, and the bridge is unbalanced.

A bolometer with maximum sensitivity to infrared rays must be able to register very small variations in temperature. This may be accomplished if the energy losses

due to thermal conductivity are reduced to a minimum, by placing the bolometer in a vacuum. In this case the sensitivity increases but so does the inertia. In cases where a low inertia is required, the sensitive element of the bolometer is placed in a tube with air; air is a good conductor of heat away from the element of the bolometer and thereby favors a rapid restoration of the element's own temperature within a short time. Depending on the type of material used for the sensitive element, bolometers are subdivided into three types: metallic, dielectric, and semiconductor.

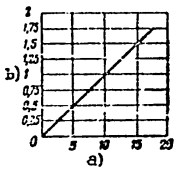

Fig. 146 - Relation between Sensitivity of Bolometer and Current
a) Current, ma; b) Sensitivity, v/w

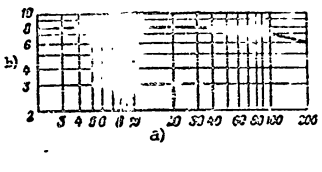

Fig. 147 - Frequency Characteristics of the Bolometer
a) Modulation frequency, cps; b) Sensitivity in relative units

The superconductor bolometers occupy a special place. Their sensitive elements are made of a metal or a semiconductor.

The principal characteristics of a bolometer as an indicator of infrared rays are its sensitivity and its inertia.

The sensitivity of a bolometer is characterized by the ratio of the voltage drop variation across the bolometer due to variation in the resistance, to the radiant flux falling on the surface of the sensitive element. Sensitivity is expressed in volts per watt (v/w) or in microvolts per microcalory per second (μv/μ cal-sec). The sensitivity is proportional to the temperature coefficient and to the applied voltage, and inversely proportional to the area of the sensitive element. The magnitude of the threshold sensitivity is determined by the noise level produced by the thermal agitation of the electrons.

The inertia, defined by the time constant τ, characterizes the rate of change of resistance of the bolometer and, consequently, also of the voltage drop across it, under the action of radiant energy. The inertia or sluggishness represents the time necessary for the change in voltage drop across the bolometer to reach a certain value (usually, 50%) with respect to the maximum value produced by the corresponding radiant flux. When a modulated radiant flux is being measured, the inertia characterizes the variation in sensitivity as a function of the frequency of the radiant flux, i.e., it becomes the frequency characteristic.

Section 83. Construction of Bolometers

Metal Bolometers

The materials used for the sensitive elements of metal bolometers are platinum, gold, nickel, antimony, bismuth, and certain other metals. These metals are used in the form of very thin foil (a few tenths of a micron thick) or of a film (of thickness down to 0.05 μ) deposited by cathode sputtering on a thin base of mica, nitrocellulose, or other nonconducting material. Electrodes of gold are deposited on the metal foil and the film itself, to improve its absorption of radiant energy, is blackened with a special composition. The sensitive element of the bolometer is placed into a tube from which the air is exhausted to a certain vacuum, or into a tube filled with hydrogen at a certain pressure. The tube, or the body of the bolometer, has a window of a material transparent to infrared rays.

The total sensitivity of a bolometer ε with an unmodulated radiant flux may be determined by the formula

$$\varepsilon = \frac{\Delta U}{q\Phi} = \frac{\alpha \Delta R_x I \Delta T}{q \Phi S} \quad [v/w] \qquad (168)$$

where ΔU = magnitude of voltage drop;

q = coefficient of absorption (degree of blackness) of the coating;

Φ = radiant flux;

α = temperature coefficient of resistance of the bolometer material;

ΔR_x = magnitude of variation of the bolometer resistance;

ΔT = temperature change of the bolometer under the action of radiant flux;

S = area of sensitive element;

I = current flowing through the bolometer.

It follows from eq.(168) that the sensitivity is directly proportional to the current flowing through the bolometer. This is illustrated in Fig 146, which represents the relation of the sensitivity and the current for a vacuum bolometer with a sensitive element of tungsten. The diagram shows that, at a current of 1.75 × × 10^{-2} amp, the sensitivity reaches 1.75 v/watt, and constantly and linearly increasing with the flux.

Table 37

Basic Data of Several Metal Bolometers

Material	Time Constant, Millisec	Sensitivity at Zero Frequency, v/w	Working Area, mm^2	Resistance, ohms	Sensitivity Threshold Watt
Nickel	5.3	0.61	5.7	4.2	9×10^{-6}
"	21.2	2.26	17.2	16	9×10^{-6}
"	4.7	1.46	4.5	64	9×10^{-6}
"	7.2	1.6	4.5	44	9×10^{-6}
"	3.6	1.61	4.5	128	9×10^{-6}
Iron	80	-	10	-	3.5×10^{-6}
Gold	3.8	4.35	2.75	200	10^{-7}

In a bolometer with a metallic film of gold, the sensitivity threshold is equal to 10^{-7} watt, the sensitivity amounts to 4.35 v/watt, and the time constant is 3.8 millisec. A gold bolometer can operate under a modulated radiant flux. The frequency characteristic of this bolometer, filled with hydrogen under a pressure of 20 mm Hg, is given in Fig.147. The diagram shows that, at irradiation frequencies of almost up to 40 cps, the sensitivity remains constant and declines smoothly only on further increase in the frequency of the flux.

Table 37 gives the basic data for several metal bolometers.

These data indicate that a bolometer of gold is preferable. It has the smallest threshold sensitivity (10^{-7} watt), and a high sensitivity (4.35 v/w), at low inertia (3.8 m sec).

Dielectric Bolometers

Figure 148 schematically shows the design of a dielectric bolometer. The sensitive element of the bolometer is the film (1) of nitrobenzene or cellophane, on which, on both sides, the gold electrodes (2) are deposited. The thickness of the nitrobenzene film is about 5×10^{-4} cm, and that of the cellophane film about 0.02 mm. The film with the electrode is attached to two bases of copper. A dielectric bolometer, with its sensitive element made of a nitrobenzene film of an area of 0.5 mm^2 and a resistance of 2000 ohms, has a sensitivity of about 300 v/w and a sensitivity threshold equal to 10^{-8} watt. The dielectric bolometer can operate with a modulated radiant flux of a frequency up to 30 cps.

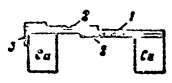

Fig.148 - Arrangement of Dielectric Bolometer: 1- Nitrobenzene film; 2- Electrodes; 3- Attachment

Semiconductor Bolometers

Bolometers of this type use layers of semiconductors as the sensitive element, e.g., a film of copper oxide or manganese, nickel, and cobalt oxides 1.5 × 0.1 mm in size and $2 \times 10^{-2} - 10^{-2}$ mm in thickness, which are applied on a glass or quartz plate. Semiconductor bolometers can operate not only in vacuo but also in air. Owing to the high temperature coefficient of resistance, which amounts to about 40% for each 1°C, these bolometers have a very high sensitivity. For example, the sensitivity of a cuprous oxide bolometer is 14,300 v/watt at a potential of 1000 v

and an ambient temperature of + 40°C.

The sensitivity of semiconductor bolometers may be determined by the formula

$$\varepsilon = \frac{U\Delta T\alpha}{\Phi S}\left(1 - e^{-\frac{t}{b}}\right) \text{ v/w} \qquad (169)$$

where U = voltage across bolometer;

ΔT = temperature rise on irradiation by the flux Φ;

S = working area;

t = time of action of radiant flux;

b = a constant.

It will be seen from eq.(169) that the sensitivity increases by an exponential law. If, for example, a bolometer of manganese, nickel and cobalt oxides has a

Table 38

Characteristics of Semiconductor Bolometers

Material	Time Constant, Millisec	Sensitivity, v/w	Working Area, mm^2	Resistance ohm	Sensitivity Threshold w
Mn, Ni, Co oxides	5.9	730	0.6	3×10^6	25.5×10^{-10}
Same	1.27	378	0.62	3×10^6	105×10^{-10}
"	1.35	3456	0.58	3×10^6	1.14×10^{-10}
"	3	100	0.6	4×10^5	2×10^{-8}
Cu oxide	220	14,300	7	1.5×10^8	6×10^{-8}

sensitivity threshold equal to 2×10^{-8} watt, at a frequency of 30 cps and a time constant of 3 m sec, then a temperature change of 2×10^{-6}°C will cause its resistance to change by 0.3 ohm, resulting in a change in voltage of 3×10^{-6} v. Table 38 gives data of a few semiconductor bolometers.

The Table shows that the smallest time constant is obtained in bolometers of cobalt, nickel and manganese oxides, which possess a high threshold and total sensitivity. Bolometers of copper oxide have a very high sensitivity but also a high inertia.

Superconducting Bolometers

The operation of superconducting bolometers is based on the phenomenon of supraconductivity. At very low temperatures, close to absolute zero, the resistance of certain materials drops to a few tenths of an ohm, and, consequently, their conductivity sharply rises. The temperature coefficient of resistance increases abruptly, greatly increasing the sensitivity of the bolometer.

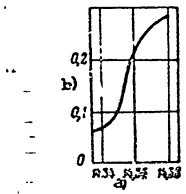

Fig.149 - Supraconductivity of Columbium Nitride at Low Temperatures
a) Temperature, °k;
b) Resistance, ohms

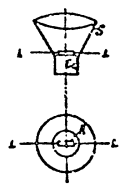

Fig.150 - Arrangement of Superconducting Bolometer of Columbium Nitride

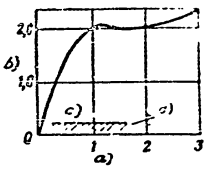

Fig.151 - Relation of Sensitivity of Bolometer to Time of Irradiation
a) Time of irradiation, millisec; b) Sensitivity in relative units;
c) Noise level;
d) $5 \cdot 10^{-6}$ μ watt

To make the sensitive elements of superconducting bolometers, tantalum is used, in which sepraconductivity starts at a temperature of 3.22-3.23°k (-269.18 to -269.17°C) or columbium nitride, in which supraconductivity starts at a temperature of 14.34-14.38°k (-258.66°C to -258.62°C), as demonstrated in Fig.149.

The principal difficulty in building superconducting bolometers of tantalum is the necessity of constructing apparatus for obtaining the extremely low temperatures and for accurately maintaining the constant temperature of the transition point to supraconductivity. It is simpler to build superconducting bolometers of

columbium nitride, since they do not require cooling such extremely low temperatures as tantalum bolometers do. The arrangement of a columbium nitride superconducting bolometer is schematically shown in Fig. 150. On a copper base (Cu) a sensitive element consisting of a columbium nitride strip L 5 mm long, 0.5 mm wide and 0.025 mm thick, prepared by heat-treating columbium in an ammonia jet, is cemented by bakelite varnish.

Table 39

Data of Superconducting Bolometers

Area of Sensitive Element, mm	Sensitivity Threshold Watt	Time Constant, Millisec	Modulation Frequency of Radiant Flux, cps
0.7	42×10^{-10}	0.9	360
1.6	186×10^{-10}	0.8	360
0.4	430×10^{-10}	1.7	360
6.4	1100×10^{-10}	4.2	360
1	5×10^{-10}	0.5	13
0.8	10×10^{-10}	0.3	13

The sensitive element is placed in the vacuum tube S, which is connected with a cooling chamber (cryostat), filled with a mixture of liquid nitrogen and hydrogen. In this chamber, a temperature of about 15°K is maintained.

Superconducting bolometers of columbium nitride have good physical properties. Figure 151 shows the relation of the sensitivity, expressed in relative units, to the time of irradiation of the bolometer by a radiant flux at a frequency of 13 cps. The diagram shows that the sensitivity reaches its maximum value within 1 millisec and half of this maximum value within 0.3 millisec. Thus the time constant is very small.

Table 39 gives a few data of superconducting bolometers of columbium nitride.

It will be seen from the data given in this Table that superconducting bolometers of columbium nitride have considerable advantages over other types of bolometers with respect to time constant, sensitivity threshold, and allowable modulation frequency of the radiant flux

Section 84. Thermistors

In recent years, considerable attention has been paid to semiconductor resistors and the possibility of their use in technology. The high negative temperature coefficient of resistance and the low electric conductivity, formerly considered drawbacks of semiconductors, was used as the basis for developing a semiconductor indicator, which was given the name of thermistor. The thermistor utilizes the property of certain semiconducting materials of sharply varying their resistance at small variations in temperature. The advantage of the thermistor as an indicator of radiant energy over the thermoelement and the bolometer is its simplicity of manufacture, and its greater durability and stability in operation.

Table 40

Characteristics of Materials for the Manufacture of Thermistors

Material	σ $ohm^{-1} \cdot cm^{-1}$	α % °C
Ag_2S	2×10^{-3}	-3.8 to -5
$CuO + Mn_3O_4$	10^{-1} to 10^{-2}	-3 to -3.2
UO_2	1.3×10^{-3}	-3.2
CuO	10^{-3} to 10^{-6}	-2.6
Cu_3O_4	1.5×10^{-3}	-2.7
TiO_2MgO	1.6×10^{-2}	-1.3
Zn	1	-0.5
$CuOCr_2O_2$	1×10^{-3}	-2.8
$Mn_3O_4 + NiO$	1×10^{-6}	-3.2
PbSe	2.4×10^{-1}	-0.8

Note. σ was measured at temperatures of + 20°C, and α, in the interval from + 16 to + 20°C.

Table 40 gives the values of the electric conductivity σ and the temperature coefficient α for materials from which thermistors can be built.

Table 40 shows that the oxides of various metals are the principal materials used for thermistors. Thermistors are made by mixing certain oxides in powder form. The resultant mixture, after adding an organic binder, is spread in a thin layer on a glass plate. The plate is dried and heated to evaporate the binder, and is then treated at high temperatures until the mixture changes into a hard mass. To obtain contacts, the ends of the plate are coated with a metal paste which is hardened by firing. Leads are soldered to the contacts. The thickness of the sensitive layer of a thermistor ranges from 0.001 to 0.004 cm, the length of the plate from 0.1-1 cm, and the thickness from 0.02 to 0.1 cm.

Table 41

Resistance of Uranium Oxide Thermistor as a Function of Temperature

t °C	R_T ohms
- 60	420,000
- 40	190,000
- 20	80,000
0	55,000
+ 16	35,500
22	28,500
31	22,000
38	18,000
56	10,500
78	6,200
98	3,950

The principal characteristics of the thermistor are as follows:

Volt-amper characteristic, indicating the relation between the value of the current flowing through the thermistor on the applied voltage.

Dissipation constant H, representing the relation between the power input in watts, dissipated in the thermistor, and the rise in its temperature as a result of this dissipation (in °C), by comparison with the ambient temperature

$$H = \frac{P}{T_T - T_0} \text{ mw/°C} \qquad (170)$$

where P = power input;

T_T = temperature of thermistor;

T_0 = ambient temperature;

The power sensitivity, ϵ_p, is the number of watts which must be dissipated to reduce the resistance of the thermistor by 1%. This quantity is determined from the relation

$$\epsilon = \frac{c}{\alpha \, 100} \qquad (171)$$

Time constant τ, the time necessary to vary the temperature of the thermistor by 63% of the difference $T_T - T_0$ at the initial instant of measurement. The current constant may also be defined by the formula

$$\tau = \frac{c}{H} \text{ sec} \qquad (172)$$

where c = heat capacity in joules per degree C (j/deg);

H = dissipation constant.

Depending on the dimensions, density and specific heat of the material, the time constant of the thermistor may vary from 10^{-3} sec to 10 min.

Thermistors, like bolometers, usually operate on a bridge circuit. The sensitivity threshold of the thermistor may be as low as 10^{-9} watt.

Let us consider the characteristics of certain types of thermistors.

Uranium Oxide Thermistors (Bibl.14)

B.T.Kolomiyets proposed heat treatment of uranium oxide in hydrogen to build thermistors of uranium oxide. The instruments obtained as a result of such treatment possess good electric conductivity, at small dimensions and low time constant. Since air has a disintegrating effect on uranium oxide, the thermistor must be placed in an exhausted glass tube.

Table 41 gives the values of the resistance R_T of a uranium oxide thermistor as a function of the ambient temperature t.

The table shows that the resistance of a thermistor drops with increasing temperature.

The relation of the current I_T to the applied voltage U_T (volt-ampere charac-

teristics) is characterized by the data given in Table 42. The table also shows that the thermistor has a sluggishness whose value is determined by the time interval

Table 42

Relation of Current I_T of an Applied Voltage U_T for a Uranium Oxide Thermistor

U_T, v	I_T, ma							
	Time Interval after Connection, sec							
	5	10	15	20	25	30	35	45
35	3.5	4.2	5.0	5.5	6.0	6.5	6.8	7.2
40	4.6	6.8	8.2	11.0	17.5	40.0	100	
45	6.0	10.0	20.0	100				
50	8.0	19.0	100					

after connection.

Thermistors of Manganese Oxide and Nickel Oxide

Figure 152 gives the volt-ampere characteristic of a thermistor of manganese oxide and nickel. At a definite value of the current, the voltage reaches a maximum

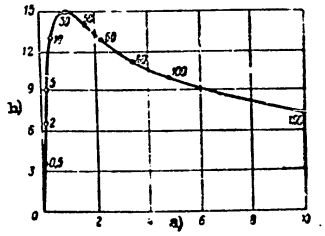

Fig. 152 - Volt-Ampere Characteristic of a Thermistor of Manganese Oxide and Nickel
a) Current, ma; b) Applied voltage, v

value and then, despite a further increase in current, decreases so that the resistance of the thermistor $h = \frac{dU}{dI}$ becomes negative.

The number on the curve gives the values of the difference $T_T - T_o$, expressed in centigrades. For each point of the curve, the ratio $\frac{U}{I}$ gives the resistance, while

Table 43

Relation of the Values of R and α of a Thermistor of Manganese Oxide and Nickel to the Temperature

Temperature of Thermistor, T_T, °C	Resistance of Thermistor R, ohms	Temperature Coefficient α, % per 1°C
-25	560,000	-6.1
0	145,000	-5.2
25	46,000	-4.4
50	16,400	-3.8
75	6,700	-3.3
100	3,200	-3
150	830	-2.4
200	305	-2
275	100	-1.5

the product $UI = H(T_T - T_o)$ gives the power dissipated. The dissipation constant H can be determined readily from the curve for the points at which the values of the difference $T_T - T_o$ are given.

Table 43 gives the resistance of a thermistor of manganese oxide and nickel, and the temperature coefficient of resistance α, as a function of the temperature of the thermistor. This thermistor is able to record a change in temperature amounting to 0.0005°C.

The table indicates that, at increasing temperature, the resistance of the thermistor drops sharply, and the temperature coefficient also diminishes, although not so markedly.

A thermistor of manganese oxide, nickel and cobalt at + 25°C has the value α = - 3.4. The dissipation constant is H = 0.1 mw/deg. The maximum allowable

STAT

temperature of heating is + 150°C. The time constant is less than 1 sec. The resistance decreases from 5000 ohms at 0°C to 95 ohms at + 150°C.

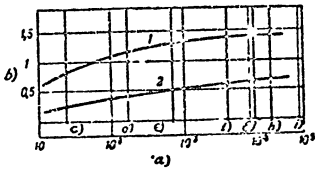

Fig. 153 - Characteristics of Stability of Operation of Thermistors:
1- Oxide of manganese and nickel; 2- Oxide of manganese, nickel, and Cobalt
a) Time in hours; b) Change in resistance, %, c) 1 Day; d) 1 Week; e) 1 Month; f) 6 Months; g) 1 Year; h) 2 Years; i) 5 Years

Figure 153 shows the characteristics of operating stability of thermistors of manganese oxide and nickel (Curve 1) and of manganese oxide, nickel, and cobalt (Curve 2), expressed in percent change of resistance as a function of the time of operation, plotted on a logarithmic scale. It is clear from the diagram that thermistors are exceptionally stable in operation. The maximum changes in resistance take place in the first month of operation, after which there is only a negligibly slight variation.

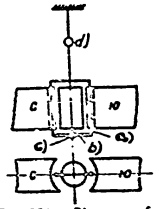

Fig. 154 - Diagram of Microradiometer
a) Frame; b) Thermocouple; c) Working space; d) Mirror

Section 85. Other Types of Nonselective Indicators of Infrared Rays

Various nonselective receptors other than thermoelements, bolometers, and thermistors, are used for recording radiant energy; these include radiometers, microradiometers, optico-acoustic and pneumatic indicators of radiant energy.

The Radiometer

The radiometric effect is based on the kinetic properties of a rarefied gas. If light plates, blackened on one side, are attached to a small glass rod, and this rod is then suspended from quartz thread in a tube with rarefied air, radiant energy striking the blackened sides of the plates will heat them and will create an unequal pressure of the residual gas on the two sides of the plates. The blackened sides of the plates will be exposed to pressure, causing the rod to rotate and twisting the suspension thread. The angle of torsion depends on the power of the radiant energy

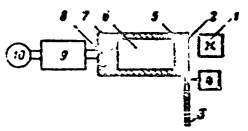

Fig. 155 - Diagram of Nevzgerov Optico-Acoustic Indicator:
1- Radiation source; 2- Apertures of modulating disk; 3- Modulating disk; 4- Motor; 5- Fluorite windows; 6- Chamber; 7- Membrane; 8- Microphone; 9- Amplifier; 10- Reproducer (telephone)

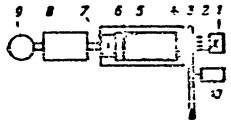

Fig. 156 - Diagram of Optico-Acoustic Indicator:
1- Radiation source; 2- Infrared rays; 3- Modulating disk, 4- Window 5- Body of chamber; 6- Membrane coated with layer of carbon black; 7- Microphone; 8- Amplifier; 9- Reproducer (telephone); 10- Motor

incident on the plates. The rotation of the system is measured by a ray reflected from a mirror attached to the suspension thread. Radiometers have high sensitivity, but the complexity of their design limits their use to the field of exact spectrometric measurements.

Microradiometer

For measuring small quantities of radiant energy, microradiometers are sometimes used. These consist of a galvanometer with a frame in the form of a thermo-

STAT

couple (Fig.154) On irradiation of the thermojunction a thermoelectromotive force arises, which induces a current in the frame and causes its rotation in the magnetic field. The displacement of a ray reflected from the mirror is used for estimating the radiant energy falling on the hot junction.

Bismuth, antimony, silver and tin are used as electrodes of the thermocouple. A receptor area of extremely thin blackened foil is sometimes placed on the hot junction itself. The frame has a single winding of copper or silver wire. To obtain a uniform and stronger magnetic field an iron core is placed within the frame.

The Optico-Acoustic Indicator

The optico-acoustic method of analyzing gases and vapors was first developed by Professor V.L.Veyngerov. The use of this method subsequently led to his constructing an optico-acoustic nonselective indicator of radiant energy. Figure 155 gives the diagram of the optico-acoustic indicator, as used for gas analysis. The radiant flux from the source (1) passes through the openings (2) of the modulating disk (3), rotated by the motor (4), and, through the fluorite window (5), strikes the chamber (6), containing the gas (or vapor) under investigation. Under the action of the interrupted irradiation, the pressure of the gas on the membrane (7) (tin foil) of the microphone (8) varies. The electric signals produced in the microphone are amplified in the amplifier (9) and fed to the reproducer (10). The variation in frequency of the current in the microphone circuit depends on the modulation frequency and the composition of the gas. By means of such a system, gases and vapors may be investigated by utilizing their ability to absorb radiant energy.

Another type of optico-acoustic indicators (Bibl.15), constructed on this principle, utilizes the variation in pressure of a thin plate coated with a layer of carbon black, under the action of interrupted irradiation. Figure 156 gives a schematic diagram of this optico-acoustic indicator. The circuit of this indicator differs from that of the gas-analyzer in that the absorber here is a layer of carbon black coating the walls of the chamber and the membrane (6) (of metal foil). Under modulated irradiation of the layer of carbon black, the absorptive, varying with the modulation frequency, produces an alternating pressure in the chamber, acting on the

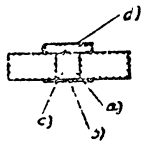

Fig.157 - Diagram of Pneumatic Indicator with Filter
a) Chamber, b) Film; c) Filter; d) Window

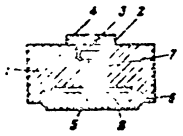

Fig.158 - Pneumatic Thermal Indicator: 1- Body of indicator; 2- Chamber of indicator; 3- Absorbing film; 4- Infrared filter; 5- Indicator film; 6- Glass wedge; 7- Tube; 8- Lower chamber

membrane (6), which is recorded by means of the reproducer or telephone (9).

The Pneumatic Indicator

Figure 157 gives a diagram of a pneumatic indicator. The chamber of such an indicator is filled with finely divided carbonized plant filler which, on absorbing radiant energy, is heated and causes a variation in the pressure of the gas in the chamber. The variation in gas pressure deforms the film covering the chamber. From the degree of deformation of this film, the value of the radiant flux can be estimated.

Such systems of pneumatic indicators were found to have inadequate sensitivity and stability, and therefore indicators of another design were developed.

Figure 158 shows another design of the thermal pneumatic indicator. The solid metal body contains the air- or gas-filled chamber (2). At one end, this chamber is closed by the film (3) which absorbs the radiant energy striking it through the infrared filter (4). The outlet from the chamber is closed by the film (5), which is deformed under the action of the expanding gas. Thus the film (5) in this design is the element that records the radiant energy absorbed by the indicator. The

deformation of the indicator film (5; is observed by an interferometric device (the glass wedge 6). To equalize the pressure and return the indicator film to the neutral position after cessation of irradiation, the slender tube (7), connecting the chamber (2) with the chamber (8), is used. The pressure in the chamber (2) is equalized through this tube in 1 sec.

The films are prepared from a colloidal mixture and are very thin. The thickness of the absorbing film (base) is only about 0.05 μ. The film is coated ("blackened") with a layer that is a good absorber of infrared rays, e.g. antimony. The indicator film is not "blackened" and its thickness is still less, as small as 0.03 μ. In later designs of indicators of this type, photoelectric methods were used for recording the deformation of the indicator film. In this case, the indicator film was made in the form of a flexible mirror, reflecting the light ray from a special light source. The thickness of the base of the absorbing film in these indicators is as small as 0.01 μ. The indicator film likewise consists of a base of about the same thickness and of an aluminum film, deposited on it as the reflecting layer.

The sensitivity threshold of pneumatic indicators is very high, reaching 10^{-10} watt. The time constant $\tau_{0.5}$ is small: only a few milliseconds.

CHAPTER X

AMPLIFICATION OF PHOTOCURRENT AND THERMOELECTROMOTIVE FORCES

Section 86. Purpose and Classification of Amplifiers

In practical use, the radiant energy to be recorded by an indicator is frequently so small that it is difficult or even impossible to utilize it directly in various devices or mechanisms. In these cases, the radiant energy is first converted into electric energy and is then amplified by means of special amplifying circuits whose basic element is usually an electron tube.

The transformation of radiant energy is accomplished by means of various indicators, whose reactions depend on the value of the radiant energy picked up. Since the radiant energy is small and its conversion takes place at low efficiency, the electric energy obtained is also very small. High amplification must therefore be used, which in some cases reaches hundreds of thousands or even hundreds of millions.

The parameters and characteristics of the amplifiers must correspond to the character of the radiant energy received and to the type of indicators that convert the radiant energy into electric energy.

The amplifiers used for amplifying photocurrents and thermoelectromotive force are subdivided, according to the power supply used, into AC and DC amplifiers.

AC amplifiers are in turn classified into two main groups, low-frequency and high-frequency amplifiers. In amplifying photocurrents and thermo-emf, low-frequency amplifiers are ordinarily used.

Resistors, chokes or transformers are used in the plate load of low-freque

amplifiers, and accordingly, such amplifiers are termed resistance, choke, or transformer amplifiers.

Occasionally, combined circuits are used, such as a rheostat transformer.

Amplifiers have different frequency pass-bands. In special broad-band amplifiers, the width of the frequency band is millions of cycles. Sometimes, on the other hand, the pass-band is measured only in tens of cycles.

DC amplifiers are subdivided into the following types: direct amplification, amplification with conversion of DC voltage into AC, and photovoltaic.

Several stages of amplification, connected in sequence, are used to obtain high amplification. The last or final stage of amplification is generally used for amplifying the power, while the preceding stages are used for amplifying the voltage. A push-pull amplification circuit is often used for the final stages of an amplifier.

Section 87. Limits of Amplification

The minimum values of the current and voltage that can be amplified are determined by the noise at the amplifier output. The noise emf limits the maximum allowable amplification factor. To amplify photocurrents and voltages, which as a rule are very small, high amplification factors (up to 10^9) are needed. The reduction of noise is therefore very important, since normal amplification is possible only where the amplified voltage (or current) is greater than the noise voltage.

Noises are due to external and internal sources. We shall accordingly term them extrinsic and intrinsic noises.

Extrinsic noises are caused by electric or mechanical sources. The noises of electric origin are due to induction by electric power plants, electric circuits, ignition systems of internal combustion engines, and other devices, or due to electromotive forces in the output circuit of the amplifier. To eliminate such noise, the entire amplifier and the lead circuit are carefully shielded. Reliable moving contacts are installed for the shields, since poor contacts may increase the noise hundreds of times.

Noises of mechanical origin are due to mechanical and acoustic influences on the amplifier, and in particular on the amplifier tubes. As a result of such influences, the so-called microphone effect of the tubes may appear. This necessitates the use of shock absorbers for the entire amplifier and its individual elements, particularly the amplifier tubes.

Even in the absence of extrinsic noise, amplification is still not unlimited. In fact, it is limited by the intrinsic noise due to the elements of the amplifier itself and to its sources of power supply. Intrinsic noises include:

Clicks and noises due to defects in the installation and contacts;

Noise in the amplifier due to its power supply sources;

Oscillation due to parasite feedback between the individual stages;

Thermal agitation noise.

To eliminate these noises, particular attention must be paid to proper installation, reliability of the contacts, elimination of feedback, and quality of the parts. When the power supply is AC, reliable filters must be used; with a DC power supply, stable noise-free storage batteries are required.

Thermal agitation noise is due to fluctuations in the electric current. Sources of such noise may be parts and tubes of the amplifier, or of the photoelement in the case of photoelectric circuits.

Noise originating in the radio part of the amplifier is customarily called circuit noise. The strongest noise arises in the resistors. Noise originating in the tubes is called tube hiss.

Thermal agitation noise in any conductor is caused by the chaotic displacement of electrons under thermal motion. The chaotic movement of charges produces voltage fluctuation at the ends of the wire. Since there is always a resistor or other radio part (capacitor, choke, transformer winding) at the amplifier input, a fluctuating voltage enters the amplifier input, causing an amplified noise voltage at the amplifier output, which limits the minimum value of the useful amplified signal.

The voltage produced by the intrinsic noises of a resistor can be calculated by

STAT

the formula

$$U_n = \frac{1}{8}\sqrt{R\Delta f} \qquad (173)$$

where U_n denotes the effective value of noise voltage in microvolts, composed of all the noise voltages with frequencies lying in the band Δf (the frequency band of the amplifier Δf is expressed in kc), while R is the resistance in k-ohm.

Tube hiss is caused by the nonuniformity of the electron flux producing the plate current, or the so-called shot effect. The direct component of the plate current is superposed by an alternating component due to the nonuniformity of the flux. This results in noise voltage at the tube output.

Noise due to the shot effect occurs in vacuum photoelements, even under constant irradiation.

Tubes are sometimes characterized by the value of the resistance equivalent to the noise produced (noise resistance).

The noise resistance R_n of a triode is inversely proportional to its transconductance and is expressed by the relation

$$R_n = \frac{2.3 \div 5}{S} \qquad (174)$$

where S is the transconductance of the triode in ma/v.

When a tube has several electrodes toward which an electron stream is flowing, the thermal agitation noise increases strongly. For this reason, the noise of a tetrode and pentrode is several times (3-5) as great as the noise of a triode.

Section 88. Amplifier Characteristics

Low-frequency DC amplifiers are characterized by the following basic quantities: amplification factor, input voltage, or amplifier sensitivity, set noise of the amplifier, power at output, frequency characteristic, and distortions introduced by the amplifier.

The amplification factor is a quantity giving the ratio of the output voltage U_{out} to the input voltage U_{in} of the amplifier. The amplification factor is expressed by the equation

$$k = \frac{U_{out}}{U_{in}} \qquad (175)$$

The value of the amplification may fluctuate over a very wide range, from units and tens (in low-frequency amplification in receptors) to hundreds of thousands and

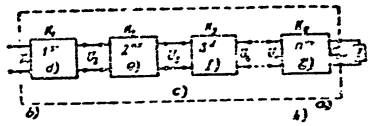

Fig. 159 - Block Diagram of a Multistage Amplifier
a) Amplifier output; b) Amplifier input; c) Amplifier; d) First stage; e) Second stage; f) Third stage; g) n^{th} stage; h) Load

even tens of millions and more (in special circuits for amplifying photocurrents and thermo emf, which in some cases require exceptionally high amplifications). In power amplification, which is effected in the output or final stages, the amplification factor is generally used merely to characterize the preliminary stages, designed to amplify the voltage.

For a multistage amplifier whose block diagram is shown in Fig. 159, the total amplification factor (k_{tot}) is defined as the product of the amplification factor of all stages:

$$k_{tot} = k_1 \cdot k_2 \cdot k_3 \ldots k_n$$

The power at the output of an amplifier is characterized by the value of the maximum power that can be obtained from the amplifier. According to the purpose of

STAT

the amplifier, its power may range from a fraction of a watt to a kilowatt. In amplifying photocurrents and thermo emf, the output power is usually small. This parameter mainly characterizes the final output stages.

In amplifying photocurrents and thermo emf, very high amplifications must often be used, in view of the small value of the input signal. The threshold sensitivity of an amplifier is characterized by the minimum voltage at its input that it can amplify. The threshold sensitivity depends on the type of amplifier, number of stages, elements of the circuit, and many other factors. One of the factors limiting the amplification is the noise at the amplifier input due to its input circuits. As already stated, the resistors, wires, and tubes produce certain nonstationary random emf which, entering the amplifier input, is amplified and produces noise at its output. Thus the set noise of an amplifier is one of the prime factors limiting amplification.

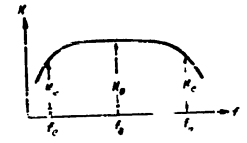

Fig.160 - Typical Frequency Characteristics of Amplifier

The degree of sensitivity is expressed by the voltage, in millivolts or microvolts, which must be imposed on the input to obtain normal amplification, i.e., to make the amplified signal greater than the voltage due to the set noise of the amplifier.

The sensitivity of amplifiers is usually measured in millivolts, microvolts, or even in fractions of a microvolt, according to the purpose of the amplifier. Photoelements may produce voltages of a fraction of a millivolt at the amplifier input, while thermoelements in some cases generate an emf of only a fraction of a microvolt. The critical sensitivity of amplifiers and the level of the set noise go as low as fractions of a microvolt.

The frequency characteristic, the frequency range, or the pass-band characterizes the frequency region in which the amplification factor fluctuates within assigned and usually narrow limits.

The required frequency limits and degree of variation in the amplification factor are determined by the purpose of the amplifier. Figure 160 shows a typical frequency characteristic, indicating the relation between the amplification factor k and the frequency in the range from f_1 to f_n indicated.

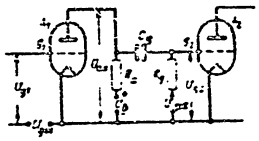

Fig.161 - Schematic Diagram of Resistor-Coupled Amplifier

The pass-band for an AC amplifier covers a wide range and may be from a few hundred to a few million cycles. The boundaries of the frequency band may be from a few cycles, for instance 5-10 (lower boundary of amplification f_1) to a few million, 2×10^6 cycles (upper boundary of amplification f_n). An amplifier usually does not give the same amplification for all frequencies, values, and shapes of the signal but introduces a certain distortion. The distortions may be due to the following causes:

Inconstancy of the amplification factor at different frequencies, resulting in frequency distortions;

Nonlinearity of the characteristic of some amplifier element (e.g., a tube);

Appearance of phase shifts between the various components of the voltage to be amplified (phase distortions);

Appearance of various nonstationary processes in the amplifier circuits.

According to the purpose of the amplifier, the role played by a given type of distortion may differ, so that the primary effort in amplifier design is to exclude the most undesirable distortions.

Let us now consider the various methods and arrangements of amplifying photocurrents and thermo emf used in infrared technology.

Section 69. Low-Frequency Resistor Amplifiers

In resistor amplifiers, the plate circuit of the preceding stage is indirectly coupled with the grid circuit of the following stage across a capacitance, so that

only alternating voltage reaches the grid of the tube

The tube of the final stage, like the useful load at the output, is most often coupled with the preceding stage across a transformer, since this makes it possible to match the parameters of the load and of the amplifier tube in a rather simple way.

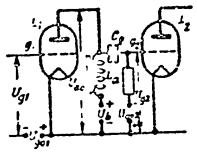

Fig. 162 - Schematic Diagram of Impedance-Coupled Amplifier

The circuit of a resistor-coupled amplifier (rheostat circuit) in Fig. 162 is characterized by the fact that the ohmic resistance R_a is here used as the useful plate load, while the coupling with the preceding stage is effected across the capacitance C_g.

A circuit of this type amplifies a wide frequency band without distortion, but has the disadvantage that a high voltage drop is obtained at the resistors R_a, thus reducing the plate voltage.

The alternating voltage obtained across the resistors R_a is fed to the grid g_2 of the tube of the following stage across the by-pass capacitor C_g which, passing the alternating voltage to be amplified, eliminates the influence of the constant component of the plate potential of the first tube.

The value of the capacitance C_g is determined by the frequencies to be amplified, and usually ranges from 10^{-3} - 1 uf. The resistance R_g, connected in the grid circuit, is equal to hundreds of thousands of ohms and is usually 5 to 10 times as great as the plate resistance. Since, in this circuit, the interstage couplings do not increase the voltage, tubes with high amplification factors (μ = 25 or more) are usually employed, most often triodes, but sometimes tetrodes and pentodes.

The values of the plate resistances are determined by the differential internal resistances of the tubes (R_i). For ordinary triodes, the plate resistance is taken equal to about $2R_i$, and for tetrodes and pentodes from $\frac{1}{3} R_i$ to $\frac{1}{5} R_i$. Although tetrodes and pentodes do have a high value of μ, they cannot yield a high amplification for the stage, owing to the considerable values of R_i, since the critical amplification of the stage cannot be higher than the product SR_a. The value of the plate resistance R_a must not exceed a certain value, since too high a resistance R_a causes a considerable voltage drop across it. Besides this, excessive distortions are created on the resistors when tetrodes and pentodes are used in amplifier circuits.

Since they have a wide frequency band without distortion, the resistor-coupled amplifier with a capacitance coupling is also used to amplify pulsating voltages, if the constant component of the pulse is small. Such an amplifier may be preferable over a DC amplifier, since the latter is usually more complicated and has higher noise, due to the shifts of the constant component (of the zero line).

Section 90. Low-Frequency Impedance-Coupled Amplifiers

In the impedance-coupled amplifier whose circuit is shown in Fig. 163, a choke is used as the useful plate load. In this case, the ohmic resistance is supplemented by an impedance L_a which completely ensures amplification of the alternating voltage. The coupling with the following stage is accomplished across the capacitance C_g.

Circuits of this type amplify low frequencies, but require rather complex chokes, usually with an iron core, and introduce distortions due to the nonuniform amplification with frequency.

By comparison with rheostat circuits, they have the advantage that a sufficient drop of the alternating voltage is produced across the choke, due to impedance, while the constant plate voltage is decreased only very li[illegible] since the resistance of chokes is low.

Circuits using impedance-coupled amplifiers are rarely used today, because of the fact that a choke is usually more complex and expensive than a resistor; in addition, these circuits, as already stated, have a less uniform amplification over the frequency band.

STAT

Section 91. Low-Frequency Transformer-Coupled Amplifiers

Transformer-coupled amplifying circuits, or transformer circuits, one of which is shown in Fig.163, are widely applied today for amplifying low frequencies, being used for amplifying not only the voltage but also the power. In these circuits, the stages are coupled by means of transformers, thus allowing the parameters of the various circuits of the system to be most rationally matched. This is particularly important in power amplification, when the following stage may produce a load due to the presence of grid currents; however, even for voltage amplification, when there are usually no grid currents, the transformer permits optimum parameters of the load circuits.

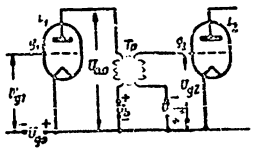

Fig.163 - Schematic Diagram of Transformer Coupled Amplifier

Transformer-coupled systems also allow a higher amplification factor per stage because of the transformer factor, and give a rather satisfactory frequency characteristic of the amplifier.

The stages are coupled across intermediate transformers, which usually have a transformation factor from 3 to 5. Like the choke, the transformer, because of its impedance, represents a high resistance for the alternating component of the plate current. At the same time the transformer, because of its low resistance, produces a small voltage drop due to the direct component of the plate current. Thus there is no marked reduction in plate current, produced by drops in the plate load in transformer hookups.

In transformer systems not only triodes are used, but also tetrodes, and pentodes. The amplification factors per stage may reach a few tens and even hundreds.

The use of transformer systems is limited mainly by the fact that their amplification is still dependent on the frequency. When a uniform amplification without distortion is required in a broad frequency band, transformer-coupled circuits are unsuitable. However, they are very convenient in instances where only a narrow frequency band need be amplified.

To obtain more uniform amplification of a broad frequency band, combined rheostat-transformer systems with amplification (Fig.164) are used in some cases.

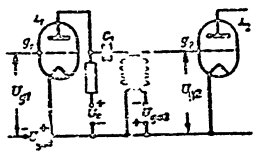

Fig.164 - Schematic Diagram of Rheostat-Transformer-Coupled Amplifier

These systems give better amplification of the low frequencies, relative to distortion, and also eliminate the magnetization of the transformer core by the direct component of the plate current which occurs in pure transformer-coupled systems along the primary winding. The main advantage of rheostat-transformer-coupled systems over other types is that, because of the transformer, the amplification per stage can be increased, the parameters of the system can be brought up their optimum value, and power amplification can be effected. Because of the low resistance of the transformer winding, the voltage drop due to the passage of current will be low and will impose no limitations on the amplifications.

On the other hand, these systems also have their disadvantages. The main drawbacks are their complexity in comparison with the rheostat or transformer-coupled system and the considerable voltage drop across the resistors, due to passage of the direct component of the plate current. Other disadvantages of the rheostat-transformer-coupled system is the frequency dependence of amplification, limiting the range of frequencies to be amplified, and a certain increase in the cost and complexity of the arrangement. The range of frequencies amplified may be from 5-10 cycles to 3×10^5 cycles.

Triodes, tetrodes, and pentodes are used in transformer-coupled systems.

Section 92. Low-Frequency Push-Pull Amplifiers

The so-called push-pull amplifier circuit, shown in Fig.165, is an improved

Section 91. Low-Frequency Transformer-Coupled Amplifiers

Transformer-coupled amplifying circuits, or transformer circuits, one of which is shown in Fig.163, are widely applied today for amplifying low frequencies, being used for amplifying not only the voltage but also the power. In these circuits, the stages are coupled by means of transformers, thus allowing the parameters of the various circuits of the system to be most rationally matched. This is particularly important in power amplification, when the following stage may produce a load due to the presence of grid currents; however, even for voltage amplification, when there are usually no grid currents, the transformer permits optimum parameters of the load circuits.

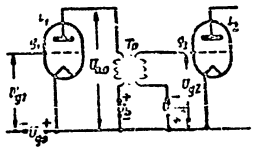

Fig.163 - Schematic Diagram of Transformer-Coupled Amplifier

Transformer-coupled systems also allow a higher amplification factor per stage because of the transformer factor, and give a rather satisfactory frequency characteristic of the amplifier.

The stages are coupled across intermediate transformers, which usually have a transformation factor from 3 to 5. Like the choke, the transformer, because of its impedance, represents a high resistance for the alternating component of the plate current. At the same time the transformer, because of its low resistance, produces a small voltage drop due to the direct component of the plate current. Thus there is no marked reduction in plate current, produced by drops in the plate load in transformer hookups.

In transformer systems not only triodes are used, but also tetrodes, and pentodes. The amplification factors per stage may reach a few tens and even hundreds.

The use of transformer systems is limited mainly by the fact that their amplification is still dependent on the frequency. When a uniform amplification without distortion is required in a broad frequency band, transformer-coupled circuits are unsuitable. However, they are very convenient in instances where only a narrow frequency band need be amplified.

To obtain more uniform amplification of a broad frequency band, combined rheostat-transformer systems with amplification (Fig.164) are used in some cases.

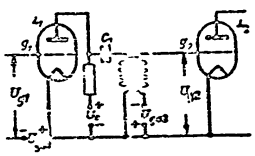

Fig.164 - Schematic Diagram of Rheostat-Transformer-Coupled Amplifier

These systems give better amplification of the low frequencies, relative to distortion, and also eliminate the magnetization of the transformer core by the direct component of the plate current which occurs in pure transformer-coupled systems along the primary winding. The main advantage of rheostat-transformer-coupled systems over other types is that, because of the transformer, the amplification per stage can be increased, the parameters of the system can be brought up their optimum value, and power amplification can be effected. Because of the low resistance of the transformer winding, the voltage drop due to the passage of current will be low and will impose no limitations on the amplifications.

On the other hand, these systems also have their disadvantages. The main drawbacks are their complexity in comparison with the rheostat or transformer-coupled system and the considerable voltage drop across the resistors, due to passage of the direct component of the plate current. Other disadvantages of the rheostat-transformer-coupled system is the frequency dependence of amplification, limiting the range of frequencies to be amplified, and a certain increase in the cost and complexity of the arrangement. The range of frequencies amplified may be from 5-10 cycles to 3×10^5 cycles.

Triodes, tetrodes, and pentodes are used in transformer-coupled systems.

Section 92. Low-Frequency Push-Pull Amplifiers

The so-called push-pull amplifier circuit, shown in Fig.165, is an improved

transformer-coupled circuit. In this arrangement, the voltage to be amplified is fed, in phase opposition, simultaneously to the grids of two tubes. The alternating components of the plate currents are thus obtained with a phase shift of 180°. When

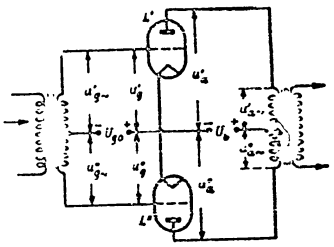

Fig. 165 - Schematic Diagram of a Push-Pull Amplifier

the alternating components of the plate currents pass through two symmetrical halves of the primary winding, the emf of each is given the same direction. As a result, the voltage induced in the secondary winding of the transformer is doubled.

Push-pull circuits have a number of advantages over ordinary amplifying circuits. They have less distortion, and the even harmonics in the plate current are eliminated or considerably attenuated. For this reason, a higher undistorted power can be obtained from the tubes.

The tube circuits are independent of the feed voltage, because of the mutual compensation introduced by the tube.

The transformer in push-pull circuits operates in such a way that the direct component of the plate circuits of both tubes produces magnetic fluxes of opposite directions in the transformer core. Due to this fact, the core of the transformer is not loaded with a constant magnetic flux. This makes it possible to build the transformer lighter and cheaper.

Push-pull circuits are used for amplifying alternating currents, especially in the output stages, when high power and low distortion must be obtained.

For more efficient operation of push-pull amplifiers, greatest possible symmetry between the two halves of the circuit is required, paying special attention to selection of the tubes.

Section 93. Direct-Current Amplification

The amplification of direct or slowly varying current and voltage involves great difficulties. If the voltages and currents to be amplified are of the direct type or

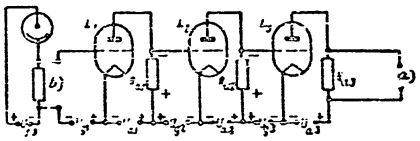

Fig. 166 - Voltistage DC Amplifier
a) Output; b) Input

have a very low frequency, it is impossible to use a circuit in which the tubes are coupled across a capacitor or transformer. In these cases, special and sometimes complicated systems must be used. If a small amplification of direct or alternating photocurrents is required, then the one-tube photocurrent amplifiers circuits discussed below are entirely suitable for this purpose.

Sometimes, the difficulties connected with amplification of direct current, make it necessary that the source of energy incident on the indicator must first be modulated to give an alternating current or voltage, which can then be amplified by the usual type of AC amplification. Such a method of amplification may be used where the indicator has a low sluggishness and has a sufficiently good frequency characteristic. In some cases, only the direct current or voltage is amplified, because modulation of the incident flux is impossible.

In the amplification of thermo emf, the difficulties are even greater, because of the small resistances of the sources of the voltage to be amplified; therefore, special amplifying circuits are used in this case.

STAT

Direct current may be amplified by combining several stages. This is the so-called circuit for the direct amplification of direct current.

In some circuits, the direct voltage is converted into alternating voltage and is then further amplified by the usual circuits for the amplification of a low-frequency alternating current (Bibl. 16).

In addition, special circuits are sometimes used to amplify direct current, such as photovoltaic amplification circuits, which are characterized by the fact that their principal components are a galvanometer, photocells, and amplifying tubes.

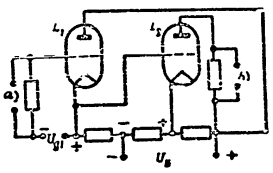

Fig. 167 - Two-Stage DC Amplifier with Voltage Divider (An Increase in Current of First Tube Increases the Current in the Second Tube)
a) Input; b) Output

Section 94. Circuits for Direct Amplification of Direct Current

To amplify constant or slowly varying current as well as pulsating currents, multistage direct amplification amplifiers are used (Fig. 165). To the amplifier input any desired DC voltage may be fed. The loads in both grid and plate circuits are pure resistances.

In circuits using direct amplification of DC, with direct interstage coupling, all the voltage drop across the plate resistance of the preceding tube is fed to the grid of the subsequent tube. However, for the subsequent tube to operate under the required conditions, an additional voltage is connected into its grid circuit, determining the grid potential and, consequently, also the plate current of the tube. On variation of the plate current of the preceding tube, the grid potential and plate current of the tube of the following stage also vary, and so on in all stages.

Each stage is fed either from a separate battery or from a common voltage divider.

Figures 167 and 168 show two hookups of two-stage DC amplifiers fed from a voltage divider. One of them (Fig. 167) gives DC amplification when the signs of the variation current at the output agree, i.e., in this hookup an increase in voltage at the amplifier input causes the plate voltage of the second output tube to increase also. The second hookup (Fig. 168) has the opposite effect: An increase in the voltage at the amplifier input in this hookup corresponds to a reduction in the plate current of the second tube. The drawbacks of these circuits are as follows.

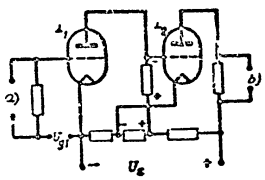

Fig. 168 - Two-Stage DC Amplifier with Voltage Divider (An Increase in Current of the First Tube Decreases the Current of the Second Tube)
a) Input; b) Output

First, the need for a high power-supply voltage, which is usually felt in multistage hookups. The value of this voltage limits the value of the plate loads and thus also the amplification of the circuits.

Secondly, the direct coupling of all stages of these circuits may lead to the appearance of oscillation and instability. When the feed is from a voltage divider, distortions of the voltages being amplified are possible, owing to their redistribution on the divider through which the current flows.

Thirdly, such hookups amplify not only the signal received but also all random noise signals, both external and internal, which likewise limits the amplification.

The set noise at the amplifier input, due to the noises of the resistor and the tube, greatly lower the amplification factor and the sensitivity of the hookup.

These circuits can operate on ordinary amplifier tubes, triodes, tetrodes, and pentodes; however, these tubes have a very high internal resistance, which makes it difficult to use them effectively in such circuits, because of the limitations imposed by the value of the feed voltage. In addition, tube bias of tetrodes and pentodes is higher than in triodes, which also limits their use in DC amplification

STAT

circuits.

A tube with a high resistance of the grid-cathode circuit has been developed especially for amplification and measurement of very low currents (10^{-14} to 10^{-17} amp). Several of the hookups in which this tube is used are described in Section 98.

Section 95. Amplification Circuits of Direct Current, for Conversion to Alternating Current (Bill.16)

To amplify direct current, converter circuits are used, in which the voltage (current) fed to the input is first converted into alternating pulsating voltage, and

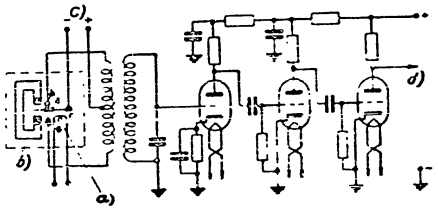

Fig.169 - Circuit for Amplifying Direct Current, Converting it into Alternating Current
a) Winding; b) Vibropack; c) Voltage to be amplified; d) To following amplification stages

is then amplified by the usual low-frequency amplification circuits.

Various systems are used for converting DC into AC: rotary commutators, vibropacks, etc.

Figure 169 shows a circuit with conversion of DC into AC by means of a vibropack. The alternating pulsating voltage obtained behind the vibropack is fed to the primary winding of the input transformer and then to the grid of the tube of the first stage. After the required amplification, the voltage is fed to the final output stage.

A vibropack consists of three main elements: a vibrating reed with a contact A, mating with the fixed contacts B and C; the exciter winding G, causing the reed to vibrate at a certain frequency, and a permanent magnet.

The exciter winding of the converter is fed by AC from the power line or from a special generator.

The DC voltage to be amplified is fed by one pole to the central point of the transformer, and by the other to the vibrating reed with the contact. When the converter is excited, the voltage being amplified arrives first at one half of the primary winding of the input transformer and then at the other half. As a result an alternating current and a magnetic flux are produced in the primary winding of the transformer, which induces in the secondary winding of the transformer an alternating emf which varies with the frequency rate of closure of the converter contacts. In such a system, the voltage being amplified is fully utilized, since it is almost continuously fed to the first or second half of the primary winding of the input transformer.

An advantage of such systems is the simplicity of all amplification stages, which consist of conventional low-frequency AC amplifiers.

The hookups of DC amplifiers, converting it to AC, are used in the amplification of very small direct currents and voltages.

Section 96. The Photoelectron Optical Amplifier

For DC amplification, photoelectron-optical amplification is sometimes used. Such a hookup was developed in 1950 by Professor E.P.Kolzarev (Bibl.17).

Figure 170 gives a schematic diagram of such an amplifier. The current or voltage to be measured is fed to the input of a sensitive galvanometer. The deflection of the galvanometer pointer is fixed by photocells connected in the grid circuit of the amplifier tubes. A bridge arrangement is used for the tubes, operating in a balanced state with the proper voltage regulation on the tube grids. A measuring instrument is connected in the diagonal of the bridge (points AE or A'B').

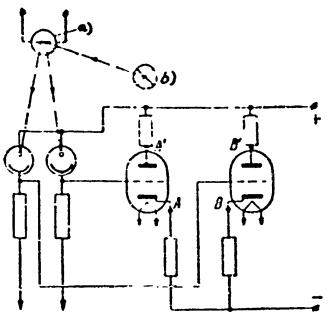

Fig. 170 - Schematic Diagram of a Photoelectron-Optical Amplifier
a) Galvanometer; b) Illuminator

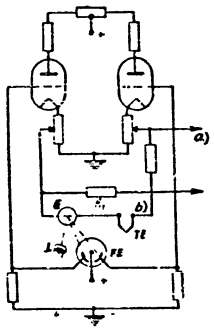

Fig. 171 - Circuit of Photoelectron-Optical Amplifier with Feedback:
G- Galvanometer; TE- Thermoelement; PE- Photoelement; R_1- Feedback Resistor; L- Illuminating Lamp
a) To measuring instrument; b) Input

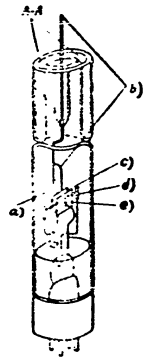

Fig. 172 - Schematic Diagram of a Vacuum-Tube Electrometer
a) Grid holder; b) Grid lead-out; c) Grid; d) Cathode; e) Plate

In the original position, no potential differences exist between the cathodes, and the measuring instrument shows no deflection. At the smallest deflection of the pointer of the input galvanometer, the currents incident on the photocells vary, thus causing the photocurrents to vary. The optical system galvanometer-photocells must be such that the variations in the fluxes at both photocells have different signs, i.e., so that, when the flux incident on one photocell increases, the flux falling on the second photocell decreases. As a result, the potentials of both grids vary and unbalance the grid circuit, thus causing the appearance of a certain potential difference in the diagonal of the bridge and, consequently also a certain current to be recorded by the instrument.

The circuits of photoelectron-optical amplification permit measuring very small emf values, particularly thermo-emf, and also low currents.

A disadvantage of such a circuit arrangement is the unavoidable sluggishness due to the resistance of the galvanometer input and of the measuring output instrument used in the circuit.

Figure 171 shows the circuit of a photoelectron-optical amplifier with negative feedback, used for decreasing the influence of vibration and making the circuit more stable. The circuit is of the high sensitivity type. A voltage of 1 mv at the input gives a full-scale (50 divisions) pointer deflection of the output measuring instrument.

Section 97. Tube for Measuring Very Low Currents

The problem of measuring and amplifying very low currents, as low as 10^{-14} to 10^{-17} amp, is quite common today. The use of high-sensitivity galvanometers for this purpose is not always possible, since their sensitivity is only 10^{-12} to 10^{-14} amp per scale division.

The use of conventional tubes is limited by the fact that the grid-cathode resistance is sometimes as high as 10^8 to 10^9 ohms. Moreover, the value of their grid currents is comparable to the value of the currents being measured. The grid cur-

STAT

rents of conventional lamps are due to thermoelectronic emission of the grid and to ions formed in the tube by incomplete vacuum.

A special tube was therefore developed for measuring very low currents. This tube is sometimes called a vacuum-tube electrometer or a tube with a high grid-cathode circuit resistance. The vacuum-tube electrometer permits measuring currents as low as 10^{-14} to 10^{-17} amp, by using galvanometers connected in its plate circuit.

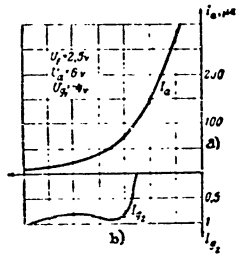

Fig. 173 - Characteristics of a Vacuum-Tube Electrometer
a) Control-grid current $\alpha \cdot 10^{-15}$;
b) I_{g_2}, μa

Figure 172 shows the circuit of such a vacuum-tube electrometer. In tubes of this type, leaks in the grid-cathode circuit are almost completely eliminated by separating the lead-outs of grid and cathode. The construction of the bulb is such that the path for the leak currents is lengthened both inside and outside, thus increasing the grid-cathode resistance. In measuring very low currents, oil is poured into the space around the grid lead-outs (A-A), improving the insulation of the grid.

To exclude the influence of ionization, the tube is operated at reduced plate voltage (4-6 v). Since, in this case, the plate voltages are very low, the tube is sometimes made with four electrodes. In this arrangement, the DC voltage is fed to the first cathode grid, while the plate grid is used as the control grid.

The cathode used in vacuum-tube electrometers operates at a low temperature. This is necessary for reducing the thermoelectronic current on the grid. In particular, thoriated cathodes are used at reduced filament voltage.

To reduce the thermoelectronic currents, the tube is usually connected at negative potential to the grid, and, in addition, the grid is placed, not between the anode and cathode (as is usual) but on both sides of the cathode.

To reduce the conductivity, quartz is used instead of glass, and special attention is paid to the quality of the tube assembly work.

To give an idea of the characteristics of such a tube, we list the data of one of the vacuum-tube electrometers:

Cathode voltage	2.5 v
Cathode current	0.110 amp
Plate voltage	+ 6 v
Voltage on screen grid	+ 4 v
Voltage on control grid	- 4 v
Resistance of grid-cathode leak	about 10^{16} ohms
Control-grid current	< 10^{-16} amp (approximately)
Plate current	40 μa
Transconductance	25 μa/v
Internal resistance	40,000 ohms
Amplification factor	1
Dimensions of tube:	
diameter	40 mm
height	60 mm

The characteristics of this vacuum-tube electrometer are given in Fig. 173.

The above data indicate that the characteristics of this electrometer are rather unusual. The amplification factor is equal to only unity, the transconductance and plate current are very small. Despite this fact these tubes make it possible, by a relatively simple but carefully executed circuit, to measure currents as low as 10^{-15} to 10^{-16} amp or even 10^{-17} amp, which corresponds to an electron flux of 60 electrons per second.

To increase the stability of the tubes, they are generally used in balanced circuits. To increase the sensitivity of the tubes, they are occasionally used in

STAT

circuits with a free control grid. No resistance is connected in the grid-cathode circuit in this case.

The tube electrometer is used not only for measuring low currents but also for measuring very high resistances, up to 10^{12} to 10^{14} ohms.

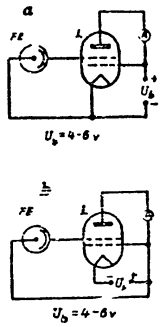

Fig. 174 - Circuit of Single-Tube Photocurrent Amplifier a- With phototube acting as grid leak; b- With phototube acting as a plate leak

Section 99. Photocurrent Amplifiers

Photocurrents may be amplified by ordinary AC or DC amplifier circuits. There are also a number of special circuits for amplifying a photocurrent. Let us consider a few of these:

Amplifiers with Extrinsic-Effect Phototube

In these circuits, the phototube is a grid leak. In the absence of irradiation, the phototube has a practically infinite resistance. In this way, when the phototube is not irradiated, the grid is disconnected from the circuit and is charged negatively by the electrons emitted by the cathode of the tube. On irradiation of the phototube, a photocurrent appears, causing the grid potential and the plate current to vary.

A tube operating in such circuits must not have its own leaks nor ionic currents acting as leaks. The grid of the tube must, therefore, be well insulated. To prevent the occurrence of ionic currents, the plate voltage is reduced to 4-6 v. However, since at such plate voltages the transconductance of triodes is small, tetrodes with a cathode grid for counteracting the space charges, are used. The vacuum-tube electrometer described in the preceding section can be used in such circuits.

The resistance of the cathode insulation of the photocell must likewise be high.

Figure 174 a is a diagram of a single-tube photocurrent amplifier. The photocell is a grid leak. With an unirradiated phototube, the grid is disconnected from the cathode and is charged to a certain potential. When a photocurrent appears, the grid begins to discharge, and its potential and, consequently, also the plate current increase, which is recorded by the instrument A in the plate circuit of the tube. Such a circuit can measure currents as low as 10^{-14} - 10^{-15} amp.

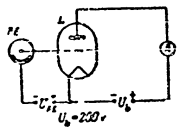

Fig. 175 - Diagram of Amplifier with Phototube

Figure 174 b shows a different photocurrent amplification system. Here the phototube is connected with the plate of the tube and is a plate leak. With unirradiated phototube, the grid is negatively charged, but when photocurrents appear, it acquires a negative charge, causing generation of currents flowing from the tube cathode to the grid and a variation in the plate current. At high radiant fluxes incident on the phototube cathode, the proportionality between the flux and the plate current of the tube is impaired, due to the fact that the grid currents are larger than the photocurrents. This circuit can therefore be used only for comparative measurements.

In the circuit shown in Fig. 175, the plate of the phototube is connected with the grid of the amplifier tube. When the phototube is not irradiated, the grid is free and is not coupled with the rest of the circuit. If a tube has a transconductance so high that, with a free grid, it has a rather high plate current, then, even under low irradiation of the phototube cathode, the grid acquires a high negative charge, which reduces or completely stops the plate current. Such a circuit may be very sensitive and give amplifications of 10^5 - 10^6 times; when tubes with very good grid insulations are used, currents as low as 10^{-14} - 10^{-16} amp can be amplified.

Ordinary Photocurrent Amplifier

In the above-described circuits, the plate current is determined by the potential acquired by the grid due to the charge present. The grid of the amplifier tube is connected with the circuit only across the phototube. In conventional amplifier

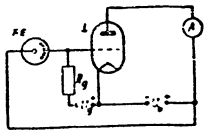

Fig. 176 - Circuit of Normal Single-Stage Photocurrent Amplifier

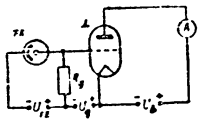

Fig. 177 - Circuits of "Inverse" Single-Stage Photocurrent Amplifier

circuits, a certain voltage is imposed on the grid, and it is this voltage that determines the plate current for a given plate voltage.

The circuit in Fig. 176 differs from those discussed above in that the resistor R_g is connected in the grid circuit. Across the resistor R_g, a voltage U_g can be imposed on the grid, this voltage determining the operating conditions of the tube at a given plate voltage. When the phototube is irradiated, a photocurrent is generated and flows across the resistor R_g, creating a voltage drop across it. In this case the grid voltage and, together with it, the plate current vary, a process which is recorded by a measuring instrument connected in the plate circuit of the tube. In this system, the plate current increases with the photocurrent.

Another version of the usual amplifier circuit (the so-called inverse circuit) is shown in Fig. 177. In this circuit, the variations of the photocurrent and the plate current of the tube are inversely proportional. With increasing photocurrent, the voltage drop across the resistor R_g and the negative voltage on the grid increase (numerically), while the plate current of the grid decreases. At a certain value of the photocurrent, the plate current of the tube can be completely stopped, and the tube will be "locked".

The resistance R_g is large, being 10^6-10^8 ohms. Its value depends on the type of tube used.

In such circuits, ordinary triodes can be used, preferably those with very low ionic currents and high leak resistance. To increase the resistance of the leak, the socket is sometimes removed from the tube and replaced by an improved tube socket, or the system is operated without either.

The current amplification in these circuits may go as high as 10^4-10^5, for a single-tube arrangement.

Compensation Circuits of Photocurrent Amplification

In the circuits just discussed, the variation in total plate current was measured. To increase the sensitivity, compensating circuits are sometimes used. Figure 178 represents one such circuit, used for measuring the variation in plate current caused by the photocurrent, without taking the direct component into consideration. This allows higher sensitivity of the circuit and the use of high-sensitivity instruments, especially galvanometers.

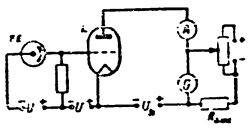

Fig. 178 - Compensation Circuit of Single-Stage Photocurrent Amplifier

All circuits for measuring current differences are very sensitive to external influences, which affect both the phototubes and the amplifying tubes. One of the causes of circuit instability is a change in the total illumination of the phototube, leading to a change in the photocurrent and, consequently, to a change in the plate current. In this case, the zero position of the pointer of the measuring instrument is disturbed.

A circuit with two photocells (Fig. 179) is sometimes used for amplification. In such arrangements, one phototube is connected so as to react only to total illumination, while the other photocell, in addition, fixes the supplementary fluxes

STAT.

incident on the cathode of the photocell, which must be measured. If the fluxes incident on both photocells vary in the same way, the plate current will not vary, since the two photocells have an opposite effect on the grid. It is only when the variation in the fluxes incident on the phototubes is unequal that the measuring instrument shows any deflection at all, and this deflection corresponds to the difference between the luminous fluxes.

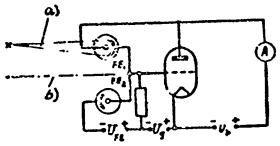

Fig. 179 - Diagram of Circuit with Two Photocells, for Compensating the Variations in Total Illumination
a) Flux being measured; b) Screen

The variation in the feed voltage of all the tube circuits also causes circuit detuning. To reduce these influences, circuits analogous to conventional bridge circuits are often used. Figure 180 shows a compensation bridge arrangement characterized by all circuits of both tubes being fed from one and the same source. While the instrument measures only the difference in plate currents. In this way, fluctuations in feed voltage would have practically no effect on the accuracy of measurement. To compensate the asymmetry introduced by the capacitance and leaks of the photoelement, a capacitor and resistor are connected in the grid circuits of the second tube. Such an arrangement, compensating the variations in feed voltage, does not remain stable at changes in the total illumination.

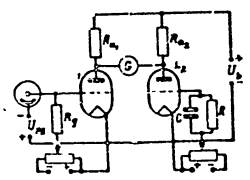

Fig. 180 - Compensation Bridge Circuit

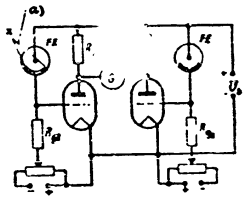

Fig. 181 - Compensation Bridge Circuit with Two Phototubes
a, Blocked flux

The circuit shown in Fig. 181 is an improvement over previous circuits. In this circuit, in order to exclude the influence of total illumination, phototubes are connected in both arms of the bridge. As a result, at equal change in the fluxes striking the phototubes, the plate currents change in the same way so that there is no change of the current in the measuring instrument. Thus the influence of total illumination is excluded and only the difference of fluxes incident on the phototubes is measured.

Bridge diagrams have a far higher stability than ordinary uncompensated circuits. A certain residual instability is explained by the incomplete symmetry of the circuit, due to the fact that its elements are not identical. For this reason, in designing such circuits, particular attention must be paid to having all elements entering into the circuit as uniform as possible.

STAT

CHAPTER XI

OPTICAL FILTERS FOR INFRARED RAYS

Section 99. Purpose of Optical Filters

The spectral composition of radiant energy from various sources and the spectral characteristics of sensitivity of the receptors of this energy vary widely. It is often necessary to change the spectrum of radiant energy of a source or the spectral characteristics of a receptor. One of the simplest methods of separating the radiant energy of a required part of the spectrum is by filtering the radiation by means of a medium having a selective transmission.

Systems designed to change the spectral composition of radiant energy are called optical filters, regardless of the region of the spectrum (visible or invisible rays). Such filters are used for the following purposes:

Isolation of the required spectrum region of the radiant energy of a source or the spectral characteristic of a receiver;

Separation of the total flux of radiation into individual spectral portions;

Separation, in photography, of definite portions of the spectrum to eliminate the effects introduced by selective scattering or absorption by the medium;

Maximum attenuation of the radiant energy in portions of the spectrum not required for the work.

Section 100. Principle of Construction and Classification of Optical Filters

All substances, to some degree, absorb the radiant energy passing through them. Radiant energy induces oscillation of the free or bound electrons in the substance (intra-atomic or intramolecular electrons), and also oscillations of the molecules or atoms. Free electrons can oscillate only with the frequency of the incident radiant energy. The absorption of radiant energy due to the oscillations of free electrons is therefore almost independent of the frequency, so that the absorption curve is uniform over the entire spectrum. If the absorption is due to oscillations of molecules, atoms, or bound electrons, then it is manifested in the form of individual absorption bands (selective absorption). Most absorption bands of infrared rays are due to molecular oscillations.

Optical filters are classified by their optical properties (spectral characteristics) or by their purpose. With respect to spectral characteristics, filters are subdivided into three classes.

Class 1, filters strongly absorbing rays of a wavelength λ less than a critical wavelength λ_T (characterizing the filter), but readily passing rays of a wavelength more than λ_T.

Such spectral characteristics in the infrared region of the spectrum are exhibited, for instance, by special classes passing radiant energy of wavelengths above 0.75-0.8 μ.

The filters in which the critical wavelength lies in the infrared region also include ebonite which passes only rays of a wavelength above 0.8 μ, wood, and paper, which begins to pass radiant energy of somewhat longer wavelengths.

Class 2, filters readily transmitting light of a wavelength $\lambda < \lambda_T$ and strongly absorptive at $\lambda > \lambda_T$, i.e., filters not passing waves longer than λ_T. Filters of this class, as far as arrangement of their zones of transmission and absorption is concerned, are the reverse of filters of class 1.

The filters of this class include sylvinite (kCl), which passes rays of wavelengths up to 21 μ, and fluorite (CaF_2), which passes wavelengths up to 10 μ, rock salt (NaCl) with a threshold near 16 μ, and quartz (SiO_2) with a boundary up to 4 μ.

Optical filters of the first two classes can be characterized as cut-off filters.

STAT

Class 3, filters strongly absorbing over the entire spectrum, except for one or several narrow wavelength regions, within which the filters readily pass radiant energy.

These filters are called band filters or monochromatic filters.

According to purpose, filters may be subdivided into two groups:

Spectral filters, isolating a relatively narrow frequency band or an entire region of the spectrum, for example, infrared or ultraviolet;

Compensation or correcting filters, which change the spectrum of a radiant flux or the spectral characteristic of a receiver, by bringing it into the required form, this group includes so-called neutral filters, which attenuate a radiant flux without changing its spectral composition.

Absorption (selective or nonselective) is a property of all substances; for this reason there are solid, liquid, and gaseous optical filters.

Solid optical filters are structurally more convenient than liquid or gaseous types, but their absorption characteristics do not always satisfy the requirements

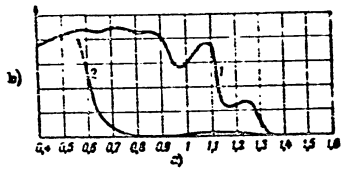

Fig. 182 - Absorption Curves of Liquid Filters for Infrared Rays
1- Absorption curve of layer of water 1 cm thick; 2- Absorption curve of 2.5% solution of cuprous chloride with a layer 2.5 cm thick;
a) Wavelength, μ; b) Absorption factor τ_λ, %

they must meet; therefore, it is sometimes necessary to use liquid and gaseous filters.

Gaseous optical filters are difficult to produce and are not durable.

Liquid filters are made in the form of a vessel with plane-parallel walls, filled with a solution of a coloring matter. The salts of certain metals (Cu, Co, Cr, Ni) or organic dyes, for example aniline dyes, are used as such coloring matters.

Some liquid filters, for example a 2% solution of cuprous chloride, with a 2.5 cm thick layer, will completely absorb infrared rays. Figure 182 shows the absorption curve (2) of a liquid filter made of a solution of cuprous chloride and, for comparison, the absorption curve (1) of a 1 cm thick water layer.

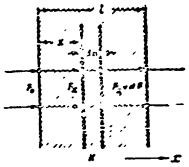

Fig. 183 - Absorption Diagram of Radiant Flux by a Filter

Section 101. Absorption of Radiant Energy in Optical Filters

The radiant flux passing through an absorbing medium is attenuated by it; at selective absorption, the attenuation of the radiant flux depends on its frequency. The radiant flux Φ passing through a medium is always less than the incident flux Φ_0. The ratio of these fluxes defines the transmission factor (or coefficient of transparency) τ:

$$\tau = \frac{\Phi}{\Phi_0} \qquad (176)$$

The absorption factor τ relates to the entire thickness of the absorbing layer.

For a monochromatic flux of wavelength λ, the ratio of the fluxes is characterized by the spectral transmission factor τ_λ.

Let us discuss the simplest case of absorption in a medium where the absorbing layer is homogeneous, while the radiant flux is monochromatic.

On an infinitely thin layer dx (Fig. 183) of a medium with an absorption factor k_x in cross section x, a flux Φ_x is incident. The absorption in this layer will be expressed by the equation

$$d\Phi = -k_x \Phi_x dx \qquad (177)$$

STAT

On integrating this expression over the entire thickness l, we obtain the value of the total absorption in a layer of a given thickness:

$$\int_0^l \frac{d\Phi}{\Phi_x} = -k_x \int_0^l dx \qquad (178)$$

At a uniform layer, when the absorption through the entire thickness is the same, we have

$$k_x = \text{const} = k$$

Solving eq.(178), we get

$$\tau = e^{-kl} \qquad (179)$$

Equation (179) shows the relation between the transmission factor τ and the length l of the path traveled by the radiant flux. The quantity k is called the extinction (or attenuation) factor and characterizes the ability of a medium to attenuate a flux of radiant energy. Equation (179) expresses the exponential law of attenuation of radiant energy.

For a monochromatic flux of a wavelength of λ, the transmission factor is

$$\tau_\lambda = e^{-k_\lambda l} \qquad (180)$$

where k_λ is the attenuation factor of a medium for wavelength λ.

In decimal logarithms, eq.(179) may be expressed as follows:

$$\tau = 10^{-k'l} \qquad (181)$$

The attenuation factor k and the absorption factor k' are connected by the relation

$$k' = k \lg_e 10 = 0.434k \qquad (182)$$

Optical filters can be characterized by the optical density D_λ of the substance composing the filter for a given wavelength. The quantity D_λ is related to the transmission factor τ_λ by the expression

$$D_\lambda = \lg \frac{1}{\tau_\lambda} = -\lg \tau_\lambda = k'_\lambda l \qquad (183)$$

Equation (183) indicates that the absorption factor characterizes the optical density of a layer of a given medium of unit thickness.

The total transmission factor of several absorbing layers is equal to the product of the transmission factors of the individual layers:

$$\tau_{\lambda\Sigma} = \tau_{\lambda 1}\, \tau_{\lambda 2}\, \tau_{\lambda 3} \cdots \tau_{\lambda n}$$

while the total optical density is equal to the sum of the densities of each layer, i.e.,

$$D_{\lambda\Sigma} = D_{\lambda 1} + D_{\lambda 2} + D_{\lambda 3} + \ldots + D_{\lambda n}$$

The total (integral) transmission factor τ_Σ of a non-monochromatic radiant flux within the band limits from λ_1 to λ_2, taking account of the distribution of the radiant energy incident over light filter on passing through it, is expressed by the formula

$$\tau_\Sigma = \frac{\Phi}{\Phi_e} = \frac{\int_{\lambda_1}^{\lambda_2} \Phi_{\lambda_e}\, \tau_\lambda\, d\lambda}{\int_{\lambda_1}^{\lambda_2} \Phi_{\lambda_e}\, d\lambda} \qquad (184)$$

Frequently, the total (integral) transmission factor τ_Σ of an optical filter is defined by taking account of the spectral characteristic of the receiver:

$$\tau_\Sigma = \frac{\Phi}{\Phi_e} = \frac{\int_0^\infty \Phi_{\lambda_e}\, v_\lambda\, \tau_\lambda\, d\lambda}{\int_0^\infty \Phi_{\lambda_e}\, v_\lambda\, d\lambda} \qquad (185)$$

STAT

where τ_λ = spectral transmission factor of the optical filter;

v_λ - spectral characteristic of the receiver;

$\Phi_{\lambda o}$ = monochromatic flux of radiant energy incident on the filter.

The total transmission factor τ_Σ is always less than unity. Part of the radiant flux falling on the filter is absorbed by the filter and heats it. When the power of the flux passing through an optical filter is great and the total transmission factor is low, the losses of radiant energy in the filter and thus also the heating of that filter, may be quite high. Therefore, whenever a filter is used, the allowable power dissipation at which the filter will still maintain its spectral characteristic and mechanical properties must be known.

The transmission factor of a filter can sometimes be defined in terms of the quantity of coloring matter in the solvent. In this case, the value of the concentration of the dye c, expressed in gm/cm^3, is introduced in eq.(181). Then,

$$\tau_\lambda = 10^{-k'cl} \qquad (186)$$

The product cl expresses the surface concentration of the dye, i.e., its quantity per unit surface of the filter. Denoting this product by N, we obtain

$$\tau = 10^{-k'N} \qquad (187)$$

The values of the surface concentration N is measured in grams of dye per m^2 of light filter.

Equation (186) is applicable to liquid and solid optical filters.

If an optical filter is made from several dyes, then the total optical density is equal to the sum of the optical densities of the individual dyes, provided that they are chemically inert with respect to one another.

For optical systems (lenses, prisms, plates) designed for work in the infrared region of the spectrum, as for infrared filters, various substances transparent to infrared rays are used: special kinds of glass, plastics, a number of crystals, and certain other materials. Figure 184 shows the transmission curves of thin plates of ebonite, mica, gelatine, and celluloid, while Fig.185 gives the spectral transmission

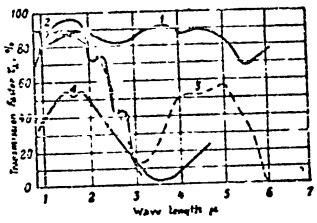

Fig.184 - Curve of Spectral Transmission Factor of Several Filters
1- Mica (0.02 mm); 2- Gelatin (0.06 mm); 3- Celluloid (0.14 mm);
4- Ebonite (0.1 mm)

characteristics for various materials. Figure 185 indicates that these materials can be used in preparing optical systems and filters for infrared rays.

Ordinary mica has a wide transmission range, while biotite, which passes infrared rays, partly blocks the visible rays. For muscovite and biotite, the transmission factor curves have an absorption zone in the area 9-10 μ, followed by a new pass-band with a maximum at about 12 μ. Such substances as gelatin and celluloid

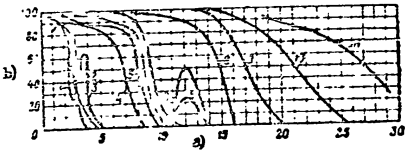

Fig.185 - Transmission Factors of Various Materials
1- Pyrex glass; 2- Plate glass; 3- Quartz; 4- Fluorospar;
5- Muscovite; 6- Biotite; 7- Fluorite; 8- Sodium fluoride;
9- Rock salt; 10- Sylvinite; 11- Potassium bromide
a) Wavelength, μ; b) Transmission factor τ_λ, %

pass infrared rays of wavelengths up to 2.5-3 μ.

Section 102. Types of Solid Optical Filters and their Characteristics

Solid optical filters are made of gelatin, colored glass or plastic, and of certain other solid substances.

Gelatin filters consists of a thin film (0.5-0.1 mm thick) of dyed gelatin. To protect it from moisture and the direct action of temperature, the film is usually placed between two plane glass plates, cemented together with Siberian balsam.

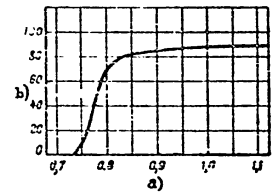

Fig. 186 - Relation between Transmission Factor of a Gelatin Optical Filter and the Wavelength
a) Wavelength, μ; b) Transmission factor τ_λ, %

Organic dyestuffs are ordinarily used to color gelatin filters.

Figure 186 gives the curve characterizing the relation between the transmission factor of a gelatin filter and the wavelength. A filter of this type readily passes infrared rays, beginning with the longest waves of the visible portion of the spectrum.

The disadvantages of gelatin color filters are the instability of their spectral characteristic with time, the low mechanical strength, and the dependence of the filter characteristics on humidity and temperature.

Glass color filters are made of glass, colored by molecular or colloidal dyes. The coloring matter used include oxy-salts of cobalt, nickel, iron, chromium, and certain other metals, as well as gold, silver, copper, cadmium selenide, or sulfide in the colloidal state.

The dyestuffs are added in very small quantities and make up only a fraction of a percent of the total mass.

Glass optical filters have the following advantages over gelatin types: heat resistance, time stability of spectral characteristic, and possibility of mass production of filters with the same characteristic.

A light filter is most completely characterized by the spectrum, the transmission curve, or the optical density curve.

Figure 187 gives the characteristics $\tau_\lambda = f(\lambda)$ and $D_\lambda = f(\lambda)$ for three types of glass color filters designed for isolating the infrared rays close to the visible

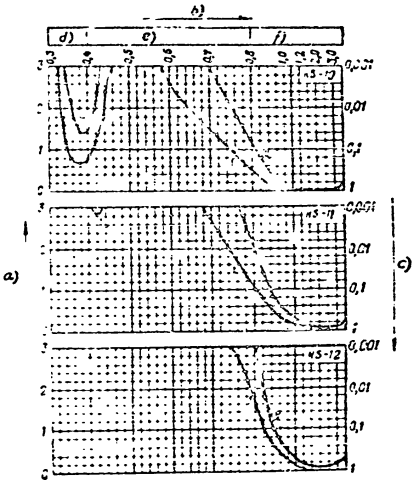

Fig. 187 - Curves of Transmission Factor τ_λ and Optical Density D_λ for Glass Filters of Different Types (KS-10, KS-11, and KS-12)
a) Optical density D_λ; b) Wavelength, λ; c) Transmission factor, τ_λ; d) Ultraviolet rays; e) Visible rays; f) Infrared rays

portion of the spectrum. For each type of these filters, two curves (1) and (2) are given, corresponding to thicknesses of 1 and 2 mm. The optical filters KS-10 and KS-11 partly transmit visible rays (red light), while the filter KS-12 fails almost completely to do so.

STAT

Figure 188 gives the spectral transmission characteristic for a glass containing manganese oxide. The characteristic shows that this glass is opaque to visible light

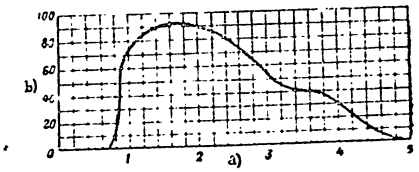

Fig. 188 - Spectral Transmission Characteristics for Glass with Manganese Oxide
a) Wavelength, μ; b) Transmission factor τ_λ, %

but readily passes infrared rays with a wavelength from about 0.9 to 2.5 μ and has its transmission threshold (τ_λ = 10%) at a wavelength close to 4.5 μ. This glass may thus serve as a good optical filter for the near infrared rays.

A number of organic dyes are used in plastic color filters, characterized by a high transmission factor in the infrared portion of the spectrum and by strong absorption in the visible portion.

Organic dyes are introduced into color filters by one of three methods:

Evaporation of a film of dye;

Deposition of a film from a colored plastic onto a glass base;

In the form of a constituent of the plastic.

Color filters prepared by the evaporation method have somewhat less favorable spectral characteristics than those prepared by the last two methods.

Cellophane, Nylon and polyvinyl compounds are generally used as films in plastic color filters.

Figure 189 gives the transmission curves for optical filters of colored celluloid film (Fig. 189a) 0.04 mm thick, of colored Nylon film (Fig. 189b), and of polyvinyl film (Fig. 189c). Color filters may have different transmission factors. These curves show that color filters of Nylon film have a lower transmission factor than color filters of celluloid film.

Color filters of polyvinyl film have a very steep transmission characteristic for infrared rays, which ensures better absorption in the visible portion. A disadvantage of these color filters is the impairment of transmission when the filter

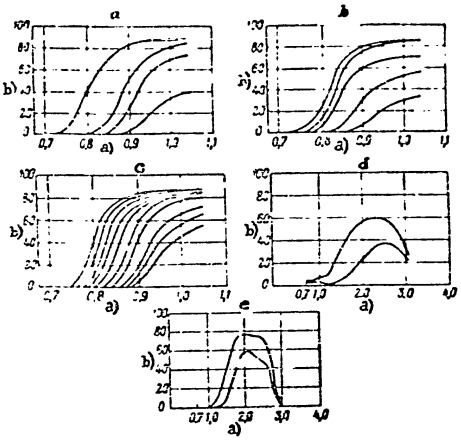

Fig. 189 - Spectral Transmission Factors of Plastic Filters
a- Celluloid, b- Nylon; c- Polyvinyl; d- Silver sulfide; e- Furane tar
a) Wavelength, μ; b) Transmission factor τ_λ, %

is heated to over 100°C. Narrow-band color filters with high transmission in the 1-2 μ region are made of silver sulfide (Fig. 189d) and furane pitch (Fig. 189e). The maximum of transmission of a silver sulfide color filter is in the spectral region of 2.4-2.6 μ.

STAT

Section 103. Nonabsorbing Color Filters

Absorbing color filters separate the required radiation with insufficient sharpness. For this reason in many cases color filters of other types are used: powder

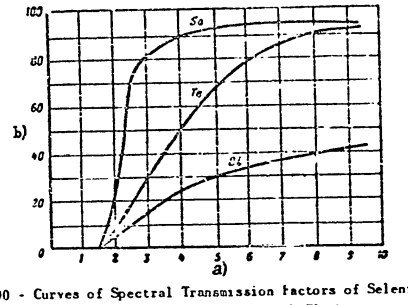

Fig. 190 - Curves of Spectral Transmission Factors of Selenium Black, Tellurium Black, and Bismuth Black
a) Wavelength, μ; b) Transmission factor τ_λ, %

filters with rough surfaces, and filters with various refractive indexes.

Powder Color Filters (Bibl. 16). The action of powder color filters is based on the diffuse scattering of incident radiant energy by particles deposited on the surface of a transparent plastic. The transmission of the filter depends on the size of the particles and increases as the dimensions of the particles and the wavelength of the ray become commensurable. For example, for the transmission of radiant energy of wavelengths from 2 to 7.5 μ, the particles must range in size from 0.22 to 2.5 μ.

Powder color filters are made of selenium, tellurium, bismuth, zinc oxide or magnesium oxide, and of certain other materials.

Figure 190 gives the curves for transmission factor variations as a function of the wavelength for several powder color filters. The selenium color filter does not transmit rays of wavelengths shorter than 1.5 μ but readily passes waves longer than 3 μ (up to 90%). Selenium filters are therefore successfully used for cutting off the descending branch of the spectral curve in the short-wave infrared region of the

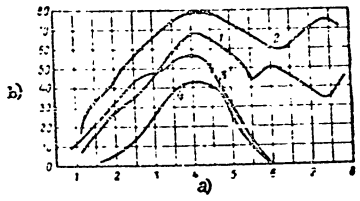

Fig. 191 - Transmission Factor of Magnesium Oxide and Zinc Oxide Color Filters
1- ZnO on mica; 2- MgO on mica; 3- ZnO on cover glass; 4- MgO on cover glass
a) Wavelength, μ; b) Transmission factor τ_λ, %

spectrum.

The curves for the transmission factors of color filters of magnesium oxide and zinc oxide, applied in powder form to mica and glass, are given in Fig. 191.

Color filters with rough surfaces are made of a material transparent to infrared rays, whose surface is roughened.

Rays of wavelengths shorter than the particle size of a rough surface, are scattered by such a surface, while rays of a wavelength considerably exceeding these dimensions, are freely transmitted. The region of wavelengths commensurable with the particle size is intermediate between the two.

The spectral transmission characteristic of radiant energy by a color filter with a rough surface depends on the dimensions and uniformity of the particles responsible for the roughness. At high nonuniformity, the color filter will transmit a wide range of wavelengths, and the transmission factor curve will be shallow. At high particle uniformity (obtained, for example, by treating the surface in a

STAT

solvent instead of mechanically), the spectral characteristic of a color filter has a sharper transition from absorption to transmission.

Figure 192 gives the spectral transmission characteristics of radiant energy for color filters with rough surfaces, prepared from rock salt. The curves A and A_1 relate to filters with rough surfaces created by a mechanical method (with carborundum powder) while the curves B and B_1 relate to filters with surfaces prepared by dissolving the surface layer of rock salt.

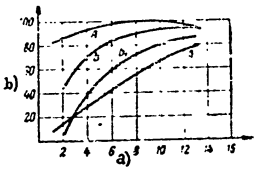

Fig. 192 - Transmission Factors of Rock-Salt Color Filters with Rough Surfaces:
A, A_1 mechanical processing;
B, B_1, treatment with solvent
a) Wavelength, μ; b) Transmission factor τ_λ, %

A disadvantage of rough surfaced filters is that their transmission characteristics do not sharply delimit the regions of diffusion and transmission.

Filters with Various Refractive Indexes.

The action of these filters is based on the diffusion of radiant energy, depending on the refractive index of the medium. Media of one substance (solid, liquid, or gaseous) with minute particles of another substance suspended on it, form an optically uniform medium, which does not scatter radiant energy, if the refractive indexes of the two substances are the same. If, however, the refractive indexes are different, the medium is optically nonuniform and therefore diffuses radiant energy. When the refractive indexes of the two substances are the same for several wavelengths but different for others, the medium is transparent to the former and opaque to the latter. Such a medium may be used as a color filter.

In the transmission of radiant energy through such a filter, that portion of it for which the refractive indexes of the two substances are different is dispersed. Only the energy of wavelengths for which the refractive indexes of the two substances are the same will pass the filter.

Table 44

Optical Characteristics and Specific Gravity of Certain Materials Transparent to Infrared Rays

Designation of Substance	Chemical Formula	Limit of Useful Transmission for Prism*	Region of Transmission	Transmission Factor	Limit of Transmission (T = 10%)	Refractive Index	Specific Gravity
	-	μ	μ	%	μ	-	g/cm²
Glass	SiO_2, Na_2CO_3, PbO etc.	2.2	up to 2-2.5	> 90	3	1.5-1.8	2.2-2.8
Fused quartz	SiO_2	-	0 2-3	> 80	4	1.46	2.02
Crystalline quartz	SiO_2	3.5	0 2-3.5	> 80	4	1.55	2.2-2.6
Lithium fluoride	LiF	-	0.12-6	> 80	8	-	2.3
Muscovite mica	-	-	up to 7	> 80	from 10-15	1.56-1.59	2.75-3
Biotite mica	-	-	up to 8	> 80	from 12-15	1.54-1.57	2.7-3.1
Fluorite (fluospar, calcium fluorite)	CaF_2	8.5	0.13-9.5	> 90	10	1.43	3.2
Sodium fluoride**	NaF	-	up to 12	> 90	16	1.3	2.7
Rock salt (sodium chloride)	NaCl	15	0.2-15.5	90-20	19	1.52	2.1-2.3
Sylvite (Potassium chloride)	KCl	21	0.2-21	90-25	24	1.47	2
Potassium bromide	KBr	29	0.21-29	> 30	31	-	2.75

* The limit of useful transmission for the prisms of spectral instruments characterizes the wavelength up to which a prism of the given material can be used.

** The materials indicated in the last four lines of the Table are readily soluble.

STAT

The width of the pass-band of the filter depends on the dispersion of the substances forming a filter, i.e., on the variation in the refractive index for various wavelengths. The greater the difference in the curves characterizing the dispersion

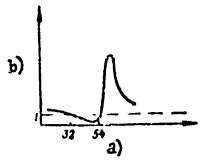

Fig. 193 - Curve for Dispersion by Rock Salt
a) Wavelength, μ; b) Refractive index

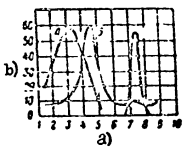

Fig. 194 - Spectral Transmission Characteristic for Filters of Powdered Quartz
a) Wavelength, μ; b) Transmission factor τ_λ, %

of the two substances, the smaller will be the spectral region isolated by the filter.

Figure 193 gives the dispersion curve for rock salt. The refractive index varies with the wavelength; at $\lambda = 32$ μ and $\lambda = 54$ μ it has the same value.

For magnesia, the maximum transmission corresponds to a wavelength of $\lambda = 12.2$ μ. If magnesia is placed in carbon tetrachloride (CCl_4), the transmission maximum is shifted to a wavelength of 9 μ, at which the refraction indexes of magnesia and CCl_4 are the same.

The spectral characteristics of transmission of powdered quartz, suspended in air (curve C), in liquid CS_2 (Curve A), and in liquid CCl_4 (curve B) are given in Fig. 194.

These data on optical filters indicate their great variety and the possibility of using them in various portions of the infrared region of the spectrum.

Table 44 gives the optical characteristics and specific gravity for a few materials transparent to infrared rays.

CHAPTER XII

OPTICAL SYSTEMS

Section 104. Purpose and Classification of Optical Systems

Optical systems serve to redistribute the flux of radiant energy in space. The source of radiation usually forms a flux scattered in all directions. The optical

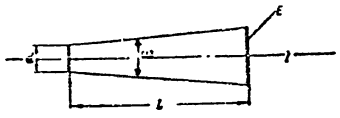

Fig. 195 - Illumination of a Screen without Lens

systems transform it into an oriented flux, thus concentrating the radiant energy and utilizing it more efficiently.

To show the efficiency of using an optical system, let us compare the illumination produced by a source of undirected radiation with the illumination produced by the same radiator with oriented radiation (by means of an optical system). Let a source of radiation have the shape of a flat plane disk (Fig. 195) of diameter d and area S, and let it have the brightness B. The luminous intensity of the source is defined by the equation

$$I = BS = B\frac{\pi d^2}{4} \qquad (188)$$

Then, at indirect illumination (without an optical system) of the plane

screen E, located at a distance l from the source of radiation, the illumination of the screen (disregarding the losses in the atmosphere) will be

$$E = \frac{I}{l^2} \qquad (189)$$

The flux incident on the screen will be

$$\Phi = I\omega \qquad (190)$$

where ω is a solid angle.

If a correcting lens (Fig. 196) is placed between the energy source illuminating the screen and the screen, itself, then the flux incident on the lens will be

$$\Phi_1 = I\omega_1 \qquad (191)$$

The illumination of the surface of the lens will become

$$E = \frac{I}{l_1^2} \qquad (192)$$

For an ideal lens, giving a correct, undistorted image, the flux $\Phi_2 = \Phi_1$ leaving it will be propagated over the solid angle ω_2. Then, the luminous intensity

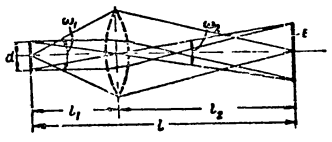

Fig. 196 - Illumination of a Screen from a Lens

leaving the lens, as it would leave a source, is defined by the relation

$$I' = \frac{\Phi_2}{\omega_2} \qquad (193)$$

and the illumination of the screen by

$$E' = \frac{I'}{l_2^2} \qquad (194)$$

The ratio between the illuminations E' and E defines the gain obtained by using an optical system. This ratio is called the optical amplification factor of the system and reads

$$k = \frac{E'}{E} \qquad (195)$$

Let us determine the relation between the optical amplification factor of the system and its diameter. From eq. (191) and (193), we obtain

$$I' = \frac{\Phi_2}{\omega_2} = \frac{I\omega_1}{\omega_2} \qquad (196)$$

The solid angles ω_1 and ω_2 are determined by the ratios of the areas of the spherical surfaces cut out of a plane, to the squares of the distances l_1 and l_2.

Considering that these angles are small, we may write

$$\omega_2 = \frac{\pi d^2}{4l_2^2} \quad \text{and} \quad \omega_1 = \frac{\pi D^2}{4l_1^2}$$

where d = diameter of light source;

D = diameter of lens.

Consequently the amplification factor of an ideal optical system (at $l_1 \approx l_2$), will be

$$k' = \frac{I'}{I} = \frac{\omega_1}{\omega_2} = \frac{D^2}{d^2} \qquad (197)$$

The amplification factor of an actual optical system (with $l_1 \approx l_2$) is determined by the relation

$$k = q\frac{D^2}{d^2} \qquad (198)$$

where q is a factor characterizing the losses in the optical system.

It will be clear from the last relation that, at increasing diameter of the optical system and decreasing size of the radiation source, the optical amplification factor of the system increases.

Equation 198 for the coefficient of optical amplification of a system holds not only for lenses but also for reflecting systems. Here D denotes the diameter of the reflector, and q that of a factor taking account of all losses, including the losses through reflection, absorption in the inside of the glass of the reflector, and the shielding of individual portions by opaque parts.

The optical amplification factor in modern searchlights reaches a few thousand.

The luminous intensity of a projector I_{pro} (in the direction of the optical axis), depending on the brightness of the source of radiation and the size of the reflector, may be determined from eqs. 188 and 198, taking account of all losses, as

$$I_{pro} = qI\left(\frac{D}{d}\right)^2 = qB\frac{\pi D^2}{4} \qquad (199)$$

where q = loss factor;

B = brightness of source of radiation.

Consequently, the luminous intensity of a projector will be

$$I_{pro} = qBS \qquad (200)$$

where $S = \frac{\pi D^2}{4}$ is the area of luminous aperture, equal to the area of projection of the reflector onto a surface perpendicular to the optical axis.

Thus, the luminous intensity of a projector is equal to the product of the brightness of the radiation source placed at the focus of the reflector, by the area of the luminous aperture and a factor allowing for the reflector losses.

The use of an optical system permits obtaining a luminous intensity considerably exceeding that of the source.

The illumination produced by a projector is defined from the usual relation

$$E = \frac{I_{pro}}{l^2} \qquad (201)$$

or, allowing for losses in the atmosphere, by the relation

$$E = q_l\frac{I_{pro}}{l^2} \qquad (202)$$

where q_l is a factor allowing for all losses in the atmosphere on the propagation path l of the radiant energy.

Optical systems are used not only in radiators but also in receptors. In this case, the optical system focuses the radiant energy incident on it and directs it onto the receptor, making it possible for the illumination of the receptor to exceed considerably the illumination of the surface of the optical system.

Optical systems can be subdivided into three groups:

Lens (dioptric) systems, in which the rays pass through a refracting medium;

Reflecting (catoptric) systems, in which the flux from the radiation source is reflected from one or more reflectors or mirrors;

Mixed (catodioptric) systems, in which lens and reflecting systems are combined.

Section 105. Basic Concepts and Laws of Optics

The action of optical systems is based on the laws of geometric optics, which determine the path of rays through an optical system and allow that path to be calculated.

The propagation of light rays in optical systems obeys the following fundamental laws:

In an optically uniform transparent medium, light rays are propagated rectilinearly and independently of each other.

The incident ray F_φ, the reflected ray F_ρ, and the refracted ray F_ψ are coplanar with the perpendicular to the refracting surface (Fig. 197).

The angle made by the incident ray with the normal equals the angle between the normal and the reflected ray.

The ratio of the sine of the angle of incidence φ and the sine of the angle of refraction ψ is a constant for the various media:

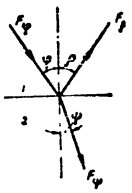

Fig. 197 - Incident (F_φ), Reflected (F_ρ) and Refracted (F_ψ) Rays at the Interface of Two Media

$$\frac{\sin\varphi}{\sin\psi} = n_{21} = \frac{n_2}{n_1} \qquad (203)$$

or

$$n_1 \sin\varphi = n_2 \sin\psi$$

where n_{21} = refractive index of the second medium with respect to the first;

n_2 and n_1 = absolute refractive indexes of the second and the first media.

The absolute refractive index of vacuum is $n = 1$ and of air, $n = 1.00029 \approx 1$.

A refracted ray is propagated in the second medium at a velocity of v_2, which is not equal to the velocity of propagation in the first medium v_1. Allowing for the inequality of the velocities of propagation of light in the different media, we may write that

$$\frac{\sin\varphi}{\sin\psi} = \frac{v_1}{v_2} \qquad (204)$$

whence

$$n_{21} = \frac{\sin\varphi}{\sin\psi} = \frac{v_1}{v_2} \qquad (205)$$

The last equation indicates that the refractive index of the second medium, relative to the first, is equal to the ratio between the speeds of propagation of light in these media.

The absolute index of refraction n is defined as the ratio of the velocity of propagation of light in vacuo (practically, also in air) to the velocity of propagation in the medium:

$$n = \frac{c}{v} \qquad (206)$$

Since the frequency ν, on passage from the first medium into another one, remains constant, while the velocity of propagation changes, the wavelength will also vary. From the well-known relations

$$\lambda = \frac{v}{\nu} \text{ and } \lambda_c = \frac{c}{\nu}$$

we obtain

$$\lambda = \frac{v}{c}\lambda_c = \frac{\lambda_c}{n}$$

where λ and λ_c are wavelengths at which energy of a frequency ν is propagated in the medium and in vacuo, respectively; while n is the absolute refractive index.

The refractive indexes for most solid and liquid substances have values from 1.3 to 2.6. Table 45 gives the values of the refractive indexes for a few substances.

Refraction Ray by a Plane-Parallel Plate. A ray passing through a plane-parallel plate is refracted twice (Fig. 198).

The ray leaving the plate is parallel to the incoming ray but is shifted with respect to its axis. The value of this shift ΔS depends on the angle of incidence, the thickness of the plate d, and the refractive indexes of the plate, of the medium from which the ray passes to the plate, and the medium into which it is passed.

STAT

The displacement of the ray is defined by the formula

$$\Delta S = d\left(1 - \frac{\tan \psi_1}{\tan \varphi_1}\right) \qquad (207)$$

At small angles of incidence, eq.(207) is transformed into

$$\Delta S = \frac{d \sin(\varphi_1 - \psi_1)}{\cos \psi_1} \qquad (208)$$

A reduction in the displacement of the ray is effected by the use of thinner plates or by reducing the angle of incidence.

Table 45

Refractive Indexes n and Critical Angles of Incidence φ_0 for Certain Substances

Substance	n	φ_0, degrees
Ice	1.31	50
Water	1.33	49
Ether	1.35	48
Ethyl alcohol	1.36	47
Glycerol	1.47	43
Benzene	1.50	42
Siberian balsam	1.54	40.5
Diamond	2.4	23.5

On passage from one medium to another, the ray is refracted in accordance with the law of refraction, eq.(203). If the light is propagated from a medium of higher refractive index n_1, when the refractive index n_1 in the medium is greater than the index n_2, then the angle of refraction ψ_1 will be greater than the angle of incidence φ (Fig.199, ray A).

With increasing angle of incidence φ_2, the angle of refraction ψ_2 increases, and, at a certain value $\varphi_2 = \varphi_0$, reaches the value $\psi_2 = \frac{\pi}{2}$.

In this case, the ray B will not be refracted in the optically less dense medium, but will slide along the interface of the media.

The angle φ_0 is called the critical angle of incidence. Any further increase in the angle of incidence will result in failure of the incident ray C to be refracted, and in its total reflection from the surface of separation between the

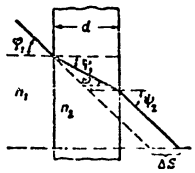

Fig.198 - Refraction of Ray by Plane-Parallel Plate

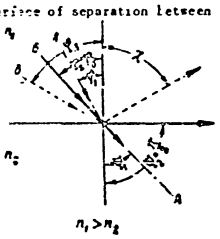

Fig.199 - Total Internal Reflection

media. This phenomenon, termed total internal reflection, takes place at angles of incidence exceeding the critical angle of incidence φ_0.

The relation $\sin \varphi > \frac{n_2}{n_1} = n_{21}$ defines the condition of total internal reflection. If a second medium (optically less dense) such as vacuum or air ($n_2 = 1$) is involved, then the condition of total internal reflection is defined as

$$\sin \varphi > \frac{1}{n_1} \qquad (209)$$

The values of the critical angles of incidence φ_0, for a few substances, are given in Table 45.

A ray incident on a medium along its boundary with air, at an angle exceeding the critical angle of incidence, is completely reflected back into the medium

The reflection of light rays on the surface of an optical part or other solid, may be specular or diffuse.

Regular, or specular, reflection is shown in Fig.200a; diffuse, or scattered,

STAT

in Fig. 200 d; mixed, in Fig. 200 b; and directed-scattered in Fig. 200 c.

The ratio of the reflected flux F_ρ to the incident flux F_φ is called the re-

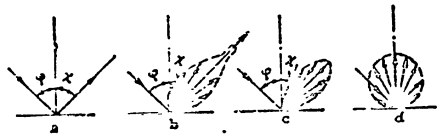

Fig. 200 - Various forms of Reflection:
a - Regular, or Specular; b - Mixed;
c - Directed-scattered; d - Diffuse,
or scattered

flection factor ρ:

$$\rho = \frac{F_\rho}{F_\varphi} \tag{210}$$

In diffuse reflection, the rays are reflected at different angles.

In regular (specular) reflection the reflection factor may also be defined by the relation

$$\rho = \frac{E}{B} \tag{211}$$

where E = illumination produced by the incident flux;

B = luminosity produced by the reflected flux.

The reflection factor depends on many causes, and, in particular, on the angle of incidence, the state of the reflecting surface, the refractive indexes and, in some cases, on the wavelength of the incident flux.

Reflection may occur on the boundary between transparent and opaque media. The curve of the relation between the reflection factor ρ and the angle of incidence φ in reflection from the surface of glass ($n = 1.5$) is given in Fig. 201. The diagram indicates that at angles of incidence not exceeding 40°, the reflection factors for a glass surface are very small (4-5%). At angles of incidence above 60°, the reflection factor increases steeply and reaches 100% at 90°.

The reflection factor for the boundary of transparent media can be defined by the formula

$$\rho = \frac{1}{2}\left\{\frac{\sin^2(\varphi - \psi)}{\sin^2(\varphi + \psi)} + \frac{\tan^2(\varphi - \psi)}{\tan^2(\varphi + \psi)}\right\} \tag{212}$$

where φ and ψ are the angles of incidence and refraction.

If a ray strikes the reflecting surface perpendicularly ($\varphi = 0°$), the coefficient of reflection is defined by the formula

$$\rho = \frac{(n_{21} - 1)^2}{(n_{21} + 1)^2} \tag{213}$$

where $n_{21} = \frac{n_2}{n_1}$ denotes the index of refraction of the second medium with respect to the first.

If the first medium is a vacuum or air, then eq. (213) takes the form

$$\rho = \frac{(n - 1)^2}{(n + 1)^2} \tag{214}$$

The reflection of rays from the surface of metals is determined not only by the refractive indexes, as in transparent media, but also by the absorption factor a of the metal, which is usually large.

If a ray strikes the surface of a metal perpendicularly ($\varphi = 0°$), the reflection factor is defined by the formula

$$\rho = \frac{(n - 1)^2 + a^2}{(n + 1)^2 + a^2} \tag{215}$$

Figure 202 a, b gives curves of the reflection factors for various polished metals, as a function of the wavelength. The curves show that the reflection factor

varies greatly for wavelengths of the visible region of the spectrum and portions close to it, but that in the infrared region of the spectrum at wavelengths of about 5-10 μ, the reflection factor remains almost constant.

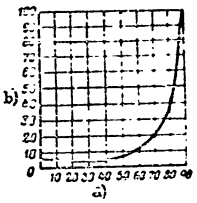

Fig. 201 - Relation between Reflection Factor and Angle of Incidence for Glass (n = 1.5)
a) Angle of Incide e, degrees;
b) Reflection factor, %

The reflection factor of some metals (Ag, Au, Cu) exceeds 90% (up to 99%) over a very wide range of wavelengths.

If the reflection factor varies as a function of the wavelength, the spectral composition of the reflected flux differs from that of the incident flux. Thus, for example, the flux reflected from certain metals (for example, gold, copper) has a different color from that of the incident flux of the visible region of the spectrum.

Section 106. Lens (Dioptric) Systems

A lens optical system usually consists of one or several lenses.

A lens is a part made of an optical material, usually glass, which has at least one spherical surface. The second bounding surface may be spherical or plane.

Lenses are characterized by the refractive indexes of the optical material of the lens, by the radii of curvature of the bounding surfaces, and by the position of the centers of curvature.

The optical properties of lenses depend on the curvature of the generatrixes of their surfaces and on the relations between the refractive index of the lens material and the refractive indexes of the adjoining media. For example, lenses thickened in the central part are of the collecting (positive) type, if they are made of glass and are in air, since the refractive index of glass is greater than that of air. Lenses whose thickness at the center is less than that at the edges, are of the dispersing (negative) type.

Lenses are thin or thick. A lens is called thin (Fig. 203) if its thickness is small relative to the radius of curvature of its surface, and if it has the distances S_1 (from the luminous point to the lens) and S_2 (from the lens to the image point). In this case, the points O_1 and O_2 may be considered to be matched with the optical center of the lens, the point C. The lines passing through the optical center of the lens C are called optical axes of the lens; the axis passing through the centers of curvature C_1 and C_2 is called the principal optical axis. A plane perpendicular to the principal optical axis of a thin lens, passing through its center and coinciding with the plane of symmetry of the lens, is called the principal plane of the lens.

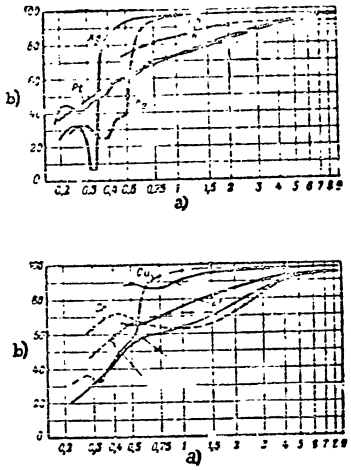

Fig. 202 - Reflection Factors of Various Metals
a) Wavelength, μ; b) Reflection factor, %;
c) Stellite; d) Steel; e) Alzak

The distances S_1 and S_2, the refractive index of the glass of the lens n (the lens being in air), and the radii of curvature of the lens surfaces r_1 and r_2, are

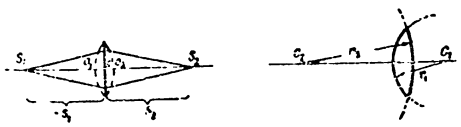

Fig. 203 - Principal Geometric Parameters of a Thin Lens

correlated by the relation

$$\frac{1}{S_2} - \frac{1}{S_1} = (n-1)\left(\frac{1}{r_1} - \frac{1}{r_2}\right) \qquad (216)$$

If rays come from infinity from right to left, the point of intersection of the rays emerging from the lens with the principal optical axis is called the rear principal focus of the lens, and is denoted by the letter F', while the distance from the principal plane to the point F' is called the rear principal focal length and is denoted by the letter f'. On their return path, the rays intersect beyond the lens in the front principal focus (F).

Assuming that $S_1 = \infty$, we obtain an equation determining the rear principal focal length as

$$\frac{1}{S_2} = (n-1)\left(\frac{1}{r_1} - \frac{1}{r_2}\right) = \frac{1}{f'} \qquad (217)$$

An analogous expression can be obtained for the front principal focal length. For a lens in air, the front and rear focal length are equal.

On substituting specific values in eqs. (216) and (217), the rule of signs must be strictly observed. It is customary to denote all segments by a plus sign if they are laid off in the direction of propagation of the rays, usually from left to right, and by a minus sign if the rays are laid off in the opposite direction. Focal lengths are measured from the center of the lens; the distances to the point of emergence and its image are measured from the focal points or from the center of the lens. The radii of curvature are considered positive if they are measured from the spherical surface to its center in the direction of propagation of the rays.

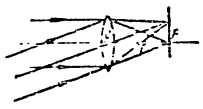

Fig. 204 - Passage of Parallel Rays through a Thin Lens

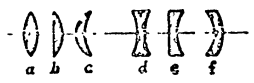

Fig. 205 - Types of Lenses:
a - Double convex; b - Planoconvex;
c - Convex-concave; d - Double concave;
e - Planoconcave; f - Concavoconvex

Planes passing through the foci, perpendicularly to the principal optical axis are called focal planes. Parallel rays passing at a certain angle toward the principal optical axis are refracted by the lens and intersect in the focal plane (Figure 204).

The images produced by lenses may be either virtual or real. An image is real if the object and its image are on different sides of the lens, i.e. if the signs of F and S are different.

An image is virtual if the signs of f and S are the same. The signs and values of the focal lengths depend on the signs and values of the radii r_1 and r_2 and on the refractive index n of the glass of the lens.

Lenses giving real images are called collecting, or positive. Lenses giving a virtual image are called dispersing, or negative.

Figure 205 shows the principal types of lenses. The positive lenses are the double-convex (a), the planoconvex (b) and the positive meniscus or convexo-concave (c) types. The negative lenses are the double-concave (d), the planoconcave (e), and the negative meniscus, or concavoconvex (f) types.

The image of any point of an object obtained after passage of rays through a

lens can be constructed by means of two rays whose intersection behind the lens will yield the image point.

In constructing an image we must start from the fundamental property of lens

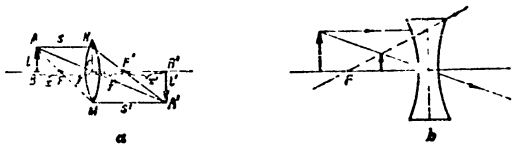

Fig. 206 - Construction of Image on Passage of a Ray through a Double-Convex (a) and a Double-Concave Lens (b)

foci: A ray parallel to the optical axis is refracted in the lens in such a way that it passes through the rear focus of the system (which is in the image space), while

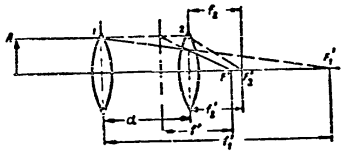

Fig. 207 - Two-Lens Optical System

a ray passing through the front focus of the lens (which is in the object space), emerges from the lens in a direction parallel to the optical axis.

In a double-convex thin lens (Fig. 206 a), the ray AK, parallel to the optical axis, will pass through the rear focus F', while the ray AM, passing through the rear focus F, after refraction, will travel parallel to the optical axis. The intersection of these two rays gives the point A', which is the image of point A.

In ideal optical systems, closely approached by thin lenses with a small relative aperture*, the ray AMA', passing through the rear focus, can be replaced by the ray ACA', passing through the optical center of the lens without refraction. The image of the point B is the point B'. Thus the image of the segment AB is obtained in the form of the segment A'B'.

The ratio of a dimension of the image l' to the corresponding dimension of the object l is called the linear enlargement of the lens and is denoted by β:

$$|\beta| = \frac{l'}{l}$$

From the similarity of the triangles AEF and KFC, and also of the triangles KCF' and A'B'F', it follows that

$$\beta = -\frac{f}{x} = -\frac{x'}{f'}$$

According to the location of the object with respect to the focus F of the lens, the image will be real or virtual, enlarged or reduced erect or inverted.

If the distance from the object to the lens is more than twice the focal length, the image will be real, reduced, and inverted. If the object is at a point between twice the focal length from the lens and the front focus, the image will be real, enlarged, and inverted. If the object is between the lens and the front focus, the image will be virtual, enlarged, and erect.

A dispersing lens, for example a double-concave lens, will give a virtual, reduced, and erect image for any position of the object (Fig. 206 b).

In thick lenses, or optical systems consisting of two thin lenses, there are two principal optical planes. Let us consider an optical system consisting of two lenses, the distance between which is less than the focal length of each lens (Figure 207).

The rays parallel to the optical axis, incident on the lens L_1, would be collected by it on the optical axis at the focus F_1'. But in the path of these rays there is the second lens L_2, which secondarily refracts the rays and collects them at the point F' on the optical axis but not coinciding with the focus of the second

* The relative aperture is the ratio between the diameter and the focal length.

lens F_2'. The point F' at which the image of point A is obtained is the real principal focus of the entire optical system.

The action of an optical system composed of two lenses is equivalent to the action of one lens of focal length F', determined from the expression

$$\frac{1}{f'} = \frac{1}{f_1'} + \frac{1}{f_2'} - \frac{d}{f_1' f_2'} \qquad (218)$$

where f_1' and f_2' are the focal lengths of each of the lenses and d is the distance between the lenses.

The linear enlargement of a two-lens system is determined, as for a thin lens, by the ratio of the dimensions of the image to the dimensions of the object.

Section 107. Light Loss in Optical Systems and the Coating of Lenses

When a radiant flux passes through an optical element, part of the radiant energy is lost. The losses of radiant energy are due to three causes:

Absorption in the substance of the optical element;

Scattering, due to optical nonuniformity of the substance of the optical element and to inadequate polishing of its surfaces;

Refraction on the interface of transparent media with different refractive indexes.

The losses due to absorption and scattering can be reduced by selecting a sufficiently transparent substance for the optical element and by carefully preparing its surface. The losses due to reflection can be reduced by means of "coating" the optical system.

From Table 44 and the transmission curves of various substances (cf. Chapter XI), an optical material of the required transparency for a given region of the spectrum may be selected (cf. Chapter XI).

Let us consider the principles of the modern methods of coating optical elements.

In the reflection of rays from a glass-air interface, 4-9% of the luminous energy is lost, depending on the kind of glass.

In thin glass plates or lenses, in which the absorption is less than 10-20%, from 9 to 20% of the radiant energy is lost, due to reflection on both surfaces of the plate, even at small angles of incidence.

The losses due to reflection increase greatly in complex optical systems consisting of a number (n) of refracting and reflecting surfaces of prisms, lenses, or plane-parallel plates. In this case, the total losses on reflection are determined as

$$\Phi = \Phi_0(1 - \rho)^n \qquad (219)$$

where Φ = radiant flux emerging from the optical system;

Φ_0 = flux incident on the system;

ρ = coefficient of reflection from one surface of an optical element.

In complex optical instruments, the total losses, mainly due to reflection, are as high as 70-90%. In addition, the reflected light is partially scattered in the

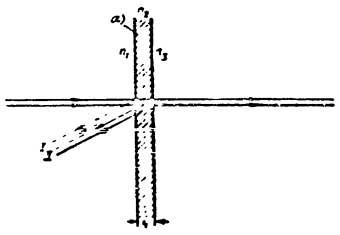

Fig. 208 - Passage of Rays through an Exposed Film
a) film

instrument itself, which still further lowers the contrast of the observed object, by forming fog or flashes.

The above examples show the importance of reducing the reflection of rays from

the boundaries of the transparent media.

In the USSR, systematic work in the coating of optical systems was started under the direction of Academician I.V.Grebenshchikov earlier than in other countries (Bibl.1). Grebenshchikov and his students developed the theoretical principles and various technological methods of coating optical elements. The coating of an optical system, consisting in the reduction of losses by reflection, is effected by covering the surface of the optical element with a thin film of a substance whose refractive index is less than that of the substance of the element. The reflection from the glass-air interface in this case is reduced, owing to the interference of the rays reflected from the interfaces air-film, and film-optical element.

Figure 208 schematically shows the course of the rays passing through the interfaces of the two media and reflected from them. The radiant flux from the air ($n_1 \approx 1$) passes through a film having the refractive index n_2 and enters the substance of the optical element having the refractive index $n_3 > n_2$. In this case, part of the radiant energy is reflected from the interfaces. If the thickness of the film is so selected that the difference in the path of two rays (I and II) reflected from the two interfaces is equal to half the wavelength of the incident ray, these rays will be absorbed due to mutual interference. As a result, the reflected radiant flux will be attenuated so that the transmitted flux will be intensified.

The fluxes of the reflected rays I and II are equal if the equation

$$\frac{(n_2 - n_1)^2}{(n_2 + n_1)^2} = \frac{(n_3 - n_2)^2}{(n_3 + n_2)^2} \qquad (220)$$

is satisfied.

By solving eq.(220), we obtain the refractive index n_2, expressed in terms of the refractive indexes n_1 and n_3:

$$n_2 = \sqrt{n_1 n_3} \qquad (221)$$

If the ray originates in air ($n_1 \approx 1$), the index of refraction of the film is determined as $n_2 = \sqrt{n_3}$.

The difference in the ray paths is equal to half the wavelength if

$$\frac{\lambda}{2} = 2d = 2hn_2 \qquad (222)$$

where h and d are, respectively, the geometric and optical thickness of the film*. The optical thickness of the film must therefore be equal to a quarter of the wavelength, $d = \frac{\lambda}{4}$, or, in the more general case, to

$$d = \left(\frac{1 + 2k}{4}\right)\lambda \qquad (223)$$

where $k = 0, 1, 2, 3...$

If the thickness of the film and its refractive index are properly selected, the reflected rays are completely absorbed, but only at a definite wavelength λ_0. At a wavelength other than λ_0, the coating effect is incomplete, and at double or half the wavelength, there is no coating effect at all. Consequently, the full coating effect is obtained at a definite wavelength, selected in accordance with the spectral characteristic of the receiver.

Section 108. Reflective (Catoptric) Systems

In reflective systems, curved reflectors are used, of the spherical** or parabolic type (Fig.209), which receive the flux from a radiation source over a definite solid angle ω and then transform it into a beam, directed along the optical axis. A reflector has two surfaces, rear and front. The front surface faces the source of radiation or the receptor, placed at the focus F. The circle bounded by the edges of the mirror is called the aperture of the reflector, while the line passing

* The optical thickness of a film is the product of the thickness of the film and its refractive index.

** A spherical reflector is a mirror whose reflecting surface has the form of part of a sphere. The radius of the sphere is the radius of curvature of the mirror.

STAT

through the center of the sphere and the principal focus F is called the optical axis of the reflector.

The diameter of the projection of the front surface of the reflector onto the plane of a cut characterizes the luminous aperture of the reflector and is called the luminous diameter or, simply, the diameter of the reflector D. The diameter

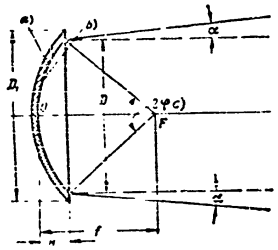

Fig 209 - Diagram and Principal Parameters of a Reflector
a) Rear surface; b) Front surface; c) φ_{max}

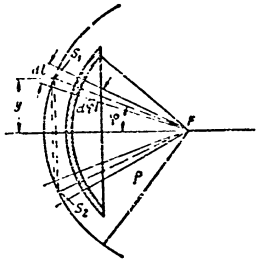

Fig.210 - Diagram for Calculating the Parameters of a Reflector

at the outside edge D_1 is called the over-all diameter.

The point at which the rays, striking an ideal reflector parallel to its optical axis, are collected is called the principal focus of the reflector F. The principal focus may be defined otherwise as the point on the optical axis at which an ideal point source of radiation may be placed to obtain a beam of parallel rays.

The vertex of the reflector O is the point of intersection of the optical axis and the front surface of the reflector, and the depth of the reflector H is the distance from the plane of the cut to the vertex of the reflector.

The distance from the vertex of the reflector to the principal focus is called the focal length f.

For actual reflectors, the concepts of the effective focus F_e and the effective focal length f_e, i.e., the distances from the effective focus to the vertex of the reflector, have been introduced. The effective focal length f_e is determined according to the permissible values of the aberrations of the reflector.

The solid angle of coverage ω is the spatial angle from the vertex at the focus of a reflector, osculating the diameter D of the reflector.

Let us determine to what the solid angle of coverage, expressed in terms of a plane angle, is equal.

An elementary annular surface $ds(\widetilde{S_1S_2})$ of a reflector (Fig.210), placed at an angle φ to the optical axis and having the angular width $d\varphi$, is equal to

$$ds = 2\pi y dl$$

and, consequently, the elementary solid angle will be

$$d\omega = \frac{ds}{r^2} = \frac{2\pi y dl}{r^2}$$

where r is the distance from focus to annular surface.

Since

$$dl = r d\varphi \text{ and } y = r \sin \varphi$$

then

$$d\omega = 2\pi \sin \varphi d\varphi$$

The total solid angle of coverage ω can be expressed in terms of the plane angle φ:

$$\omega = \int_0^{\varphi_{max}} d\omega = 2\pi(1 - \cos \varphi_{max}) \qquad (224)$$

The total flux of the reflector is the sum of the fluxes produced by the separate zones. The zones are not equivalent, and the value of each of them is characterized by the luminosity factor of the zone, M_z.

STAT

The luminous value of the zone is determined by the ratio of the area of the zone to the total area of the reflector, i.e., by $\frac{S_\varphi}{S}$. Table 45 gives the luminosity

Table 45

Luminous Values of Zones of a Reflector (in %), and Relative Luminous Apertures A for Various Angles of Coverage $2\varphi_{max}$

Angle of Coverage, $2\varphi_{max}$	A	Zone, degrees								
		0-10	10-20	20-30	30-40	40-50	50-60	60-70	70-80	80-90
180	-	1	2.5	4.0	6.0	8.5	11.5	16.0	21.5	30
160	3.4	1.0	3.0	6.0	8.5	12.5	16.5	22.5	30.0	-
120	2.3	2.5	7.0	12.5	18.0	26.0	34.0	-	-	-
100	1.8	3.5	10.5	19	28.0	39.0	-	-	-	-
80	1.5	6	17	31	46	-	-	-	-	-
60	1.1	11.0	32	57	-	-	-	-	-	-

factors of the zones for reflectors with various angles of coverage; it also gives the values of the relative luminous aperture A.

Reflectors can be subdivided into two groups: shallow, in which the plane angle of coverage is $2\varphi_{max} < 180°$, and deep, in which $2\varphi_{max} > 180°$ (Fig.211).

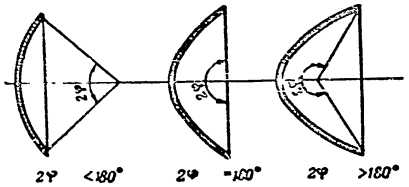

Fig.211 - Types of Reflectors

Reflectors with an aperture in the central part are also used. They are called reflectors with a blind (central) aperture (Fig.212). In view of the relatively small area of the aperture and its screening by some structure located at the focus, such reflectors hardly differ in efficiency from total reflectors.

Reflectors are spherical, parabolic, elliptic, or hyperbolic, according to the shape of their cross section.

Spherical and parabolic reflectors are most widely used. The latter, when the the form of the parabola is exactly followed, yield a parallel beam if a point

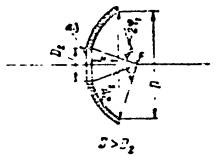

Fig.212 - Reflectors with Blind (Central) Aperture
a) Blind aperture

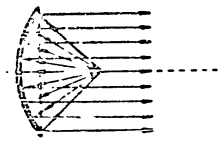

Fig.213 - Parallel Pencil of Rays from Ideal Parabolic Reflector

source of radiation is placed at the focus of the reflector; these reflectors collect, at the focal point, all parallel rays incident on the reflector (Fig.213). When the radiation source, placed at the focus of the reflector, is of finite size, the rays reflected from a parabolic mirror diverge within the limits of some small angle 2 a (cf.Fig.209). The angle of divergence of the rays depends on the ratio of the dimensions of the radiator to the focal length of the reflector. Actual reflectors give a more divergent beam than ideal ones, due to the imperfection of the optical system and the presence of aberrations (errors introduced by an actual optical system into an image and manifested in the form of blurring of the image are called aberrations).

If the radiating body is of finite dimensions, the total beam of rays may be considered as the sum of separate elementary beams produced by all points of the reflector. In this case, each elementary beam will have an axis parallel to the

STAT

optical axis, and its angle of divergence will be determined by the ratio of the focal length to the dimensions of the radiation source.

Let us determine the angle of divergence of a beam with a spherical radiation source having a radius of r and placed at the focus F of a parabolic reflector. Under these conditions,

$$\sin \alpha_\varphi = \frac{r}{\rho_\varphi}$$

For a parabola

$$\rho_\varphi = f \sec^2 \frac{\varphi}{2}$$

Consequently,

$$\sin \alpha_\varphi = \frac{r}{f} \cos^2 \frac{\varphi}{2}$$

It is clear from this that the maximum value of the angles α_φ will be at $\varphi = 0$. In this case,

$$\alpha_{max} = \frac{r}{f}$$

The angle of dispersion of the beam β equals twice the angle α_{max}, i.e.,

$$\beta = 2\alpha_{max} = \frac{2r}{f} \qquad (225)$$

Because of the scattering of the rays within the limits of the angle β, the axial luminous intensity I of a projector will not remain constant at various distances from the reflector. Only beginning at a certain distance L_o, which is called the distance of total radiation or the distance of beam formation, can the beam be considered formed. Beyond this distance, the axial luminous intensity remains constant (diverging beam), and there the law of inverse squares can be applied, determining the illumination at the distance L:

$$E = \frac{I}{L^2} k \qquad (226)$$

where I = axial luminous intensity of the projector;

L = distance from the reflector to the point illuminated;

k = attenuation factor due to losses in the atmosphere.

The value of L_o depends on the focal length, the angle of coverage or the diameter of the reflector, and on the form and dimensions of the radiation source. Ordinarily, this is considerably greater (a few tens or hundreds of times) than the focal length. Photometric measurements with reflectors are sufficiently reliable only beyond the limits of the distance L_o, also called the photometric distance.

The optical systems of reflectors, just like lenses, are characterized by the following basic parameters:

Area or diameter of luminous aperture of the optical system;

Angle of coverage or focal length;

Relative luminous aperture, equal to the ratio of the diameter of the optical system to the focal length;

Magnitude of aberrations;

Losses in the optical system (by absorption and by reflection).

A radiation source is characterized by brightness, dimensions, and form. Optical systems and radiation sources are characterized by spectral characteristics.

Reflectors are of metal or glass.

In metal reflectors, a layer of reflecting metal is deposited on a solid (or sheet metal) base. Solid metal reflectors are durable and little subject to mechanical damage, but they are heavy and undergo some deformation in time, which leads to a change in their qualities. Reflectors of sheet metal are less durable and are made only in small sizes.

Aluminum, chromium, rhodium, or gold are used as reflecting metals. Silver, which has a good reflection factor, rapidly tarnishes in air and is therefore not

STAT

used for metal reflectors.

In glass reflectors, the reflecting medium is deposited on the rear surface of a glass form (in projector-type reflectors) or on its front surface.

A layer of silver about 1 micron thick is used as the reflecting layer, deposited on the rear surface of a glass form. Because of the use of silver, such glass reflectors have a higher reflection factor than metal reflectors, but they are heavier and less durable. Their principal drawback, however, is the fact that the radiant energy passes twice through the glass layer, thus causing additional energy losses. In addition, a supplementary correction of the form of both surfaces (front and rear) is necessary to eliminate, as far as possible, aberration of the reflector; in uncorrected reflectors, aberrations introduce extensive distortions.

Glass does not transmit waves longer than 2-2.5 μ, making such reflectors entirely unsuitable for rays of longer wavelengths.

The reflecting layer deposited on the rear face is covered with a protective layer of another metal. Galvanically deposited copper is often used as a protective layer. The copper layer is coated with varnish and paint. On the outside, the reflecting layer is protected by the glass.

Glass reflectors with a reflecting layer deposited on the front surface can be used regardless of the wavelength of the radiant energy. The spectral characteristics of such reflectors are determined by the reflecting layer, while the glass serves only as a base, giving the reflector the necessary shape. In this case, the reflecting layer is not protected by glass on the outside, therefore, only metals not sensitive to external influences or easily protected from them by protective layers can be used as the reflecting layer.

Figure 202 gives the curve of the reflection factor for a special kind of aluminum. The graph shows that the reflection factors of this type aluminum are very high and remain almost constant over a wide range of wavelengths. The aluminum layer obtained is sufficiently sturdy and not a bject to the influence of atmospheric conditions.

Such reflectors (with the reflecting layer deposited on the front surface) are more efficient than reflectors of the first type, since there is no energy loss in the glass and no distortions due to aberrations of the glass. In addition, the form of glass reflectors does not change in time.

The efficiency of operation of both metal and glass reflectors depends on the properties of the surface. Any dirt, scratches, or moisture will lower the efficiency, which means that reflectors always require cautious handling and careful treatment.

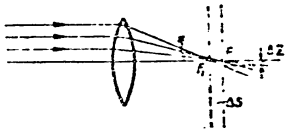

Fig.214 - Spherical Aberration

One of the favorable properties of reflectors with a front specular layer is the fact that, in most cases, this type is completely free of chromatic aberration, i.e., produces almost no changes (at least for infrared rays) in the spectral composition of the reflected flux.

Section 109. Distortion of Images in Optical Systems

In actual optical systems, an incident parallel beam of rays, after passing through the system (or after being reflected from it) is not collected at the focus, but intersects the axis of the system at different points; therefore, instead of the image of a point, a blurred spot is formed.

The magnitude of the error (aberration) depends on the luminous diameters of the optical elements of the system and on the angles of inclination of the rays passing through that system to the optical axis.

Ideal optical systems have no aberration. Optical systems with small luminous apertures approach such systems since they are free of chromatic aberrations when the depicted object is small and located near the optical axis.

Aberrations may be longitudinal, when the optical system introduces distortions in the image points of an object coinciding with the optical axis, or transverse.

STAT

when the image points located within a certain field of view are distorted.

In optical systems with spherical surfaces (lenses or reflectors), parallel rays are not collected at a single point, due to aberration. The further the incident ray passes from the axis of the optical system (Fig.214), the greater will be the distance from the focal point at which the emergent ray intersects the axis of the system. This phenomenon is called spherical aberration. The radius ΔZ of the blurred spot obtained instead of the point-image characterizes transverse spherical aberration, while the area ΔS characterizes longitudinal (or zonal) aberration. The relation between transverse and longitudinal aberrations is expressed by the relation $\frac{\Delta Z}{\Delta S} = \tan u$, where u is the angle at which the extreme ray intersects the axis of the system.

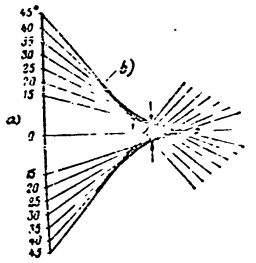

Fig.215 - Circle of Diffusion of Reflected Pencil of Rays
a) Zones in degrees, b) Caustic

The size of the blurred spot obtained on the screen as a result of spherical aberration is small when the screen is placed in the plane of the principal focus. As the screen is displaced from the focus toward the optical system, the size of the spot diminishes at first and then begins to increase again.

Spherical aberration is always produced by any spherical surface of a lens or reflector. Such aberration can be reduced by using a combination of various lenses having aberrations of opposite signs. However, aberration usually cannot be completely eliminated; as a rule, a certain residual aberration remains.

Parabolic reflectors of an ideally precise form have no spherical aberration.

The rays striking the surface of a spherical reflector (fig.215), after reflection from it, do not converge in a single point but are dispersed in a circle of small diameter, which is called the circle of minimum diffusion. This is due to the fact that the pencil of rays is reflected from individual concentric surfaces of the reflector, called zones, and converges at certain points called the focal length of the zones.

Since there are several foci in a reflector, it is necessary to use, in exact calculations, the effective focal length, determined from the expression

$$f_{eff} = \frac{\Sigma f_{zone} W_z}{\Sigma W_z}$$

where Σf_{zone} = sum of focal lengths of all zones;

W_z = factor of relative luminous value of a zone, by which we mean the expression, in percent, of the portion of each zone that participates in creating luminous intensity.

Parabolic reflectors generally used in projectors exhibit the following types of aberration:

Longitudinal relative aberration ε, representing the ratio of the difference between the effective focal length of the reflector and the focal length of a definite zone, to the effective focal length of the reflector,

$$\varepsilon = \frac{f_{eff} - f_{zone}}{f_{eff}} \qquad (227)$$

Longitudinal absolute aberration Δf, representing the difference between the effective focal length of the reflector and the focal length of a definite zone,

$$\Delta f = f_{eff} - f_{zone} \qquad (228)$$

Angular aberration δ, representing the angle formed by the ray with the optical axis,

$$\delta = \frac{\Delta f}{(f + \frac{R^2}{4f})^2} \qquad (229)$$

STAT

where R is the radius of the zone and f the distance to the principal focus of the reflector.

Figure 216 graphically shows the longitudinal absolute and angular aberrations. If a pencil of parallel rays strikes a lens at a certain angle to the optical axis, the image point is obtained in the form of an asymmetric blurred spot. This form of aberration is called the coma aberration*.

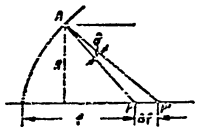

Fig. 216 - Longitudinal and Angular Aberrations of a Reflector

The image in this case is sharp only at the point of intersection between the optical axis and the principal ray or closely adjacent rays, while the other rays give an indistinct image. The size of the spot of the coma aberration depends on the relative aperture of the system $A = \frac{D}{f}$ and on the angle of inclination of the beam to the axis (angular field of view**).

At a large angular field of view, the image of a plane object is not produced in a plane perpendicular to the optical axis but on a certain curved surface. Such distortions are produced by what is called astigmatism*** and by the curvature of the field of the optical system (curvature of the image plane). In aberrations of this type, a point remote from the optical axis is imaged in the form of an oval spot.

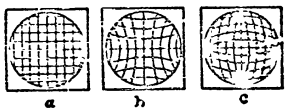

a b c

Fig. 217 - Aberrations of Distortion
a - Ideal image; b - Positive distortion; c - Negative distortion

Distortions introduced by the optical system, which depend on the angles formed between a ray coming from a given point of the object and the optical axis, are called aberrations of distortion. The system in this case produces an unequal variation in the linear dimensions of different parts of the object image, from the center to the periphery of the image plane. This form of aberration leads to impairment of the similarity between the object and its image, i.e., to a modification of the linear image scale.

Figure 217 shows the character of the changes due to aberration of distortion. If a uniform grid (Fig. 217 a) takes the form shown in Fig. 217 b, the aberration is called positive, or pillow-shaped distortion; if the grid takes the form shown in Fig. 217 c, the aberration is called negative or barrel-shaped distortion.

In evaluating aberration, the concept of the caustic or caustic surface is introduced. The caustic is an envelope of refracted or reflected rays (cf. Fig. 215). The shape and size of the caustic depend on the value and character of the aberrations of the optical system. The caustic of a symmetric optical system is symmetric and is characterized by length and transverse dimensions.

The distortions introduced by the optical system may differ for different wavelengths. Aberrations depending on the wavelength of the incident radiation are called chromatic aberrations; they also exist for infrared rays, particularly if the spectrum of these rays is wide.

Chromatic aberration is explained by the phenomenon of dispersion (resolution of a complex ray into the component rays of the spectrum) resulting from a change in the refractive index of the substance of an optical system and depending on the wavelength. The degree of dispersion differs for different substances, and usually increases for regions of the spectrum which approach the limit of transmission of the substance.

Chromatic aberration may be manifested in the form of chromatism of position or in the form of chromatism of enlargement.

In chromatism of position, the focal points of different wavelengths do not

* Coma in Greek means hair.

** The angle including the area bounded by the field of view.

*** Deformation of a pencil of rays. The rays do not converge in a single point, but form two lines of intersection located at different distances.

STAT

coincide. As a result, the luminous spot is imaged by a point of one color, surrounded by colored circles formed by rays of other wavelengths.

In chromatism of enlargement, the focal length differs for different wavelengths; the image of an object thus has its own scale for each wavelength.

Thus there exist, in optical systems, seven principal forms of aberrations: spherical, coma, astigmatism, curvature of field, distortion, chromatism of position, and chromatism of enlargement. The degree of aberration depends on the relative aperture of the optical system (A) and on the angle of inclination of the beam to the optical axis (w).

The aberrations of the simplest optical systems are defined by the following formula (Bild.20) (for unit focal length):

spherical aberration: $\rho_1 = \frac{1}{8} k_1 A^3$;

aberration of coma*: $\rho_2 = \frac{1}{4} k_2 A^2 w$;

astigmatism: $\rho_3 = a - b = k_3 A w^2$;

curvature of field: $\rho_4 = \frac{1}{4} k_4 A w^2$;

distortion: $\Delta l' = k_5 w^3$;

chromatism of position** $\rho_\lambda = k_6 A$

chromatism of enlargement: $\Delta l' = k_7 w$

In the above formulas, the following notations have been adopted: ρ = radius of the circle of diffusion; a and b = axes of the elliptical image point; $\Delta l'$ = = displacement of image point from the position corresponding to the ideal optical system; k_{1-7} = aberration factors for different lenses or reflectors.

The significance of each aberration depends both on its magnitude and on the conditions under which an optical system is used. Which of the above enumerated aberrations is most harmful and must be excluded can be determined only for each concrete practical case of using an optical system. Each aberration can be reduced or almost completely eliminated by a combination of lenses with aberrations of different signs, and also by proper selection of the types of glass for the optical elements and calculation of the design parameters of the optical elements of the system.

* The major axis of the coma aberration is $3\rho_2$, and its maximum width is $2\rho_2$.

** Chromatic aberration occurs only in lens systems.

Section 110. Compound Mirrors and Mirror-Lens Systems

Compound Mirror Systems

Compound optical systems consist of several mirrors or lenses. In compound mirror systems, consisting of several concave or convex mirrors, the larger mirror

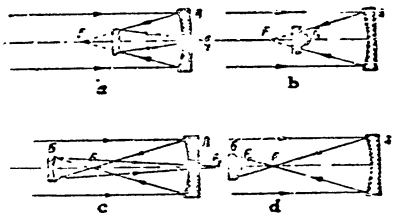

Fig.218 - Compound Mirror Systems
a - Prefocal elongating system; b - Prefocal shortening system, c - Postfocal elongating system; d - Postfocal shortening system

determines the effective aperture and is the main or principal, mirror. The smaller mirrors effect only the convergence of the rays and are secondary mirrors. Such systems may also have plane mirrors, but these do not modify the optical characteristics of the system.

Figure 218 shows four characteristic optical mirror systems, to which all existing compound systems can be reduced. The mirror A is the principal mirror, B is the secondary mirror. The secondary mirror is placed in front of the focus of the principal mirror (Fig.218 a,b) or behind it (Fig.218 c,d). In the former case, the systems are called prefocal, in the latter, postfocal. Mirrors are either concave or convex. The secondary mirrors shorten or lengthen the focal lengths of the

STAT

system.

A compound mirror system, for example, can be used for producing a parallel beam beyond the mirror (Fig. 219 a,b) passing through an aperture in the principal mirror.

The change in focal length permits constructing more compact optical systems in many cases. An example of such a system is the system developed by Professor D.D.Maksutov (Fig. 220). To reduce the over-all size, the plane mirror C in this system, which changes the direction of the rays, is placed beyond the focus of the

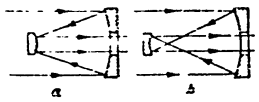

Fig. 219 - Mirror Systems to Obtain Parallel Beams

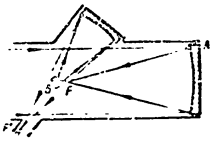

Fig. 220 - Schematic Optical Diagram of Mirror Telescope Developed by Professor D.D.Maksutov

principal mirror A. The secondary mirror B does not shield the principal mirror so that its diameter may be larger, while the over-all dimensions of the system remain practically unchanged.

Mirror-Lens Systems

Ordinary optical systems, both lens and mirror, always exhibit some form of aberration.

To reduce the aberrations, so-called corrected mirror-lens (mixed) systems are used, in which the lens of the larger lens or mirror is combined with a smaller lens or mirror. The larger lens determines the diameter of the effective aperture of the system, while the smaller lens serves to reduce the aberrations introduced by the principal lens or mirror.

Mirror-lens systems may be used for rays of the visible and infrared regions of the spectrum. Let us consider a few of the most typical mirror-lens systems.

Mirror-Lens System with Lens Close to the Focus. A paraboloic mirror (ideal) has no spherical aberration, but the image formed by it is distorted because of other

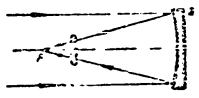

Fig. 221 - Mirror-Lens System with Lens Close to Focus

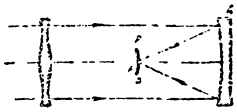

Fig. 222 - Mirror-Lens System with Correcting Lens
a) PFP - Focal area

aberrations, particularly coma. To reduce the latter, the lens system B, consisting of several lenses (in the simplest case two lenses, a positive and a negative lens) is placed close to the focus in the path of the convergent beam (Fig. 221).

The drawbacks of such a system are the complex design, the expense (since large glass surfaces of good quality are required), and the additional losses by reflection from the lens surfaces and by absorption in the glass.

Such correcting lenses can also be used for spherical mirrors, but in this case the lens must also be corrected for spherical aberration. It is possible but irrational to build such systems, because the lenses are very complex and also limit the power, the luminous aperture, and the field of view of the optical system.

Mirror-Lens System with Correcting Lens. In ordinary mirror telescopes, the principal mirror is not protected from outside influences such as dust, sweating, mechanical damage, and the direct temperature effects. In addition, the convection currents of air in the tube distort the image. All disadvantages of an open tube are eliminated in the mirror telescope with a correcting lens (Fig. 222).

Correction of the image is accomplished by placing in front of the spherical mirror A the lens B with a diameter equal to the diameter of the beam cross section. With one plane of the lens B deformed in a certain way, this reduces not only the

spherical aberration but also the aberration of coma and astigmatism. The aberration of field curvature is not reduced in this system. For this reason, the locus of sharp images is not a plane but the surface of the sphere PFP, known as the focal area; consequently, the surface on which the image is to be depicted must be convex (according to the shape of the focal area).

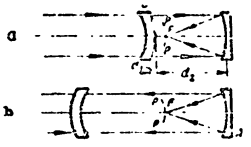

Fig. 223 - Maksutov Meniscus Systems

The principal drawback of these systems is the difficulty in building correcting lenses and the light losses in the correcting lens systems.

The Maksutov Meniscus Systems

In 1941, Professor D.D.Maksutov proposed the use of a meniscus to correct the aberrations of mirrors. Since the spherical aberration of a meniscus may have either sign and, in addition, a meniscus is achromatic, it may serve as a very effective correcting element in catodioptric systems. If the meniscus is properly located with respect to the mirror, it will also correct the coma.

Figure 223 shows the simplest meniscus system. In this diagram, A is a concave spherical mirror and B an achromatic meniscus. With a properly selected spherical aberration of the meniscus and a properly selected distance between the meniscus and the mirror, the system will not only be achromatic and free of spherical aberration, but will also have its coma corrected, i.e., it will be an aplanatic system, giving a true, undistorted, and aberration-free image. Only the curvature of the field will remain uncorrected.

The meniscus is arranged with its convexity (Fig 223 a) or its concavity (Figure 223 b) facing the reflecting surface.

The Maksutov meniscus systems permit construction of a powerful optical system with a large field of view and reduced aberrations. It is simpler to build a meniscus of the required form than any other correcting system. A meniscus may be used in any optical system to reduce its aberration and to simplify the system.

STAT

CHAPTER XIII

PASSAGE OF INFRARED RAYS THROUGH THE ATMOSPHERE

Section 111. Composition of the Atmosphere

The atmosphere is a medium consisting of a mixture of gases and water vapor, with foreign particles suspended in it. The size of the particles ranges from 5×10^{-6} to 5×10^{-3} cm.

The principal constant constituents of the lower (ground) layer of the atmosphere are nitrogen (78.03%) and oxygen (20.99%). The remaining gases entering into the composition of air (argon, hydrogen, carbon dioxide, neon, helium, krypton and xenon), make up less than 1% all told.

The water-vapor content of the air varies as a function of several factors, particularly the air temperature and the atmospheric pressure. At increasing temperature, the water-vapor content of the air increases.

In the lowest layer of the air, a certain quantity of foreign impurities is always present, which may be minute water droplets, produced by condensation of water vapor, smoke particles, dust particles of organic or mineral origin, and bacteria.

The state of the atmosphere when the predominant impurities are solid particles, like dust or smoke, is called haze.

Various degrees of concentration of liquid particles (water droplets) lead to the formation of haze, fogs of various densities, clouds, and rain.

The presence of any form of impurity in the atmosphere makes it turbid and adversely affects the conditions for the passage of infrared rays. The ratio between the energy I, passing through a layer of atmosphere of thickness x, to the energy I_0 entering that layer is called the transparency, or the transparency factor of the given layer, and is usually denoted by the letter τ. It is customary to express the factor τ in percent per km.

Section 112. Absorption of Infrared Rays by Gases and Water Vapor

Infrared rays are absorbed and scattered in the atmosphere by the molecules of various atmospheric gases, and also by solid particles and water droplets (fogs).

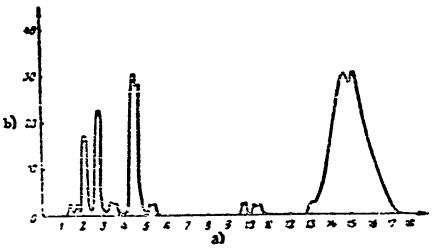

Fig. 224 - Absorption Bands of Carbon Dioxide in the Atmosphere
a) Wavelength, μ; b) Absorption factor, %

When infrared rays pass through the atmosphere, they are selectively absorbed by ozone, carbon dioxide, and water vapor. The degree of absorption is defined by the absorption factor A, which characterizes the attenuation of the radiation when it passes through an atmospheric layer of unit thickness. A number of empirical and semi-empirical formulas have been proposed for its calculation.

The absorptive power of ozone may be neglected, since the percentage content of ozone in the lowest layer of air is insignificant, except for a period following a thunderstorm, when the ozone content of the air is sharply increased. Ozone has absorption bands at wavelengths of 4.7 and 9.6 μ.

STAT

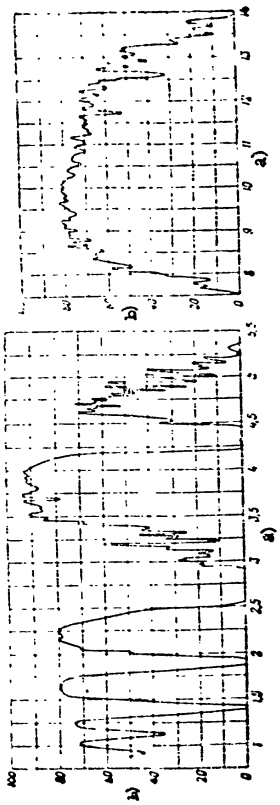

Fig.225 - Pass-Bands of Infrared Rays in the Atmosphere
a) Wavelength, μ; b) Transmission, %

Carbon dioxide is characterized by intense absorption bands at wavelengths of 2.05 μ, 2.6 μ, 4.3 μ, and particularly at 12.8-17.3 μ (Fig.224).

The latter of these bands, together with the absorption bands of water vapor, is the cause of the almost total absorption of infrared rays by the atmosphere, beginning at 14-15 μ. The absorptive action of carbon dioxide in the first two parts

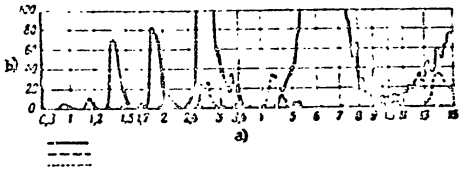

Fig.226 - Absorption Bands of Water Vapor, Carbon Dioxide and Ozone
a) Wavelength, μ; b) Absorption factor, %; c) Water vapor; d) Carbon dioxide; e) Ozone

of the spectrum may be disregarded, since its content in air is small relative to that of water vapor, while water vapor more strongly absorbs infrared rays.

Water vapor is the greatest absorber of infrared rays and has intense absorption bands at various wavelengths. Consequently, the absorption has a selective character, i.e., it primarily affects certain portions of the spectrum. The strongest absorption bands of water vapor are the following wavelength regions (the figures indicate the centers of the bands): 0.94, 1.13, 1.38, 1.46, 1.87, 2.66, 3.15, 6.26, 11.7, 12.6, 13.5, and 14.3 μ.

In these portions of the spectrum, the energy of the infrared rays passing through the atmosphere is absorbed to a considerable extent. Alongside of the absorption bands in water vapor there are also pass-bands, through which the energy of the infrared rays passes without appreciable absorption.

Figure 225 shows the pass-bands of infrared rays in the atmosphere, in the 1-14 μ region.

STAT

As will be seen from the figure, in the wavelength regions of 1-1.1; 1.2-1.3, 1.6-1.75; and 2.1-2.4 μ, the transmission reaches 80%, and in the region 3.4-4.2 μ it exceeds 90%. In the 8-12 μ band, the average transmission extends from 60 to 70%, and for some lines exceeds 80%.

The location of the absorption zones of water vapor, carbon dioxide, and ozone is given in Fig. 226. The relative values of the absorption bands of these components of the atmosphere are taken on an arbitrary scale, since their percentage content in the atmosphere varies.

Section 113. Attenuation of the Flux of Infrared Rays Due to Scattering

When infrared rays pass through a layer of atmosphere containing minute suspended particles, whose refractive index differs from that of the medium, part of the radiant energy is scattered in all directions by the molecules of air. This phenomenon is called molecular scattering. The work of the prominent Soviet scientist, Academician L.I.Mandel'shtam, has shown that the inhomogeneities of the atmosphere, causing the scattering of the radiation energy, are accumulations of air molecules of various density, due to the chaotic thermal motion of the molecules.

According to theoretical studies, the scattering of radiant energy by particles whose dimensions are small with respect to its wavelength, is inversely proportional to the fourth power of the wavelength. Consequently, the scattering increases with decreasing wavelength. The energy scattered by such particles can be defined by the scattering factor ε°, characterizing the degree of attenuation of the radiation in unit thickness of the atmosphere, as a result of interaction of the radiant flux with the molecules of the medium, resulting in a redistribution of energy:

$$\varepsilon^\circ = \frac{\pi^2(n^2-1)^2}{2N\lambda^4}(1+\cos^2\varphi) \qquad (230)$$

where n = refractive index of the particle substance;

N = number of particles in unit volume;

φ = angle between direction of the incident ray and direction of the scattered ray;

λ = wavelength.

The scattering factor depends on the angle φ and on the properties of the medium. It follows from eq.(230) that at $\varphi = 0°$ and 180°, the scattering reaches a maximum.

The total attenuation of the energy I of the infrared rays in a layer of atmosphere of thickness x, due to the scattering of energy and its absorption, is characterized by the attenuation (extinction) factor k°.

The attenuation factor is the quantity obtained by adding the diffusion and absorption factors, and is of a dimension inverse to the length, for example 1/m.

To determine the attentation factor, we may use the formula

$$I = I_0 e^{-k^\circ x} = I_0 e^{-(\varepsilon+\varepsilon^\circ)x} \qquad (231)$$

where I_0 = energy of radiation before passing a layer of thickness x;

I = energy of radiation after passing the layer;

e = base of natural logarithms.

Equation (231) is known as the exponential law of attenuation of energy.

The relation between the luminous intensity and direction of the diffused rays, for particles of various sizes, is shown in Fig. 227. This diagram shows the indicatrices of diffusion constructed by Professor V.V.Shuleykin for particles with progressively increasing diameters (a, b, c, d). The hatched part shows the proportion of polarized rays, i.e., of rays vibrating in a certain definite direction.

With increasing size of the particles, the indicatrices become asymmetric and elongated in the forward direction. In the case of large-size particles, the forward scattering (in the direction of the arrow) may be 10 times as great as the backward scattering. The angle of maximum scattering φ by small particles is 90°, and by large particles 120°. The proportion of polarized light decreases with in-

creasing particle diameter.

In addition to scattering by air molecules, there is also scattering by water droplets formed in the atmosphere by condensation of water vapor on cooling of the

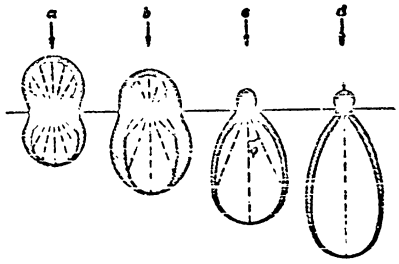

Fig. 2.7 - Indicatrices of Diffusion

air, and by particles of the impurities present in the atmosphere (ground dust, haze, and soot). The condensation of water vapor requires particles that can serve as nuclei, or centers of condensation. Particles of dust, haze, the salts sodium chloride and magnesium chloride, as well as atmospheric ions, may serve as such nuclei of condensation in the atmosphere.

The number of condensation nuclei in the air varies. Over the surface of the ocean, the number of nuclei is 100-150 per cm^3, over large industrial centers with strongly turbid atmosphere their number reaches 150,000 per cm^3.

The number of condensation nuclei in a definite volume of air determines the size of the particles formed on the condensation of water vapor. When the number of nuclei is large, very minute particles are obtained, with a diameter of about 5×10^{-5} cm. Such particles form haze.

Experimental data show that haze leads to a certain attenuation of infrared rays. Thus, for example, over a distance of 10 km, the attenuation of infrared rays of a wavelength of 3 μ amounts to not more than 0.013%.

In the presence of haze, when the visibility does not exceed 1 km (for visible rays), the use of infrared rays gives an advantage of a factor of about 2 to 4 in range of visibility, by comparison with the range for visible rays.

Section 114. Passage of Infrared Rays through Fog

Investigations on the passage of infrared rays through natural and artificial mists frequently lead to contradictory results. This is explained by the different conditions under which the measurements are made.

The conditions of passage of infrared rays through fog on dry land differ from the conditions of passage through fog over an ocean surface or a coast. The composition of fog in a city, and especially in a large center, differs greatly from the composition of a fog in the fields, outside the city, etc. The conditions of passage of infrared rays through natural and artificial fogs also differ considerably. It is impossible to produce a stable artificial fog. The instability of such a fog can be demonstrated by the fact that two measurements, separated by only a short time interval, yield entirely differently results. Despite the difference in the literature data, a number of useful conclusions on the passage of infrared rays through fog can be drawn.

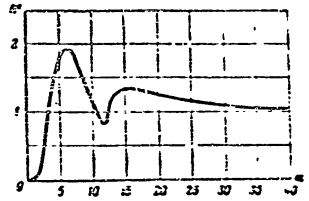

Fig. 2.8 - The Scattering Function k'

Passage of Infrared Rays through Natural Fogs

A state of the atmosphere saturated by water droplets at which the visibility range (for visible rays) does not exceed 800-1000 m, is called fog. Natural fogs are formed as a result of currents of warm moist air flowing over a cold surface, or as a result of the cooling of the lowest layers of air due to the rapid cooling of the soil after sunset.

STAT

Natural fogs are subdivided, according to the character of their formation, into intramass and frontal. Intramass fogs are in turn subdivided into radiation fogs and advective fogs.

Radiation fogs occur on strong cooling of the earth's surface due to thermal radiation in clear weather, causing the air to become supersaturated and moisture to condense.

Advective fogs are formed on invasion of a warm moist air front into a zone of lower temperature.

Frontal fogs occur on the displacement of a front of air masses in air with a high moisture content.

As a result of studies of the passage of infrared rays through natural fog, formulas were proposed for determining the brightness of rays that have passed through a layer of thickness x, and to determine the scattering factor as a function of the radius of the droplets.

If the original intensity of a ray is I_0, then after passage of the ray through a fog it will decrease to the value

$$I = I_0 e^{-2\pi N \rho^2 x k'} \qquad (232)$$

where ρ = radius of droplets;

N = number of droplets in 1 cm^3 of fog;

e = base of natural logarithms;

k' = a function depending on the droplet radius and on the wavelength.

If the refractive index of the medium is n = 1, the value of k' will be proportional to the diffusion factor

$$\varepsilon^\circ = 2\pi\rho^2 k' \qquad (233)$$

i.e.,

$$k' = \frac{\varepsilon^\circ}{2\pi\rho^2} \qquad (234)$$

On the basis of these formulas curves were constructed (Fig.223) that express the relation between k' and a quantity

$$\alpha = \frac{2\pi\rho}{\lambda}$$

The diagram shows that the curve $k' = f(\alpha)$ has maxima at $\alpha = 6.2$ and $\alpha = 15$, and a minimum at $\alpha = 11.2$. After reaching the maximum value of k' at $\alpha = 15$, the curve smoothly descends. In the region of maximum values of α scattering of short-wave rays exists and at its minimum value, scattering of long-wave rays.

The numerical values of k' and α are given in Table 47.

Table 47

Values of α and k'

α	k'	α	k'	α	k'	α	k'
1	0.06	6	1.95	11	0.87	20	1.35
2	0.27	7	1.9	11.2	0.82	25	1.15
3	0.82	8	1.7	12	1.0	30	1.09
4	1.45	9	1.4	13	1.25	35	1.06
5	1.83	10	1.12	15	1.35	40	1.03

The scattering factor ε° can be calculated from the values of k' given in Table 47.

The curves of $\varepsilon^\circ = f(\lambda)$, given in Fig.229 were constructed for various particle radii ρ, measured in centimeters for wavelengths up to 100 μ. It will be seen from Fig.229 that, for the shorter wavelengths, the scattering is determined only by the radius of the particles and is almost independent of the wavelength (provided that the wavelength is considerably less than the radius of the particles). Maximum scattering takes place when the wavelength equals the radius of the scattering particles.

For fog with particles of a radius of $\rho = 0.5$ μ, the slope of the curve for

STAT

the coefficient k', as a function of the wavelength, is given in Fig.230. Obviously, beginning with the region 0.5 μ, the diffusion of long waves decreases, i.e., the transparency increases. For particles of a radius of ρ = 1 μ, the reduction in diffusion and the increase in transparency take place beginning with the region 1 μ.

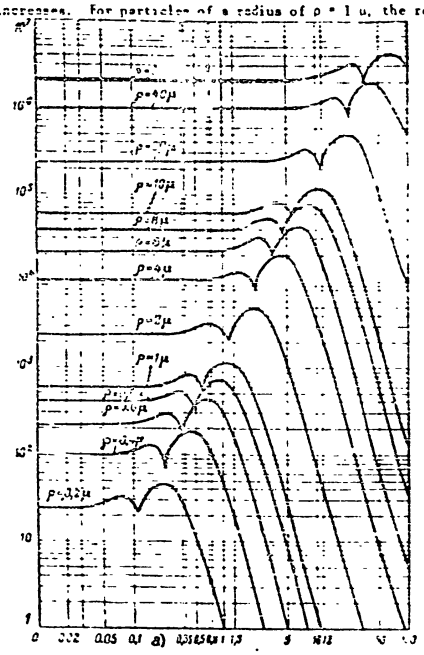

Fig.229 - Curves for the Relation ε' = f( ) at Various Sizes of the Fog Droplets
a) Wavelength, μ

For particles of a radius of ρ = 2 μ, the maximum scattering is shifted toward longer wavelengths (about 2 μ). For particles of still greater radius, the scattering maxima are shifted still further toward the long-wave portion of the spectrum.

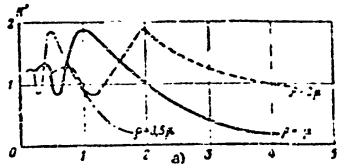

Fig.230 - Relation between the Scattering Function k' and the Wavelength for Various Sizes of Fog Droplets
a) Wavelength, μ

On the basis of Figs.229 and 230 the following conclusions can be drawn:

The scattering of infrared rays is considerably less than the scattering of visible rays at a radius of the scattering particles not exceeding 0.4 μ;

Part of the infrared rays (the long-wave ones) are scattered less than visible rays if the radius of the particles does not exceed 2 μ.

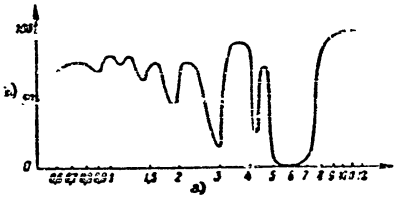

Fig.231 - Passage of Infrared Rays through a Natural Light Mist
a) Wavelength, μ; b) Transmission, %

If the radius of the scattering particles is more than 20 μ, waves longer than 1000 μ, i.e. millimeter radio waves, will pass without excessive scattering.

Consequently, when infrared rays pass through an atmosphere of reduced transparency, the size of the mist droplets is of decisive importance.

Figure 231 shows the curve of transmission of infrared rays by a natural light mist of optical density 0.14 per kilometer. The graph indicates that, in a light mist, the transmission of infrared rays is as high as 90% in the 3-4 μ region and is equal to 100% in the 8-12 μ region. The existing absorption bands are due to water vapor.

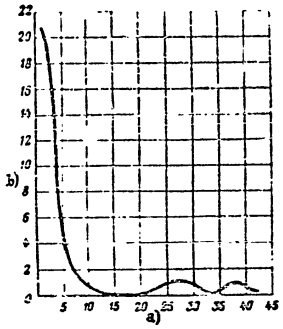

Fig. 232 - Relation between Number of Droplets per cm³ of Mist and Their Size
a) Radius of droplets, μ; b) Number of particles per cm³

Thus, in a mist, no increase of transparency can be expected for the near infrared rays, due to the fact that, as a rule, the particles of mist have a radius greater than 3-5 μ.

The radii of mist droplets vary over a wide range, from 1 to 60 μ, but droplets of a radius greater than 25 μ are encountered relatively seldom.

Mist droplets of a radius of 60 μ and above change into rain drops. Measurements in heavy fogs, with visibility not exceeding 2000 m, show that the most frequently encountered mist droplets have a radius equal to 4 μ (Fig. 232).

Passage of Infrared Rays through Artificial Fogs

In 1930, Anderson studied the passage of visible and infrared rays through an artificial aqueous mist. By means of filters, he isolated the bands 0.7-1.2 μ and 1.65-2.7 μ. His problem included determination of the absorption as a function of concentration and the size of the mist particles.

The data obtained by Anderson are given in Table 48.

Thus, the presence of small particles in a fog, together with large particles, make the fog more transparent for infrared rays than for visible rays.

It will be seen from Table 48 that the permeability of fog for infrared rays is higher than for visible rays, and that infrared rays are transmitted more readily

Table 48

Permeability of Fog in % for Infrared Rays (After Anderson)

What \ Wavelength μ	0.49	0.53	0.56	0.7	0.7-1.2	1.65-2.7
Of small particles	32.5	32.5	40	44	60	68
Of large particles	40	39	38	40	50	73

through fog of small particles than through fog of large particles.

Section 110. Transparency of the Atmosphere for Infrared Rays

As a result of several measurements of the transparency of the atmosphere, it has been established that, near the earth's surface, the atmosphere is more transparent for infrared rays than for visible rays. The results of the measurements are given in the form of curves, in Figs. 233 and 234.

The above material permits certain conclusions as to the ability of infrared rays to pass through the atmosphere.

In the case of a transparent atmosphere and also in presence of haze and light mist, when the range of visibility is above 1000 m, infrared rays of wavelengths up to about 1.5 μ are transmitted considerably better than visible rays. This is explained by the fact that the radius of the scattering particles is considerably less than 1 μ.

In a heavy fog, where the visibility range is less than 300 m, infrared rays of wavelengths up to 1.5 μ are completely absorbed, since the radius of the scattering particles is more than 1 μ. Infrared rays of wavelengths from 4 to 12 μ, depending on the kind of fog and the character of the particle-size distribution, may pass better than visible rays, if particles of sizes smaller than the wavelengths of the transmitted rays passing predominate in the mist.

STAT

In artificial mists, in which the radius of the particles usually does not exceed 0.2-1μ, infrared rays pass better than visible rays; for wavelengths of 2 μ,

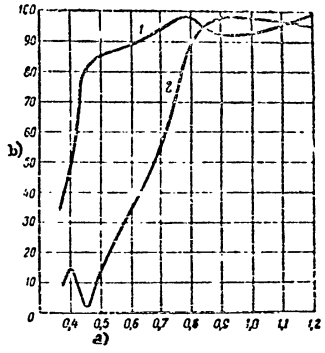

Fig. 233 - Transparency of the Atmosphere at Various Altitudes for Infrared Rays:

1 - Altitude [illegible] km; 2 - Altitude 2.5 km
a) Wavelength, μ; b) Transparency, %

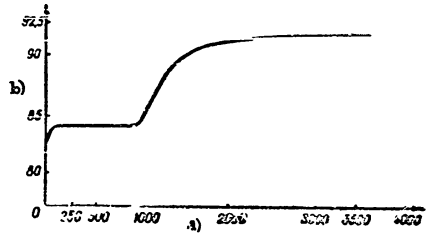

Fig. 234 - Relation between Transparency of the Atmosphere for Infrared Rays and Altitude
a) Altitude, m; b) Transparency, %

they pass more than 20 times better. However, it must be borne in mind that, in artificial mists, the particle radius increases in time, causing the passage of infrared rays to become more difficult.

In rain, when the minimum particle radius is approximately equal to 60 μ, infrared rays have no advantages in transmission since scattering no longer depends on the wavelength.

On the basis of these conclusions, the possibility of using infrared rays under various atmospheric conditions can be estimated.

BIBLIOGRAPHY

1. Lukovskiy, Ye.A. - Principles of Optics. Elements of Illumination Engineering. VOYENIZDAT (1949)

2. Mikheyev, M.A. - Principles of Heat Transmission. Second Ed. GOSENERGOIZDAT (1949)

3. Latvin, A.M. - Theoretical Principles of Heat Engineering. GOSENERGOIZDAT (1944)

4. Khvostikov, I.A. - Surveying, Observation, and Signaling Through Fog. GOSTEKHIZDAT (1942)

5. Ivanov, A.P. - Electric Light Sources, Part I. GONTI (1938)

5a. Karyakin, N.A. - Projectors. GOSTEKHIZDAT (1944)

6. Levitskaya, M.A. - Infrared Rays. AN SSSR (1935)

7. Chudakov, P.A. - Mercury-Arc Light Sources. Izv. VETA im. S.M. Budennogo, 13 (1936)

8. Ivanov, A.P. - Loc. Cit Part II

9. Likhoniitskiy, S.D., Blyudzin, A.P. - Illumination Engineering. VETAS (1941)

10. - Elektrichestvo, No. 10, 38 (1947)

10a. Ivanov, A.P. - Electric Light Sources, Part II. GOZENERGOIZDAT (1948)

11. Rubetskiy, I.A. - Secondary-Electronic Instruments. Stenographic Text of Lecture. Pravda (1951)

12. Vlasov, V.F. - Vacuum Electric Instruments. SVYAZIZDAT (1939)

13. - Modern Bolometers. Zhur.tekh.fiziki, 20(6; (1950)

14. Kolomets,B.T. - Thermistors. Elektrichestvo,No.3 (1947)

15. Luchin,S.M. - Electro-Optico-Acoustic Phenomena in Soot. Zhur.tekh.fiz. 16(10)(1946)

16. Preobrazhenskiy,V.P. - Measurements and Instruments of Heat Engineering. GOSENERGOIZDAT (1946)

17. Rokharev,V.P. - A Photoelectrooptical Amplifier. Usp.fiz.nauk 44 (1951)

18. Cherni and Reder - Usp.fiz.nauk 25(1),103

19. Grebenshchikov,I.V. et al. - Coating of Optical Systems. AN SSSR (1948)

20. Maksutov,D.D. - Astronomical Optics. GOSTEKHIZDAT (1946)

TABLE OF CONTENTS

STAT

STAT

STAT